Queen Mary
University of London

Thesis submitted for the degree of
Doctor of Philosophy

Inflation: Connecting Theory with Observables

Zachary Kenton

Supervisors

Prof. Steven Thomas & Dr David J. Mulryne

July 19, 2017

Centre for Research in String Theory
School of Physics and Astronomy
Queen Mary University of London

Tell your son to stop trying to fill your head with science - for to fill your heart with love is enough! – Richard Feynman

This thesis is dedicated to Mum and Hubie who have supported me in every aspect of my life. This thesis wouldn't have been possible without their love and encouragement.

Know that for the human mind there are certain objects of perception which are within the scope of its nature and capacity; on the other hand, there are, amongst things which actually exist, certain objects which the mind can in no way and by no means grasp: the gates of perception are closed against it. Further, there are things of which the mind understands one part, but remains ignorant of the other; and when man is able to comprehend certain things, it does not follow that he must be able to comprehend everything.

– Rambam (Maimonides), *The Guide for the Perplexed*

Abstract

Information about the very early universe can be accessed from observations of the cosmic microwave background (CMB) radiation and the later formation of large-scale structure (LSS) that are produced from cosmological perturbations of the early universe. The most developed theoretical explanation for the origin of these perturbations is the theory of inflation, in which the early universe undergoes a period of accelerated expansion, amplifying quantum fluctuations to macroscopic size, which act as the seeds for the CMB anisotropies and the cosmic web of the LSS. The work in this thesis aims to connect the theory of inflation to properties of these observables in a highly detailed way, suitable for future high-precision astronomical surveys. After some introductory review chapters, we begin with new research on a study of inflation from string theory, deriving an observably-large value of the tensor-to-scalar ratio, which had been previously difficult to achieve theoretically. The next study investigates the link between the observed CMB power asymmetry and non-Gaussianity, including a novel non-zero value for the trispectrum. Next we study soft limits of non-Gaussian inflationary correlation functions, focussing first on the squeezed limit of the bispectrum and then generalizing to soft limits of higher-point correlation functions, giving results valid for multi-field models of inflation.

Acknowledgements

Firstly I would like to thank Mum and Hubie, who have supported me with love and kindness all the way through my studies. Thanks also to Dad and Steph, and to my brother Russell for being there for me.

Roxana, my muse, your love, kindness and creative spirit inspired the latter parts of this thesis. I'm very lucky to have you in my life.

Throughout my PhD studies I've had two fantastic supervisors, Steve Thomas and David Mulryne, who have guided me on the research in this thesis. Steve supported me from before I even began my PhD, sharing with me his vast knowledge across a broad range of physics topics from string theory to cosmology, and from observations to instrumentation. He supervised me in a relaxed yet supportive way, allowing me the freedom to follow my own research interests at every stage. His exceptional kindness is felt by all who work with him.

David has been my academic mentor and key collaborator, later becoming my second supervisor halfway through my PhD. Working with David has been so enjoyable - he has always been interested in what I've got to say, my calculations and the ideas I have. His technical expertise has been invaluable, as has his guidance on my academic career. He is at once a great friend and my academic inspiration.

I have many people I wish to thank from earlier in my mathematical studies. In particular I would like to thank my directors of studies at Cambridge, Stephen Cowley, Vladimir Dokchitser and Mark Spivack for guiding me along my undergraduate and masters in mathematics. Stephen Cowley, in particular, has been a long-term advisor to me, offering sharp insights along with his own unique humour. I wish to thank Daniel Baumann for sharing his extensive knowledge on cosmology with me, his fantastic lectures and for continued support since I graduated. Thanks also to Adam Solomon, a supervisor turned mentor turned friend.

I would like to thank those who have hosted me for various seminars and discussions including Adam Solomon, Mark Trodden, Sarah Shandera and Matthew Kleban for hosting me during my visit to the USA, Enrico Pajer and Daniel Baumann for hosting me in the Netherlands and Johannes Noller, Christian Byrnes, Kostas Skenderis and Ivonne Zavala for invitations to speak at their seminars in the UK.

For their feedback on some of the drafts of the published material contained in this thesis I wish to thank Enrico Pajer, Shailee Imrith, David Seery, Raquel Ribeiro, Takeshi Kobayashi and Christian T. Byrnes.

I'd like to thank all the CRST PhD students I've shared an office with over the years: Sam Playle, Rob Mooney, David Garner, Brenda Penante, James McGrane, Felix Rudolph, Paolo Mattioli, Edward Hughes, Martyna Kostacinska, Emanuele Moscato, Joe Hayling, Rodolfo Panerai, Chris Lewis-Brown, Arnau Koemans Collado, Matteo Parisi, Ray Otsuki and Zoltan Laczko. Thanks for putting up with my constant bad jokes and for making our office such an enjoyable place to work. It's been great to work with such caring, fun and interesting people. I'd also like to thank all the CRST academics, in particular David Berman for hilarious discussions on all manner of things, physics and beyond academia.

Thanks to all the Cosmology and Relativity group who I've worked alongside, particularly Sophia Goldberg, Viraj Sanghai, Karim Malik, Tim Clifton, Alex Leithes, Ellie Nalson, Pedro Carrilho, John Ronayne, Jessie Durk, Charlie Pittordis, Kit Gallagher, Jorge Venegas and Louis Coates. It's been so great to have been included in your research group during my PhD.

Thanks also to the administrative staff in the SPA, especially Lucie Bone, Karen Wilkinson, Jessica Henry and Sarah Cowls.

It's been a pleasure to connect with some amazing PhD students along the way - thanks to Tom Charnock, Rebecca Kennedy, Peter Jones, Zoe Slade, David Edwards, William Woodhead, Giulia Ferlito, Elliot Banks, Yvette Welling, Drian van der Woude and Sebastian Cespedes.

Thanks to my old housemates Ed, Callum, July, Tom and my Moish housemates Tanya, Andrew, Ben, Hannah, Em and Roxy - you've all made my life so much fun and give me so much happiness.

I'd also like to thank my friends that I've neglected at various times during my PhD, in particular, Callum, Nicole, Wills, David, Theo, Maz, Sinead, Mark, George, Javal, Gilboy, Rob, Becca, Simon, Elz, Bruce, Joëlle and Emma, plus many others I don't have space to thank here.

I have been supported by an STFC Studentship throughout my PhD.

Declaration

I, Zachary Kenton, confirm that the research included within this thesis is my own work or that where it has been carried out in collaboration with, or supported by others, that this is duly acknowledged below and my contribution indicated. Previously published material is also acknowledged below.

I attest that I have exercised reasonable care to ensure that the work is original, and does not to the best of my knowledge break any UK law, infringe any third party's copyright or other Intellectual Property Right, or contain any confidential material.

I accept that the College has the right to use plagiarism detection software to check the electronic version of the thesis.

I confirm that this thesis has not been previously submitted for the award of a degree by this or any other university.

The copyright of this thesis rests with the author and no quotation from it or information derived from it may be published without the prior written consent of the author.

Signature:

Date: July 19, 2017

Details of collaboration and publications:

This thesis describes research carried out with my supervisors Prof. Steven Thomas and Dr David J. Mulryne, which was published in [1–4]. It also contains some unpublished material. Where other sources have been used, they are cited in the bibliography.

Contents

1 Introduction **10**

2 Inflation **13**

2.1 Classical Dynamics of Inflation 13
2.1.1 Single-Field Slow-Roll 14
2.1.2 Single-Field Non-Canonical 15
2.1.3 Multiple Fields 16
2.2 Quantum Fluctuations in Inflation 17
2.2.1 Spatially Flat Gauge 18
2.2.2 Curvature Perturbations 19
2.2.3 Gravitational Waves 21
2.2.4 Non-Gaussianity 23
2.2.5 The $in-in$ Formalism 24
2.2.6 The δN Formalism 25
2.2.7 Numerical Techniques for Inflationary Correlation Functions . . 29
2.3 Observables 29
2.3.1 Cosmic Microwave Background 29
2.3.2 Large Scale Structure 33
2.3.3 ΛCDM Model 34
2.3.4 Primordial Gravitational Waves 34
2.3.5 Constraints on Primordial Non-Gaussianity 35
2.3.6 Alternatives to Inflation 38

Part 1 Theory - String Theory and Inflation **40**

3 Elements of String Theory for Inflation **41**

3.1 Actions 41
3.2 Compactifications 42
3.3 Moduli Stabilization 48
3.4 Conifolds 52
3.4.1 The Singular Conifold $M^\sharp$ 54

3.4.2 The Deformed Conifold . . . 57
3.4.3 The Resolved Conifold . . . 59
3.4.4 Gauge/Gravity Correspondence . . . 60
3.5 String Inflation . . . 65
3.6 The Weak Gravity Conjecture . . . 67

4 D-branes in the Warped Resolved Conifold 74
4.1 Introduction . . . 74
4.2 D-brane Potential in the Warped Resolved Conifold . . . 78
4.3 Natural Inflation Model . . . 84
4.3.1 Preview . . . 84
4.3.2 D3-brane in the WRC . . . 89
4.3.3 Wrapped D5-brane in the WRC . . . 92
4.4 Conclusion . . . 98

Part 2 Observables 101

5 Asymmetry and Non-Gaussianity 102
5.1 Introduction . . . 102
5.2 Generating the Asymmetry . . . 104
5.3 Conclusion . . . 111

6 The Squeezed Limit of the Bispectrum in Multi-Field Inflation 113
6.1 Introduction . . . 113
6.2 The squeezed limit of the bispectrum with δN . . . 116
6.2.1 Field evolution between different crossing times . . . 117
6.2.2 The field-space bispectrum in the squeezed limit . . . 119
6.2.3 The squeezed limit of the bispectrum of ζ . . . 121
6.3 Scale dependence . . . 124
6.3.1 Spectral index of the halo bias . . . 124
6.3.2 Tilts of the reduced bispectrum in the squeezed limit . . . 125
6.4 Employing the Γ formalism in concrete models . . . 126
6.4.1 Calculating Γ: sum-separable potential . . . 127
6.4.2 Single-source models . . . 129
6.4.3 Multiple-source models: the mixed curvaton-inflaton model . . . 130
6.5 Conclusion . . . 133

7 The Separate Universe Approach to Soft Limits 135
7.1 Introduction . . . 135
7.1.1 Correlations of the Curvature Perturbation . . . 138

7.2 Soft Limits . . . 139
7.2.1 Soft Limit Expansion . . . 139
7.2.2 Simple Examples . . . 140
7.2.3 Soft Limit Diagrams . . . 144
7.2.4 Examples Using Diagrams . . . 145
7.2.5 Inequalities Between Soft Correlation Functions . . . 149
7.3 Explicit Expressions . . . 151
7.3.1 The Γ expansion . . . 151
7.3.2 Field-Space Correlation Functions . . . 152
7.3.3 Explicit Examples . . . 153
7.4 Conclusion . . . 158

8 Conclusion **159**

A Appendices for D-branes in the Warped Resolved Conifold **164**
A.1 D-brane Backreaction . . . 164
A.2 Corrections from the 4D Ricci Scalar . . . 169
A.3 Wrapped D5-branes and the b-Axion . . . 175

B Appendix for the Squeezed Limit of the Bispectrum **177**
B.1 Reduction to single field case . . . 177
B.2 Recovering Seery & Lidsey result in near-equilateral limit . . . 178
B.3 Squeezed limits of graviton correlators . . . 178
B.4 Reduction to Byrnes *et al.* . . . 180
B.5 Reduction to Dias *et al.* . . . 181
B.6 Tilt of reduced bispectrum in the squeezed limit . . . 182

C Appendix for the Separate Universe Approach to Soft Limits **185**
C.1 The background wave method . . . 185
C.2 Reduction to Single Field Result . . . 187
C.3 Γ Diagrams . . . 188

Bibliography **189**

Chapter 1

Introduction

The standard Big Bang theory is incomplete - it doesn't explain why temperature variations are correlated on scales which, according to the standard Big Bang picture, were never originally in causal contact.

In order to address this *horizon problem*, and the related *flatness problem* and the *magnetic monopole problem*, the standard Big Bang theory needs to be augmented. The leading solution is to presume an epoch of *Cosmological Inflation* [5], in which the early universe undergoes a period of accelerated expansion, before beginning its hot standard Big Bang phase.

At the classical level, inflation solves the above problems, allowing for the large scales to be in causal contact early in the history of the universe and become correlated. At the quantum level, inflation stretches quantum fluctuations to macroscopic size, later becoming the perturbations we observe in the cosmic microwave background radiation and the later formation of large-scale structure.

However, the precise microphysics necessary to give successful inflation remains unclear. In order to give the required acceleration, the simplest theoretical models suppose the universe is filled with a source for the acceleration that has an energy density that remains nearly constant whilst the universe expands. This is starkly different to any kind of ordinary matter/energy we have previously observed, which instead dilutes as the universe expands.

Thus, it is a well-motivated topic to study the microphysics of inflation. At the time of writing, there is no universally-accepted agreement on the true microphysics of inflation. There are a large number of competing theoretical models, each of which comes with its own predictions for observables. The aim of this thesis is to further the understanding of the link between theoretical models and their corresponding predictions of observables. This fits into the overarching aim of the subject that aims to discern the true underlying microphysics of inflation.

With each new experiment that provides information about the early universe, our

models become more refined and constrained. Thus, it is necessary to have precise theoretical predictions in order to be able to keep up with new experiments. The results of this thesis provide precise theoretical predictions from a range of models which have observables that may be detected in the near-future. I hope that the legacy of this thesis is that it will be useful in the future work of determining the underlying physics of inflation using future observations.

This thesis focusses on two broad approaches to inflation: the top-down approach and the bottom-up approach. In the top-down approach, a well-motivated high-energy theoretical model is assumed - in our case, string theory - and inflationary observables are predicted. This approach is captured in Part I of this thesis, covering string theory and inflation. In Part II of this thesis we consider the bottom-up approach, where one is agnostic about the high-energy UV complete theory, and instead works with a low-energy effective theory, which is supposed to be generic enough to capture a range of high-energy models. In this thesis we work with multi-field models of inflation, which are well-motivated enough to be considered generic from string theory constructions. For these multi-field models we calculate inflationary observables, looking for observational signatures which would imply a multi-field model of inflation.

A brief outline of this thesis is as follows.

In Chapter 2 we give an overview of inflation, covering theoretical topics in the classical picture of inflation and the quantum fluctuations in inflation, and then move on to observables in inflation.

In Part I we cover string theory and inflation. This part begins with an introductory chapter, Chapter 3, on elements of string theory for inflation. It's by no means a thorough introduction to string theory, but at least serves as some introduction to the necessary computational formulae for the next chapter. Chapter 4 contains original work from Kenton & Thomas, [1], titled *D-brane Potentials in the Warped Resolved Conifold and Natural Inflation*, where a model of natural inflation is derived from a string theory D-brane model in the warped resolved conifold geometry.

In Part II we cover observables, with a particular focus on primordial non-Gaussianity. The theme that links this part of the thesis is the coupling of long-wavelength modes to short-wavelength modes that is a signature of a type of non-Gaussianity produced in some multi-field inflation models.

Chapter 5 contains the original work of Kenton, Mulryne and Thomas, [2], in which the observed CMB power asymmetry is produced using a long-wavelength mode of a second light field, to modulate the short-wavelength power. The non-Gaussianity required in this model contains a novel non-zero trispectrum in addition to a non-zero bispectrum.

In Chapter 6, we review the work of Kenton and Mulryne [3], titled *The squeezed limit of the bispectrum in multi-field inflation* which gives the first calculation of the

squeezed limit of the bispectrum produced by inflation with multiple light fields, where one long-wavelength mode acts as a background for the two shorter-wavelength modes.

Chapter 7 presents the work of Kenton and Mulryne [4], titled *The Separate Universe Approach to Soft Limits*, in which we generalize the results of Chapter 6 to include any soft limit of any higher-point inflationary correlation function for multi-field models.

We conclude the thesis in Chapter 8 summarizing our findings and pointing to future ideas in this field.

The appendices contain some calculational details which are not central for a first read-through of this thesis, but which are all original and important for the consistency of the presented calculations of the main parts of the thesis.

Chapter 2

Inflation

2.1 Classical Dynamics of Inflation

Inflation solves the horizon problem by assuming a spatially-flat Friedmann–Robertson–Walker (FRW) expansion with metric

$$ds^2 = -dt^2 + a^2(t)d\vec{x}^2 \ , \tag{2.1}$$

which at early times has a period of accelerated expansion, in which the scale factor undergoes $\ddot{a} > 0$. This is equivalent to a shrinking Hubble radius $\frac{d}{dt}(aH)^{-1} < 0$ or that $\epsilon \equiv -\dot{H}/H^2 < 1$, where the Hubble factor is $H = \dot{a}/a$. In order for inflation to last long enough for inflation to solve the horizon problem, typically 60 e-folds, one also requires $\eta \equiv \dot{\epsilon}/(\epsilon H) < 1$. The de Sitter limit, $\epsilon \to 0$, corresponds to exponential growth $a(t) \sim e^{Ht}$, with H approximately constant. The Einstein equations for this FRW universe supported by a perfect fluid, with pressure P and energy density ρ, take the form

$$3M_p^2 H^2 = \rho \tag{2.2}$$

$$6M_p^3(\dot{H} + H^2) = -(\rho + 3P), \tag{2.3}$$

where M_p is the reduced Planck mass, with $M_p^{-2} \equiv 8\pi G = (2.4 \times 10^{18}\text{GeV})^{-2}$, and we work in natural units where $\hbar = c = 1$.

The accelerated expansion of inflation then requires a source with an equation of state $w \equiv P/\rho < -1/3$. The simplest example of such a source is a scalar field with a positive potential energy and negligible kinetic energy, although there are other possibilities that we will also consider.

2.1.1 Single-Field Slow-Roll

Arguably the simplest model of inflation uses a single, slowly-rolling (which we define shortly) scalar field, called the inflaton ϕ, which is minimally coupled to gravity with the following action

$$S = \int d^4x\sqrt{-g}\left[\frac{M_p^2}{2}R - \frac{1}{2}(\partial\phi)^2 - V(\phi)\right]. \tag{2.4}$$

In an FRW background the Klein-Gordon equation for the inflaton is

$$\ddot{\phi} + 3H\dot{\phi} + \frac{\partial V}{\partial\phi} = 0\ , \tag{2.5}$$

where the Hubble rate is determined by the Friedmann equation

$$H^2 = \frac{1}{3M_p^2}\left[\frac{1}{2}\dot{\phi}^2 + V\right]. \tag{2.6}$$

These can be combined to form the equation

$$\dot{H} = -\frac{1}{2}\frac{\dot{\phi}^2}{M_p^2}. \tag{2.7}$$

We can then write ϵ in terms of the dynamics of ϕ as

$$\epsilon = \frac{3\dot{\phi}^2}{\left[\dot{\phi}^2 + 2V\right]}. \tag{2.8}$$

The field is said to be slowly-rolling when the potential dominates over the kinetic energy, $V \gg \frac{1}{2}\dot{\phi}^2$, and in this case inflation occurs, since $\epsilon \ll 1$. Inflation persists if the acceleration of the field is also small $|\ddot{\phi}| \ll 3H|\dot{\phi}|$. In this model, one can define the slow-roll parameters

$$\epsilon_V \equiv \frac{M_p^2}{2}\left(\frac{1}{V}\frac{\partial V}{\partial\phi}\right)^2, \tag{2.9}$$

$$\eta_V \equiv \frac{M_p^2}{V}\frac{\partial^2 V}{\partial\phi^2}. \tag{2.10}$$

In the case of slow-roll, which is the conditions $V \gg \frac{1}{2}\dot{\phi}^2$ and $|\ddot{\phi}| \ll 3H|\dot{\phi}|$, then $\{\epsilon_V, \eta_V\} \sim \{\epsilon, \eta\}$, so that arranging $\epsilon_V, \eta_V \ll 1$ gives that $\epsilon, \eta \ll 1$. Note that achieving inflation in this single-field slow-roll setup requires the potential to be rather flat - this can be hard to arrange from a top-down perspective, something we will investigate in later chapters of this thesis.

There is a huge range of slow-roll inflationary models - they can be classified by the type of potential. Here we just pick a couple of examples, highlighting *Natural Infation*, which will be investigated in Chapter 4. For a more general review of inflationary models, see for example, [6].

Chaotic Inflation – probably the simplest single-field slow-roll inflationary model is chaotic inflation [7], where the potential is a monomial $V(\phi) = \mu^{4-p}\phi^p$, $p > 0$, where μ has dimensions of mass.

Natural Inflation – In natural inflation [8], the potential is sinusoidal,

$$V(\phi) = \Lambda^4 \left[1 - \cos\left(\frac{\phi}{f}\right)\right] \tag{2.11}$$

where Λ is a scale with dimensions of mass and the parameter f also has dimensions of mass and is referred to as the 'decay constant'. These models were originally motivated by modelling the inflaton as a pseudoscalar axion, although the term natural inflation is now used for any inflation model with a sinusoidal potential. Axions enjoy an approximate continuous shift symmetry at the perturbative level, but this gets broken to a discrete shift symmetry by non-perturbative quantum effects. With the shift symmetry, models of natural inflation are natural in an effective field theory sense, with the shift symmetry protecting against corrections which don't respect the symmetry.

2.1.2 Single-Field Non-Canonical

There is an alternative single-field theory to the single-field slow-roll theory, which we refer to here as $P(X, \phi)$ type theories [9], with action

$$S = \int d^4x\sqrt{-g}\left[\frac{M_p^2}{2}R + P(X,\phi)\right] \tag{2.12}$$

where $X \equiv -\frac{1}{2}(\partial\phi)^2$, and P is an arbitrary function. The corresponding stress-energy tensor is a perfect fluid form with pressure P and energy density $\rho = 2XP_{,X} - P$, where $P_{,X}$ denotes a partial derivative of P with respect to X. The Klein-Gordon equation and Friedmann equation are

$$\frac{d}{dt}\left(a^3 P_{,X}\dot{\phi}\right) = a^3 P_{,\phi} \tag{2.13}$$

$$H^2 = \frac{1}{3M_p^2}\left(2XP_{,X} - P\right). \tag{2.14}$$

The inflationary parameter ϵ can be written in terms of $P(X, \phi)$ as

$$\epsilon = \frac{3XP_{,X}}{2XP_{,X} - P}. \tag{2.15}$$

The condition for inflation, $\epsilon < 1$, now becomes a condition on the function $P(X, \phi)$. A special case of $P(X, \phi)$ models is DBI inflation [10], in which $P(X, \phi)$ takes the following form

$$P(X, \phi) = -T(\phi) \left[\sqrt{1 - \frac{2X}{T(\phi)}} - 1 \right] - V(\phi), \tag{2.16}$$

where $T(\phi)$ is an arbitrary function. Note that here one does not necessarily need a flat potential in order to achieve inflation, because the higher-derivative kinetic terms effectively slow down the scalar field motion, in contrast to the case of canonical kinetic terms relying on a flat potential to slow down the motion of the scalar field.

2.1.3 Multiple Fields

Models of inflation with multiple fields (also known as multi-field inflation models) arise generically when we try to embed inflation into a fundamental theory, such as string theory or supergravity, whose low energy effective field theory involves multiple degrees of freedom.

Here we consider the simplest case of slow-roll multi-field inflation, considering only scalar fields. More complicated scenarios are also possible. We suppose there is more than one scalar field varying during inflation, $\phi_i(t) = (\phi_1(t), \phi_2(t), \cdots)$. Different authors have different definitions of multi-field inflation. If the inflationary trajectory is just a straight line, we can rotate the field basis to align with the straight trajectory and then the classical dynamics are indistinguishable from single-field inflation. However, the quantum dynamics will be different from single-field inflation. For this reason, we define multi-field inflation to occur whenever there is more than one light field present, regardless of the curvature of the inflationary trajectory.

The Klein-Gordon equation and Friedmann equation for multi-field inflation are

$$\ddot{\phi}_i + 3H\dot{\phi}_i + \partial_i V = 0 \tag{2.17}$$

$$3H^2 = \frac{1}{3M_p^2} \left[\frac{1}{2} \sum_i \dot{\phi}_i^{\,2} + V \right] \tag{2.18}$$

where $\partial_i \equiv \frac{\partial}{\partial \phi_i}$ and $V = V(\phi_i)$. Notice that even if there is no explicit coupling between the multiple fields in the potential, through the Friedmann equation, they are still gravitationally coupled. In single-field slow-roll inflation, the Hubble damping during slow-roll inflation forces all trajectories to approach an attractor solution, where all local variables such as the Hubble rate and field time-derivatives are all determined by the local value of the single field (see e.g. [11]). Thus, any dependence on the initial field and field time-derivative values of the trajectories are lost. However, in

multi-field inflation, there can be a continuous family of trajectories in phase space, where local variables depend on more than one field's local value. These trajectories don't converge to an attractor and so there will be dependence on the initial field and field time-derivative values. This allows non-adiabatic field perturbations to survive on superhorizon scales during multi-field inflation.

An interesting example of multi-field inflation is *assisted inflation* [12], in which inflation occurs with a large number of fields, each with a steep exponential potential, whose combined effect of Hubble damping is to create an effective potential with an exponential potential which is much less steep, providing inflation.

Another example is *Hybrid Inflation* [13], where there is an inflaton field, ϕ, and a tachyonic waterfall field, ψ, with potential

$$V_{\rm Hybrid} = V_0 + m_\phi^2\phi^2 + \frac{1}{2}(g^2\phi^2 - m_\psi^2)\psi^2 \tag{2.19}$$

where inflation ends when the instability in the ψ field is triggered at a critical value of ϕ. One should note that in most hybrid inflation models, although there is more than one field, usually only one of the fields, say ϕ, is light, with a small effective mass $d^2V/d\phi^2 \ll H^2$, with the other fields being heavy.

A final important example of a multi-field model, which we mention briefly now, is the curvaton model [14–16] (see also [17, 18] for earlier related ideas), in which a second light field is present during inflation, whose initial energy density is negligable. Depending on the type of curvaton scenario, the quantum fluctuations of the curvaton contribute different amounts towards the primordial curvature perturbation. We turn to these inflationary quantum fluctuations next.

2.2 Quantum Fluctuations in Inflation

We have so far considered the classical dynamics of inflation, which solve the horizon problem. Moreover, the quantum theory of inflation can also give a primordial microscopic explanation for the observed temperature anisotropies in the cosmic microwave background (CMB) radiation and the origin of large scale structure (LSS). The basic idea is that quantum fluctuations of the inflaton (or other fields) seed the perturbations in the local density after inflation which then leads to variations in the CMB and LSS. It's worth remarking that inflation was not engineered specifically to do this, and the origin of these perturbations comes as a consequence of considering inflation quantum mechanically. Heuristically, inflation stretches perturbations on small, subhorizon scales, to larger superhorizon scales.

In the classical dynamics of inflation section, we considered homogeneous background scalar fields, $\phi_A(t)$, in a homogeneous FRW background metric. Now we con-

sider inhomogeneous perturbations to the homogeneous background fields. We must also have inhomogeneous metric perturbations about the homogeneous FRW background metric. The perturbed FRW metric, to linear order in scalar perturbations is [11]

$$ds^2 = -(1+2A)dt^2 + 2a\partial_i B dx^i dt + a^2\left[(1-2\psi)\delta_{ij} + 2\partial_{ij}E + h_{ij}\right]dx^i dx^j. \quad (2.20)$$

Here $i, j, ...$ refer to spatial indices. Any vector can be split into a the gradient of a scalar and a divergenceless vector, which we refer to as the vector part, and similarly for rank-2 tensors. Considering this definition of scalar, vector and tensorial parts, the field equations for the scalar and tensor parts decouple to linear order, and vector perturbations vanish at linear order for inflation due to scalar fields [19]. The tensor perturbations h_{ij} are transverse and traceless and are coordinate gauge-independent. They describe primordial gravitational waves.

The three-dimensional intrinsic Ricci scalar curvature of constant-time hypersurfaces is given by

$${}^{(3)}R = \frac{4}{a^2}\nabla^2\psi. \quad (2.21)$$

We'll express different gauges in terms of ψ in the next section.

2.2.1 Spatially Flat Gauge

There are a number of gauge choices that are taken in the literature. A common choice is *spatially flat gauge*, in which $\psi = 0$ and hence ${}^{(3)}R = 0$. We can split the scalar fields into terms of background and perturbations in this flat gauge,

$$\phi_i(t, \vec{x}) = \phi_i(t) + \delta\phi_i(t, \vec{x}). \quad (2.22)$$

The linear order scalar field perturbation field equation, in spatially flat gauge, for each fourier mode, with comoving wavenumber k, (which we suppress here) in a linear order perturbed FRW spacetime is

$$\delta\ddot{\phi}_i + 3H\delta\dot{\phi}_i + \left[V_{,ij} + \left(\frac{k}{a}\right)^2\delta_{ij} - \frac{1}{M_p^2 a^3}\frac{d}{dt}\left(\frac{a^3\dot{\phi}_i\dot{\phi}_j}{H}\right)\right]\delta\phi_j = 0. \quad (2.23)$$

At leading order in the slow-roll approximation, we can neglect the interaction terms to obtain

$$\delta\phi_i{}'' + 2H\delta\phi_i{}' + \left(a^2 V_{,ii} + k^2\right)\delta\phi_i = 0, \quad (2.24)$$

where we switched to conformal time, τ, defined through $ad\tau = dt$, denoting $d/d\tau$ with

a prime $'$. Small scale fluctuations, which are subhorion, $k \gg aH$, are under-damped and behave like free oscillators. Deep inside the horizon, the fluctuations should be indistinguishable from free field fluctuations in flat space, leading to the normalization

$$\delta\phi_i \to \frac{e^{-ik\tau}}{a\sqrt{2k}} \text{ , as } \tau \to -\infty. \tag{2.25}$$

During inflation, aH increases, and modes which begin subhorizon start to exit the horizon, $k = aH$, and eventually end up superhorizon, $k \ll aH$. Light fields, with potential $V_{ii} \ll H^2$, have perturbations which become over-damped on superhorizon scales, and essentially freeze-in at their horizon exit value, (2.25), evaluated at horizon exit, $k = aH$. This gives the two-point correlation function for scalar field perturbations [20, 21]

$$\Sigma_{ij}(k) = \frac{H_k^2}{2k^3}\delta_{ij}, \tag{2.26}$$

$$\text{where } \langle\delta\phi_i(\vec{k})\delta\phi_j(\vec{k}')\rangle = \delta(\vec{k}+\vec{k}')\Sigma_{ij}(k). \tag{2.27}$$

In the above, H_k^2 denotes H^2 evaluated at the horizon exit time, t_k, such that $k = a(t_k)H(t_k)$, where $k = |\vec{k}|$.

2.2.2 Curvature Perturbations

The curvature perturbation on uniform-density hypersurfaces, denoted ζ, has the definition (at linear order in perturbation theory)

$$\zeta \equiv \psi + \frac{H}{\dot{\rho}}\delta\rho \tag{2.28}$$

The curvature perturbation orthogonal to comoving worldlines is

$$\mathcal{R} = \psi - \frac{H}{\rho + P}\delta q \tag{2.29}$$

where the scalar part of the three-momentum perturbation is $\partial_i\delta q$.

On superhorizon scales, $\mathcal{R} = -\zeta$, since by the Einstein equations,

$$-\mathcal{R} - \zeta = -\frac{2}{3}\frac{H\rho}{\dot{\rho}}\left(\frac{k}{aH}\right)^2\left[\psi + a^2H\left(\dot{E} - \frac{B}{a}\right)\right]. \tag{2.30}$$

We note that ζ is conserved on superhorizon scales if the system reaches an adiabatic limit [22, 23]. In single-field models of inflation, the non-adiabatic pressure vanishes on superhorizon scales, and hence ζ can be calculated a little after horizon exit, remaining constant independently of the details of reheating or on the physics of the end of inflation. In contrast, in multi-field models of inflation, there can in general be non-

adiabatic perturbations, and hence ζ can evolve on superhorizon scales until the system reaches an adiabatic limit.

According to the separate universe assumption, a curvature perturbation can be written as a local perturbation to the scale factor as [22, 24, 25]

$$a(t, \mathbf{x}) = a(t)e^{\psi(t,\mathbf{x})} \tag{2.31}$$

on large scales. Choosing the t-slicing to be such that the spatial hyper surfaces have uniform-density (UD) leads to $\psi_{\rm UD}(t, \mathbf{x}) \equiv \zeta(t, \mathbf{x})$, while a flat t-slice is defined by $\psi_{\rm flat}(t, \mathbf{x}) = 0$. These are the non-linear generalizations of the curvature perturbations we introduced above in linear perturbation theory. Following common convention in the literature, we refer to this non-linear ζ as the *uniform-density curvature perturbation.*

We'll now consider the form of the second-order action for the comoving curvature perturbation for a single-field $P(X, \phi)$ type model using action given in Eq. (2.12), which first appeared in [26]. It's given by

$$S_2 = \int d^3\vec{x}d\tau \; a^2 z \left(\zeta'^2 - c_s^2(\partial\zeta)^2\right), \tag{2.32}$$

where τ is conformal time, a prime denotes a derivative with respect to τ, and z and c_s are defined through

$$c_s^2 \equiv \frac{P_{,X}}{P_{,X} + 2XP_{,XX}} \; , \tag{2.33}$$

$$z \equiv \frac{\epsilon}{c_s^2} \; , \tag{2.34}$$

where ϵ was defined in Eq. (2.15). Here, c_s is the speed of sound of the fluctuations, which, for a subluminal theory, can be ≤ 1. For simplicity we'll consider a slow-variation model, where ϵ and c_s are slowly-varying. This requires $\eta \equiv \dot{\epsilon}/(H\epsilon) \ll 1$ and $s \equiv \dot{c_s}/(Hc_s) \ll 1$.

This allows us to introduce a new, canonically normalized field v such that $v \equiv y\zeta$, where $y^2 = 2M_p^2 a^2 z$. This canonical field has time-dependent mode functions $v_k(\tau)$ which satisfy the Mukhanov-Sasaki equation

$$v_k'' + \left(c_s^2 k^2 - \frac{y''}{y}\right) v_k = 0. \tag{2.35}$$

This is the single-field, non-canonical version of Eq. (2.24), with a canonically normalized field (one could have written Eq. (2.24) in terms of a similar Mukhanov variable - the presentation here highlights that one can equivalently look at the field equation or at the related Mukhanov-Sasaki equation). Initial conditions are computed by treating ζ as a quantum field in a classical inflationary background. The Fourier modes are

promoted to quantum operators

$$\hat{v}_{\vec{k}} = v_k(\tau)\hat{a}_{\vec{k}} + h.c. \tag{2.36}$$

At early enough times, all modes are deep inside the horizon, and each mode feels like it's in Minkowski space and behaves like a free oscillator with zero point fluctuations

$$v_k(t) \to \frac{e^{-ikc_s\tau}}{a\sqrt{2kc_s}} \text{ , as } \tau \to -\infty. \tag{2.37}$$

The fluctuation freezes at the value it took at sound horizon crossing, $c_s k = aH$. Transforming back to ζ, we get the power spectrum of ζ defined by

$$\langle \zeta_{\mathbf{k_1}} \zeta_{\mathbf{k_2}} \rangle = P_\zeta(k_1)(2\pi)^3 \delta(\mathbf{k_1} + \mathbf{k_2}), \tag{2.38}$$

where

$$P_\zeta(k) = \frac{1}{4}\frac{H^2}{M_p^2 \epsilon c_s k^3}. \tag{2.39}$$

In the above, the quantities on the right-hand side are evaluated at the sound horizon crossing time. One often defines the dimensionless power spectrum

$$\mathcal{P}_\zeta(k) \equiv \frac{k^3}{2\pi^2} P_\zeta(k) = \frac{1}{8\pi^2}\frac{H^2}{M_p^2 \epsilon c_s}. \tag{2.40}$$

Any time-dependence of H and c_s become scale-dependence of the power spectrum. Perfect scale-invariance is given by $\mathcal{P}_\zeta(k) = const.$, and deviations from scale invariance are captured by the scalar spectral tilt

$$n_s - 1 \equiv \frac{d\log \mathcal{P}_\zeta(k)}{d\log k} = -2\epsilon - \eta - s \tag{2.41}$$

where the right hand side holds for this slowly-varying single-field $P(X, \phi)$ model. Typically, inflation requires $\{\epsilon, |\eta|, |s|\} \ll 1$, hence predicting a near-scale invariant power spectrum. Since we require that inflation ends at some time, we know that $\{\epsilon, \eta, s\}$ can't all be zero, and hence perfect scale-invariance is not predicted in realistic models of inflation. All this held for a single-field, but the story is more complicated for multi-field inflation, and is covered in Subsec. 2.2.6 when we review the δN formalism.

2.2.3 Gravitational Waves

Inflation predicts a spectrum of primordial gravitational waves due to the tensor perturbations to the spatial metric, h_{ij}, as appeared in Eq. (2.20). Expanding the Einstein-

Hilbert action to quadratic order in h gives

$$S_2 = \frac{M_p^2}{8} \int d^3\vec{x} d\tau \; a^2 \left((h'_{ij})^2 - (\partial h_{ij})^2 \right) \tag{2.42}$$

and a similar calculation to that of the curvature perturbations gives a dimensionless tensor power spectrum

$$\mathcal{P}_t(k) \equiv \frac{k^3}{2\pi^2} P_t(k) = \frac{2}{\pi^2} \frac{H^2}{M_p^2}, \tag{2.43}$$

and a tensor spectral tilt

$$n_t \equiv \frac{d \log \mathcal{P}_t(k)}{d \log k} = -2\epsilon. \tag{2.44}$$

Observations usually constrain the tensor to scalar ratio, $r \equiv \mathcal{P}_t / \mathcal{P}_\zeta$.

Using the formula for the tensor power spectrum (2.43), and the observed value for the amplitude of the scalar power spectrum, $\ln(10^{10} A_s) \approx 3.062$, where $\mathcal{P}_\zeta(k_0) = A_s$ at the Planck pivot scale of $k_0 = 0.05 \text{Mpc}^{-1}$, we can write a relation between the energy scale of inflation and the value of r, [27]

$$E_{\text{inf}} \equiv (3 M_p^2 H^2)^{1/4} \approx 8 \times 10^{-3} \left(\frac{r}{0.1} \right)^{1/4} M_p. \tag{2.45}$$

We see that gravitational waves from inflation are only observable in the near-future if inflation occured near the GUT scale, 10^{16}GeV.

The Lyth bound [28], relates observable levels of gravitational waves to a super-Planckian field displacement for the inflaton,

$$\frac{\Delta\phi}{M_p} > \mathcal{O}(1) \left(\frac{r}{0.01} \right)^{1/2} \tag{2.46}$$

where the order one constant depends on how r varies with number of efolds N, and on how many e-folds of inflation are required, as set by the temperature of reheating. Note that models will not necessarily saturate the Lyth bound and may exceed it by some way.

This super-Planckian field displacement is perhaps problematic from an effective field theory perspective. While at the low energy level, gravitational backreaction is under control (since the potential is sub-Planckian) and radiative stability is not a problem (there is a shift symmetry which makes the inflaton mass technically natural), there is a problem when one considers couplings of the inflaton to the UV degrees of freedom necessary for the ultraviolet completion of gravity. Intregrating out UV fields

of mass Λ with order-unity couplings to the inflaton give an effective Lagrangian [29]

$$L_{\rm eff}[\phi] = L_{\rm LE}[\phi] + \sum_{i=1}^{\infty}\left(\frac{c_i}{\Lambda^{2i}}\phi^{4+2i} + \frac{d_i}{\Lambda^{2i}}(\partial\phi)^2\phi^{2i} + \frac{e_i}{\Lambda^{4i}}(\partial\phi)^{2+2i} + \cdots\right) \tag{2.47}$$

where LE denotes the low energy Lagrangian that we began with, the c_i, d_i, e_i are dimensionless order-one Wilson coefficients and the omitted terms are higher order in derivatives. The masses of the fields should be $\Lambda \lesssim M_p$, so that one sees these corrections will typically become important for super-Planckian field displacements and render the effective Lagrangian non-flat over super-Planckian distances.

In Chapter 4 of this thesis we investigate a string theory model of inflation where a super-Planckian displacement occurs and where we explicitly derive the effective Lagrangian, finding that in this particular example, the effective Lagrangian is flat in this direction of field space. However, we will see that the required model is not perfect and seems a little contrived. However, it is important evidence that typical expectations from effective field theory arguments can be evaded in certain top-down constructions.

2.2.4 Non-Gaussianity

The Planck data contains about 50 million pixels. An enormous amount of data compression occurs in reducing this to the CMB power spectrum, which contains about a thousand multipole moments. This can only be justified if the primordial perturbations were drawn from a Gaussian distribution with random phases. In principle, there is more information that can be gleaned from the CMB anisotropies, contained in deviations from the Gaussian distribution.

We separate different origins for a non-Gaussian CMB:

1. *Primordial non-Gaussianity*: the primordial curvature perturbation can have non-Gaussian statistics produced in the early universe during inflation, or an alternative.

2. *Other non-Gaussianity*: non-Gaussianity can arise from later time effects too. For example, it may occur due to the non-linear relation between ζ and the temperature anisotopy at the time of recombination. It may also occur from astrophysical foreground effects such as lensing due to galaxies and galaxy clusters.

We focus on the first type of source, primordial non-Gaussianity, in this thesis. It should be noted that in order to extract this primordial signature, we must understand and quantify the other sources, though we don't study these effects in this thesis.

In Subsec. 2.2.2 we looked at the two-point correlation function of ζ, captured by the power spectrum. If the primordial perturbations are perfectly isotropic and

Gaussianly distributed, then all of the statistical information is contained within the power spectrum. However, many models can give a similar power spectrum, so to distinguish between them we need to look at deviations from Gaussianity. Information about the non-Gaussian aspect of the distribution is contained within higher-order correlation functions, with the primary diagnostic being the three-point correlation function. This is captured by the bispectrum, B_ζ, of the curvature perturbation defined by

$$\langle \zeta_{\mathbf{k_1}} \zeta_{\mathbf{k_2}} \zeta_{\mathbf{k_3}} \rangle = B_\zeta(k_1, k_2, k_3)(2\pi)^3 \delta(\mathbf{k_1} + \mathbf{k_2} + \mathbf{k_3}). \tag{2.48}$$

We can define the kernels, G_n, of the n-point correlation functions

$$\langle \zeta_{\mathbf{k_1}} \cdots \zeta_{\mathbf{k_n}} \rangle = G_n(k_1, \ldots, k_n)(2\pi)^3 \delta(\mathbf{k_1} + \cdots + \mathbf{k_n}). \tag{2.49}$$

A Gaussian distribution has $G_{2n} \propto P_\zeta^n$ and $G_{2n+1} = 0$. The kernel of the four-point function is called the trispectrum, denoted T_ζ. Often observational constraints are given in terms of a reduced dimensionless kernel. For example, the reduced bispectrum is defined as

$$f_{\rm NL}(k_1, k_2, k_3) \equiv \frac{5}{6} \frac{B_\zeta(k_1, k_2, k_3)}{[P_\zeta(k_1)P_\zeta(k_2) + (k_1 \to k_2 \to k_3)]}. \tag{2.50}$$

2.2.5 The $in - in$ Formalism

Central to inflationary cosmology is the calculation of inflationary correlation functions. In this section we focus on quantum mechanical effects which generate non-Gaussianity before or during horizon exit. In the next section, Sec 2.2.6 we focus on classical effects which can generate non-Gaussianity after horizon exit. The calculation of inflationary correlation functions differs to the calculation of the S-matrix in applications of quantum field theory to standard particle physics. For the S-matrix, one computes

$$\langle out|S|in\rangle = \langle out(+\infty)|in(-\infty)\rangle \tag{2.51}$$

interpreted as the probability for a state in the far past, $|in\rangle$, to transition to a state $|out\rangle$ in the far future. However, for inflationary correlation functions, we are interested in equal-time expectation values of operators, taken in the state corresponding the vacuum in the far past - since in the far past the wavelengths are much smaller than the horizon and hence the interaction-picture fields will have the same form as in Minkowski space, due to the equivalence principle. This state is called the Bunch-Davies vacuum state, denoted $|in\rangle$, taken to be the interacting theory vacuum at time t_i, in the far past. Thus the formalism we now present is called The $in - in$ Formalism, where expectations of

operators, $\mathcal{O}(t)$, where $t > t_i$, are taken in two $|in\rangle$ states

$$\langle \mathcal{O}(t) \rangle = \langle in|\mathcal{O}(t)|in\rangle \,. \tag{2.52}$$

To compute the right-hand-side of (2.52) we evolve $\mathcal{O}(t)$ back to time t_i, using the perturbed Hamiltonian $\delta H = H_0 + H_{\rm int}$, where H_0 is the free (quadratic) Hamiltonian and $H_{\rm int}$ is the interacting Hamiltonian, which in this formalism has to be treated as a perturbation to the free Hamiltonian, allowing for a perturbative expansion. The result is [30] (see also [31–35])

$$\langle \mathcal{O}(t) \rangle = \langle 0|\bar{T} e^{i\int_{-\infty(1-i\epsilon)}^{t} H_{\rm int}(t')dt'} \mathcal{O}(t) T e^{-i\int_{-\infty(1+i\epsilon)}^{t} H_{\rm int}(t'')dt''} |0\rangle \,, \tag{2.53}$$

where $|0\rangle$ is the free theory vacuum, and $T(\bar{T})$ is the (anti-)time-ordering symbol. One can then perturbatively expand the exponentials, organising the expansion with Feynman diagrams, with the leading order term corresponding to the tree level result, and higher orders corresponding to loop results. This formalism can be applied to calculate, for example, the three-point correlator of ζ at horizon crossing time, allowing for a calculation of non-Gaussianity using this method.

In [36], Maldacena calculated that for single-field, slow-roll models, the non-Gaussianity was of order the slow-roll parameters, with the detailed answer given by

$$\langle \zeta_{\vec{k}_1} \zeta_{\vec{k}_2} \zeta_{\vec{k}_3} \rangle = (2\pi)^3 \delta(\vec{k}_1 + \vec{k}_2 + \vec{k}_3) \frac{H^4}{\dot{\phi}^4} \frac{H^4}{M_p^4} \frac{1}{\prod(2k_i^3)} \mathcal{A}(k_i) \tag{2.54}$$

$$\mathcal{A}(k_i) \equiv 2\frac{\ddot{\phi}}{H\dot{\phi}} \sum k_i^3 + \frac{\dot{\phi}^2}{H^2} \left[\frac{1}{2} \sum k_i^3 + \frac{1}{2} \sum_{i \neq j} k_i k_j^3 + 4 \frac{\sum_{i>j} k_i^2 k_j^2}{k_1 + k_2 + k_3} \right] . \tag{2.55}$$

This result gives a reduced bispectrum that is of order $\mathcal{O}(\epsilon, \eta)$ and as we will see in the section on observations, this is out of reach of current and future observational probes of non-Gaussianity.

2.2.6 The δN Formalism

In Sec. 2.2.5 we considered non-Gaussianity from quantum mechanical effects before and during horizon exit. In this section we review the δN formalism which can be used to calculate the correlation functions of ζ, including non-Gaussian contributions arising from non-linearities after horizon exit when all modes have become classical.

Scalar perturbations to the spatial part of the metric on a fixed-time hypersurface can be written as a local perturbation to the scale factor giving a spatially dependent definition of the scale factor as in Eq. (2.31), as parametrized by ψ. The local number of e-folds which occurs between two time slices of the perturbed spacetime, labeled by

T and t_u respectively, with $T < t_u$, is a function of position and is given by

$$N(T, t_u, \mathbf{x}) \equiv \int_T^{t_u} \frac{\dot{a}(t, \mathbf{x})}{a(t, \mathbf{x})} dt = \int_T^{t_u} H(t) dt + \psi(t_u, \mathbf{x}) - \psi(T, \mathbf{x}) \tag{2.56}$$

while the unperturbed number of e-folds is given by $N_0(T, t_u) \equiv \int_T^{t_u} H(t) dt$. Taking the T-slices to be flat, and the t_u-slices to be uniform density gives

$$\zeta(t_u, \mathbf{x}) = N(T, t_u, \mathbf{x}) - N_0(T, t_u) \equiv \delta N(t_u, \mathbf{x}) \tag{2.57}$$

which is the celebrated δN formula [37]. We note that δN doesn't depend on the initial time T [22]. Typically T is taken to be some time after all the modes involved in a given correlation function have exited the horizon (for the bispectrum this means $T > t_3$). If the system becomes adiabatic ζ is also independent of t_u and so the later time t_u should be the time at which adiabaticity is reached. If it doesn't become adiabatic, then t_u can be taken to be the time at which the correlations are required (see for example the discussion in Ref. [38]).

To use this formalism in practice, we must employ the separate universe approximation [39, 40] to cosmological perturbation theory. This states that on super-horizon scales positions in the perturbed universe evolve independently of one another, and do so according to the same equations as the unperturbed cosmology, so that every position can be treated as a 'separate universe'. The number of e-folds which occur at every position can therefore be calculated using the local conservation and Friedmann equations in that separate universe.

For an inflationary model with n scalar fields, ϕ_i, where i runs from one to n, we can split the field values on any flat slice into background and perturbed parts $\phi_i(t, \mathbf{x}) = \phi_i(t) + \delta\phi_i(t, \mathbf{x})$. In later chapters, we use uppercase indices $A, B, ...$ which run over all degrees of freedom. Further demanding that the slow-roll equations of motion are satisfied at time T, such that $3H^2 = V(\phi_i)$ and $3H\dot{\phi}_i = -V_{,i}$, the initial conditions at time T for the perturbed cosmology become dependent only on $\phi_i(T, \mathbf{x})$. Consequently, the number of e-folds to any subsequent time slice becomes a function only of the initial field values, even if the cosmology evolves away from slow-roll. In particular, we can write

$$N(T, t_u, \mathbf{x}) = N((\phi_i(T, \mathbf{x})), t_u) = N((\phi_i(T) + \delta\phi_i(T, \mathbf{x})), t_u) \tag{2.58}$$

which gives

$$\zeta(\vec{x}) = N((\phi_i(T) + \delta\phi_i(T, \mathbf{x})), t_u) - N_0(\phi_i(T), t_u). \tag{2.59}$$

One can then Taylor expand in the initial flat slicing field perturbations, which in

Fourier space leads to [37, 41]

$$\zeta_{\mathbf{k_1}} = N_i^{(T)} \delta\phi_{i,\mathbf{k_1}}^{(T)} + \frac{1}{2} N_{ij}^{(T)} (\delta\phi_i^{(T)} \star \delta\phi_j^{(T)})_{\mathbf{k_1}} + ... \tag{2.60}$$

$$\text{where } N_i^{(T)} \equiv \frac{\partial N_0}{\partial \phi_i^{(T)}}\,, \tag{2.61}$$

and where $\star$ denotes convolution. The additional vector (boldface) subscript indicates wavevector and the superscript in brackets is a shorthand indicating evaluation time

$$\phi_i^{(T)} \equiv \phi_i(T) \tag{2.62}$$

which we use from now on.

The correlation functions of the field perturbations are defined as

$$\langle \delta\phi_{i,\mathbf{k_1}}^{(T)} \delta\phi_{j,\mathbf{k_2}}^{(T)} \rangle = \Sigma_{ij}^{(T)}(k_1)(2\pi)^3 \delta(\mathbf{k_1} + \mathbf{k_2}) \tag{2.63}$$

$$\langle \delta\phi_{i,\mathbf{k_1}}^{(T)} \delta\phi_{j,\mathbf{k_2}}^{(T)} \delta\phi_{k,\mathbf{k_3}}^{(T)} \rangle = \alpha_{ijk}^{(T)}(k_1, k_2, k_3)(2\pi)^3 \delta(\mathbf{k_1} + \mathbf{k_2} + \mathbf{k_3}) \tag{2.64}$$

such that the power spectrum [37] and bispectrum [41] of ζ are given by

$$P_\zeta(k_a) = N_i^{(T)} N_j^{(T)} \Sigma_{ij}^{(T)}(k_a) \tag{2.65}$$

$$\begin{aligned} B_\zeta(k_1, k_2, k_3) =& N_i^{(T)} N_j^{(T)} N_k^{(T)} \alpha_{ijk}^{(T)}(k_1, k_2, k_3) \\ &+ N_i^{(T)} N_{jk}^{(T)} N_l^{(T)} \left[\Sigma_{ij}^{(T)}(k_1)\Sigma_{kl}^{(T)}(k_2) + (k_1 \to k_2 \to k_3)\right] \end{aligned} \tag{2.66}$$

where the arrows indicate there are two additional terms formed by cyclic permutations.

For light, canonically normalized fields, the field-space correlation function for a given wavenumber takes a very simple form at the time the wavenumber crosses the horizon[1] (and from which the δN formalism can be employed), one finds (as explained in (2.26)) [20, 21]

$$\Sigma_{ij}^{(1)}(k_1) = \frac{{H^{(1)}}^2}{2k_1^3} \delta_{ij}, \tag{2.67}$$

where $H^{(1)} \equiv H(t_1)$, and t_1 is the horizon exit time of k_1, where $k_1 = a(t_1)H(t_1)$.

In the most common application of δN, one assumes a near-equilateral momentum regime, where all the wavenumbers are approximately equal, $k_1 \approx k_2 \approx k_3$ and thus the horizon crossing times of the three wavenumbers involved in the bispectrum can be identified with a single time, t_*, such that $t_1 \approx t_2 \approx t_3 \approx t_*$. In this regime, it is then common to make the simple choice $T = t_*$.

[1] Strictly speaking this result is the form the two-point function takes once the decaying mode present at horizon crossing has been lost, written in terms of horizon crossing parameters.

For canonical slow-roll inflation, one can take[2]

$$\Sigma_{ij}^{(*)}(k_1) \approx \frac{H^{(*)2}}{2k_1^3}\delta_{ij}\,, \tag{2.68}$$

and similarly for the other wavenumbers, k_2 and k_3. Moreover, Seery & Lidsey [43] used the in-in formalism to calculate $\alpha_{ijk}^{(*)}(k_1, k_2, k_3)$ in the close to equilateral momentum configuration at the time t_*. They found

$$\begin{aligned}&\alpha_{ijk}^{(*)}(k_1, k_2, k_3)\\ &= \frac{4\pi^4}{k_1^3 k_2^3 k_3^3}\left(\frac{H^{(*)}}{2\pi}\right)^4 \sum_{6\text{ perms}} \frac{\dot{\phi}_i^{(*)}\delta_{jk}}{4H^{(*)}}\left(-3\frac{k_2^2 k_3^2}{k_t} - \frac{k_2^2 k_3^2}{k_t^2}\left(k_1 + 2k_3\right) + \frac{1}{2}k_1^2 - k_1 k_2^2\right)\end{aligned} \tag{2.69}$$

where the sum is over the six permutations of (ijk) while simultaneously permuting the momenta (k_1, k_2, k_3) where i is associated with k_1, j is associated with k_2 and k is associated with k_3. We emphasize that this result assumed that the three k modes crossed the horizon at roughly the same time and cannot be trusted when the crossing times are too different[3], as in the case of the highly squeezed limit, $k_1 \ll k_2 \approx k_3$, which we will consider later in this thesis.

Sticking with the near-equilateral configuration, with $k_1 \approx k_2 \approx k_3$, and taking the δN initial time $T = t_*$, the results (2.67) and (7.47) can then be used together with Eqs. (2.65)-(5.4) to give the well-known expression [41], valid when $f_{\rm NL}(k_*) \gg \mathcal{O}(\epsilon)$,

$$f_{\rm NL} \approx \frac{5}{6}\frac{N_i^{(*)}N_{ij}^{(*)}N_j^{(*)}}{(N_l^{(*)}N_l^{(*)})^2}\,, \tag{2.70}$$

where (2.69) has been used to demonstrate that the second term in Eq. (2.66) must dominate over the first term if $f_{\rm NL}$ is to be large – i.e. the contribution from α is neglected [44]. Eq. (2.70) retains a dependence on k_* through the horizon crossing time t_*, and the relation that $k_* = a(t_*)H(t_*)$.

Given that it retains this dependence on the crossing scale, which is a measure of the overall scale of the bispectrum in the near-equilateral configuration, the bispectrum calculated above is sometimes referred to as quasi-local (to be contrasted with the local shape, in which $f_{\rm NL}$ is independent of all three k's). Differentiating (2.70), Byrnes *et*

[2]The leading order in slow-roll correction to this [20, 21, 42] is to replace $\delta_{ij} \mapsto \delta_{ij} + 2cu_{ij}$, where $c \equiv 2 - \log 2 - \gamma$, with γ the Euler-Masheroni constant, and $u_{ij} = -(\log V)_{,ij}$, but we will not use this correction in this thesis.

[3]This is because in evaluating the time integrals of the in-in calculation, the time-dependent coefficients of the field perturbations were all evaluated at the common horizon crossing time, t_*, of the near-equilateral modes. This can't be done if the modes exit at largely different times, as is the case in the highly squeezed limit.

al. [45] gave an expression for the tilt of $f_{\rm NL}$, denoted $n_{f_{\rm NL}}$, for equilateral triangles

$$n^{(*)}_{f_{\rm NL}} \equiv \frac{\mathrm{d}\log|f_{\rm NL}|}{\mathrm{d}\log k} = \frac{(n^{(*)}_i + n^{(*)}_j + n^{(*)}_{ij})N^{(*)}_i N^{(*)}_{ij} N^{(*)}_j}{N^{(*)}_l N^{(*)}_{lm} N^{(*)}_m} - 4\hat{n} \tag{2.71}$$

$$\text{where } n^{(*)}_i \equiv \frac{1}{H}\frac{\mathrm{d}\log N^{(*)}_i}{\mathrm{d}t_*}, \qquad n^{(*)}_{ij} \equiv \frac{1}{H}\frac{\mathrm{d}\log N^{(*)}_{ij}}{\mathrm{d}t_*} \qquad \text{and } \hat{n} \equiv \frac{n^{(*)}_i N^{(*)}_i N^{(*)}_i}{N^{(*)}_j N^{(*)}_j}. \tag{2.72}$$

2.2.7 Numerical Techniques for Inflationary Correlation Functions

The in-in formalism can be used to accurately calculate inflationary correlation functions analytically for many single-field models, while other models, such as those including features, require a numerical implementation [46–49].

Recently, there has been progress on performing numerical computations of inflationary correlation functions for multi-field models, with automation of the power spectrum and bispectrum in canonical multi-field inflation being completed in [50–52]. This includes all relevant effects at tree level. It relies on numerical routines which solve the *Moment Transport* differential equations [53–57].

This is to be compared with previous codes such as Pyflation [58] and MultiModeCode [59] which numerically compute the power spectrum from canonical multi-field models, and [60] which numerically computes the power spectrum from curved field space multi-field models.

2.3 Observables

In this section we relate the results of the theoretical calculations of Sections 2.1 and 2.2 to observations of the cosmic microwave background (CMB) radiation and large-scale structure (LSS).

Using the separate universe approach, Wands et al. [40] showed that ζ is conserved on superhorizon scales when the non-adiabatic pressure perturbation is negligable, independent of the gravitational field equations (to be contrasted with Weinberg's approach [61]). In order to compare late-time observables with early universe physics, it's necessary to know the evolution of perturbations up until the point at which adiabaticity is reached, and from then onwards one can apply this conservation law.

2.3.1 Cosmic Microwave Background

Once perturbations reenter the horizon they lead to the observed CMB anisotropies. The curvature perturbation lead to fluctuations in the energy density, $\delta\rho$. When the universe expands and gets sufficiently cool, neutral hydrogen forms, capturing electrons

allowing photons to decouple, creating the CMB. The temperature of the CMB gets anisotropies (relative to the background temperature $T_0 = 2.7K$) resulting from $\delta\rho$. The temperature anisotropies, $\Delta T(\vec{n})$, have the spherical harmonic expansion

$$\frac{\Delta T(\vec{n})}{T_0} = \sum_{l=0}^{l=\infty} \sum_{m=-l}^{m=+l} a_{lm} Y_{lm}(\vec{n}). \tag{2.73}$$

The multipole moments can be combined into an angular power-spectrum

$$C_l^{TT} = \frac{1}{2l+1} \sum_m \langle a_{lm}^* a_{lm} \rangle \,. \tag{2.74}$$

It is these C_l's that CMB observations can constrain. They can also be related to the primordial power spectrum via

$$C_l^{TT} = \int d\log k \mathcal{P}_\zeta(k) (\Delta_{l,T}^s(k))^2, \tag{2.75}$$

where the *Transfer Function*, $\Delta_{l,T}^s(k)$, describes the imprint on the temperature perturbations (T) from the evolution of the initial scalar (s) fluctuations from horizon entry time to the recombination time and projection effects from recombination time to today. It depends only on known physics, and is computed by numerically solving coupled Einstein-Boltzmann equations [62–64].

Recombination wasn't instantaneous, and during the time it took for electrons and protons to combine into neutral hydrogen the photons developed a quadrupolar anisotropy in the local electron rest frame, leading to an anisotropy of the CMB polarization. The polarization anisotropy can be broken into parity even (E) and parity odd (B) mode parts. Symmetry forbids scalar modes from forming B modes and hence detecting B modes would signal the presence of primordial tensors (gravitational waves).

Examples of the corresponding transfer functions for scalar (s) and tensor (t) perturbations into temperature, T, and E- and B-mode polarizations are shown in Fig. 1.

The observed data for the temperature power spectrum, TE cross correlation and EE power spectrum are shown in Fig. 2 assuming the Planck best fit ΛCDM cosmology and a nearly scale-invariant spectrum as predicted by inflation. The CMB anisotropies have coherent phases, as demonstrated by the series of peaks and troughs in the power spectra, due to constructive and destructive interference. In the absence of coherence, the first peak in the TE cross-correlation wouldn't be present [66]. Inflation predicts coherent phases for its perturbations since modes are frozen on superhorizon scales and start evolving when they reenter the horizon - this time being common for all modes

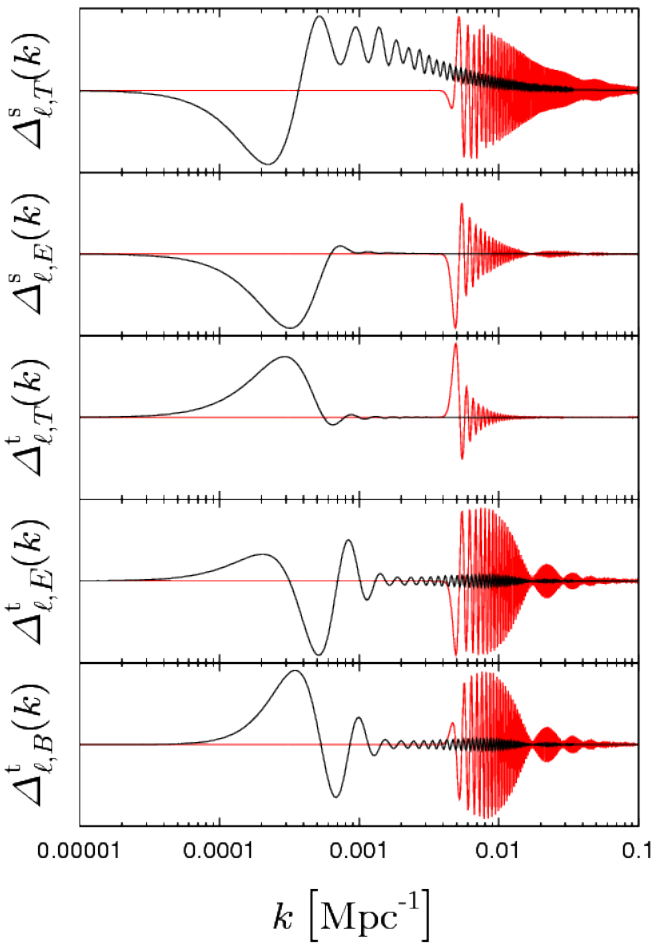

Figure 1: From Planck et al. [65]. Comparison of transfer functions for the scalar and tensor modes into T, E, and B modes. These functions are plotted for two representative values of the multipole number: $l = 2$ (in black) and $l = 65$ (in red).

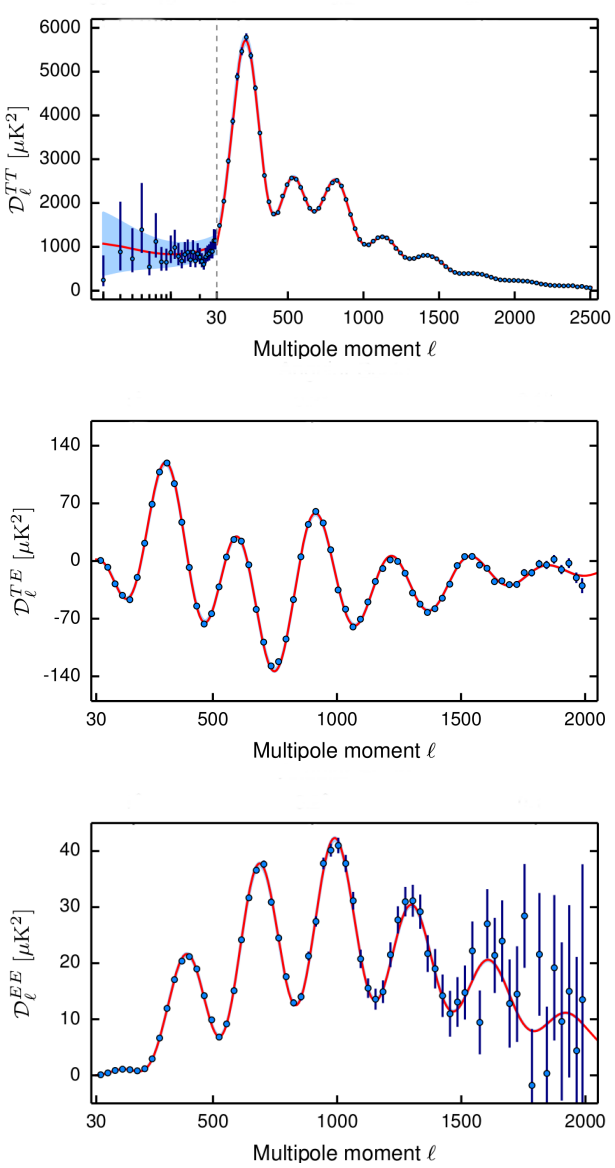

Figure 2: From Planck et al. [65]. Angular power spectra, with $\mathcal{D}_l \equiv l(l+1)C_l$. Blue points are averages of binned data points. Red line is theoretical curve for Planck's best fit ΛCDM cosmology.

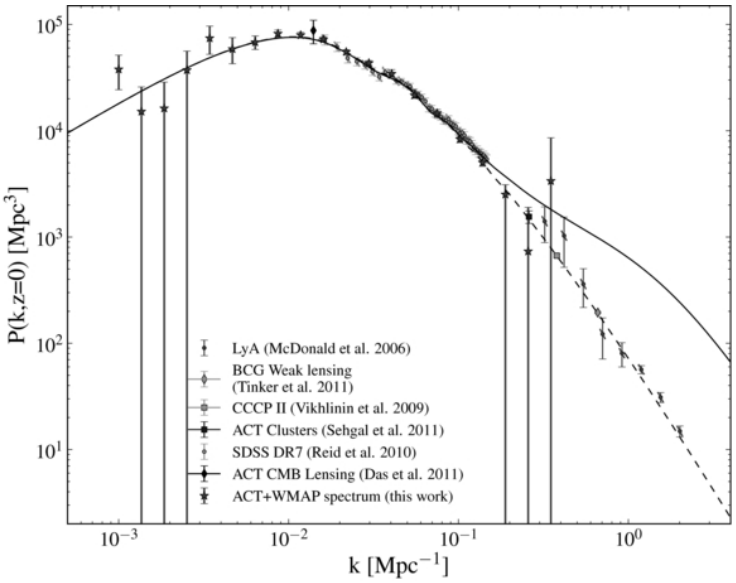

Figure 3: Figure adapted from Hlozek et al. [69]. Combination of measurements of the dark matter density power spectrum. Solid line is non-linear while dashed line is linear

with distinct $\vec{k}$ but with the same wavenumber k. Alternative theories of structure formation, such as cosmic strings, have perturbations with incoherent phases, and as such are now strongly ruled out by CMB observations.

2.3.2 Large Scale Structure

At recombination, the density fluctuations are small, but gravity causes them to grow with time, and they eventually produce the large-scale structure of the universe. At linear order in the perturbations, the dark matter density contrast δ has a power spectrum, $P_\delta(z,k)$ that can be related to the inflationary scalar power spectrum via

$$P_\delta(z,k) = T_\delta^2(z,k)\mathcal{P}_\zeta(k) \tag{2.76}$$

where the dark matter transfer function $T_\delta^2(z,k)$ can be determined by perturbation theory on large scales [67] and via numerical N-body simulations on small scales [68]. One way of probing the dark matter density directly is gravitational lensing, however, more common is the observation of some biased baryonic tracer, such as galaxies and clusters. On large scales the dark matter density contrast can be linearly related to the density contrast of the baryonic tracer, δ_g, via a local bias factor

$$\delta(z,\vec{x}) = b(z)\delta_g(z,\vec{x}). \tag{2.77}$$

However, on small scales, the density becomes non-linear (as can the bias). The dark matter density power spectrum is shown in Fig. 3.

Parameter	Planck TT + lowP + lensing (68%)
$\Omega_b h^2$	0.02226 ± 0.00023
$\Omega_c h^2$	0.1186 ± 0.0020
Ω_Λ	0.692 ± 0.012
τ	0.066 ± 0.016
$\ln(10^{10} A_s)$	3.062 ± 0.029
n_s	0.9677 ± 0.0060

Table 1: ΛCDM model parameter constraints from Planck 2015 [72]

A scale-dependent shift in the bias can be introduced by primordial non-Gaussianity, see, for example, [70, 71]. This will be of interest to us in the chapter on the squeezed limit of the bispectrum, to which the scale-dependence of the bias is particularly sensitive.

The oscillations present in the CMB are also present in the dark matter power spectrum, since the Einstein equations couple the photon-baryon fluid to the dark matter density, producing Baryon Acoustic Oscillations.

2.3.3 ΛCDM Model

The standard model of cosmology is referred to as the ΛCDM model and contains just six free parameters: the physical baryon density today, $\Omega_b h^2$, the physical cold dark matter density today, $\Omega_c h^2$, the dark energy density today divided by the critical density, Ω_Λ, the optical depth, τ, the scalar amplitude A_s and the scalar spectral index n_s for the power law ansatz for the initial conditions

$$\mathcal{P}_\zeta(k) = A_s \left(\frac{k}{k_0} \right)^{n_s - 1} \tag{2.78}$$

where the pivot scale is $k_0 = 0.05\ \mathrm{Mpc}^{-1}$. Note that h is defined by the Hubble constant at the present day, $H_0 = 100\ h\ \mathrm{km\ s^{-1}\ Mpc^{-1}}$. This base ΛCDM model assumes a spatially-flat universe with negligable contributions from tensor modes to the CMB temperature fluctuations.

The best-fit constraints on the ΛCDM parameters from Planck 2015 [72] are given in Table 1.

2.3.4 Primordial Gravitational Waves

Adding a tensor component to the base ΛCDM, the joint polarization data from Planck 2015 and BICEP2, Keck Array and Planck (BKP) data [73] gives the upper limit on the tensor-to-scalar ratio $r < 0.09$ at pivot scale $k_0 = 0.002\ \mathrm{Mpc}^{-1}$ [72]. The allowed parameter space region in the $n_s - r$ plane is shown in Fig. 4, along with theoretical

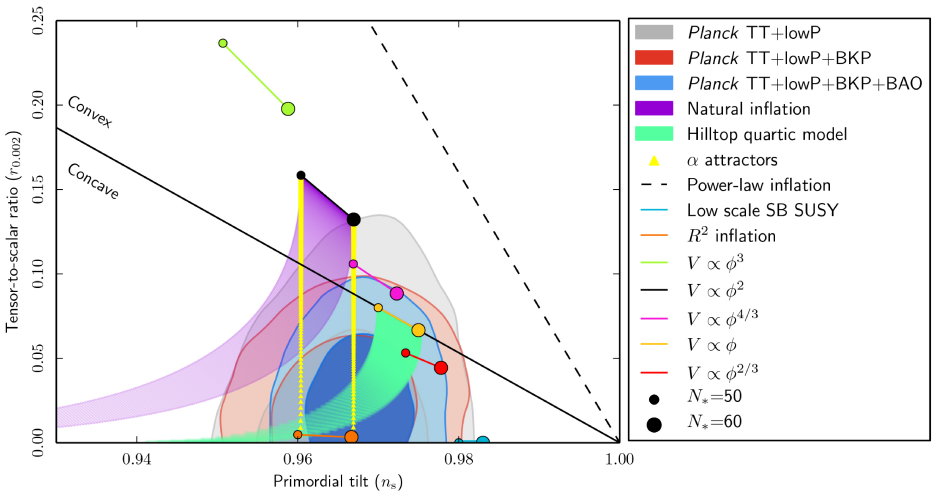

Figure 4: Figure from Planck 2015 [65]. Marginalized joint 68% and 95% CL regions for n_s and r at $k_0 = 0.002$ Mpc^{-1} from combination of Planck and BICEP2/Keck Array and/or BAO data compared with the theoretical predictions of selected inflationary models. Note that the marginalized joint 68% and 95% CL regions have been obtained by assuming no running of the scalar spectral index, dns/ dlnk = 0.

predictions of these parameters for selected inflationary models.

These contour plots should be compared to the data from BICEP2 alone [74], which suggested a detection of $r = 0.20^{+0.07}_{-0.05}$. However, it was later found that the BICEP2 analysis included modelling of the level of dust contamination which is now thought to be too low. With the original BICEP2 data, it appeared to favour inflationary models such as *Natural Inflation*, with a cosine potential $\cos(\phi/f)$, where the decay constant f is super-Planckian. For this reason, in Chapter 4, we consider such a model of Natural Inflation derived from string theory, in order to explore whether an observably large r can be derived in a string theory construction.

We note now, however, that using the combined Planck TT + lowP + BKP + BAO data, as in the blue region in Fig. 4, puts natural inflation into mild tension with observations and so there is now less motivation for studying these inflationary models from an observational perspective. However, from a theoretical perspective, they are still interesting.

There are future experiments looking for primordial B-modes, including EBEX [75], BICEP3 [76], ABS [77], SPIDER [78] and CLASS [79] on degree scales, and SPTPol [80], POLARBEAR [81] and ACTPol [82] on arcminute scales. A detection from any of these would require a natural inflation model to have a super-Planckian decay constant.

2.3.5 Constraints on Primordial Non-Gaussianity

The primary diagnostic of primordial non-Gaussianity comes from the bispectrum of the curvature perturbation. Data can't constrain an entirely free function, so first a shape

template needs to chosen and then an amplitude for this shape can be constrained from the data. The Planck collaboration has tested for non-Gaussian signals parameterized by the following shape templates

$$B_{\rm local}(k_1,k_2,k_3) \equiv \frac{6}{5} f_{\rm NL}^{\rm local} \left(P_1P_2 + \text{perms.}\right) \tag{2.79}$$

$$B_{\rm equil}(k_1,k_2,k_3) \equiv \frac{3}{5} f_{\rm NL}^{\rm equil} \left(6(P_1^3P_2^2P_3)^{1/3} - 3P_1P_2 - 2(P_1P_2P_3)^{2/3} + \text{perms.}\right) \tag{2.80}$$

$$B_{\rm ortho}(k_1,k_2,k_3) \equiv \frac{3}{5} f_{\rm NL}^{\rm ortho} \left(18(P_1^3P_2^2P_3)^{1/3} - 9P_1P_2 - 8(P_1P_2P_3)^{2/3} + \text{perms.}\right) \tag{2.81}$$

where $P_i = P_\zeta(k_i)$ for $i = 1, 2, 3$. We now give some physical intuition for these choices of shape templates:

Local: This shape arises from the following local ansatz in real space for the non-Gaussian random variable ζ, in terms of a Gaussian random variable ζ_G

$$\zeta(\vec{x}) = \zeta_G(\vec{x}) + \frac{3}{5} f_{\rm NL}^{\rm local} \left[\zeta_G^2(\vec{x}) - \langle \zeta_G^2(\vec{x}) \rangle\right]. \tag{2.82}$$

The signal in this template peaks in the squeezed configuration, $k_1 \ll k_2 \sim k_3$. Under mild assumptions[4] all single-field inflationary models predict an unobservably small signal in the squeezed configuration, and hence, since the local shape peaks in the squeezed configuration, all single field models with these assumptions won't produce a signal for the local shape template. On the other hand, some multi-field models of inflation may predict a shape similar to the local shape template, with the amplitude of the predicted $f_{\rm NL}^{\rm local}$ dependant on the model details. The strong constraint on $f_{\rm NL}^{\rm local}$ in Table 2 thus constricts models of multi-field inflation. To be clear though, it does not rule out *all* models of multi-field inflation. On the other hand, a detection of a non-zero $f_{\rm NL}^{\rm local}$ would rule out all single field models under the mild assumptions.

The reason some multi-field models of inflation can give rise to local non-Gaussianity of the curvature perturbation is that there can be a non-linear transfer of superhorizon Gaussian or non-Gaussian isocurvature perturbations of an additional field into the adiabatic density perturbations. Since this typically occurs on superhorizon scales, it is local in real space, correlating large and small scale Fourier modes.

Equilateral: This shape can arise in single-field inflationary models with higher-derivative interactions in the inflaton Lagrangian, i.e. non-canonical kinetic terms. Note that derivative interactions are suppressed when one scale is far outside the horizon, and so we expect these derivative interaction non-Gaussianities to be small in the squeezed configuration and hence we expect them to peak close to the equilateral configuration $k_1 = k_2 = k_3$. This is indeed the case for the equilateral template. From

[4] assuming a Bunch-Davies initial state and that the classical solution is a dynamical attractor [83,84].

Shape	ISW-lensing subtracted (68%)
$f_{\rm NL}^{\rm local}$	0.8 ± 5.0
$f_{\rm NL}^{\rm equil}$	-4 ± 43
$f_{\rm NL}^{\rm ortho}$	-26 ± 21

Table 2: Results for the $f_{\rm NL}$ parameters of the primordial local, equilateral, and orthogonal shapes, from Planck 2015 [85].

the higher-derivative interactions one can associate a sound speed with which perturbations propagate - this sound speed is often related to the amplitude via $f_{\rm NL}^{\rm equil} \sim c_s^{-2}$, and hence for small sound speeds, the equilateral non-Gaussianity can be large.

Orthogonal: This shape also arises in single-field inflationary models with higher-derivative interactions, and is orthogonal to both the equilateral and local shapes, where the dot product between two bispectra shapes is defined as

$$B_1 \cdot B_2 \equiv \sum_{\vec{k}_i} \frac{B_1(k_1, k_2, k_3) B_2(k_1, k_2, k_3)}{P_1 P_2 P_3} \tag{2.83}$$

where the sum is taken over all physical closed triangles in momentum space. This is a sum for a finite number of observations or an integral for theoretical calculations.

The observational constraints on the $f_{\rm NL}$ parameters for these shapes are shown in Table 2. These constraints are strong, but still allow for future detections of multiple field models, single-field models with non-canonical kinetic terms and deviations from Bunch-Davies initial states.

Future experiments may be able to probe non-Gaussianity to even higher precision. However, the observations from the CMB alone are now nearly at their limit, since Silk damping washes away primordial information for multipoles above $l \approx 2000$. More modes are accessible through LSS measurements, since these galaxy surveys probe three dimensions, rather than the two dimensions of the CMB sphere. Some current and future surveys and their expected error on detecting $f_{\rm NL}$ are shown in Table 3. It is necessary to further understand non-linearities in the dark matter evolution in order to take full advantage of these LSS experiments. In addition, we need a better grip on the non-linear behaviour of the halo bias and redshift space distortions. Some recent work towards extending to non-linear scales involves the effective theory of LSS [86–97].

Both LSS and CMB experiments are limited to scales inside $\{10^{-4} - 1\}$ Mpc^{-1}, the upper limit coming from non-linear dynamics for LSS and Silk damping for the CMB. We can probe smaller scales, $\{50 - 10^4\}$ Mpc^{-1} using CMB spectral distortions, [98]. The μ-distortion can be used to constrain the integrated primordial power spectrum over this range of very small scales. Further, cross-correlations between the temperature anisotropy on large scales and the μ-distortion on very small scales can be used to probe the squeezed limit of the primordial bispectrum. The autocorrelations of the μ-

Survey	$\sigma(f_{\rm NL})$
SDSS LRG	5.62
BOSS	3.34
Big-BOSS	2.27
HETDEX	3.65
CIP	1.03
EUCLID	0.92
WFIRST	1.11

Table 3: Current and future LSS surveys. Adapted from [29].

distortion can be used to probe the primordial trispectrum on very small scales. See [99] for recent work on this. These might be detectable with future experiements such as PIXIE [100] and PRISM [101].

2.3.6 Alternatives to Inflation

There are a number of alternatives to the inflationary paradigm, including, but not limited to, String Gas Cosmology, Cosmic Strings, Bouncing Models, Varying Speed of Light Models, and Ekpyrotic/Cyclic Scenarios. These try to address some of the theoretical shortcomings of the inflationary paradigm, such as the 'patch' and 'overshoot' problems, where the initial position of the inflaton field on the inflationary potential needs to be on a patch flat enough for inflation to occur and the initial velocity needs to be small. In addition, inflation is geodesically incomplete towards the past, and so is not a complete theory, and itself requires its own initial conditions. Moreover, there is the problem of eternal inflation and the associated measure problem: for generic initial conditions, there are regions in which statistically rare, large quantum fluctuations push the inflaton back up the potential prolonging inflation. The region that continues inflating can dominate the volume of the universe and inflation never ends - except in small pockets where inflation ends at random times. Because of the random nature of these end times, these pockets where inflation has ended may or may not be sufficiently flat to solve the horizon problem. Without a measure which determines how likely these pockets are, it's impossible to know what this kind of eternal inflation predicts.

However, each of these alternatives to inflation has its own problems and could potentially be ruled out by future observations. For example, the Ekpyrotic scenario (see [102] for a review) doesn't predict an observably large B-mode polarization signal, whereas inflation does. If a B-mode signal is observed, this could rule out the Ekpyrotic scenario. Similarly, Ekpyrotic scenarios generically predict a larger level of non-Gaussianity, which currently constrains the Ekpyrotic model parameters to a small allowed window [85].

Nonetheless, inflation remains the most developed theoretical explanation for the

horizon problem. Some of the problems of inflation may be addressed when embedding it in a more fundamental theory, such as string theory - a topic we turn to in the next chapter.

Part 1

Theory - String Theory and Inflation

Chapter 3

Elements of String Theory for Inflation

String theory is a major area of modern research in theoretical physics spanning a vast literature, with the grand aim of providing a consistent theory of quantum gravity. It is the most developed candidate theory of quantum gravity available and hence it makes sense for us to study cosmology in string theory - although there are less well-developed alternatives. In this chapter we don't aim to give a full introduction to string theory, which instead can be found in many textbooks, for example [103–105]. Instead we aim to give the bare essentials needed for studies of inflation in string theory, with bias towards preparing the reader for Chapter 4 where a model of inflation from branes in the warped resolved conifold is presented. Much of the introductory parts of this chapter follow the textbooks *String Theory and M-Theory* [106] and *Inflation and String Theory* [29].

3.1 Actions

There are five supersymmetric string theories which are interrelated through dualities. Here we focus just on Type IIB string theory with Chapter 4 in mind. The low energy limit of Type IIB string theory is a ten-dimensional supergravity theory, with effective action, in Einstein frame, given by

$$S_{\rm IIB} = -\frac{1}{2\kappa_{10}^2}\left[\int_{M_{10}} d^{10}X\sqrt{|g|}\left(R - \frac{|\partial\tau|^2}{2({\rm Im}\tau)^2} - \frac{|G_3|^2}{2{\rm Im}\tau} - \frac{|\tilde{F}_5|^2}{4\cdot 5!}\right) + \frac{1}{4i}\int_{M_{10}}\frac{C_4\wedge G_3\wedge\overline{G}_3}{{\rm Im}\tau}\right] \tag{3.1}$$

Here, the NS-NS 2-form is B_2 with field strength $H_3 = dB_2$ and the R-R forms present in Type IIB are C_0, C_2 and C_4 with field strengths $F_5 = dC_4$, $F_3 = dC_2$. These give

the following combination of forms and field strengths,

$$\tilde{F}_5 \equiv F_5 - \frac{1}{2}C_2 \wedge H_3 + \frac{1}{2}B_2 \wedge F_3, \qquad G_3 \equiv F_3 - \tau H_3 \tag{3.2}$$

where the axiodilaton is $\tau = C_0 + ie^{-\Phi}$, with Φ the dilaton. Here $\kappa_{10} = \frac{1}{2}(2\pi)^4 g_s l_s^4$, with l_s the string length (related to α' via $l_s^2 = \alpha'$) and g_s the string coupling. We must impose self duality of $\tilde{F}_5 = \star_{10}\tilde{F}_5$ by hand.

In addition to strings, string theory also contains higher-dimensional objects. Dp-branes are $p+1$-dimensional objects charged under the C_{p+1} R-R field via the electric coupling, known as the Chern-Simons term,

$$S_{CS} = i\mu_p \int_{\Sigma_{p+1}} \sum_n C_n \wedge e^{\mathcal{F}} \tag{3.3}$$

where $\mathcal{F}_{ab} \equiv B_{ab} + 2\pi\alpha' F_{ab}$, where B_{ab} is the pullback of the NS-NS 2-form to the Dp-brane worldvolume, Σ_{p+1}. Here μ_p is the brane charge, related the Dp-brane tension, T_p, via $\mu_p = g_s T_p$, where the tension is

$$T_p = \frac{1}{(2\pi)^p g_s (\alpha')^{(p+1)/2}}. \tag{3.4}$$

The sum in (3.3) runs over all R-R forms and only combinations which are $p+1$-forms contribute to the integral. This is a higher-dimensional generalization of the coupling of a charged point particle to a gauge potential.

The low energy effective action for D-branes is the DBI action in Einstein frame

$$S_{DBI} = -T_p \int_{\Sigma_{p+1}} d^{p+1}\sigma \sqrt{-\det(G_{ab} + \mathcal{F}_{ab})} \tag{3.5}$$

where the metric and 2-form are pullbacks onto the brane worldvolume. The complete bosonic action for Dp-branes is then

$$S_{Dp} = S_{DBI} + S_{CS}. \tag{3.6}$$

3.2 Compactifications

Solutions of string theory, also known as a string theory *vacua*, are solutions to the equations of motion of the effective theory, leading to a worldsheet theory without anomalies. For critical superstring theory, a geometric solution has a ten-dimensional spacetime, $\mathcal{M}_{10}$, with coordinates X^M.

In cosmology we are interested in a 4D spacetime, $\mathcal{M}_4$ with coordinates x^μ, so we

consider a compactification of string theory

$$\mathcal{M}_{10} = \mathcal{M}_4 \times Y_6 \tag{3.7}$$

for Y_6 a compact manifold with coordinates y^m.

In a *vacuum compactification*, with no sources of stress-energy, the metric on $\mathcal{M}_{10}$ can be split as a direct product on the spaces

$$ds_{10}^2 = \eta_{\mu\nu} dx^\mu dx^\nu + g_{mn} dy^m dy^n, \tag{3.8}$$

and since this is a 10D vacuum solution, we must have $R_{\mu\nu} = R_{mn} = 0$.

However, the equations of motion can admit non-vacuum solutions, since the ten-dimensional action contains more fields than just the metric, each of which contributes stress-energy. These non-vacuum solutions contain sources that can give rise to *warped compactifications* with a warped product metric

$$ds_{10}^2 = \mathcal{H}^{-1/2}(y) g_{\mu\nu} dx^\mu dx^\nu + \mathcal{H}^{1/2}(y) \tilde{g}_{mn} dy^m dy^n, \tag{3.9}$$

where $\mathcal{H}(y)$ is the warp factor, and now $\tilde{g}_{mn}$ is not necessarily Ricci-flat. We can get to a 4D effective theory by exploring one of the following options:

Kaluza Klein Compactification: We can compute the 4D effective action by performing a Kaluza Klein reduction on the 10D action. As long as the size of the extra dimensions is much smaller than the lengthscale of the experiment performed at low energy, these extra dimensions can't be seen, but there are important effects from their topology on the spectrum and symmetries of the 4D theory.

Brane-World Scenario: We can identify the four large dimensions with a brane embedded in a 10D spacetime. Warping can lead to interesting hierarchies, like the Randall-Sundrum scenario [107].

We focus in this thesis on the Kaluza Klein picture.

Supersymmetric Compactifications

Type IIB string theory has $(2, 0)$ supersymmetry (SUSY) in 10D, which is maximal, with 32 supercharges. We hope that the 4D effective theory from a string compactification inherits some SUSY for a number of reasons:

- The hierarchy problem of the standard model: $\mathcal{N} = 1$ SUSY at high energy in the 4D theory, broken at some scale above the standard model energy scale, would alleviate the hierarchy problem of the standard model, and so protect the Higgs mass.

- SUSY ensures the three gauge couplings of the standard model converge at the

GUT scale.

- Calculations are a lot simpler for $\mathcal{N} = 1$ SUSY. Second order equations of motion become first order with the constraints of SUSY.

Compactifying on a highly symmetric space preserves the maximal $\mathcal{N} = 8$ SUSY in the 4D theory, which is phenomenologically unrealistic. More attractive are compactifications on a Calabi-Yau three-fold (CY) which preserves one quarter of the supersymmetries of the 10D theory, which for Type IIB gives $\mathcal{N} = 2$ SUSY in 4D. Note that $\mathcal{N} = 2$ SUSY in 4D at low energies would be unrealistic, as it doesn't allow chiral fermions, but we can orbifold down from $\mathcal{N} = 2$ to $\mathcal{N} = 1$ SUSY as desired - more details on this can be found in *Inflation and String Theory* [29] and references therein.

We digress briefly now on the main ingredients of $\mathcal{N} = 1$ supergravity in four dimensions that will be useful throughout this chapter, before looking in more detail at Calabi-Yau manifolds. The bosonic field content of four-dimensional $\mathcal{N} = 1$ supergravity is the metric, gauge potentials and complex scalars Φ_i. The low-energy theory of the scalars is captured by the superpotential $W(\Phi_i)$, a holomorphic funtion of the Φ_i, and the Kähler potential $K(\Phi_i, \bar{\Phi}_i)$, a real analytic function of the Φ_i. Neglecting gauge interactions, the scalars have the Lagrangian

$$L = -K_{i\bar{j}}\partial^\mu \Phi^i \partial_\mu \Phi_{\bar{j}} - V_F \tag{3.10}$$

$$\text{where } V_F = e^{K/M_p^2}\left(K^{i\bar{j}} D_i W D_{\bar{j}} W - \frac{3}{M_p^2}|W|^2\right). \tag{3.11}$$

Here $K_{i\bar{j}} = \partial_i \partial_{\bar{j}} K$ is the Kähler metric, $K^{i\bar{j}}$ its inverse, and $D_i W = \partial_i W + \frac{1}{M_p^2}(\partial_i K)W$. The superpotential and Kähler potential can be calculated from the ten-dimensional compactification as we will see in a later section.

Calabi-Yau Compactifications

In order to define a Calabi-Yau three-fold, we need the following definitions:

A **complex n-manifold** is a real $2n$-manifold with real coordinates $y^m, m = 1, 2, ..., 2n$ and complex coordinates $z^a, a = 1, 2, ..., n$, with conjugates $\overline{z}^{\overline{a}}$, such that the transition functions are biholomorphic and there exists a tensor, $\mathcal{I}$, with components in complex coordinates:

$$\mathcal{I}_a^b = i\delta_a^b, \mathcal{I}_{\bar{a}}^{\bar{b}} = -i\delta_{\bar{a}}^{\bar{b}}, \tag{3.12}$$

$$\mathcal{I}_a^{\bar{b}} = 0 = \mathcal{I}_{\bar{a}}^b. \tag{3.13}$$

If we are given a real $2n$-manifold, then it's a complex manifold if the real manifold

admits a tensor $\mathcal{I}^m_n$ satisfying the following two properties

$$\mathcal{I}^n_m \mathcal{I}^p_n = -\delta^p_m \tag{3.14}$$

$$N^p_{mn} \equiv \mathcal{I}^q_m \partial_{[q} \mathcal{I}^p_{n]} - \mathcal{I}^q_n \partial_{[q} \mathcal{I}^p_{m]} = 0, \tag{3.15}$$

then $\mathcal{I}$ is called the *complex structure*.

A **Hermitian manifold** is a complex manifold with a Riemannian metric g_{mn} such that

$$g_{ab} = 0 = g_{\bar{a}\bar{b}} \tag{3.16}$$

A **Kähler manifold** is a Hermitian manifold on which the *Kähler form*, J, defined by

$$J \equiv i g_{a\bar{b}} dz^a \wedge d\bar{z}^{\bar{b}} \tag{3.17}$$

is closed

$$dJ \equiv (\partial + \bar{\partial}) J = 0. \tag{3.18}$$

Then, locally, we must have

$$g_{a\bar{b}} = \partial_a \bar{\partial}_{\bar{b}} \mathcal{K} \tag{3.19}$$

where $\mathcal{K}(z, \overline{z})$ is called the *Kähler potential*, and $J = i\partial\overline{\partial}\mathcal{K}$.

A **Calabi-Yau three-fold** (CY), Y_6, is a complex 3-manifold (real 6-manifold), which is compact and Kähler, which also satisfies one (equivalently all) of the following conditions

- Y_6 is Ricci flat,
- *Reduced holonomy*: $Hol(Y_6) \subseteq SU(3)$. A generic 3-fold has $Hol(Y_6) = SU(4)$,
- Vanishing first Chern class, $c_1 = 0$,
- The manifold admits a *holomorphic* $(3,0)$*-form*: $\Omega = f(z^i) dz^1 \wedge dz^2 \wedge dz^3$,
- There are other more technical definitions involving fibre bundles (see, for example, Nakahara [108]).

Note that the above conditions are equivalent for a Kähler 3-manifold. It is not known whether the number of topologically distinct, compact CY's is finite. Examples include submanifolds of complex projective spaces, e.g a quintic hypersurface in $\mathbb{C}P^4$. However, we don't know the explicit form of the metric on any compact CY. In our study of

inflation in string theory, we will require the metric and as such, we will look to conifolds - non-compact cousins of CYs - on which we know the metric. We will study these conifold spaces in depth later. For now we look at moduli, which arise as deformations of CYs.

Deformations of Calabi-Yau spaces

We can relate different CYs by smooth deformations of the parameters which give their shape and size. These parameters are called *moduli*. The moduli parametrize the space of possible expectation values of massless scalar fields in 4D. These are undetermined because they feel no potential, i.e. the effective potential is independent of these moduli.

There are two types of continuous deformations of Y_6 to consider:

1. Deformations of the p-form fields, giving rise to b_p moduli fields, where b_p is the p-th Betti number of the manifold. These deformations give rise to *axion* moduli.

2. Metric deformations of the 10d metric g_{MN} gives a 4d metric $g_{\mu\nu}$ and a set of massless scalar fields coming from the internal coordinates y^m. There will also be moduli from fluctuations of the 6D internal metric g_{mn}.

Call $\mathcal{E}(Y_6)$ the internal moduli space: i.e. the part of the moduli space depending on deformations of the internal 6D metric g_{mn} on Y_6. Consider fluctuations, δg_{mn}, of the internal 6D metric g_{mn}, which satisfy

$$R_{mn}[g + \delta g] = 0, \tag{3.20}$$

so that we are deforming to another CY. Equation (3.20) leads to a set of differential equations for δg_{mn}. The coefficients of the independent solutions to these equations are the moduli. These equations for δg_{mn} decouple into pure components δg_{ab} and mixed components $\delta g_{a\bar{b}}$. This means that $\mathcal{E}(Y_6)$ itself contains two types of moduli:

- The *complex-structure moduli*, which are deformations of the complex-structure $\mathcal{I}_n^m$ on Y_6. These correspond to non-zero δg_{ab} (and $\delta g_{\bar{a}\bar{b}}$), since deforming the complex-structure allows for these. The new manifold can be Hermitian because as well as adding pure type perturbations, one also deforms the complex structure in such a way that new coordinates on the manifold are such that Hermiticity holds.

- The *Kähler moduli* which are deformations of the complexified Kähler form $\mathcal{J} \equiv B + iJ$ on Y_6. Here B is the compactified NS-NS two-form, which is a (1,1)-form $B_{a\bar{b}}$ on Y_6. These deformations correspond to non-zero $\delta g_{a\bar{b}}$, since the Kähler form is $J = ig_{a\bar{b}}dz^a \wedge d\bar{z}^{\bar{b}}$.

From the decoupling of the CY equations (3.20), the internal moduli space $\mathcal{E}(Y_6)$ locally factorizes into a space of *complex-structure moduli*, $C^{2,1}(Y_6)$, and a space of *Kähler-structure moduli*, $K^{1,1}(Y_6)$

$$\mathcal{E}(Y_6) = C^{2,1}(Y_6) \times K^{1,1}(Y_6). \tag{3.21}$$

Finally, let's explicitly write down the moduli of each of these spaces.

Complex-structure moduli – For the complex-structure moduli space, $C^{2,1}(Y_6)$, the deformations $\delta g_{\overline{a}\overline{b}}$ (and similarly for δg_{ab}) can be written

$$\delta g_{\overline{a}\overline{b}} = -\frac{1}{||\Omega||^2}\zeta^I(x)[\chi_I]_{cd\overline{b}}\overline{\Omega}_{\overline{a}}{}^{cd} \text{ where } ||\Omega||^2 \equiv \frac{1}{3!}\Omega_{abc}\overline{\Omega}^{abc} \tag{3.22}$$

where Ω is the CY holomorphic $(3,0)$-form; the $\{\chi_I, I = 1, ..., h^{2,1}\}$ are a basis for the Dolbeault cohomology group $H^{2,1}(Y_6)$, with Hodge number $h^{2,1}$, formed of the harmonic $(2,1)$-forms χ_I

$$\chi_I = \frac{1}{2}[\chi_I]_{ab\overline{c}}\, dz^a \wedge dz^b \wedge d\overline{z}^{\overline{c}} \text{ with } [\chi_I]_{ab\overline{c}} = -\frac{1}{2}\Omega^{\overline{d}}_{ab}\frac{\partial g_{\overline{c}\overline{d}}}{\partial \zeta^I}, \tag{3.23}$$

and the $\zeta^I(x)$ are local coordinates on the complex structure moduli space $C^{2,1}(Y_6)$, i.e the *complex-structure moduli* – they are scalar fields from the four-dimensional perspective.

Kähler moduli – For the Kähler moduli space, $K^{1,1}(Y_6)$, the deformations $\delta g_{a\overline{b}}$ and $\delta B_{a\overline{b}}$ can be combined into deformations of the complexified Kähler form $\mathcal{J}$ and written

$$\delta\mathcal{J} = t^\alpha(x)\omega_\alpha \tag{3.24}$$

where the $\{\omega_\alpha, \alpha = 1, ..., h^{1,1}\}$ are a basis of harmonic $(1,1)$-forms for $H^{1,1}(Y_6)$, with Hodge number $h^{1,1}$, and the $t^\alpha(x)$ are a set of $h^{1,1}$ four-dimensional massless scalar fields - the *Kähler moduli*.

Axions – The original QCD axion is a pseudoscalar field which enjoys the continuous Peccei-Quinn shift symmetry $a \mapsto a+const.$ which is broken to a discrete shift symmetry $a \mapsto a+2\pi$ by the effects of QCD instantons through a coupling of the axion to the QCD instantons. In string compactifications, there are moduli (in addition to the complex-structure and Kähler moduli above), called *Axions*, (referred to also as closed-string axions) which come from compactifying the gauge potentials of the NS-NS and R-R form fields. For example, one can expand the ten-dimensional R-R 2-form C_2 into a basis of harmonic $(1,1)$-forms for $H^{1,1}(Y_6)$,

$$C_2 = C_2(x) + c^\alpha(x)\omega_\alpha \tag{3.25}$$

where $C_2(x)$ is a four-dimensional 2-form and $c^\alpha(x)$ are the axion moduli. Classically, the axions have a continuous shift symmetry $c \mapsto c + const.$ (where we drop the index α) inherited from the gauge symmetry of the ten-dimensional p-forms from which they are compactified. This continuous shift symmetry holds to all orders in perturbation theory, but is spontaneously broken to a discrete shift symmetry, $c \mapsto c + 2\pi$, by quantum non-perturbative effects such as worldsheet instantons and Euclidean D-branes wrapping cycles in the higher dimensional spacetime.

The above three types of moduli are closed string moduli. There are also open string moduli, such a Dp-brane position moduli – these will be of central importance in Chapter 4.

3.3 Moduli Stabilization

Some of the closed string moduli arising from CY compactification in type IIB string theory were discussed earlier. For a generic CY, there will be *many* moduli. This is both a blessing and a curse. One may hope that one of these moduli is a candidate for our inflaton field, as it has a completely flat potential. However, one must then also account for the many other moduli. The many complex-structure moduli and Kähler moduli need to be stabilized, since the positive vacuum energy during inflation tends to drive these moduli along directions which reduce the vacuum energy, and abruptly end inflation.

For single-field inflation we then have a delicate balancing act to perform: stabilizing many moduli, while allowing for one flat direction to inflate from. We need to find vacua (solutions of string theory) in which all of the moduli have positive mass squared, where these masses are large compared to the mass of the inflaton. In the following section we look for leading contributions to the moduli potential.

We note here that multiple-field models of inflation are generically expected from string compactifications - most constructions which stabilize some moduli while keeping one light for inflation will generically keep a whole family of fields light by a similar process. However, the majority of top-down string theory models of inflation aim to model inflation as a single-field low energy model.

Flux Compactifications

One can fix the complex-structure moduli and the dilaton at the classical level using so-called flux compactifications. Following the seminal work of [109], these warped geometries arise naturally when local brane sources are present, and fluxes are non-trivial. Compactifications on such backgrounds are known as flux compactifications.

At leading order in α' and g_s, the type IIB action for bosonic fields, together with

local sources, is given in the Einstein frame as

$$S = S_{\rm IIB} + S_{\rm loc} \tag{3.26}$$

where $S_{\rm IIB}$ is the IIB action, (3.1), and $S_{\rm loc}$ is the action for the local sources, formed from actions of the type (3.6).

We assume a warped background metric ansatz

$$ds^2 = e^{2A(y)} g_{\mu\nu} dx^\mu dx^\nu + e^{-2A(y)} \tilde{g}_{mn} dy^m dy^n. \tag{3.27}$$

We have a maximally symmetric external 4D spacetime, $\mathcal{M}_4$, with metric $g_{\mu\nu}(x)$ and an internal unwarped space $\tilde{Y}_6$ with metric $\tilde{g}_{mn}(y)$. The warp factor is denoted $\mathcal{H}(y) \equiv e^{-4A(y)}$. We denote the warped internal 6D space without a tilde Y_6, with warped metric $g_{mn} = \mathcal{H}(y)^{1/2} \tilde{g}_{mn}$. Here, and in what follows, a tilde denotes use of the unwarped 6D metric $\tilde{g}_{mn}$ (except for $\tilde{F}_5$, which is just conventional notation in supergravity). Note that if the warp factor is shifted by a constant, this can be absorbed into a rescaling of the x^μ coordinates, so that only the functional dependence of $\mathcal{H}(y)$ is important.

For $\tilde{F}_5$ we take the ansatz

$$\tilde{F}_5 = (1 + \star_{10})\ d\alpha(y) \wedge \sqrt{-\det g_{\mu\nu}} dx^0 \wedge dx^1 \wedge dx^2 \wedge dx^3. \tag{3.28}$$

Similarly to the warp factor, shifts of $\alpha(y)$ by a constant are irrelevant for $\tilde{F}_5$.

The inclusion of local sources, such as D-branes, leads to a non-trivial warp factor, producing a warped metric, together with non-vanishing fluxes. Varying the action leads to the Bianchi identity [109]

$$d\tilde{F}_5 = H_3 \wedge F_3 + 2\kappa_{10}^2 T_3 \star_6 \rho_3^{\rm loc} \tag{3.29}$$

where $\star_6$ is the hodge dual in the warped 6D internal space with metric g_{mn}. Here $\rho_3^{\rm loc}$ is the D3-brane charge density from the local sources. Using the warped spacetime (3.27), and the 5-form flux (3.28), the Bianchi identity (3.29) becomes

$$\tilde{\nabla}^2 \alpha = i e^{2A} \frac{G_{mnp} \star_6 \overline{G}^{mnp}}{12 {\rm Im}\tau} + 2e^{-6A} \partial_m \alpha \partial^m e^{4A} + 2\kappa_{10}^2 e^{2A} T_3 \rho_3^{\rm loc} \tag{3.30}$$

with $\tilde{\nabla}^2$ the Laplacian with respect to the unwarped internal 6D metric. The trace of the Einstein equations can be written [109], [110],

$$\tilde{\nabla}^2 e^{4A} = \mathcal{R}_4 + \frac{\kappa_{10}^2}{2} e^{2A} J^{\rm loc} + e^{2A} \frac{G_{mnp} \overline{G}^{mnp}}{12 {\rm Im}\tau} + e^{-6A} (\partial_m \alpha \partial^m \alpha + \partial_m e^{4A} \partial^m e^{4A}) \tag{3.31}$$

where

$$J^{\text{loc}} \equiv \frac{1}{4}\left(\sum_{M=4}^{9} T^{\text{loc}}{}_{M}{}^{M} - \sum_{M=0}^{3} T^{\text{loc}}{}_{M}{}^{M}\right). \tag{3.32}$$

Note that the local stress-energy tensor $T^{\text{loc}}{}_{MN}$ is contracted using the full 10D metric. The 4D Ricci scalar $\mathcal{R}_4$ is not present when the external spacetime is taken to be Minkowski [109], but in the case of inflation, we take the external 4D spacetime to be quasi-de Sitter, with $\mathcal{R}_4 \approx 12H^2$ [110]. We can combine (3.30) and (3.31) to give

$$\begin{gathered}\tilde{\nabla}^2\Phi_- = \mathcal{R}_4 + \frac{e^{8A(y)}}{6\text{Im}\tau}|G_-|^2 + e^{-4A(y)}|\partial\Phi_-|^2 + 2\kappa_{10}^2 e^{2A(y)}(J^{\text{loc}} - T_3\rho_3^{\text{loc}}) \\ \text{where } \Phi_- \equiv e^{4A(y)} - \alpha(y), \qquad G_- \equiv \star_6 G_3 - iG_3.\end{gathered} \tag{3.33}$$

Note that Φ_- is insensitive to constant shifts.

For the time being, we work in the noncompact warped volume limit for the internal geometry, $\text{vol}(Y_6) \to \infty$. But the warped volume is related to the reduced Planck mass M_p by

$$M_p^2 = \frac{\text{vol}(Y_6)}{\kappa_{10}^2} \tag{3.34}$$

so that $M_p \to \infty$ in this noncompact limit. Then by the Friedmann equation, $H^2 = V/(3M_p^2) \to 0$, so that the Ricci scalar for dS space vanishes $\mathcal{R}_4 \to 0$. We will later consider corrections from taking the compact limit with finite M_p. In the noncompact limit, (3.33) becomes

$$\tilde{\nabla}^2\Phi_- = \frac{e^{8A(y)}}{6\text{Im}\tau}|G_-|^2 + e^{-4A(y)}|\partial\Phi_-|^2 + 2\kappa_{10}^2 e^{2A(y)}(J^{\text{loc}} - T_3\rho_3^{\text{loc}}). \tag{3.35}$$

Many well-understood local sources satisfy a BPS-like condition $J^{\text{loc}} \geq T_3\rho_3^{\text{loc}}$. D3-brane sources saturate this, while D5-branes satisfy but don't saturate it. Integrating (3.35) and assuming no boundary contribution at infinity, the LHS will vanish as it's a total derivative. But since each term on the RHS is positive semi-definite, each must individually vanish at leading order, giving an imaginary self-dual (ISD) solution $G_- = 0$ and $\Phi_- = 0$.

The four-dimensional effective description of an ISD flux compactification can also be derived from a four-dimensional Kähler potential and a four-dimensional Gukov-Vafa-Witten flux superpotential, W, of $\mathcal{N} = 1$ supergravity [111]

$$K = -2\log(\mathcal{V}) - \log(-i(\tau - \bar{\tau})) - \log(-i\int_{\tilde{Y}_6} \Omega \wedge \bar{\Omega}), \tag{3.36}$$

$$W = \int \Omega \wedge G_3 \ , \tag{3.37}$$

where Ω is the holomorphic 3-form associated to the Calabi-Yau. $\mathcal{N} = 1$ supersymmetry is preserved if G_3 is a primitive $(2,1)$-form [109].

Note that the Kähler potential is of *no-scale type*

$$\sum_{i,\bar{j}=t^\alpha} K^{i\bar{j}} \partial_i K \partial_{\bar{j}} K - 3 = 0. \tag{3.38}$$

Since G_3 depends on the axiodilaton and Ω depends on the complex-structure moduli, (3.37) is independent of the Kähler moduli. Since the Kähler potential is of no-scale type, the resulting scalar potential, V_F, stabilizes only the complex-structure moduli and axiodilaton. The Kähler moduli are assumed lighter than the complex-structure moduli and axiodilaton, and so once these heavier moduli have been integrated out, the Kähler moduli can then be stabilized by another mechanism, which we come to later.

To see how the fluxes stabilize the complex structure moduli, let's define the following basis of 3-cycles A^I, B_J for $I, J = 0, ..., h^{2,1}$ on the complex structure moduli space, $C^{2,1}(Y_6)$, where

$$A^I \cap B_J = -B_J \cap A^I = \delta^I_J \text{ and } A^I \cap A^J = B_I \cap B_J = 0. \tag{3.39}$$

One can then choose to turn on quantized F_3 or H_3 $(2,1)$-form fluxes through the A, B cycles, for example,

$$\frac{1}{2\pi\alpha'} \int_A F_3 = 2\pi M \qquad \text{and} \qquad \frac{1}{2\pi\alpha'} \int_B H_3 = -2\pi K. \tag{3.40}$$

These fluxes allow for the superpotential to be written in terms of the complex structure moduli. Since SUSY is preserved, one can minimize the scalar potential by imposing the vanishing of the derivative of the superpotential with respect to the complex structure moduli, which stabilizes the complex structure moduli values at the minimum.

In a flux compactification with non-zero G_3, the complex-structure moduli $\zeta^A(x)$ and the axiodilaton τ experience a potential, coming from the following term in the 10D type IIB action (3.1)

$$V_{\text{flux}} = \frac{1}{2\kappa_{10}^2} \int d^{10}X \sqrt{|g|} \left[-\frac{|G_3|^2}{2\text{Im}\tau} \right]. \tag{3.41}$$

However, at leading order in α' and g_s, the Kähler moduli have vanishing potential. Also, the vacuum energy is zero, not positive, as would be hoped for in an inflationary model.

Quantum perturbative corrections (see e.g. [112, 113]) and non-perturbative cor-

rections (e.g. from gluino condensation [114–119]) to the effective four-dimensional supergravity potential can provide a potential for the Kähler moduli, but this will lead to an AdS vacuum with negative vacuum energy. This needs to be made positive for inflation, so we require an uplifting mechanism, which may require the inclusion of anti-D-brane sources. The two leading ideas for Kähler moduli stabilization are the KKLT scenario [120] and the Large Volume Scenario [121]. The KKLT mechanism relies on a balance between the classical flux superpotential with fine-tuned fluxes to make this contribution comparable in size to the non-perturbative superpotential. The LVS mechanism consists of regions of Kähler moduli space where some cycles are exponentially fine-tuned to be larger than others, allowing for a balance of the leading α' correction with the non-perturbative superpotential. Here we don't go into the details of either of these constructions or the uplifting mechanism, referring the reader instead to [29] and references therein.

3.4 Conifolds

Moving away from moduli stabilization, we now go into more detail on the geometry of conifolds. As was mentioned earlier, the metric on a compact Calabi-Yau (CY) is not explicitly known – though progress has been made numerically, for example in [122,123]. If we wish to study physics on CY spaces, we need the metric to do calculations.

But we do know the explicit metric on a certain class of non-compact CY's, called *conifolds*, which are intimately related to their compact CY cousins. Conifolds are similar to manifolds, except they can contain conical singularities.

Being non-compact, conifolds aren't the whole story for a compactification. In order to compactify, one cuts off the conifold at some finite length and glues it onto a bulk to form a Calabi-Yau. The metric on the bulk is not specified and the analysis is restricted to local physics done in the conifold region.

Conifold singularities of the moduli space

Note that there is room for confusion here - to be clear, let's emphasize that we will find that the moduli space of CY's can have singularities corresponding to conifold spaces. A particular conifold space itself can in general have conical singularities and is non-compact.

To see the relation between conifolds and CY's, note that when we compactify we are interested in the classical low energy effective action, in which the heavy fields have been integrated out. The moduli space $\mathcal{M}(Y_6)$ of CY's contains singularities, that is, points where the classical low energy effective action description breaks down. An example of such a singularity is a *conifold singularity*. To describe this we need *special*

coordinates, X^I, on $C^{2,1}(Y_6)$ where

$$X^I = \int_{A^I} \Omega. \tag{3.42}$$

We then take the complex structure moduli $\zeta^I = X^I/X^0$.

The conifold singularity occurs when one of the special coordinates on $C^{2,1}(Y_6)$, e.g. X^1, vanishes, and the metric on $C^{2,1}(Y_6)$ develops a curvature singlarity - which we call a *conifold singularity*.

The conifold singularity arises because the classical low energy effective action breaks down near the conifold singularity point as certain massive states that were integrated out actually become light, so it is inconsistent to integrate these out. The states are Euclidean D3-branes wrapping certain 3-cycles called *special Lagrangian cycles* (more details in [106]).

Topologically equivalent CY's live within a certain section of the CY moduli space. Sections of the CY moduli space for topologically distinct CY's abutt on each other, connected at conifold singularity points. Topologically distinct CY's can be connected to one another by finite-length curves in the moduli space, which pass through a conifold singularity [124–127].

In order to pass smoothly through one of these conifold singularities in the moduli space, it is necessary to smooth out the conical singularities of the conifolds themselves, which can be done in two distinct ways: *resolution* and *deformation*.

But since the conifold singularity is not a bone-fide part of the moduli space, it's not constrained to be compact - in fact, it corresponds to a conifold space, which is non-compact.

Since the conifold singularity occuring in the moduli space of compact CY's corresponds itself to a non-compact CY, it is most convenient to smooth out the moduli space conifold singularity in the moduli space of non-compact CY's. This is like excising a small ball in the vicinity of the conifold singularity of the moduli space of compact CY's and replacing it with the moduli space of non-compact CY's. Now, in the vicinity of the conifold singularity in moduli space, we can smooth out our singularity using the resolution or the deformation of the conifold.

To see how the smoothing works, we begin with the *Singular Conifold*, labelled $M^\sharp$ (sharp for singular), which is the non-compact CY associated to the conifold singularity of the moduli space. We'll find that $M^\sharp$ is the transition point linking two topologically distinct smooth non-compact CY's (see Fig. 5): the *resolved conifold*, *RC*, and the *deformed conifold*, *DC*. We'll now give details of each of these geometries in turn.

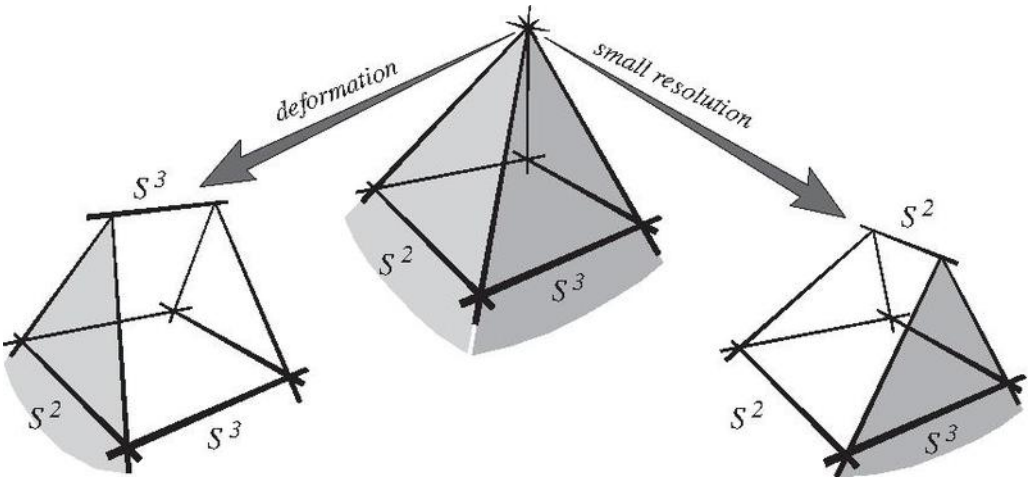

Figure 5: Left to right: deformed conifold DC (with an S^3 at the tip), singular conifold $M^\sharp$ (with a sharp tip) and resolved conifold RC (with an S^2 at the tip).

3.4.1 The Singular Conifold $M^\sharp$

We'll give descriptions of the singular conifold space using a few different coordinate systems, to enable us to see the connection to the resolved conifold and the deformed conifold more easily.

w^i *Coordinates:* We can locally describe the singular conifold $M^\sharp$ in complex coordinates w^i, $i = 1, ..., 4$, where each w^i is a vector $\in \mathbb{C}_4$, as the cone given by the following equation

$$\sum_{i=1}^{4} (w^i)^2 = 0. \tag{3.43}$$

Note that this describes a (complex) cone, as if $\vec{w}$ is a solution, then so is $\alpha\vec{w}$, for $\alpha \in \mathbb{C}$ so that the space consists of complex lines through the origin.

Let r be the (real) radial coordinate on the cone. The base of the cone is defined to be the manifold given by the intersection of the solution space of (3.43) with a sphere of radius r in $\mathbb{C}^4$:

$$\sum_{i=1}^{4} |w^i|^2 = r^2. \tag{3.44}$$

The base is topologially $S^3 \times S^2$. To see this, let $\vec{w} = \vec{x} + i\vec{y}$, and we look at the real and imaginary parts from the equations (3.43) and (3.44), giving

$$\vec{x} \cdot \vec{x} = \frac{r^2}{2} \qquad \vec{y} \cdot \vec{y} = \frac{r^2}{2} \qquad \vec{x} \cdot \vec{y} = 0. \tag{3.45}$$

The first equation describes an S^3. For each point $\vec{x}$ of this S^3, the third equation

restricts $\vec{y}$ to be a 3-vector, which, in combination with the second equation defines an S^2. The base is then an S^2 fibred over an S^3, which must be trivial, so that the base is topologically just $S^3 \times S^2$. Finally, since it is a cone, the singular conifold has a *conical singularity* at $w^i = 0$.

We emphasise that the moduli space of CY's has *conifold* singularities, while the associated non-compact CY associated to such a point in the moduli space itself has a *conical* singularity - an important distinction that is muddled by confusingly similar terms!

(X, Y, U, V) *Coordinates:* The singular conifold can alternatively be described by complex coordinates (X, Y, U, V) subject to

$$\det W = XY - UV = 0 \tag{3.46}$$

$$\mathrm{Tr} W^\dagger W = r^2 \tag{3.47}$$

where the coordinates are related to the w^i via

$$W = \begin{pmatrix} X & U \\ V & Y \end{pmatrix} = \begin{pmatrix} w^3 + iw^4 & w^1 - iw^2 \\ w^1 + iw^2 & -w^3 + iw^4 \end{pmatrix}. \tag{3.48}$$

(3.46) is one complex condition on $\mathbb{C}^4$, and so describes a 3-complex dimensional space. The conical singularity is now at $(X, Y, U, V) = (0, 0, 0, 0)$.

$(X, Y, U, V, \lambda_1, \lambda_2)$ *Coordinates:* Away from $(X, Y, U, V) = (0, 0, 0, 0)$, this space can be equivalently defined on the coordinates $(X, Y, U, V, \lambda_1, \lambda_2) \in \mathbb{C}^4 \times P\mathbb{C}^1$ (here $P\mathbb{C}^1$ is complex projective space) subject to the restriction

$$\begin{pmatrix} X & U \\ V & Y \end{pmatrix} \begin{pmatrix} \lambda_1 \\ \lambda_2 \end{pmatrix} = \begin{pmatrix} 0 \\ 0 \end{pmatrix}, \text{ where } (\lambda_1, \lambda_2) \neq (0, 0). \tag{3.49}$$

Recall that since $(\lambda_1, \lambda_2) \in P\mathbb{C}^1$, we can't have both $\lambda_1 = 0$ and $\lambda_2 = 0$. This is two complex conditions on 5 complex coordinates, giving a 3-complex dimensional space. The description in these coordinates breaks down at the conical singularity $(X, Y, U, V, \lambda_1, \lambda_2) = (0, 0, 0, 0, \lambda_1, \lambda_2)$.

(A_i, B_j) *Coordinates:* We can solve the cone equation for the singular conifold

$$\det W_{ij} = 0 \tag{3.50}$$

by introducing four new complex coordinates A_i, B_j, $i = 1, 2$ and $j = 1, 2$ with

$$W_{ij} = A_i B_j. \tag{3.51}$$

This is because W_{ij} is a 2×2 matrix with vanishing determinant, so it must be rank

one, and so can be decomposed as (3.51) for unconstrained A_i, B_j. But in order to satisfy the base equation (3.47) we require

$$A_i^\dagger A_i B_j^\dagger B_j = (|A_1|^2 + |A_1|^2)(|B_1|^2 + |B_1|^2) = r^2. \tag{3.52}$$

But we can obtain the same W_{ij} if we rescale

$$A_i \mapsto \lambda A_i \text{ and } B_j \mapsto \lambda^{-1} B_j \text{ for } \lambda \in \mathbb{C}^*. \tag{3.53}$$

Away from the conical singularity, we can choose to fix λ by demanding

$$|A_1|^2 + |A_2|^2 - |B_1|^2 - |B_2|^2 = 0. \tag{3.54}$$

The base equation (3.52) now becomes

$$|A_1|^2 + |A_1|^2 = r = |B_1|^2 + |B_1|^2. \tag{3.55}$$

But since the definition of W_{ij} given in (3.51) is invariant under

$$(A_i, B_j) \mapsto (e^{i\alpha} A_i, e^{-i\alpha} B_j), \tag{3.56}$$

for the same α, we should make the following identification

$$(A_i, B_j) \sim (e^{i\alpha} A_i, e^{-i\alpha} B_j). \tag{3.57}$$

This means the base is given by the coset space

$$T^{1,1} = \frac{SU(2) \times SU(2)}{U(1)}. \tag{3.58}$$

The equations (3.55) and (3.51) enjoy a global $SU(2) \times SU(2)$ symmetry, with one $SU(2)$ acting on the left of A_i and the other $SU(2)$ acting on the right of B_j

$$A_i \mapsto L_{ik} A_k \text{ and } B_j \mapsto B_l R_{lj}^\dagger. \tag{3.59}$$

There is also a global $U(1)$ symmetry acting as $(A_i, B_j) \mapsto e^{iR/2}(A_i, B_j)$. From this we see that the global continuous symmetry group of $T^{1,1}$ is $SU(2) \times SU(2) \times U(1)$.

$(r, \psi, \theta_1, \phi_1, \theta_2, \phi_2)$ Coordinates: We can describe the singular conifold with coordinates $(r, \psi, \theta_1, \phi_1, \theta_2, \phi_2)$, in which the metric on the singular conifold can be written

rather simply [128]

$$ds^2_{M^\sharp} = dr^2 + r^2 \left[\frac{1}{9} \left(d\psi + \sum_{i=1}^{2} \cos\theta_i d\phi_i \right)^2 + \frac{1}{6} \sum_{i=1}^{2} \left(2d\theta_i^2 + \sin^2\theta_i d\phi_i^2 \right) \right] \tag{3.60}$$

Here r is the radial conical coordinate over the $T^{1,1}$. We see that the metric describes a S^1 fibre bundle over an $S^2 \times S^2$ fibre-bundle-base, with 2ψ the coordinate on the S^1 and (θ_1, ϕ_1) coordinates on one S^2, and (θ_2, ϕ_2) on the other S^2.

We can rewrite the angular part of the metric in the convenient basis of 1-forms $\{g^i\}$:

$$g^1 = \frac{e^1 - e^3}{\sqrt{2}} \qquad g^2 = \frac{e^2 - e^4}{\sqrt{2}} \tag{3.61}$$

$$g^3 = \frac{e^1 + e^3}{\sqrt{2}} \qquad g^4 = \frac{e^2 + e^4}{\sqrt{2}} \tag{3.62}$$

$$g^5 = e^5 \tag{3.63}$$

where

$$e^1 = -\sin\theta_1 d\phi_1 \qquad e^2 = d\theta_1 \tag{3.64}$$

$$e^3 = \cos\psi \sin\theta_1 d\phi_2 - \sin\psi d\theta_2 \qquad e^4 = \sin\psi \sin\theta_1 d\phi_2 + \cos\psi d\theta_2 \tag{3.65}$$

$$e^5 = d\psi + cos\theta_1 d\phi_1 + cos\theta_2 d\phi_2. \tag{3.66}$$

Then the metric is diagonal

$$ds^2_{M^\sharp} = dr^2 + r^2 \left[\frac{1}{9}(g^5)^2 + \frac{1}{6} \sum_{j=1}^{4} (g^j)^2 \right]. \tag{3.67}$$

The conical singularity is at $r = 0$, and the base metric is

$$ds^2_{T^{1,1}} = \frac{1}{9}(g^5)^2 + \frac{1}{6} \sum_{j=1}^{4} (g^j)^2. \tag{3.68}$$

3.4.2 The Deformed Conifold

To get to the deformed conifold from the singular conifold we begin in w^i coordinates and replace the cone equation (3.43) with

$$\sum_{A=1}^{4} (w^A)^2 = \epsilon^2 \tag{3.69}$$

for some $\epsilon \in \mathbb{R}$. The base is $T^{1,1}$ as before. Decomposing w^i into real and imaginary parts we get

$$\vec{x} \cdot \vec{x} + \vec{y} \cdot \vec{y} = r^2 \tag{3.70}$$

$$\vec{x} \cdot \vec{x} - \vec{y} \cdot \vec{y} = \epsilon^2. \tag{3.71}$$

For $r > \epsilon$, the surfaces $r = const.$ are $S^3 \times S^2$. But the surface $r = \epsilon$ is just an S^3 of non-zero radius, because the S^2 has shrunk to zero radius. We can continously range to $\epsilon = 0$ and reach the singular conifold.

Klebanov-Strassler [129] gave the metric for the deformed conifold. We have coordinates on the deformed conifold $(\tau, g^1, g^2, g^3, g^4, g^5)$, where τ is a radial coordinate (different to r for the singular conifold) and the g^i are as above. The metric is

$$\begin{aligned} ds_D^2 = \frac{1}{2}\epsilon^{4/3} K(\tau) \Bigg\{ & \frac{1}{3K(\tau)^3}[d\tau^2 + (g^5)^2] + \cosh^2(\tau)[(g^3)^2 + (g^4)^2] \\ & + \sinh^2(\tau)[(g^1)^2 + (g^2)^2] \Bigg\} \\ \text{where } K(\tau) = & \frac{(\sinh(2\tau) - 2\tau)^{1/3}}{2^{1/3}\sinh(\tau)}. \end{aligned} \tag{3.72}$$

For large τ we can introduce a new radial coordinate r via

$$r^2 \equiv \frac{3}{2^{5/3}}\epsilon^{4/3} e^{2\tau/3} \tag{3.73}$$

and then the metric tends to

$$ds_D^2 \to dr^2 + r^2 ds_{T^{1,1}}^2 \text{ for large } \tau. \tag{3.74}$$

But in the $\tau \to 0$ limit, the angular part of the metric degenerates to the metric of a round metric on S^3

$$d\Omega_{S^3}^2 = \frac{\epsilon^{4/3} 2^{1/3}}{3^{1/3} 8} \left[\frac{1}{2}(g^5)^2 + (g^3)^2 + (g^4)^2 \right], \tag{3.75}$$

and the other two angular directions, corresponding to the S^2 fibred over the S^3, shrink like τ^2.

Note that we can also use (A_i, B_j) coordinates on D, defined analagously to the singular conifold.

3.4.3 The Resolved Conifold

To get to the resolved conifold from the singular conifold $M^\sharp$, we begin in $(X, Y, U, V, \lambda_1, \lambda_2)$ coordinates, together with a condition similar to (3.49). The space is defined as

$$R = \left\{ (X, Y, U, V, \lambda_1, \lambda_2) \in \mathbb{C}^4 \times P\mathbb{C}^1 | \begin{pmatrix} X & U \\ V & Y \end{pmatrix} \begin{pmatrix} \lambda_1 \\ \lambda_2 \end{pmatrix} = 0, \text{ where } (\lambda_1, \lambda_2) \neq (0,0) \right\}. \tag{3.76}$$

Note that this space differs from the conifold, in that we now include $(X, Y, U, V, \lambda_1, \lambda_2) = (0, 0, 0, 0, \lambda_1, \lambda_2)$ as a legitimate region of our manifold. Indeed, in this region (λ_1, λ_2) can take any values, and so we have a whole S^2 here. Note, these coordinates for R are not global, and only work in patch e.g. where $\lambda_1 \neq 0$. In this patch the solution to (3.49) is

$$\begin{pmatrix} X & U \\ V & Y \end{pmatrix} = \begin{pmatrix} -U\alpha & U \\ -Y\alpha & Y \end{pmatrix} \tag{3.77}$$

$$\alpha = \frac{\lambda_2}{\lambda_1}\ , \tag{3.78}$$

which defines a 3-complex dimensional space (U, Y, α). It will be helpful to have an equivalent description of the resolved conifold in (A_i, B_j) coordinates, defined similarly to the singular conifold, but replacing (3.54) with

$$|A_1|^2 + |A_2|^2 - |B_1|^2 - |B_2|^2 = u^2 \tag{3.79}$$

where $u \in \mathbb{R}$ is known as the blow-up parameter. By taking $u \to 0$ we continuously recover the singular conifold.

The metric on the resolved conifold, R, in the 6 real coordinates $(r, \psi, \theta_1, \phi_1, \theta_2, \phi_2)$ (note we follow the convention that these coordinates have the same names as, but are distinct from, the singular conifold coordinates) [130, 131]

$$\begin{aligned} ds_R^2 = {} & \kappa^{-1}(r)dr^2 + \frac{1}{9}\kappa(r)r^2(d\psi + \cos\theta_1 d\phi_1 + \cos\theta_2 d\phi_2)^2 \\ & + \frac{1}{6}r^2(d\theta_1^2 + \sin^2\theta_1 d\phi_1^2) + \frac{1}{6}(r^2 + 6u^2)(d\theta_2^2 + \sin^2\theta_2 d\phi_2^2) \\ \text{where } \kappa(r) = {} & \frac{r^2 + 9u^2}{r^2 + 6u^2}. \end{aligned}$$

Again, in the large r limit the metric will asymptote to the large r limit of the singular conifold. But as $r \to 0$ in R, we see that the S^3 shrinks to zero size, and we are left with an S^2 of radius u.

We see that we can follow a continous path in the moduli space of non-compact

CY's from the non-singular deformed conifold to the topologically distinct resolved conifold by passing through the singular conifold.

3.4.4 Gauge/Gravity Correspondence

Conifolds are important in the *Gauge/Gravity Correspondence*, providing further insight to the AdS/CFT correspondence. For this reason they have been well studied in string theory constructions. Before we get on to cosmological applications of conifolds, we'll review their importance for the gauge/gravity correspondence. Conifold geometries help to generalize notions from the original $AdS_5 \times S^5$/CFT correspondence [132]. We are interested in compactifying on certain CY spaces Y_6. Since we know the explicit metric on the conifold, which we view as a cone over the base $X_5 = T^{1,1}$, we may wish to know about the gauge/gravity correspondence on spaces like $AdS_5 \times X_5$. This was done in [129, 130, 133, 134].

Original $AdS_5 \times S^5$/CFT

Consider a stack of N D3 branes placed in 10D Minkowski space. The stack sources a non-trivial background solution for type IIB supergravity. In the string frame, the geometry is given by the warped metric

$$ds^2 = \mathcal{H}^{-1/2}(r)\eta_{\mu\nu}dx^\mu dx^\nu + \mathcal{H}^{1/2}(r)(dr^2 + r^2 d\Omega_5^2) \tag{3.80}$$

with warp factor

$$\mathcal{H}(r) = 1 + \frac{L^4}{r^4} \tag{3.81}$$

$$\text{where } L^4 = 4\pi g_s N \alpha'^2 \tag{3.82}$$

$$= 4\pi g_s N \alpha'^2 \frac{\pi^3}{\text{vol}(\text{S}^5)}. \tag{3.83}$$

Taking the $r \to 0$ limit the metric becomes, with $z = L^2/r$,

$$ds^2 = \frac{L^2}{z^2}(-dt^2 + d\vec{x}^2 + dz^2) + L^2 d\Omega_5^2. \tag{3.84}$$

This is $AdS_5 \times S^5$, with AdS_5 and S^5 each of radius L. The continous global symmetry group of $AdS_5 \times S^5$ is $SO(2,4) \times SU(4)$.

The $r \to 0$ limit of type IIB supergravity (SUGRA) on $AdS_5 \times S^5$ corresponds to the low energy limit of a *dual gauge theory*. This dual gauge theory is $\mathcal{N} = 4$ Super-Yang-Mills (SYM) in 4D flat space, with gauge group $SU(N)$. Note that this is a superconformal field theory (SCFT). It is the low energy limit of the gauge theory living on the worldvolume of the stack of N D3's. The $SU(N)$ gauge theory living on

the brane must have $\mathcal{N} = 4$ Poincaré SUSY as D3-branes are $\frac{1}{2}$-BPS, and so break half the total number of SUSY's. The YM coupling is related to the string coupling via $g_{YM} = g_s^{1/2}$. The continuous global symmetry of the CFT has maximal bosonic subgroup $SO(2,4) \times SU(4)_R$, which matches the continuous global symmetry group of the gravity side.

If we change the S^5 to some $X_5 \neq S^5$ we will break some of the $SU(4)$ symmetry. The gauge theory dual to $AdS_5 \times X_5$ must then include some breaking of the $SU(4)_R$ symmetry.

Operators in the CFT are mapped to SUGRA modes through a matching of the scaling dimension of the operator to the mass of the KK mode from compactifying the SUGRA mode on S^5.

Changing the S^5 to $T^{1,1}$

Now we change the setup slightly, following [133, 134]. We place the stack of N D3's at a conical singularity in the 6D internal space, which we take to be the singular conifold $M^\sharp$, a cone over the base $T^{1,1}$ which has continuous global symmetry group $SU(2) \times SU(2) \times U(1)$.

The gauge/gravity correspondence then becomes the conjecture that IIB SUGRA on $AdS_5 \times T^{1,1}$ is dual to the low energy limit of the worldvolume gauge theory on the D3-branes placed at the singularity. The warped metric sourced by the stack placed at the conical singularity is

$$ds^2 = \mathcal{H}^{-1/2}(r)\eta_{\mu\nu}dx^\mu dx^\nu + \mathcal{H}^{1/2}(r)(dr^2 + r^2 ds^2_{T^{1,1}}) \tag{3.85}$$

$$\mathcal{H}(r) = 1 + \frac{L^4_{T^{1,1}}}{r^4} \tag{3.86}$$

$$L^4_{T^{1,1}} = 4\pi g_s N \alpha'^2 \frac{\pi^3}{\mathrm{vol}(T^{1,1})} \tag{3.87}$$

$$= 4\pi g_s N \alpha'^2 \frac{27}{16} \text{ for the singular conifold.} \tag{3.88}$$

More generally, a warped metric of the form

$$ds^2 = \mathcal{H}^{-1/2}(r)\eta_{\mu\nu}dx^\mu dx^\nu + \mathcal{H}^{1/2}(r)(dr^2 + r^2 ds^2_{X_5}) \tag{3.89}$$

is called a *warped throat geometry*, where the throat is a cone over X_5.

Going back to $X_5 = T^{1,1}$, and taking again the $r \to 0$ limit (close to the branes, and so close to the singularity) the metric becomes,

$$ds^2 = L^2_{T^{1,1}} \left(\frac{1}{z^2}(-dt^2 + d\vec{x}^2 + dz^2) + ds^2_{T^{1,1}} \right) \tag{3.90}$$

with $z = L^2_{T^{1,1}}/r$. This is the metric on $AdS_5 \times T^{1,1}$ (which is unwarped as it's a direct product metric), with AdS_5 of radius $L_{T^{1,1}}$. Similarly to the S^5 case, this $r \to 0$ limit corresponds to the low energy limit of a dual gauge theory on the worldvolume of the D3's near the conical singularity. We highlight the $SU(2) \times SU(2) \times U(1)$ continuous global symmetry of $T^{1,1}$, most evident in the (A_i, B_j) coordinate description given by $W_{ij} = A_i B_j$ in (3.51).

In this scenario, since we have compactified on a (non-compact) CY, we retain only 1/4 of the original SUSY so that in the dual gauge theory there will only be $\mathcal{N} = 1$ SUSY in 4D. This dual gauge theory was constructed in [133]. It is an $\mathcal{N} = 1$ SCFT in $D = 4$, with continuous global symmetry group $SU(2) \times SU(2) \times U(1)_R$. It is an $SU(N) \times SU(N)$ gauge theory, coupled to:

- two chiral superfields $\tilde{A}_i, i = 1, 2$ in the $(\mathbf{N}, \bar{\mathbf{N}})$ rep of $SU(N) \times SU(N)$. These also transform as a doublet under one of the global $SU(2)$'s.
- and two chiral superfields $\tilde{B}_j, j = 1, 2$ in the $(\bar{\mathbf{N}}, \mathbf{N})$ rep of $SU(N) \times SU(N)$. These also transform as a doublet under the other global $SU(2)$.

These fields are written in a suggestive notation to compare to the dual supergravity coordinates (A_i, B_j). Under the $U(1)_R$ R-symmetry both $\tilde{A}_i, \tilde{B}_j$ have charge 1/2. Thus, the global continuous symmetries of the dual gauge theory and the supergravity description match.

This theory has a superpotential which is fixed up to normalization by the global $SU(2) \times SU(2) \times U(1)_R$ symmetry to be

$$W = \lambda_1 \epsilon^{ij} \epsilon^{kl} \mathrm{tr}(\tilde{A}_i \tilde{B}_k \tilde{A}_j \tilde{B}_l), \tag{3.91}$$

so that W has R-charge 2, as required for a superpotential.

To show that the classical field theory describes N D3-branes moving in the singular conifold geometry, we take the superfields to have diagonal expectation values

$$\langle \tilde{A}_i \rangle = \mathrm{diag}(a_i^{(1)}, ..., a_i^{(N)}) \qquad \langle \tilde{B}_j \rangle = \mathrm{diag}(b_j^{(1)}, ..., b_j^{(N)}). \tag{3.92}$$

These diagonal VEVS mean the F-term supergravity equations from the superpotential for a SUSY vacuum are automatically satisfied. Define the $4N$ complex coordinates

$$n_{ij}^{(r)} = a_i^{(r)} b_j^{(r)}, \text{ for } r = 1, ..., N \tag{3.93}$$

which, when subject to satisfying the D-term supergravity equations, and gauge invariance conditions, reduce to a system of $3N$ independent complex variables. For each r,

they satisfy

$$\det_{i,j} n_{ij}^{(r)} = 0 \tag{3.94}$$

which is the equation satisfied by complex coordinates on the singular conifold (3.46), with n_{ij}^r viewed as a collection of r coordinates W_{ij}^r on the singular conifold. So the $4N$ coordinates $n_{11}^{(r)}, n_{12}^{(r)}, n_{21}^{(r)}, n_{22}^{(r)}$, $r = 1, ..., N$ are naturally associated with the positions of the D3-branes on the conifold. For a stack we have just 3 complex coordinates

$$n_{ij}^r = \bar{n}_{ij} \text{ for all } r, \tag{3.95}$$

describing the position of the stack in the singular conifold.

Positioning the stack at the conical singularity $W_{ij} = 0$ corresponds to giving zero VEVs for the fields $\tilde{A}_i, \tilde{B}_j$. This leads to the precise conjecture that type IIB string theory on $AdS_5 \times T^{1,1}$, with N units of R-R flux through $T^{1,1}$ is equivalent to $SU(N) \times SU(N)$ gauge theory, with two copies of $(\mathbf{N}, \overline{\mathbf{N}}) \oplus (\overline{\mathbf{N}}, \mathbf{N})$, flowing to an IR fixed point, (which is the conformal theory, with zero VEVs for $\tilde{A}_i, \tilde{B}_j$), and then perturbing by the superpotential (3.91).

Deforming the Conifold

Here we outline the necessary steps in realizing the dual gauge theory to a supergravity solution with a warped metric involving the deformed conifold as the unwarped 6D internal space - following the work of [129].

- Begin with the *unwarped singular conifold* of Section 3.4.4 . The metric factorizes into an unwarped $AdS_5 \times T^{11}$ in the IR limit. On each side of the correspondence this involves:
  - Supergravity: placing N D3's at $r = 0$ on the singular conifold.
  - Gauge theory: No VEVs given to fields $\tilde{A}_i, \tilde{B}_j$. This is an $\mathcal{N} = 1$ $SU(N) \times SU(N)$ gauge theory, which is superconformal.
- Next consider the geometry of the *warped singular conifold*. The warped metric is $ds^2 = \mathcal{H}^{-1/2}(r) ds^2_{\mathbb{M}_4} + \mathcal{H}^{1/2}(r) ds^2_{M^\sharp}$. On each side of the correspondence this involves:
  - Supergravity: M fractional D3-branes placed at the conical singularity, $r = 0$, of the singular conifold, together with N D3's near, but not at, $r = 0$.
  - Gauge theory: Fields $\tilde{A}_i, \tilde{B}_j$ given diagonal VEVs, while $\det N_{ij} = 0$ still holds both classically and quantum mechanically. This is an $\mathcal{N} = 1$, $SU(M+N) \times SU(N)$ gauge theory which is no longer conformal as the superpotential

(3.91) is turned on. There is an *RG cascade* to an $SU(M+p) \times SU(p)$ gauge theory. The moduli space of such vacua is exactly $M^\sharp$.

- We now consider the geometry of the *warped deformed conifold* (WDC). The warped metric is $ds^2 = \mathcal{H}^{-1/2}(\tau) ds^2_{\mathbb{M}_4} + \mathcal{H}^{1/2}(\tau) ds^2_{DC}$, for the deformed conifold. On each side of the correspondence this involves:
  - Supergravity: We have M units of 5-form flux through the S^3 of the deformed conifold, and we've cascaded down to having only one D3-brane, which is at some position (A_i, B_j) in D.
  - Gauge theory: We have an $\mathcal{N} = 1$, $SU(M+1)$ gauge theory. The fields $\tilde{A}_i, \tilde{B}_j$ are given non-zero VEVs, corresponding to the position of the D3-brane on the SUGRA side. We have $\det N_{ij} = 0$ classically, but when we include quantum effects, there is chiral symmetry breaking which leads to $\det N_{ij} = \epsilon^2$, so that the moduli space of vacua is exactly the deformed conifold.

Resolving the Conifold

After seeing how the deformed conifold arises naturally in the gauge/gravity correspondence, we now look at the analogous picture for the resolved conifold, following the work of [130]. Here we outline the steps in realizing the dual gauge theory to a supergravity solution with a warped metric involving instead the resolved conifold as the unwarped 6D internal space.

- We begin with the unwarped singular conifold, just as in the deformed case.
- We again consider the geometry of a *warped singular conifold*, but this time without any fractional D3-branes. The warped metric is $ds^2 = \mathcal{H}^{-1/2}(r) ds^2_{\mathbb{M}_4} + \mathcal{H}^{1/2}(r) ds^2_{M^\sharp}$
  - Supergravity: In this case we just have a stack of N D3-branes near, but not at, $r = 0$, and no fractional D3-branes, as the resolved conifold doesn't support three-form flux, since the S^3 shrinks to zero size.
  - Gauge theory: The fields $\tilde{A}_i, \tilde{B}_j$ are given VEVs, but these are subject to the operator $\mathcal{U} \equiv \frac{1}{N} Tr(|\tilde{B}_1|^2 + |\tilde{B}_2|^2 - |\tilde{A}_1|^2 - |\tilde{A}_2|^2)$ having zero VEV, $\langle \mathcal{U} \rangle = 0$. The moduli space of these vacua is exactly the singular conifold $M^\sharp$.
- We now consider the geometry of the *warped resolved conifold* (WRC). The warped metric is $ds^2 = \mathcal{H}^{-1/2}(r, \theta) ds^2_{\mathbb{M}_4} + \mathcal{H}^{1/2}(r, \theta) ds^2_R$, for the resolved conifold R. On each side of the correspondence this involves

- Supergravity: We have a stack of N D3-branes's localized at any r on the resolved conifold. We can place them at the north pole of the finite-radius S^2 at $r = 0$. Since this chooses an angle on the S^2, we must now have angular dependence, as well as radial, in the Green's function associated to this source, and so there is angular dependence in the warp factor.
- Gauge theory: The fields $\tilde{A}_i, \tilde{B}_j$ are given VEVs and now we can have $\langle \mathcal{U} \rangle = u^2 \neq 0$. This u^2 is the resolution parameter of the resolved conifold. From this we see the moduli space of these vacua is exactly the resolved conifold.

Thus we have seen how the warped deformed conifold and the warped resolved conifold arise naturally in the gauge/gravity correspondence. This acts as motivation for investigating models of inflation from string theory compactified using these geometries, as we will do in Chapter 4.

3.5 String Inflation

In the previous sections of this chapter we have studied Calabi-Yau compactifications and their associated moduli, the stabilization of these moduli and mentioned how a de Sitter vacuum can be generated. These Calabi-Yau compactifications involve many moduli – scalar fields in four-dimensions, which, after stabilization have very complicated potentials and interactions.

This is to be contrasted with what we are intending to model - inflation - which, in it's simplest form requires a single field which is slowly-rolling requiring a single scalar field with a near-flat potential. It was originally hoped that one of the CY moduli may provide such a scalar field, but it is tricky to arrange for one of the fields to be the inflaton, while stabilizing the others, except for in contrived scenarios.

There are the following inflaton candidates from string theory

- *Brane moduli*: the positions of spacetime-filling branes in the internal 6D space can be moduli for the 4D effective theory. The positions can be time dependent, leading to FRW expansion. The branes feel a potential through interactions with other sources in the internal space. Controlling the brane potential to keep it flat enough is highly non-trivial. A large range of inflationary models can be produced from brane moduli.

- *Kähler moduli*: Here the inflaton is identified with time-dependent deformations of volumes of even-dimensional cycles in the CY. Promising models have lead to saddle-point inflation models.

- *Complex-structure moduli*: In type IIB, these are normally stabilized by flux compactifications, so don't provide a promising inflaton candidate. But in type

IIA string theory the complex-structure moduli may be more natural inflaton candidates.

- *Axions*: Compactifications lead to many axion fields, one of which could be a candidate for the inflaton. These can potentially give rise to large field inflation, with an observably large value for the tensor-to-scalar ratio.

The inflationary models derived from each of these candidates depends rather sensitively on the details of the construction, so there may not be an easy way to distinguish between these candidates observationally.

In this thesis we focus on using the brane moduli to give inflation. In the next chapter, Chapter 4, we will explicitly construct an original model of *natural inflation* coming from a brane moduli model. A complete review of inflation in string theory would require a lot more space – see the excellent book [29] for a more general presentation of string theory and inflation.

Before moving on to Chapter 4 we say a little more about axions for inflation. The discrete shift symmetry, due to non-perturbative quantum effects, constrains the axion Lagrangian to be schematically

$$L = -\frac{1}{2}f^2(\partial a)^2 - \Lambda^4\left[1-\cos(a)\right] + \cdots \tag{3.96}$$

where f is called the axion decay constant, with mass dimension one, and Λ is a mass scale, and higher terms contain higher-order terms in derivatives and from multi-instanton corrections which come exponentially suppressed. The canonically normalized field $\phi \equiv fa$ has periodicity $2\pi f$. Note that these axions can be used to produce *natural inflation* models from compactifications, mentioned in the previous chapter. The decay constant can be derived from dimensional reduction. For illustrative purposes, an unwarped symmetric toroidal compactification on a torus with lengthscale L produces (see for example, [29])

$$\frac{f^2}{M_p^2} \sim \frac{\alpha'^2}{L^4}. \tag{3.97}$$

We note that computational control requires the lengthscale of the compactified geometry, L, be much bigger than the string length, $L \gg l_s = \sqrt{\alpha'}$, so that the decay constant for these closed-string axions is much below the Planck scale. This has important observational consequences, in that a Planck scale f can generate a nearly observable level of gravitational waves. In Chapter 4 we will instead look at if a Planck scale f can be derived in a D-brane model of natural inflation.

3.6 The Weak Gravity Conjecture

In the final part of this section on the elements of string for inflation, we present original, unpublished work related to the Weak Gravity Conjecture.

The *Weak Gravity Conjecture* (WGC) [135] amounts to the statement that gravity is the weakest force in a theory of quantum gravity. The original arguments in favour of the conjecture relate to avoiding a zoo of stable black hole remnants. The original WGC involves 1-form gauge fields, and this can be generalized to p-form gauge fields via the *Generalized Weak Gravity Conjecture* (GWGC).

More precisely, the four-dimensional electric version of the GWGC states that there must exist a $(p-1)$-dimensional object, with tension T, which couples electrically to a p-form Abelian gauge field, with coupling g, such that

$$T \lesssim g M_p \tag{3.98}$$

where M_p is the four-dimensional reduced Planck mass. Interpreting this, it means that the electrostatic force between charged objects is stronger than the gravitational force – i.e. gravity is the weakest force in this sense.

The conjecture can be used to constrain string axion models of inflation, and the result (3.97) that we showed earlier, which bounds the decay constant of the axion derived as the integral of a p-form over a p-cycle, can be interpreted as a result due to the weak gravity conjecture. Here we demonstrate this following similar analyses to [136,137], extending these works to allow for warped compactifications. The motivation for the following computation is to see whether warping helps to avoid the weak gravity conjecture constraints on the decay constant for closed string axions. In [138], it was claimed that warping the weak gravity conjecture aids open-string D-brane models to achieve a super-Planckian decay constant. As we will find out, it doesn't help for the closed-string axions and the effects of warping cancel out in the computation. Below we present a short investigation into the effects of warping on the decay constant for closed-string axion models.

Consider a ten-dimensional spacetime $\mathcal{M}$ with coordinates X^M, $M = 0, ..., 9$, which splits into a four-dimensional spacetime, M_4, with coordinates x^μ, $\mu = 0, ..., 3$ and a six-dimensional space X_6 with coordinates y^m, $m = 4, ..., 9$.

The 10-dimensional metric takes the following warped form

$$ds_{10}^2 = G_{MN} dX^M dX^N = \mathcal{H}^{-1/2}(y) ds_{\text{FRW}}^2 + \mathcal{H}^{1/2}(y) ds_{\text{CY}}^2 \tag{3.99}$$

where the four-dimensional unwarped metric is FRW

$$ds_{\text{FRW}}^2 = \tilde{g}_{\mu\nu}^{\text{FRW}} dx^\mu dx^\nu = -dt^2 + a(t)^2 d\vec{x}^2 \tag{3.100}$$

and the six-dimensional unwarped CY metric is

$$ds^2_{\rm CY} = \tilde{g}_{mn} dy^m dy^n. \tag{3.101}$$

We denote the warped four-dimensional and warped six-dimensional metrics by $g^{\rm FRW}_{\mu\nu} \equiv \mathcal{H}^{-1/2}(y)\tilde{g}^{\rm FRW}_{\mu\nu}$ and $g_{mn} \equiv \mathcal{H}^{1/2}(y)\tilde{g}_{mn}$ respectively.

One can read off the reduced Planck mass as the coefficient sitting in front of the Einstein-Hilbert term in the type IIB bosonic supergravity action

$$S_{EH} = -\frac{1}{2\kappa^2_{10}} \int_{\mathcal{M}} d^{10}X \sqrt{-G} R_{10} = -\frac{M_p^2}{2} \int_{M_4} d^4x \sqrt{-g} R_4 \tag{3.102}$$

where

$$M_p^2 = \frac{1}{\kappa^2_{10}} \int_{X_6} d^6y \sqrt{\tilde{g}} \mathcal{H}(y) \tag{3.103}$$

with $\kappa^2_{10} = \frac{1}{2}(2\pi)^7(\alpha')^4 g_s^2$.

The original QCD axion is a pseudoscalar field which enjoys the continuous Peccei-Quinn shift symmetry $a \mapsto a + const.$ which is broken to a discrete shift symmetry $a \mapsto a + 2\pi$ by the effects of QCD instantons through a coupling of the axion to the QCD instantons (we follow the conventions of [137]).

We look at closed-string axions which arise in compactifications from integrating q-form gauge potentials over q-cycles, which we denote Σ_q, in the compact space X, as in [137]. The gauge symmetry lives on D$(3+q)$-branes extended along the four non-compact directions and wrapped around Σ_q in X. Decay constants for these axions have previously been analysed in an unwarped setting, and here we present results allowing for a warped compactification. In this section, we will denote the warp factor at the position of the D$(3+q)$-branes (assumed to be stationary) by h_0. Dimensional reduction of the bulk Einstein-Hilbert action gives the following expression for the reduced Planck mass

$$M_p^2 = \frac{1}{\kappa^2_{10}} \int_{X_6} d^6y \sqrt{\tilde{g}} h(y) \approx \frac{4\pi h_0 \tilde{V}_X}{l_s^8 g_s^2} \tag{3.104}$$

where we have approximated the warped volume by the warp factor evaluated at h_0 - assumed to be typical - multiplied by the unwarped volume of the six-dimensional space, $\tilde{V}_X$. In what follows we will assume X is a symmetric internal space, where R is a linear scale of X, so that $\tilde{V}_X = xR^6$, with x of order one, depending on the details of X.

In this setup, the axions enjoy a continuous shift symmetry $a \mapsto a + const.$ both classically and at the perturbative quantum level, but is broken to a discrete shift

symmetry $a \mapsto a + 2\pi$ by quantum non-perturbative instanton effects, giving rise to a periodic potential.

Here we present a computation of the decay constants from the ten-dimensional theory - an alternative is to deduce them from the effective Kähler potential of the dimensionally reduced four-dimensional theory.

The axions in the closed string sector arise from the NS-NS 2-form, B_2, and R-R q-forms, C_q, with indices along the internal directions of the wrapped q-cycle Σ_q. The R-R forms appear in the bulk supergravity action as

$$-\frac{2\pi}{l_s^{8-2q}} \int \frac{1}{2} F_{q+1} \wedge \star F_{q+1} + 2\pi \int C_q \tag{3.105}$$

where $F_{q+1} = dC_q$ and the NS-NS form appears in the bulk supergravity action with kinetic term

$$-\frac{2\pi}{g_s^2 l_s^4} \int d^{10}X \frac{1}{2} |dB_2|^2 \tag{3.106}$$

where we've followed the normalization of [137] so that our field strengths have integer periods. The conventional form fields are related to ours by $C_{q,conv} = l_s^q C_q$ and $B_{2,conv} = l_s^2 B_2$.

The four-dimensional axions, $b_\alpha(x)$ and $c_\alpha(x)$, are then given via the associated phases $2\pi \int_{\Sigma_2} B_2$ and $2\pi \int_{\Sigma_q} C_q$, through the expansions

$$B_2 = \frac{1}{2\pi} \sum_\alpha b_\alpha(x) \omega_\alpha(y) \qquad\qquad C_q = \frac{1}{2\pi} \sum_\alpha c_\alpha(x) \omega_\alpha(y) \tag{3.107}$$

where ω_α are a basis for the cohomology class $H^q(X, \mathbb{Z})$ such that $\int_{Q_\alpha} \omega_\beta = \delta_{\alpha\beta}$, with Q_α being a basis for the homology class $H_q(X, \mathbb{Z})$, with $\alpha = 1, ..., \dim(H_q(X, \mathbb{Z}))$, where $q = 2$ for the b-axions.

We'll focus for now on the c-axions, with the b-axion decay constant, f_b, related to the c-axion decay constant, f_c, by $f_c^2 = g_s^2 f_b^2$ for $q = 2$.

Upon dimensional reduction one finds the $c_\alpha(x)$ axion kinetic action

$$S_c = -\frac{1}{2} \frac{1}{2\pi l_s^{8-2q}} \sum_{\alpha,\beta} \int_X \omega_\alpha \wedge *_6(\omega_\beta) \int d^4x \sqrt{g_{\text{FRW}}} g^{\mu\nu}_{\text{FRW}} \partial_\mu c_\alpha \partial_\nu c_\beta \tag{3.108}$$

We now insert the relevant warp factors. We begin with the term

$$\int_X \omega_\alpha \wedge *_6(\omega_\beta) \sim \int_X \sqrt{\left(h_0^{1/2}\right)^6} \left(h_0^{-1/2}\right)^q \omega_\alpha \wedge \tilde{*}_6(\omega_\beta) \tag{3.109}$$

$$\sim h_0^{3/2-q/2} x R^{6-2q} \tag{3.110}$$

where in the first line we included warp factors coming from the determinant and q factors of the inverse metric that appear in the Hodge dual (note that $*_6$ is the Hodge dual with respect to the warped six-dimensional metric, $\tilde{*}_6$ is the Hodge dual with respect to the unwarped six-dimensional metric), and in the second line we assumed that the warp factor is roughly constant over X, and used that $\tilde{V}_X = xR^6$. The four-dimensional integral part gives

$$\int d^4x\sqrt{g_{\rm FRW}}g^{\mu\nu}_{\rm FRW}\partial_\mu c_\alpha\partial_\nu c_\beta = h_0^{-1/2}\int d^4x\sqrt{\tilde{g}_{\rm FRW}}\tilde{g}^{\mu\nu}_{\rm FRW}\partial_\mu c_\alpha\partial_\nu c_\beta \tag{3.111}$$

so that for a typical c-axion

$$S_c \sim -\frac{1}{2}\frac{h_0^{1-q/2}xR^{6-2q}}{2\pi l_s^{8-2q}}\int d^4x\sqrt{\tilde{g}_{\rm FRW}}\tilde{g}^{\mu\nu}_{\rm FRW}\partial_\mu c\partial_\nu c \tag{3.112}$$

so that the axion decay constant is

$$f_c^2 = \frac{h_0^{1-q/2}xR^{6-2q}}{2\pi l_s^{8-2q}} \tag{3.113}$$

and the ratio with the Planck mass is

$$\frac{f_c^2}{M_p^2} = \frac{g_s^2 h_0^{-q/2}}{2\pi}\left(\frac{l_s}{R}\right)^{2q}. \tag{3.114}$$

For the supergravity approximation to be valid, one needs that $R > l_s$. We can see from this that if $q > 0$, the right hand side can be large if the value of h_0 is small enough.

We now consider the breaking of the continuous shift symmetry, coming from the corresponding q-form gauge invariances of the ten-dimensional theory, to discrete shift symmetries by non-perturbative instanton effects.

We here give a brief summary of instantons relevant for our purposes. Instantons appear in four-dimensional gauge theories as classical solutions to the Euclidean equations of motion, obeying the self-duality condition $\star_4 F = F$, and are labelled by an integer called the instanton number $n = \frac{1}{8\pi^2}\int \mathrm{tr}\ F\wedge F$. Because of the self duality, the classical action for a gauge n-instanton is $S_{\mathrm{cl},n} = 8\pi^2 n/g^2 = nS_{\mathrm{cl},1}$ for gauge coupling g. This classical solution to the Euclidean equations of motion gives a strength $e^{-S_{\mathrm{cl},n}}$ to the tunneling process in the Lorentzian theory.

For concreteness we focus here on the NS-NS two-form, B_2, which is coupled to a worldsheet instanton (where the string worldsheet wraps a topologically non-trivial 2-cycle Σ_2). The n-instanton sector generates a potential for the axion, in which the continuous shift symmetry is spontaneously broken to a discrete shift symmetry, with

the potential including terms proportional to the strength

$$e^{-S_{\mathrm{cl},n}} = \exp\left(-\frac{2\pi n}{l_s^2}\int_{\Sigma_2}(J + il_s^2 B_2)\right) \tag{3.115}$$

where $J = ig_{i\bar{j}}dz^i \wedge d\bar{z}^{\bar{j}}$ is the Kähler form. This combination of J and B_2 appears because this is the complexified Kähler form with our convention for the normalization of B_2. Now we use that $\int_{\Sigma_2} J = h_0^{1/2}\tilde{V}_{\Sigma_2}$, with $\tilde{V}_{\Sigma_2}$ the unwarped volume of the 2-cycle, giving

$$e^{-S_{\mathrm{cl},n}} = \exp\left(-\frac{2\pi n h_0^{1/2}\tilde{V}_{\Sigma_2}}{l_s^2}\right)\exp\left(-inb\right) \tag{3.116}$$

where for simplicity we've dropped the α label and just written a single axion b. Here one can see that for $n = 1$, b is now periodic with period 2π. At level n, the potential develops substructure on scale $2\pi/n$. For the canonical field $\phi_b \equiv f_b b$, the potential is periodic with period $2\pi f_b/n$. Because of the exponential suppression, only terms with $n \lesssim n_{\mathrm{max,b}}$ contribute, where

$$n_{\mathrm{max,b}} \equiv \frac{l_s^2}{2\pi h_0^{1/2}\tilde{V}_{\Sigma_2}}. \tag{3.117}$$

We now assume that $\tilde{V}_{\Sigma_2} \sim R^2$, where R was a linear scale of X, i.e. that the 2-cycle has the same parametric lengthscale as the enveloping space X. We now drop factors of 2π since we are working parametrically. We use (3.114) with $f_c^2 = g_s^2 f_b^2$ for $q = 2$ to write R/l_s in terms of f_b/M_p, to give

$$n_{\mathrm{max,b}} \sim \frac{f_b}{M_p} \tag{3.118}$$

independently of h_0. Thus the potential for ϕ_b has substructure on scale $2\pi f_b/n_{\mathrm{max,b}} \sim 2\pi M_p$.

We now note two things. Firstly, even if $f_b > M_p$, the substructure for the canonical field is still $2\pi M_p$. Secondly, it wasn't obvious, but this is independent of the warping. Warping doesn't help to make the field range larger than M_p, once instanton effects have been taken into account.

For the c-axions a similar cancellation in warp factors occurs. This time there are Euclidean Dq-branes wrapping non-trivial $q+1$-cycles, n times, with strength

$$e^{-S_{\mathrm{cl},n}} = \exp\left(-nT_q\int_{\Sigma_{q+1}} d^{q+1}x\sqrt{\det g|_{\Sigma_{q+1}}}\right)\exp\left(-nig_sT_q\int_{\Sigma_{q+1}} C_{q+1}\right). \tag{3.119}$$

The first factor contributes up to

$$n_{\rm max,c} \sim \frac{g_s l_s^q}{h_0^{q/4} \tilde{V}_{\Sigma_q}} \tag{3.120}$$

We now assume that $\tilde{V}_{\Sigma_q} \sim R^q$, where R was a linear scale of X, i.e. that the q-cycle has the same parametric lengthscale as the enveloping space X. We use (3.114) to write R/l_s in terms of f_c/M_p to give

$$n_{\rm max,c} \sim \frac{f_c}{M_p} \tag{3.121}$$

which again is independent of h_0, and the factors of g_s have cancelled out to give an answer analogous to the b-axion. Thus the potential for $\phi_c = f_c c$ has substructure on scale $2\pi f_c/n_{\rm max,c} \sim 2\pi M_p$. This same result holds for any q. For $q = 2$ we see the same result for C_2 as B_2, which is a consequence of $SL(2,\mathbb{Z})$ symmetry of type IIB string theory [136].

To conclude, for closed-string axions warping does not help to alleviate the issue of obtaining a potential which is flat on super-Planckian scales, due to instanton effects.

We now ask if this result can be interpreted in terms of the Weak Gravity Conjecture (WGC), allowing for warping. The four-dimensional Generalized Weak Gravity Conjecture (GWGC) states that there must be a $(p-1)$-dimensional object, with tension T, which couples electrically to a p-form Abelian gauge field, with coupling g, such that

$$T \lesssim g M_p \tag{3.122}$$

where M_p is the four-dimensional reduced Planck mass.

In our case, we have a 0-form gauge field, which is the axion, and it couples to a (-1)-dimensional object, an instanton, which has tension given by the instanton action $T = S_{\rm cl,1}$. The coupling can be read off from dimensionally reducing the Chern-Simons term in the D$(3+q)$-brane action

$$2\pi \int_{W_{3+q}} C_q \wedge \frac{{\rm tr} F \wedge F}{8\pi^2} = \sum_\alpha \frac{1}{f_{c,\alpha}} \int_{\Sigma_Q} \omega_\alpha \int_{M_4} \frac{\phi_{c,\alpha} {\rm tr} F \wedge F}{8\pi^2} \tag{3.123}$$

where C_q is the background R-R form and F is the worldvolume gauge field strength, and where W_{3+q} is the $4+q$-dimensional brane worldvolume and M_4 is the four-dimensional spacetime. Dropping the α subscript, we see that for the canonical ϕ_c, the coupling is $1/f_c$. The GWGC is then

$$S_{\rm cl,1} \lesssim \frac{M_p}{f_c}. \tag{3.124}$$

If we want to be able to ignore instanton contributions to the potential, then we require a large instanton action $S_{\text{cl},1} \gg 1$. The GWGC then implies that $f_c/M_p \ll 1$.

Conversely, if you want $f_c/M_p \gg 1$, then the GWGC implies you must have a very small instanton action, and so there will be contributions to the potential from the instanton effects. The scale of variation at level n is $\Lambda = 2\pi f_c/n$, which comes with a factor $e^{-S_{\text{cl},n}} = e^{-nS_{\text{cl},1}}$, and so we must keep up to level $n \sim S_{\text{cl},1}^{-1}$, which by the GWGC is $n \gtrsim f_c/M_p$, leading to variation scale $\Lambda \lesssim 2\pi M_p$, i.e. the potential is no longer flat on the scale $2\pi f_c$, instead there is variation on scale $\Lambda \lesssim 2\pi M_p$.

Note finally that the warping didn't come into the GWGC argument anywhere, as we found out in the explicit computation.

In the next chapter, Chapter 4, we will investigate whether a Planckian decay constant can arise in a warped compactification using a d-brane as the inflaton, rather than an axion.

Chapter 4

D-branes in the Warped Resolved Conifold

4.1 Introduction

This chapter contains material from Kenton & Thomas [1], titled *D-brane Potentials in the Warped Resolved Conifold and Natural Inflation*, done in collaboration with my supervisor, Steven Thomas.

In this chapter we investigate a model of natural inflation from string theory, which can produce a value of the tensor-to-scalar ratio which may be observable by near-future experiments.

The natural inflation model comes with a Planckian decay constant, which is unusual compared to many other string theory models of natural inflation, in which a closed string axion comes with a sub-Planckian decay constant.

Since publication of these results there has been a lot of interest in this work – most notably [138] which builds on our findings and attempts to interpret them in terms of the Weak Gravity Conjecture.

Our model requires the investigation of D-brane dynamics in the background of the warped resolved conifold (WRC) throat approximation of Type IIB string compactifications on Calabi-Yau manifolds. When we glue the throat to a compact bulk Calabi-Yau, we generate a D-brane potential which is a solution to the Laplace equation on the resolved conifold. We can exactly solve this equation, including dependence on the angular coordinates. The solutions are valid down to the tip of the resolved conifold, which is not the case for the more commonly used deformed conifold. This allows us to exploit the effect of the warping, which is strongest at the tip.

The inflationary model occurs near the tip, using an angular coordinate of a D5-brane in the WRC which has a discrete shift symmetry, and feels a cosine potential, giving us a model of natural inflation. A Planckian decay constant is achieved whilst

maintaining control over the backreaction. This is because the decay constant for a wrapped brane contains powers of the warp factor, and so can be made large, while the wrapping parameter can be kept small enough so that backreaction is under control.

In Section 4.2 we consider a compactification of the six extra dimensions on the warped resolved conifold.

In Section 4.3 we apply our string theory compactification to a model of natural inflation [8, 139–141]. In contrast to many previous studies of natural inflation from a controlled string theory, we are able to achieve a Planckian decay constant. This is because our axion is an open string modulus - a D-brane position modulus - rather than a closed string axion formed from integrating a p-form over a p-cycle.

As mentioned in detail in Chapter 3, Calabi-Yau compactifications involve many closed string moduli, including complex structure moduli, Kähler moduli and the axiodilaton. It was originally hoped that one of these closed string moduli may provide a candidate scalar field for inflation. In Type IIB supergravity, the complex structure moduli and the axiodilaton can be stabilized classically via flux compactifications [109], which involve a warped spacetime. The Kähler moduli are not stabilized classically and are instead fixed by quantum perturbative and non-perturbative effects [142], [143].

In general it's difficult to stabilize all the closed string moduli, while maintaining a flat potential for just one or two of them, in order to give a simple inflationary model. A more promising approach is to stabilize all the closed string moduli and then inflate using open string brane moduli, arising from spacetime-filling branes whose coordinates within the internal 6D space are moduli for the 4D effective theory [144]. The branes feel a potential through interactions with other sources in the internal space. The warping helps to keep the brane potential flat, which is desired for inflation.

Here we briefly summarise the sections on conifolds in Chapter 3. In order to study the dynamics of branes in warped spacetimes, we require the metric on the internal unwarped 6D Calabi-Yau space. However, no explicit metric is known on any global compact Calabi-Yau space. The best we can do is to approximate the Calabi-Yau by a noncompact throat region, which is Ricci flat and Kähler, and on which we know the metric. We can then cut off the throat at a finite length and glue it on to a compact bulk Calabi-Yau, on which the metric is unknown. Research is constricted to obtaining inflation from D-branes confined to the warped throat region, where the metric is known. The singular conifold (SC) is one example of a Ricci flat, Kähler throat on which the metric is known [145]. The SC lives at a singular point within the moduli space of Calabi-Yau manifolds. It is a cone over a $T^{1,1} \equiv [SU(2) \times SU(2)]/U(1)$ base, and so it contains a conical singularity at its tip (not to be confused with the singular point within the moduli space). We can smooth out this conical singularity in two topologically distinct ways, whilst preserving the Ricci flat and Kähler conditions, leading to the deformed conifold (DC) and the resolved conifold (RC). The DC and

RC are both noncompact, and the metric is known explicitly in each case [145–149] and [150].

The DC is the usual choice when one is interested in stabilizing the closed string moduli and inflating within the *same* throat, because the DC can support a non-trivial (2,1)-form flux which can stabilize the complex structure moduli and the axiodilaton while preserving supersymmetry [111, 143]. This flux is also responsible for the warping of the full 10D solution, known as the warped deformed conifold (WDC) [149]. The DC has been used for previous examples of brane inflation in a warped throat, for example [142].

The RC, on the other hand can't support topologically non-trivial (2,1)-form flux. This means the complex structure moduli and axiodilaton can't be stabilized in the same manner as the DC. Indeed, the RC on its own has no complex structure moduli to stabilize, and so it is no surprise that the flux mechanism used to stabilize the complex structure modulus of the DC is not suitable here[5]. However, we can still produce a warped 10D spacetime by placing a stack of N D3-branes at the tip of the RC, extended along the 4 noncompact spacetime directions. The resulting 10D spacetime is called the warped resolved conifold[6] (WRC) [150, 155].

In this chapter we do not explicitly address the issue of closed string moduli stabilization. Instead, we assume that these are stabilized by some mechanism at a higher energy scale, decoupled from the open string brane moduli, which remain light. This allows us to investigate the inflationary dynamics from branes in the WRC.

This assumption does not seem so strange when one remembers that the throat region is only an approximation to a fully compactified Calabi-Yau manifold. Multi-throat scenarios have been considered in which different throats are attached to different parts of the bulk Calabi-Yau [156–160]. One of these other throats could support fluxes and or other mechanisms to stabilize the closed string moduli at a high energy scale. An additional warped throat may be necessary to embed the standard model, and another to uplift to a dS vacuum. With this multi-throat picture in mind, we assume an RC throat in which inflation occurs, and allow for other throats in which fluxes may be present which stabilize the complex structure moduli. It is beyond the scope of this thesis to investigate closed string moduli stabilization in the WRC - we focus instead on the cosmological phenomenology of inflation in the WRC.

In Section 4.3, we model the inflaton as one of the angular coordinates of a probe wrapped D5-brane moving within the tip region of the WRC. This angular coordinate

[5] The authors of [151] have analysed SUSY breaking ISD (1,2) fluxes on the RC, which are allowed if Poincare duality is broken either through non-compactness or through having a compact but non-CY manifold. It would be interesting to see if this work can be extended to the case of the WRC which we are considering.

[6] This is not to be confused with the similarly named *resolved warped deformed conifolds* of [152, 153] based on the work of [154].

is periodic, and so has a shift symmetry, appearing in the brane potential inside a cosine. Once rescaled to have canonical kinetic terms, it appears with a decay constant, set by the choice of D-brane. In this way, we find a model of natural inflation from string theory. In taking a path in field space along the angular direction, we evade the Baumann-McAllister bound which limits the field range, and hence the tensor-to-scalar ratio, when the motion is only in the radial direction [161].

Finally, it should be noted that this work has a more general context beyond its application to the model of natural inflation presented in Section 4.3. The authors of [110, 162–165] have developed a systematic programme investigating the various corrections to the D-brane potential, corresponding to the potential on the Coulomb branch of the dual gauge theory, for perturbations of the Lagrangian. This includes various compactification effects, such as the deformation of the throat from gluing it to the bulk, the inclusion of IASD fluxes and a finite 4D curvature. The approach makes use of perturbative expansions around a Calabi-Yau background, requiring knowledge of the eigenfunctions of the Laplace operator on the unperturbed, unwarped Calabi-Yau background. Since the WDC has been extensively studied for moduli stabilization, the DC geometry was used to derive explicit expressions for the D-brane potential.

However, the eigenfunctions of the Laplace operator on the DC are only known in the region well away from the tip of the DC. Interestingly, exact analytic solutions to the Laplace equation on the RC are known. In contrast to the DC case, these solutions are valid anywhere within the RC [155]. Thus by studying the WRC we are able to provide a new explicit example of the general formalism developed in [110, 162–165], which extends deeper into the IR. Thus, aside from inflationary applications, we believe studying D-brane dynamics in the WRC geometry is an interesting new avenue to explore from the perspective of the holographic dual gauge theory.

This chapter is structured as follows. In Section 4.2 we review the supergravity background arising from flux compactifications of 10D Type IIB string theory, focussing on the various sources that can contribute to the D-brane potential. We also introduce the geometry of the WRC. In Section 4.3 we apply this to produce a natural inflation model from a D-brane in the WRC. We find that for the simple case of a D3-brane it's not possible to obtain a Planckian decay constant. Indeed, in the WDC case, it was shown in [166] that one can generate a Planckian decay constant from a large number of D3-branes, but the backreaction effects cannot then be ignored. By considering instead a wrapped D5-brane with flux we find that we can choose parameters such that the decay constant is Planckian, while the backreaction remains small. We conclude in Section 4.4 and provide scope for future research. We gather more technical aspects, such as estimations of the backreaction in Appendix A.1 and corrections to the potential coming from the 4D Ricci scalar in Appendix A.2.

4.2 D-brane Potential in the Warped Resolved Conifold

As we have stated already, we don't know the explicit metric on any smooth compact Calabi-Yau in 3 complex dimensions. One way forward is to approximate a region of the fully compactified manifold with a section of a noncompact throat, which satisfies the Ricci flat and Kähler condition, upon which we know the metric. We then cut off this noncompact throat and glue it onto a bulk compact Calabi-Yau producing a fully compactified geometry. If we assume that the physics we're interested in is localised within the throat region then we have access to an explicitly known metric. We can try to quantify the effects of the gluing procedure via perturbative expansions, assuming the gluing region is suitably far away.

The moduli space of Calabi-Yau threefolds has curvature singularities called conifold singularities. The space associated to the conifold singularity is known as *the singular conifold* (SC) [145], which is a cone over the coset space $T^{1,1}$. On the plus side, it's Ricci flat and Kähler, and we know the explicit metric on it. However, it's noncompact and has a conical singularity at the tip, $r = 0$. There are two topologically distinct ways of removing the conical singularity of the SC, while preserving the Ricci flat and Kähler conditions, arriving at *the deformed conifold* (DC) [149] and *the resolved conifold* (RC) [150], [155]. For each of these, the metric is explicitly known. These are all noncompact, and must be truncated and glued to a bulk compact Calabi-Yau, as discussed in Section 4.2.

We often speak of a warped throat spacetime, which is a 10D warped spacetime (3.27) involving a noncompact throat as the unwarped 6D space, $\tilde{Y}_6$, which can be approximated by a cone over some X_5 base in the large r limit. These throats are a general family which include the SC, the DC and the RC.

We will take the internal unwarped 6D manifold to be the RC, using the coordinates $y^m = (r, \psi, \theta_1, \phi_1, \theta_2, \phi_2)$ in which the metric takes the form [150]

$$\begin{aligned} ds^2_{\text{RC}} = \tilde{g}_{mn} dy^m dy^n =& \kappa^{-1}(r) dr^2 + \frac{1}{9}\kappa(r) r^2 (d\psi + \cos\theta_1 d\phi_1 + \cos\theta_2 d\phi_2)^2 \\ &+ \frac{1}{6} r^2 (d\theta_1^2 + \sin^2\theta_1 d\phi_1^2) + \frac{1}{6}(r^2 + 6u^2)(d\theta_2^2 + \sin^2\theta_2 d\phi_2^2), \end{aligned} \tag{4.1}$$

with

$$\kappa(r) = \frac{r^2 + 9u^2}{r^2 + 6u^2}. \tag{4.2}$$

Here u is called the *resolution parameter*, which has dimensions of length. This naturally defines a dimensionless radial coordinate $\rho \equiv r/(3u)$. As $r \to 0$ the second and third parts of (4.1) vanish, corresponding to a shrinking S^3 with coordinates (ψ, θ_1, ϕ_1),

leaving an S^2 with coordinates (θ_2, ϕ_2) of radius u.

One can consider the 10D geometry sourced by placing a stack of N D3-branes extended along the noncompact 4 spacetime dimensions, appearing pointlike localized at the north pole, $\theta_2 = 0$, of the S^2 at the tip of the RC [155]. The resulting geometry is a warped spacetime called the warped resolved conifold (WRC), with 10D metric [150], [155]

$$ds^2 = \mathcal{H}^{-1/2}(\rho, \theta_2) ds^2_{\text{FRW}} + \mathcal{H}^{1/2}(\rho, \theta_2) ds^2_{RC} \tag{4.3}$$

where we have taken the 4D spacetime to be FRW, for our cosmological application, and the 6D unwarped space is the RC.

The warp factor, $\mathcal{H}(\rho, \theta_2)$, is the solution to the Green's function equation for the Laplace operator on the RC. An exact expression for the WRC warp factor is [155]

$$\mathcal{H}(\rho, \theta_2) = (L_{T^{1,1}}/3u)^4 \sum_{l=0}^{\infty} (2l+1) H_l^A(\rho) P_l[cos(\theta_2)], \tag{4.4}$$

with the $T^{1,1}$ lengthscale set by $L^4_{T^{1,1}} = (27/4)\pi N g_s l_s^4$. The P_l are the Legendre polynomials, and the radial functions $H_l^A(\rho)$ are given in terms of the ${}_2F_1(a, b, c; z)$ hypergeoemetric functions as

$$H_l^A(\rho) = \frac{2\tilde{C}_\beta}{\rho^{2+2\beta}} \, {}_2F_1(\beta, 1+\beta, 1+2\beta; -1/\rho^2) \tag{4.5}$$

$$\text{where } \tilde{C}_\beta = \frac{\Gamma(1+\beta)^2}{\Gamma(1+2\beta)}, \qquad \beta = \sqrt{1 + (3/2) l(l+1)}. \tag{4.6}$$

Since localizing the stack at the north pole specifies an angle, the warp factor must now have both angular and radial dependence - whereas the warp factors only depend on the radial coordinate in the case where the internal geometry is the SC or the DC, and is an assumption usually made for generic warped throats. This motivates us to explore branes moving in the angular directions within the WRC, where the warping also acts in the angular direction.

The gauge gravity correspondence for a stack of D-branes near a conical singularity of a cone over an X_5 base was investigated in generality in [167] where strings on $AdS_5 \times X_5$ correspond to a certain dual $\mathcal{N} = 1$ gauge theory. Theories where the stack of D-branes are localized at a point on the resolution of an orbifold have also been considered, for example in [168] for $\mathbb{C}^3/\mathbb{Z}_3$.

The WRC has been investigated from the point of view of the gauge gravity correspondence in [155], which found the dual gauge theory living on the stack to be a 4D $\mathcal{N} = 1$, $SU(N) \times SU(N)$ gauge theory coupled to two chiral superfields $A_i, i = 1, 2$ in the $(\mathbf{N}, \overline{\mathbf{N}})$ representation of $SU(N) \times SU(N)$; and two chiral superfields $B_j, j = 1, 2$

in the $(\overline{\mathbf{N}}, \mathbf{N})$ representation of $SU(N) \times SU(N)$. The fields A_i, B_j are given VEVs such that the operator

$$\mathcal{U} \equiv \frac{1}{N} Tr(|B_1|^2 + |B_2|^2 - |A_1|^2 - |A_2|^2) \tag{4.7}$$

has VEV $\langle \mathcal{U} \rangle = u^2$. The moduli space of these vacua has exactly the geometry of the RC, with resolution parameter u.

Gluing a Warped Throat to a Bulk Calabi-Yau

For model building purposes we first take the noncompact limit, with an infinitely long warped throat. This gives an imaginary self-dual (ISD) flux solution, defined by $G_- = 0$ and $\Phi_- = 0$. However, note that a 10D geometry with an infinitely long warped throat does not lead to 4D dynamical gravity, as M_p is infinite.

To remedy this, we cut off the warped throat at some large radial distance r_{UV}, and glue it to a compact bulk Calabi-Yau. The metric on the bulk is not known, but the metric on the warped throat is explicitly known for certain warped throats, such as the SC, the DC and the RC. For this reason we try to get inflation to occur within the warped throat. Although this may not be generic, it allows us to do calculations. Perturbations of Φ_- arise as a result of this gluing procedure and are solutions to the Poisson equation (3.33), written in terms of the warp factor as

$$\tilde{\nabla}^2 \Phi_- = \mathcal{R}_4 + \frac{\mathcal{H}^{-2}}{6\mathrm{Im}\tau} |G_-|^2 + \mathcal{H} |\partial \Phi_-|^2 + 2\kappa_{10}^2 \mathcal{H}^{-1/2} (J^{\mathrm{loc}} - T_3 \rho_3^{\mathrm{loc}}). \tag{4.8}$$

We will assume that the gluing will induce corrections of $\mathcal{O}(\delta)$ to Φ_-, for some small δ, and we assume corrections to G_- are of the same order. We will assume also that the local terms don't contribute at this order. The G_- and Φ_- terms appear on the RHS of (4.8) at second order in δ, so that the leading order perturbation of Φ_- in the large throat limit is a solution to the homogeneous Laplace equation, so we denote it with subscript h,

$$\tilde{\nabla}^2 \Phi_h = 0. \tag{4.9}$$

This distinguishes it from Φ_- which is the full solution to the Poisson equation arising when we consider the effect of a non-negligible $\mathcal{R}_4$, where the leading order correction to $\Phi_- = 0$ from the gluing is given by

$$\tilde{\nabla}^2 \Phi_- = \mathcal{R}_4 \tag{4.10}$$

so that Φ_- includes Φ_h, but also the particular solutions to the Poisson equation.

The solutions of (4.9) and (4.10) will depend on the unwarped internal 6D geometry.

In this part of the thesis we consider solutions to the Laplace equation (4.9) for the DC and the RC geometry respectively. In Appendix A.2 we consider solutions to the Poisson equation (4.10) for the RC.

Gluing the Deformed Conifold

Unfortunately, the exact solutions to the Laplace equation (4.9) are not known for the deformed conifold. Progress has only been made in the mid-throat region [164] , $r_{\rm IR} \ll r \ll r_{UV}$, where the geometry approximates that of the singular conifold, with the 10D metric approaching $AdS_5 \times T^{1,1}$.

We can expand the solution in terms of the eigenfunctions $Y_L(Z_i)$ of the 5D Laplacian on $T^{1,1}$ as

$$\Phi_h(y) = \sum_L \Phi_L(r) Y_L(Z_i) \tag{4.11}$$

where Z_i are the angular coordinates on $T^{1,1}$. Here, the multi-index $L \equiv (l_1, m_1, l_2, m_2, R)$, labels the $SU(2)_1 \times SU(2)_2 \times U(1)_R$ quantum numbers under the corresponding isometries of $T^{1,1}$.

But the equation for the radial part, $\Phi_L(r)$, has no known analytic solution for the DC, and can only be solved numerically [169]. Limited to the mid-throat region, Φ_h can be expanded in powers of $r/r_{\rm UV}$ as [165]

$$\Phi_h(r, Z_i) \approx \sum_L c_L \left(\frac{r}{r_{\rm UV}}\right)^{\Delta(L)} Y_L(Z_i) \tag{4.12}$$

$$\text{where } \Delta(L) \equiv -2 + \sqrt{6[l_1(l_1+1) + l_2(l_2+1) - R^2/8] + 4} \tag{4.13}$$

where c_L are constant coefficients.

The lowest value of $\Delta(L)$ will give the leading contributions for $r < r_{\rm UV}$. The lowest value is $\Delta(L) = 3/2$, for $L = (1/2, 1/2, 1/2, 1/2, 1)$ [164]. But the $U(1)_R$ symmetry of $T^{1,1}$ is broken in the DC to a discrete $\mathbb{Z}_2$, so only modes with $R = 0$ are allowed, forbidding the $\Delta(L) = 3/2$ mode. The next smallest mode, $\Delta(L) = 2$, for $L = (1, 0, 0, 0, 0)$ or $L = (0, 0, 1, 0, 0)$ is allowed, and comes with an angular term $Y_L \sim \cos\theta_i$. This mode was analyzed in [170] in the DBI limit.

The coefficients c_L appearing in (4.12) are undetermined, apart from their small size. The authors of [171], [172] have taken a statistical approach to investigating warped D3-brane inflation in this approximation. For example, [172] explores the parameter space spanned by the first 12 c_L coefficients and determining the success/failure of the model in each case. However, a flat field space metric was used instead of a curved conifold metric which was corrected for in [173] and appeared in a corrected version of [172]. This statistical approach has been restricted to the mid-throat region of the

singular conifold, but could also be applied to the RC geometry we consider in this work, with the benefit of not being restricted to lie in the mid-throat region.

Gluing the Resolved Conifold

For the RC we can again expand Φ_h in the $Y_L(Z_i)$, but in this case the radial part of the Laplace equation can be solved exactly on the resolved conifold in terms of hypergeometric functions [155], which was not the case for the DC.

In this work, we are interested in probing the tip of the WRC, so we focus on solutions of the Laplace equation which are invariant under the $SU(2)_1 \times U(1)_\psi$ which rotates the (θ_1, ϕ_1) and ψ coordinates of the shrinking S^3 which has zero radius at the tip[7]. This leaves us (ρ, θ_2, ϕ_2), from which we now drop the subscripts.

There are two particular independent solutions to the radial part of the Laplace equation on the RC, invariant under the $SU(2)_1 \times U(1)_\psi$. They are $H_l^A(\rho)$, given in (4.5), and $H_l^B(\rho)$, given by

$$H_l^B(\rho) = {}_2F_1(1-\beta, 1+\beta, 2; -\rho^2). \tag{4.14}$$

The most general solution to the Laplace equation with the given isometries is

$$\Phi_h(\rho, \theta, \phi) = \sum_{l=0}^{\infty} \sum_{m=-l}^{m=l} [a_l H_l^A(\rho) + b_l H_l^B(\rho)] Y_{lm}(\theta, \phi). \tag{4.15}$$

This solution is valid *anywhere* within the WRC throat, in particular near the tip. This is a much better situation compared to the WDC, where the solution is only valid in the mid-throat region. The coefficients are undetermined, yet small, $a_l, b_l = \mathcal{O}(\delta)$.

For completeness, we give the asymptotics of the two radial functions $H_l^A(\rho)$ and $H_l^B(\rho)$ [155]

$$\begin{aligned} \frac{2}{\rho^2} + 4\beta^2 \log\rho + \mathcal{O}(1) \quad &\overset{0\leftarrow\rho}{\longleftarrow} \quad H_l^A(\rho) \quad \overset{\rho\to\infty}{\longrightarrow} \quad \frac{2\tilde{C}_\beta}{\rho^{2+2\beta}} \\ \mathcal{O}(1) \quad &\overset{0\leftarrow\rho}{\longleftarrow} \quad H_l^B(\rho) \quad \overset{\rho\to\infty}{\longrightarrow} \quad \mathcal{O}(\rho^{-2+2\beta}). \end{aligned} \tag{4.16}$$

In Appendix A.2 we will consider solutions to the Poisson equation (4.10) on the RC, which gives corrections to Φ_- in the limit of a finite but large throat.

[7] It should be emphasised there is no particular reason other than simplicity in focussing on solutions with the given isometries. We focus on dynamics at the tip, as this is new analytic territory compared to that available for the WDC. Note that studying dynamics along the whole throat is calculable in the WRC but we leave this interesting problem to a future investigation.

Moduli Stabilization

Previous studies [109], [143], [142] have stabilized the complex-structure moduli and axiodilaton using the DC as the internal 6D unwarped metric. The DC has Hodge numbers $h^{2,1} = 1, h^{1,1} = 0$ [174] so there is only one complex-structure modulus to stabilize – the deformation parameter of the deformed conifold, z. Since $h^{2,1} = 1$, one can turn on primitive $(2,1)$-form fluxes which preserve $\mathcal{N} = 1$ SUSY. The third betti number is $b_3 = 2+2h^{2,1} = 4$, so there are 4 non-trivial 3-cycles in the DC. One of these, the A-cycle, is associated to the finite size S^3 at the DC tip. There is an associated 3-cycle, B, which intersects this A-cycle exactly once.

One can then choose to turn on the following quantized $(2,1)$-form fluxes through the A, B cycles

$$\frac{1}{2\pi\alpha'}\int_A F_3 = 2\pi M \qquad \text{and} \qquad \frac{1}{2\pi\alpha'}\int_B H_3 = -2\pi K. \tag{4.17}$$

These fluxes allow for the superpotential to be written in terms of z. Since SUSY is preserved, one can minimize the scalar potential by imposing $D_z W = 0$ which stabilizes z, by solving $D_z W = 0$ for z. In the noncompact DC, the axiodilaton is not fixed by the superpotential - instead it is frozen in the Klebanov-Strassler solution.

In the noncompact DC limit, with an infinitely long throat, the DC B-cycle degenerates to infinite size. When the DC is cut off and glued to a compact bulk Calabi-Yau, the B-cycle becomes finite. The gluing will generically increase $h^{2,1}$ for the entire manifold, meaning there are more complex-structure moduli to stabilize. Assuming one can first stabilize z near the conifold point $z = 0$, the additional complex-structure moduli can be stabilized while preserving $\mathcal{N} = 1$ supersymmetry using the superpotential generated by the fluxes. In this compact case, the axiodilaton is no longer frozen, as in the KS solution. It is now fixed by including $(2,1)$-form fluxes over the remaining two 3-cycles distinct from A and B. This contributes to W, and one can then impose $D_\tau W = 0$, near $z = 0$ and solve for τ, which preserves $\mathcal{N} = 1$ SUSY [109].

The RC on the other hand has Hodge numbers $h^{2,1} = 0, h^{1,1} = 1$ [174] so there are no complex-structure moduli to stabilize, instead there is a single Kähler modulus, the resolution parameter u. Since $h^{2,1} = 0$, there are no cohomologically nontrivial closed $(2,1)$-forms, so one can't turn on fluxes which preserve $\mathcal{N} = 1$ SUSY. The third betti number is $b_3 = 2 + 2h^{2,1} = 2$, so there are 2 non-trivial 3-cycles in the RC, on which $(3,0)$-form fluxes could be turned on, and these would classically fix the axiodilaton. However, these fluxes will break $\mathcal{N} = 1$ SUSY, and so the equation determining the vev of the axiodilaton would be obtained by minimizing the full scalar potential, rather than just solving $D_\tau W = 0$. It would be interesting to compare the energy scale at which SUSY would need to be broken to fix the axiodilaton in this way, compared to the energy scale at which SUSY is broken when uplifting to a dS mimimum, as in [143].

The Kähler modulus u would need to be stabilized by non-perturbative effects, [142]. This may also fix the axiodilaton, without the need for breaking SUSY. It is outside the scope of this thesis, but it would be interesting to investigate in future work at what value u is fixed at, and its possible mixing with the open string brane moduli.

When the compact case is considered, the bulk Calabi-Yau may have a different topology, allowing for $h^{2,1} > 0$, and so SUSY preserving primitive $(2,1)$-form fluxes may be turned on, stabilizing the additional complex-structure moduli and the axiodilaton.

Indeed, there have been multi-throat scenarios proposed, [156], in which the standard model is required to be situated in a seperate throat to that where inflation occurs, and to where the anti-branes, which end inflation, are located. Since this scenario allows for these extra throats, it doesn't seem too much to ask that there is another warped throat in the compactification, perhaps a WDC throat, which allows stabilization of the complex-structure moduli. Perhaps it's too much to hope that one throat will be able to do everything: stabilize, inflate, produce the standard model and give a dS vacuum.

In addition, it has been suggested that there might be a mild hierarchy between the scales at which the closed string moduli and open string moduli are stabilized, so that the two problems are approximately decoupled [175]. This serves as motivation for us to investigate brane inflation in the WRC.

4.3 Natural Inflation Model

4.3.1 Preview

In this section we produce a model of natural inflation using a D-brane in the WRC geometry, which has a Planckian decay constant, meaning it can give a value for the tensor-to-scalar ratio which is possibly large enough for future surveys to find, which for the purpose of this chapter we take to be 0.1. Although the model may appear contrived, the point is that it is a proof-of-concept model, which provides a counterexample to the claim that all string theory models predict an unobservably small value of the tensor-to-scalar ratio.

In more detail, we are interested in modelling inflation using the open string moduli arising as the coordinates of a probe D-brane within the WRC geometry, which are scalar fields of the 4D effective theory. The probe approximation means ignoring any backreaction coming from the mobile brane, onto the WRC supergravity background, which is itself sourced by the stack of N D3-branes at the north pole of the S^2 at the tip of the RC. Note that N must be large for the SUGRA solution to be valid, so that for a single probe D3-brane, the backreaction should be negligable. The backreaction for a probe D5-brane is discussed in Appendix A.1.

In the original warped throat models of inflation, motion in the angular directions is assumed stabilized before inflation begins, with inflation occurring along a radial path. But the Baumann-McAllister (BM) bound implies a stringent upper bound on the scalar-to-tensor ratio r for motion along the radial path [161]. In this work we instead look to inflate along the angular direction θ_2, where the BM bound no longer restricts r, as pointed out in [176].

Indeed, contrary to the WSC and WDC, the simplest form of the warp factor for the WRC has dependence on both ρ and θ_2, so for the WRC one might expect interesting motion in the ρ and θ_2 directions. More general models can be considered where the brane also moves in the other directions - we defer this more complicated study to future investigation.

Brane motion in both the radial and one angular direction of the WDC was considered in [170,177–180], however, the majority of the trajectory was in the radial direction. This was done in the DBI limit, where the brane motion is ultrarelativstic. Studies of brane inflation with multiple fields were considered more generally in [176, 181, 182].

In this work, we will instead show that for a suitable choice of coefficients in the homogeneous solution Φ_h in (4.15), ρ rapidly approaches a minimum value near the tip of the WRC. The brane then follows a path in the angular direction θ_2 down to the minimum of the potential[8]. It is the latter motion which will generate the 50-60 e-folds of inflation. We can set the initial conditions to be such that we begin at the minimum in the radial direction and just off to the side of the maximum of the potential in the θ_2 direction, which we now relabel as $\theta_2 \equiv \theta$, without ambiguity.

Using this setup we will construct an explicit original model of *natural inflation* [8, 139–141] i.e. an inflationary model for the inflaton σ, with the potential

$$V(\sigma) = \Lambda^4 \left[1 + \cos\left(\frac{\sigma}{f}\right)\right]. \tag{4.18}$$

The observationally favoured values for the number of e-foldings N, the scalar spectral tilt n_s, together with a value for the tensor-to-scalar ratio r which may be large enough to be observed in the near future are given by the parameter choice of energy scale $\Lambda = M_{\rm GUT} \approx 10^{16}$GeV and decay constant $f \sim m_p \sim 5M_p \approx 1.2 \times 10^{19}$GeV, for m_p the Planck mass, and M_p the reduced Planck Mass [141] .

We will derive a potential of the form (4.18) by considering brane potentials of the general form

$$V = \frac{M_p^2}{4}\Big\{\varphi(y) + \lambda\left[\overline{\Phi}_-(y) + \Phi_h(y)\right]\Big\} \tag{4.19}$$

[8] We shall see that with this choice of coefficients, the potential is flat along the other 4 angular directions and so we can choose to set these anglular fields to zero.

where $\varphi(y)$, λ, $\overline{\Phi}_-(y)$ and $\Phi_h(y)$ depend on the choice of probe D-brane. The term $\varphi(y)$ arises from the noncancellation of DBI and Chern-Simons (CS) terms in the slow roll limit, and also includes any constants independent of the brane position which contribute to the 4D energy density. The $\Phi_h(y)$ term is the nonconstant solution to the homogeneous Laplace equation on the RC. The $\overline{\Phi}_-(y)$ term is the inhomogeneous part of the solution to the Poisson equation, present only when considering corrections from the Ricci scalar. This is explained in more detail in Appendix A.2. The factor of λ is a constant which depends on the choice of probe D-brane.

The $\Phi_h(y)$ term is independent of the choice of probe brane, and one can freely choose the coefficients of independent solutions of the Laplace equation. We choose to keep two independent solutions to the Laplace equation, but this is by no means a unique choice. It is motivated only by our aim of reaching a potential related to the natural inflation potential.

One solution we keep is non-normalizable for large ρ, with charges

$$L = (l_1, m_1, l_2, m_2, R) = (0, 0, 1, 0, 0) \tag{4.20}$$

which is present for the choice of non-zero b_1, and takes the form

$$H_1^B = \frac{3}{2}(3\rho^2 + 2)\cos\theta. \tag{4.21}$$

This term is desirable because of its cosine term. Our model will take the inflaton field σ to be the canonical scalar field Θ, proportional to the angular coordinate θ. The normalisation of Θ in terms of θ will determine f in (4.18), and depends on the choice of probe D-brane.

We will also keep one mode which is normalizable for large ρ, with charges

$$L = (l_1, m_1, l_2, m_2, R) = (0, 0, 0, 0, 0) \tag{4.22}$$

which is present for nonzero a_0, and takes the form

$$H_0^A = \frac{1}{\rho^2} - \log\left(\frac{1}{\rho^2} + 1\right). \tag{4.23}$$

Taking $a_0 > 0$ gives a large positive contribution near $\rho = 0$. Thus, our choice of coefficients leads to the homogeneous solution to the Laplace equation on the RC, Φ_h, given by

$$\Phi_h = \frac{a_0}{\rho^2} - a_0 \log\left(\frac{1}{\rho^2} + 1\right) + \frac{3}{2} b_1 \left(3\rho^2 + 2\right) \cos\left(\frac{\Theta}{5M_p}\right). \tag{4.24}$$

In Subsection 4.3.2, we consider a probe D3-brane. This has $\lambda = 4T_3/M_p^2$, and a

constant $\varphi(\rho) = V_0$. This is because the DBI and CS terms exactly cancel in the slow roll limit for a D3, but other sources contribute to the 4D energy density to give the constant V_0. This constant sources a mass term, $\overline{\Phi}_- \sim m^2\rho^2$ at leading order in small ρ, when one includes the $\mathcal{R}_4$ contribution [110]. This mass term, when combined with the large positive wall from the H_0^A term will give a radial minimum at small ρ.

In Subsection 4.3.3, we consider a probe wrapped D5-brane with electric flux turned on in the wrapped directions. In this case, $\varphi(\rho)$ is not constant, and depends on ρ quadratically, $\varphi(\rho) \sim \rho^2$. This arises from the non-cancellation of the DBI and CS terms in the slow roll expansion of the action. This ρ^2 term will again give a radial minimum at small ρ when combined with the large positive contribution for small ρ from the H_0^A term. In Appendix A.2 we show that $\varphi(\rho) \sim \rho^2$ sources a quartic term in $\overline{\Phi}_-$, with a large positive coefficient. However, this quartic term is subleading in the small ρ limit.

Our work differs from previous works deriving natural inflation from closed string axions in string theory, which arise from integration of a p-form over a p-cycle in the compact space, see Section 3.6. For these closed string axions, a periodic potential can arise in the 4D effective theory when the continuous axion shift symmetry is spontaneously broken to a discrete shift symmetry, due to nonperturbative effects arising from worldsheet instantons or Euclidean D-brane instantons. The decay constant for each closed string axion is set by the kinetic terms, which depend on the type of axion used. However, these decay constants turn out to be generically sub-Planckian, by looking at the kinetic terms for these axions and relating them to the compactification volume, and hence the Planck mass, together with the validity of the α' expansion [136,137,183].

It should be noted that although one can't generically obtain a Planckian decay constant for a single closed string axion from a controlled string theory, there may be additional structure which allows one to obtain a Planckian effective decay constant. For example, in *Aligned Natural Inflation* [184, 185], the extra structure involves two interacting closed string axions with sub-Planckian decay constants, which after a suitable amount of fine tuning aligns to produce a direction in axion field space which has a Planckian effective decay constant. Further extensions to more than two axions were investigated in [186]. Embedding axion alignment in string theory was recently explored in [187], using gaugino condensation on magnetized or multiply-wound D7-branes, however closed string moduli stabilization was not addressed in this model. In [188], moduli stabilization was included in both KKLT and LVS regimes, with non perturbative effects in the superpotential used to produce the alignment, or the alternative *Hierarchical Axion Inflation* [189]. Another embedding of Aligned Natural Inflation in IIB orientifolds was discussed in [190], using C_0 and C_2 R-R axions in the LVS regime.

A separate model, *N-flation* [191], motivated by *Assisted Inflation* [12], and similar

proposals [192–194], use many light non-interacting closed string axions which contribute to one effective axion direction with a Planckian effective decay constant. The masses of the axions can be made hierarchically lighter than the Kähler moduli [195]. However, the large number of axions requried [196] can renormalize the Planck mass, spoiling the achievement of a Planckian decay constant. N-flation and Aligned Natural Inflation can be combined as in [197–199].

Axion Monodromy Inflation encompasses a related class of models which achieve large field inflation from closed string axions in specific brane backgrounds from string theory and F-theory. The brane backgrounds explicitly break the axionic shift symmetry of the potential, giving rise to monodromy [183, 200–205]. Inflation can continue through many cycles of the axion field space, with an effective field range which is much larger than the original period of the axion, giving large field inflation. However, the axion monodromy models generically suffer from a large backreaction problem, coming from a large D3-brane charge and/or backreaction from the branes themselves [206]. These backreaction difficulties are alleviated when the monodromy mechanism is combined with the idea of alignment, in a model known as *Dante's Inferno*, where the inflaton takes a gradual spiral path in 2D axion field space [207]. Alternative monodromy models use D7-brane position moduli with a shift symmetry broken by a flux superpotential [208], or the Ignoble Approach of [209] where the axion mixes with a topological 4-form field strength to produce the monodromy. Possible embeddings of natural inflation in supergravity were investigated recently in [210]. A review of axion inflation in the Planck era is given in [211].

Our natural inflation model doesn't use any of the above closed string axions as the inflaton, and so a Planckian decay constant is not ruled out *a priori*. Our inflaton is instead an open string modulus, identified with the position of the brane in an angular direction on the RC. It has a discrete shift symmetry, which is set by the internal geometry, with the decay constant set by the normalization of the kinetic term. Thus, our model shares more similarity to models of spinflation [170]. However, we also differ from the setup of [170], because we explore the use of the RC rather than the DC geometry. Also, we use a probe wrapped D5-brane with flux, rather than a probe D3-brane without flux, and we probe the tip rather than the mid-throat region. The combination of these choices allows us to select a Planckian decay constant, which we then check is suitable for a controlled supergravity approximation, and doesn't produce a large backreaction.

In previous work, inflation from a brane moving in an angular direction was found to be rather ineffective [170, 171, 178]. In these models the initial conditions were such that the brane starts far from the tip and where the major contribution to the number of e-folds was from the radial motion towards the tip. However, in our model we make a different choice of initial conditions, such that the brane begins at the tip and due to

the steep potential in the radial direction, experiences no motion in the radial direction. All of the inflationary e-folds occur along the angular direction. The flatness in the angular direction is a result of the choices of initial radial position (bringing a large warp factor), the use of a wrapped D5-brane (rather than a D3-brane) and turning on 2-form flux through the wrapped dimensions of the brane (allowing for a nonzero CS potential from the gluing to a bulk Calabi-Yau).

4.3.2 D3-brane in the WRC

To begin, we review how the potential, V, felt by a single slowly moving probe D3-brane in a warped throat geometry is related to Φ_- via $V = V_0 + T_3\Phi_-$ [162].

Consider a probe D3-brane, with worldvolume coordinates χ^a extended along the four noncompact directions, M_4. The action has contributions from the DBI term and the Chern-Simons term

$$S_{D3} = -T_3 \int_{M_4} d^4\chi \sqrt{-\det(P_4[g_{MN} + B_{MN} + 2\pi\alpha' F_{MN}])} + T_3 \int_{M_4} P_4[C_4] \tag{4.25}$$

where P_4 is the pullback of the brane worldvolume to M_4. We assume 4D isotropy and homogeneity, relevant for cosmological spacetimes, meaning we should consider time-dependent internal coordinates $y^m(t)$. Substituting a general warped 10D metric g_{MN} of the form (3.27)

$$ds^2 = \mathcal{H}^{-1/2}(y) g^{\text{FRW}}_{\mu\nu} dx^\mu dx^\nu + \mathcal{H}^{1/2}(y)\tilde{g}_{mn} dy^m dy^n \tag{4.26}$$

together with the ansatz (3.28) for C_4 and taking $B_2 = 0 = F_2$ gives the effective 4D Lagrangian density

$$\mathcal{L} = -T_3 \mathcal{H}^{-1}(y)\sqrt{1 - \mathcal{H}(y)\tilde{g}_{mn}\dot{y}^m\dot{y}^n} + T_3\alpha(y). \tag{4.27}$$

For slowly rolling fields, we can expand the square root in (4.27), to give

$$\mathcal{L} \approx \frac{1}{2} T_3\, \tilde{g}_{mn}\dot{y}^m\dot{y}^n - V(y) \tag{4.28}$$

where the D3-brane potential $V(y)$ will be

$$V(y) = V_0 + T_3(\mathcal{H}^{-1}(y) - \alpha(y)) = V_0 + T_3\Phi_-. \tag{4.29}$$

Here V_0 is a constant extracted from Φ_-, since Φ_- as defined in (3.33) is invariant under constant shifts, so that now Φ_- doesn't include a constant term. For an exact ISD solution, $\Phi_- = 0$, and so the D3-brane feels no potential in this slow roll limit. The leading order potential then comes from the $\mathcal{O}(\delta)$ corrections to Φ_- coming from

the gluing of the warped throat to the bulk Calabi-Yau.

The other regime, in which the brane is moving relativistically, is called DBI inflation. In this case, the motion is constrained by the causal speed limit, set by the positivity inside the square root in (4.27). This can lead to inflation, even if the potential is steep, because of the noncanonical kinetic terms. In this work we only consider the slowly rolling regime, and defer investigation of the DBI limit to a future investigation.

Natural Inflation from a D3-brane?

In this section we show our first attempt at realising natural inflation using a slow rolling D3-brane probe. We will find that we can't have a Planckian decay constant in a consistent manner. In Subsection 4.3.3 where we consider a probe wrapped D5-brane with flux, we'll find instead that we can consistently choose a Planckian decay constant.

Consider the WRC metric restricted to the (ρ, θ) subspace

$$ds^2 = u^2 \left[9 \left(\frac{\rho^2 + 2/3}{\rho^2 + 1} \right) d\rho^2 + \left(\frac{3}{2}\rho^2 + 1 \right) d\theta^2 \right]. \tag{4.30}$$

Now we make a coordinate transformation to canonical coordinates (Z, Θ), so that the kinetic terms appearing in the D3-brane slow roll Lagrangian (4.27) will be canonical

$$\frac{1}{2} T_3 \, \tilde{g}_{mn} \dot{y}^m \dot{y}^n \approx \frac{1}{2} T_3 u^2 \left[9 \left(\frac{\rho^2 + 2/3}{\rho^2 + 1} \right) \dot{\rho}^2 + \left(\frac{3}{2}\rho^2 + 1 \right) \dot{\theta}^2 \right] \tag{4.31}$$

$$= \frac{1}{2}\dot{Z}^2 + \frac{1}{2}\dot{\Theta}^2. \tag{4.32}$$

In the small ρ limit, near the tip, the desired coordinates are given by

$$\rho = \frac{1}{u\sqrt{6T_3}} Z \tag{4.33}$$

$$\theta = \frac{1}{u\sqrt{T_3}} \Theta. \tag{4.34}$$

We now examine the potential (4.19) for the D3-brane, with our choice of homoegenous solutions to the Laplace equation, in terms of these canonical coordinates. It is

$$\begin{aligned} V(Z, \Theta) = V_0 + T_3 \Bigg[& \frac{m^2 Z^2}{6u^2 T_3} + \frac{2a_0 u^2 T_3}{3Z^2} - a_0 \log\left(1 + \frac{2u^2 T_3}{3Z^2} \right) \\ & + \frac{3b_1}{4} \left(4 + \frac{9Z^2}{u^2 T_3} \right) \cos\left(\frac{\Theta}{u\sqrt{T_3}} \right) \Bigg]. \end{aligned} \tag{4.35}$$

This will have a stable minimum in Z at Z_{min}. If inflation begins at Z close to Z_{min} and sufficiently off to the side of the ridge along the Θ direction, the motion will be

mostly in the Θ direction. We then identify $f = u\sqrt{T_3}$ for a D3-brane.

We now investigate whether one can arrange for the decay constant $f = u\sqrt{T_3}$ to be of order $5M_p$. Note that in our conventions, $T_3 = [(2\pi)^3 g_s l_s^4]^{-1}$, and $\kappa_{10} = \frac{1}{2}(2\pi)^4 g_s l_s^4$. We require

$$25M_p^2 = u^2 T_3 = \frac{u^2}{(2\pi)^3 g_s l_s^4}, \tag{4.36}$$

but we also have that the reduced Planck mass is related to the warped volume of the Calabi-Yau by $M_p^2 = V_6^w \kappa_{10}^{-2}$. We take the throat length to be $r_{\rm UV} \gg r_{\rm min}$. Throughout the region $r_{\rm min} \ll r < r_{\rm UV}$, the space is approximately $AdS_5 \times T^{1,1}$ and the warp factor goes like $\mathcal{H} \sim L^4_{T^{1,1}}/\rho^4$, where $L^4_{T^{1,1}} = (27/4)\pi g_s N l_s^4$. Under the assumption that $V^w_{throat} \gtrsim V^w_{bulk}$, we get

$$M_p^2 \gtrsim \kappa_{10}^{-2} \mathrm{vol}(T^{1,1}) \int_{r_{\rm min}}^{r_{\rm UV}} y^5 \mathcal{H}(y) dy \approx \frac{N r_{\rm UV}^2}{2(2\pi)^4 g_s l_s^4}. \tag{4.37}$$

Near the tip of the WRC the Planck mass receives a contribution

$$\frac{N r_{\rm min}^2}{g_s l_s^4}, \tag{4.38}$$

which will only contribute to (4.37) by multiplication of an order one factor for $r_{\rm min} \lesssim r_{\rm UV}/50$. This is because in the small ρ part of the WRC throat, where we are near to the N D3-branes, the space is locally $AdS_5 \times S^5$ and the warp factor is $\mathcal{H} \sim L^4_{S^5}/y^4$, now with y the distance to the North Pole, where the N D3's are located.

In order to match (4.36) to (4.37) we must take the throat length $r_{\rm UV}$ to be

$$r_{\rm UV}^2 \approx \frac{4\pi u^2}{25N} \ll u^2, \text{ for large } N \gg 1. \tag{4.39}$$

But u is the natural length scale of the RC. To have the length of the throat $r_{\rm UV}$ hierarchically smaller than u seems unnatural, since we assumed a very long throat for the noncompact limit, and also for the M_p approximation coming mainly from the throat. It seems we can't consistently choose $f = 5M_p$ for a D3-brane.

Finally, for a later comparison with the D5-brane case, we note that turning on a constant electric flux of $\epsilon < 1$ on the D3-brane gives a factor $(1-\epsilon^2)^{1/2}$ in front of the DBI part of the action, with the CS part of the D3 action left unchanged. This leads to a non-cancellation of the inverse warp factor, and so the following potential term appears

$$V = T_3 \left[(1-\epsilon^2)^{1/2} - 1 \right] \mathcal{H}^{-1}. \tag{4.40}$$

But we note that this comes with a negative sign, and so acts to destabilize the overall potential, making it unsuitable for achieving a stable minimum in Z. In the D5-brane case, this non-cancellation will come with the opposite sign, as then the flux appears in the CS action.

4.3.3 Wrapped D5-brane in the WRC

In this section we'll find that for the probe wrapped D5-brane with flux, we can obtain $f \approx 5M_p$, corresponding to $r = 0.1$, within the long throat approximation. In this case the non-cancellation of the DBI and CS terms works to our advantage, giving a quadratic term in the potential with a positive coefficient.

We consider the same WRC background but this time we place a probe D5-brane in it, with 4 of it's dimensions extended along the 4 noncompact spacetime directions and wrap the remaining two spatial dimensions around a 2-cycle Σ_2 inside the compact space p times. We also turn on an F_2 flux on the D5-brane through Σ_2.

The action for the p-wrapped D5-brane with worldvolume coordinates ξ^α and worldvolume W_5 is

$$S_{D5} = S_{DBI-D5} + S_{CS-D5} \tag{4.41}$$

$$\begin{aligned} &= -T_5 \int_{W_5} d^6\xi \sqrt{-\det(P_6[g_{MN} + B_{MN} + 2\pi\alpha' F_{MN}])} \\ &\quad + T_5 \int_{W_5} P_6\left[C_6 + C_4 \wedge (B_2 + 2\pi\alpha' F_2)\right] \end{aligned} \tag{4.42}$$

where P_6 is the pullback of a 10D tensor to the 6D brane worldvolume, and $T_5 = [(2\pi)^5 g_s l_s^6]^{-1}$.

It's important to distinguish between the *embedding* of the D5-brane in the 10D spacetime, and the *wrapping* of the D5 on a 2-cycle Σ_2 in the 6D internal space.

The embedding is a relation between the brane worldvolume coordinates ξ^α and the 10D spacetime coordinates x^M, given as $\xi^\alpha = k^\alpha(x^M), \alpha = 0, ..., 5$ for some function k^α. Similarly to [212], we choose the simple embedding

$$\xi^\alpha = (x^0, x^1, x^2, x^3, \theta_1, \phi_1). \tag{4.43}$$

We specify the wrapping on the 2-cycle Σ_2 in the 6D internal space by taking $6 - 2 = 4$ relations on the internal y^m coordinates

$$r = \text{constant} \qquad \theta_2 = f(\theta_1) = -\theta_1 \tag{4.44}$$

$$\psi = \text{constant} \qquad \phi_2 = g(\phi_1) = -\phi_1. \tag{4.45}$$

With this choice of embedding and wrapping, the pullback of the 10D metric g_{MN} to

the 6D D5-brane worldvolume is

$$P_6[g]_{\alpha\beta} = \frac{\partial X^M}{\partial \xi^\alpha}\frac{\partial X^N}{\partial \xi^\beta} g_{MN}, \tag{4.46}$$

which takes the following diagonal form

$$P_6[g]_{00} = -\mathcal{H}^{-1/2}(1 - \mathcal{H}v^2) \tag{4.47}$$

$$P_6[g]_{ii} = a^2\mathcal{H}^{-1/2} \tag{4.48}$$

$$P_6[g]_{\theta_1\theta_1} = \frac{1}{3}\mathcal{H}^{1/2}(r^2 + 3u^2) \tag{4.49}$$

$$P_6[g]_{\phi_1\phi_1} = \frac{1}{3}\sin^2\theta_1\mathcal{H}^{1/2}(r^2 + 3u^2), \tag{4.50}$$

where there's no summation implied on the ii component, and we restrict to only have motion in the r, θ_2 directions, so that the speed squared of the brane is

$$v^2 = \left(\frac{r^2 + 6u^2}{r^2 + 9u^2}\right)\dot{r}^2 + \frac{1}{6}\left(r^2 + 6u^2\right)\dot{\theta}_2^2. \tag{4.51}$$

We choose to turn on a worldvolume flux F_2, of strength q along the wrapped 2-cycle, so that its pullback has the following non-zero components

$$P_6[2\pi\alpha' F_2]_{\theta_1\phi_1} = 2\pi\alpha'\frac{q}{2}\sin\theta_1 = -P_6[2\pi\alpha' F_2]_{\phi_1\theta_1}. \tag{4.52}$$

As an aside, we note that we have chosen to turn on an F_2 worldvolume flux, but we could also have turned on a B_2 worldvolume flux, as discussed in Appendix A.3. The wrapped D5-brane would lead to a potential for the b-axion associated with integrating this B_2 over the wrapped 2-cycle. This b-axion was used to as the inflaton in models of axion monodromy inflation [200]. However, for suitable initial conditions on the size of b, this term will not affect our inflationary dynamics from the position modulus of the wrapped D5-brane.

Now we have the following term in the DBI part of the action

$$S_{DBI-D5} = -pT_5\int_{M_4\times\Sigma_2} d^4x d\theta_1 d\phi_1\sqrt{-\det(P_6[g + 2\pi\alpha' F_2])} \tag{4.53}$$

$$= -pT_5\int_{M_4} d^4x a^3 4\pi\mathcal{H}^{-1}\mathcal{F}(r,\theta_2)^{1/2}\sqrt{1 - \mathcal{H}v^2} \tag{4.54}$$

$$\text{where } \mathcal{F}(r,\theta_2) \equiv \frac{\mathcal{H}}{9}(r^2 + 3u^2)^2 + (\pi\alpha' q)^2. \tag{4.55}$$

Now we need to do a slow roll expansion, and check what terms multiply the kinetic terms, and then define new coordinates which have canonical kinetic terms. In the 4D Lagrangian density, (with a^3 absorbed into the integration measure) the coefficient of

$\frac{1}{2}v^2$ in the expansion of the square root is

$$4\pi p T_5 \mathcal{F}(r,\theta_2)^{1/2}. \tag{4.56}$$

Since the open string modulus has mass dimensions, we expect this modulus to be affected by the warping. In the case of the D3-brane, the warp factors exactly cancelled in (4.27) to give (4.28) with 4D canonical fields with no powers of the warp factor. However, in the case of a wrapped D5-brane, we see this cancellation no longer occurs, with dependence on the warp factor to the power of 1/2 as set by $\mathcal{F}^{1/2}$ in (4.54).

If we neglect $\mathcal{O}(\alpha'^2 q^2)$ and take the AdS limit of the throat, we would get $\mathcal{F} \sim R^4/9$ giving the same result as found in [212]. However, we are interested in the *small* r region of the throat, near the stack, where we will fix $r = r_{\rm min} \ll r_{\rm UV}$.

In contrast to the D3-brane case, we can now take $r_{\rm UV} \sim u$, so that the length of the throat is of order the resolution parameter, which is the natural lengthscale of the WRC geometry. This is because we have more freedom in the model from the wrapping number p.

For the moment let's take the following assumption on the size of the flux q

$$q \lesssim \frac{1}{\pi}\left(\frac{u}{r_{\rm min}}\right)^2 \sqrt{4\pi g_s N}, \tag{4.57}$$

which means that to leading order in $u/r_{\rm min}$, $\mathcal{F}$ has behaviour

$$\mathcal{F}(r,\theta_2)^{1/2} \approx \frac{u^2 L_{S^5}^2}{r_{\rm min}^2} \approx \left(\frac{u}{r_{\rm min}}\right)^2 l_s^2 \sqrt{4\pi g_s N} \tag{4.58}$$

with the q^2 term possibly contributing only an $\mathcal{O}(1)$ numerical factor in front of this. Here $L_{S^5}^4 = 4\pi g_s N l_s^4$ is the fourth power of the $AdS_5 \times S^5$ radius, which is the near stack geometry created by the N D3's.

Decay Constant f

The canonical kinetic coordinate Θ is

$$\Theta \equiv \frac{u^2}{r_{\rm min}} (4\pi p T_5 L_{S^5}^2)^{1/2} \theta_2. \tag{4.59}$$

The dominant contribution to the Planck mass from a long warped throat of length $r_{\rm UV} \sim u$ is

$$M_p^2 \gtrsim \kappa_{10}^{-2}\ {\rm vol}(T^{1,1}) \int_0^u y^5 \mathcal{H}(y) \approx \frac{N u^2}{2(2\pi)^4 g_s l_s^4}. \tag{4.60}$$

We want the decay constant f to be $5M_p$ for observable tensor modes, which occurs

for the canonical field Θ in (4.59) when we set the coefficient of θ_2^2 to be equal to $25M_p^2$. Using the reduced Planck mass from the volume of the throat (4.60), we find that this requires

$$p \sim \frac{25}{4\pi}\left(\frac{r_{\min}}{u}\right)^2 \sqrt{\frac{N\pi^3}{4\pi^2 g_s}}. \tag{4.61}$$

Note that there is dependence on the ratio $(r_{\min}/u)^2$, which is small for $r_{\min}$ near the tip. This will be helpful for keeping the backreaction under control, as we will show in Appendix A.1.

Scale of Inflation

We now wish to set the scale of inflation to be $M_{\rm GUT}$. Writing the action for the D5-brane minimally coupled to gravity in an FRW spacetime and expanding in slow roll fields gives

$$S_{D5} = \int_{M_4} d^4x\sqrt{g_{\rm FRW}}\left[\frac{M_p^2}{2}\mathcal{R}_4 + \frac{1}{2}\dot{Z}^2 + \frac{1}{2}\dot{\Theta}^2 - V\right] \tag{4.62}$$

$$\text{where } V = \frac{M_p^2}{4}\left[\varphi(y) + \lambda\Phi_-\right] \tag{4.63}$$

and

$$\Phi_- = \overline{\Phi}_- + \Phi_h \tag{4.64}$$

$$\varphi(y) = \frac{4}{M_p^2}4\pi p T_5 \mathcal{H}^{-1}\left(\mathcal{F}^{1/2} - l_s^2\pi q\right) \tag{4.65}$$

$$\lambda = \frac{4}{M_p^2}4\pi^2 l_s^2 T_5 pq. \tag{4.66}$$

We are aiming for a natural inflation type potential, which we derive from the homogeneous solution (4.24). We want the cosine term to be

$$V = M_{GUT}^4 \cos\left(\frac{\Theta}{5M_p}\right). \tag{4.67}$$

We now ask what value of q is required to match the coefficient of $\cos(\Theta/5M_p)$ in (4.63) to be M_{GUT}^4, in the small ρ limit. From (4.63), (4.66) and (4.24), this requires

$$4\pi^2 l_s^2 T_5 pq 3b_1 = M_{GUT}^4. \tag{4.68}$$

Taking $b_1 = \delta B$, with $B = \mathcal{O}(1)$, the LHS becomes

$$4\pi^2 l_s^2 T_5 pq 3 b_1 \approx 2.1 \times 10^{-2} \frac{N^{1/2}}{g_s^{3/2} l_s^4} \left(\frac{r_{\min}}{u}\right)^2 \delta B q. \tag{4.69}$$

The GUT scale is $M_{\rm GUT} = 10^{16}\text{GeV} \approx 4 \times 10^{-3} M_p$ and using the reduced Planck mass from (4.60) gives

$$M_{\rm GUT}^4 \approx 2.6 \times 10^{-17} \frac{N^2 u^4}{g_s^2 l_s^8}, \tag{4.70}$$

meaning we need to take q of order

$$q \approx 1.2 \times 10^{-15} \frac{N^{3/2}}{g_s^{1/2} \delta B} \left(\frac{u}{l_s}\right)^4 \left(\frac{u}{r_{\min}}\right)^2 \tag{4.71}$$

to get the desired GUT scale.

Backreaction of a Wrapped D5-brane

Unlike the D3-brane, the D5-brane can backreact on both the warp factor and the internal geometry. The backreaction on the internal geometry is possibly lethal to the assumption that the leading order terms in the potential are small, coming from the gluing of the warped throat to the CY. We should check that our chosen values for p, in (4.61), and q, in (4.71), are small enough so that backreaction effects are negligable.

Table 4 summarizes the data we take for various parameters. The model is fairly robust to small changes in these values.

Parameter	B	g_s	N	u	δ	$r_{\min}$	$\sin\theta_2$
Data	1	10^{-1}	10^4	$50 l_s$	10^{-2}	l_s	10^{-2}

Table 4: Compactification data for our model

Before we check that the backreaction from the wrapped D5-brane is under control, we can first check the value of q, given in (4.71) for the scale of inflation to be the GUT scale, against the constraint we already imposed on it in (4.57) for the approximation of $\mathcal{F}^{1/2}$ in (4.58). We require

$$1.2 \times 10^{-15} \frac{N^{3/2}}{g_s^{1/2} \delta B} \left(\frac{u}{l_s}\right)^4 \left(\frac{u}{r_{\min}}\right)^2 \lesssim \frac{1}{\pi} \left(\frac{u}{r_{\min}}\right)^2 \sqrt{4\pi g_s N} \tag{4.72}$$

$$\Leftrightarrow \frac{N}{B g_s \delta} \left(\frac{u}{l_s}\right)^4 \lesssim 9.4 \times 10^{14} \tag{4.73}$$

independent of the value of $r_{\min}$. For the data in Table 4, we have

$$\frac{N}{Bg_s\delta}\left(\frac{u}{l_s}\right)^4 \sim 6.25\times 10^{13} \lesssim 9.4\times 10^{14} \tag{4.74}$$

as required.

In Appendix A.1 we show further that for this choice of data, the backreaction is under control. We calculate the size of the backreaction on the warp factor and on the internal geometry, and find that they are small compared to what is produced by the stack.

The Stable Radial Minimum

We now confirm that we can find a stable radial minimum in ρ for our potential. Using our chosen p in (4.61) and q in (4.71), and the data in Table 4 we get

$$\varphi(y) = \frac{4}{M_p^2}4\pi u^2 pT_5\mathcal{H}^{-1/2} \approx \frac{180}{u^2}\rho^2 \tag{4.75}$$

$$\lambda = \frac{4}{M_p^2}4\pi^2 l_s^2 T_5 pq \approx 4\frac{M_{\rm GUT}^4}{\delta M_p^2} \approx \frac{0.2}{\delta u^2} \approx \frac{20}{u^2} \tag{4.76}$$

where we've used that $M_{\rm GUT} = 4\times 10^{-3}M_p$, and

$$M_p^2 = \frac{Nu^2}{2(2\pi)^4 g_s l_s^4} \approx \frac{2\times 10^8}{u^2} \tag{4.77}$$

for our data. Then we have

$$\lambda M_p^2/4 \approx 100 M_{\rm GUT}^4. \tag{4.78}$$

We note that in the potential there is the term

$$\frac{M_p^2}{4}\varphi(\rho) \approx M_{\rm GUT}^4 880\rho^2 \tag{4.79}$$

coming from the non-cancellation of DBI and CS terms. The leading order behaviour of the potential for small ρ is then

$$V \approx M_{\rm GUT}^4\left[880\rho^2 + \frac{A_0}{\rho^2} + 2A_0\log\rho + 3B_1\cos\left(\frac{\Theta}{5M_p}\right)\right], \tag{4.80}$$

where we have kept the ρ^2 term from $\varphi(y)$, since it comes with a large coefficient, but neglected positive powers of ρ from Φ_h in the small ρ limit.

We now look for a minimum $\rho_{\min}$ small enough that our selected data $r_{\min}\sim u/50$ is valid. This means that we require $\rho_{\min}\sim 1/150 \approx 7\times 10^{-3}$.

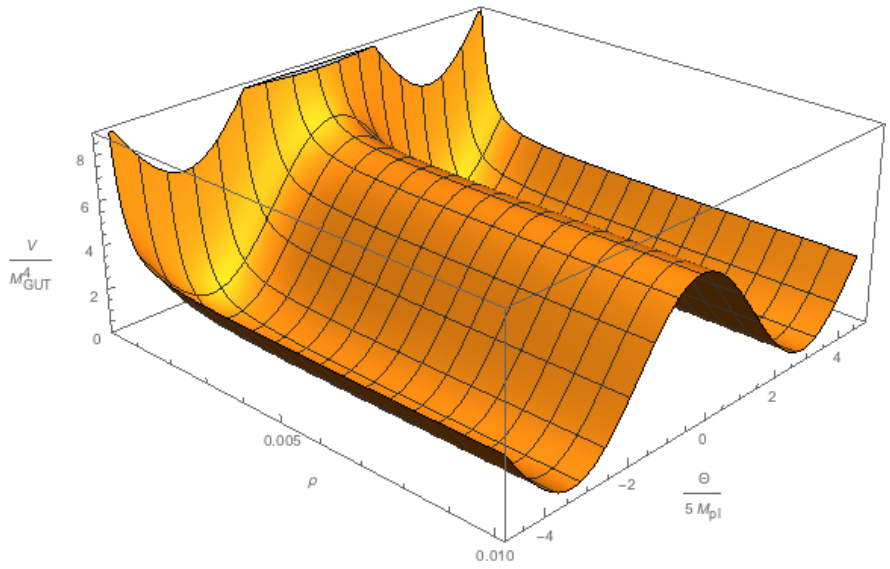

Figure 6: Natural inflation potential for the D5-brane

This requires us taking $A_0 \approx 10^{-5}$, which gives us $\rho_{min} \approx 10^{-2}$. This is a bit of fine-tuning, but the only restriction we have on the a_i is that they are less than $\mathcal{O}(\delta) = 10^{-2}$. The fact that we've taken all the other a_i as zero is at least consistent with having a very small a_0.

Once we have stabilized in the ρ direction at ρ_{min}, the effective potential is only in the Θ direction, and has the form of the natural inflation potential. A plot of the potential, with this value of A_0 and $B = 1$ is shown in Figure 6.

We could include the correction from the Ricci scalar, calculated in Appendix A.2, which contributes at leading order with a quartic term in ρ with a large coefficient. This changes the potential to

$$V \approx M_{\rm GUT}^4 \left[880\rho^2 + 4500\rho^4 + \frac{A_0}{\rho^2} + 2A_0 \log\rho + 3B_1 \cos\left(\frac{\Theta}{5M_p}\right)\right]. \tag{4.81}$$

However, the position of the minimum is highly insensitive to the addition of this term in the small ρ limit. A priori, one might have expected corrections to contribute towards the position of the minimum, but it seems the dominant feature is the small value of A_0.

4.4 Conclusion

In this chapter we have investigated D-brane potentials in the background of the warped resolved conifold (WRC) and applied this to give a model of natural inflation. The potentials arise as perturbations to the ISD solution from the gluing of the warped

throat to a bulk Calabi-Yau. These perturbations are the solutions to the Laplace equation on the unwarped resolved conifold (RC). We know the exact solutions to this equation, valid anywhere within the throat, in particular at the tip. This is not the case for the warped deformed conifold geometry, in which the solutions to the Laplace equation on the deformed conifold are only valid in the mid-throat region, far from the tip. This allowed us to exploit the effect of the warping, which is strongest at the tip. We inflated using a periodic angular coordinate which had a potential involving a cosine of this coordinate, giving us a model of natural inflation. We now summarise how we achieved a Planckian decay constant for our natural inflation potential, given the difficulty this has posed in previous attempts at embedding natural inflation in string theory.

A crucial ingredient in this respect is the choice of inflating with a D5-brane rather than a D3-brane. Using first a D3-brane, we found that we couldn't obtain a Planckian decay constant. Increasing the number of D3's increases the decay constant but the amount required has been shown to yield a large backreaction [166].

We then considered instead a wrapped D5-brane probe, with electric flux turned on along the wrapped directions. We found it was possible to get a Planckian decay constant for this probe and simultaneously set the energy scale of inflation to be the GUT scale, whilst maintaining control over the backreaction and supergravity approximation. This is because the pullback of the DBI action to the D5-brane worldvolume produces a dependence on the warp factor through the term $\mathcal{F}^{1/2}$, which is not present in the case of the D3-brane.

The term $\mathcal{F}$ is proportional to the warp factor and by setting the initial conditions such that the D5-brane begins at a small radial displacement compared to the length-scale u, allows for $\mathcal{F}^{1/2}$ to be large, as emphasised in (4.58). Since the decay constant f is proportional to $p\mathcal{F}^{1/2}$, as shown in (4.56), one can achieve a Planckian value for the decay constant by either a large p or a large $\mathcal{F}^{1/2}$. In our case we choose $\mathcal{F}^{1/2}$ to be large, as it has already been shown that choosing a large p would lead to a large backreaction as the brane would become very heavy. Having some moderate wrapping $p > 1$ is helpful however, since in the case of no wrapping a Planckian decay constant can only be achieved for an extreme hierarchy of $r_{min} \ll u$, which would be difficult to achieve. The choice of moderate p and the initial radial position of the D5-brane near the tip allows for a Planckian f.

The presence of 2-form flux q is not crucial for the Planckian f, as it does not enter directly into the expression for f, as long as we use the $AdS_5 \times S^5$ approximation valid near the stack of branes at the tip. However, q does appear in the CS action for the D5-brane, and so a non-zero q is crucial in order to get a cosine potential term in the first place, coming from the solution to the Laplace equation on the resolved conifold. By (4.66), this potential is proportional to q and so this can be chosen to set the overall

energy scale of the natural inflation potential to be M_{GUT}.

We found that we could tune one coefficient of a solution to the Laplace equation to arrange for a stable minimum in the radial direction which is very close to the tip. The slope of the potential was found to be much greater in the radial direction than in the angular direction. We can arrange for inflation to begin once the brane has stabilized in the radial direction, with inflation solely along the angular direction. Enough e-folds are produced if inflation begins near the top of the potential in the angular direction.

Estimates of the backreaction for the case of a wrapped D5-brane were presented in Appendix A.1 where it was shown that there is a choice of stringy parameters for which the supergravity and probe brane approximations are valid. In Appendix A.2, we investigated corrections to the potential when the noncompact limit approximation is relaxed, to include the effects of a nonzero 4D Ricci scalar. This involved solving the Poisson equation on the RC, using the Green's function method outlined in [162]. The leading order term only contributed at fourth order in the small radial coordinate, subleading to other terms in the potential. It had a very small effect on the value of the radial coordinate at the minimum.

Future work, outside the scope of this thesis, could explore more general motion in both the radial and the other angular directions in the WRC. We focussed in this chapter on slow roll inflation in an angular direction near the tip of the WRC. This could also be extended to the case of relativistic branes and to a DBI spinflation scenario on the WRC. Given that one knows the explicit form of the solutions of the Laplace equation and the Green's function on the whole of the RC, one could easily broaden this study to explore other regions of the RC throat.

We have not presented how to stabilize the closed string moduli within the RC throat, as it can't support non-trivial (2,1)-form flux, required to stabilize the bulk complex structure moduli and the axiodilaton, whilst preserving $\mathcal{N} = 1$ supersymmetry. Future work could investigate complex structure moduli stabilization in the RC - in particular, supersymmetry breaking (3,0)-fluxes may present a way forward, and may lead to supersymmetry broken at a high scale. One could also ask how Kähler moduli stabilization is affected, and its cosmological implications. This could also impact on the stabilization of the axiodilaton as well. In addition, the idea of the decoupling of closed string moduli from open string moduli could be pursued.

Finally, an interesting broad question arising from this work is whether observable values of r can be achieved in general from D3-brane inflation and to what extent one is forced to consider objects such as wrapped D5-branes or other brane constructions in order to produce a large value of r within a warped throat setup.

Part 2

Observables

Chapter 5

Asymmetry and Non-Gaussianity

This chapter contains material discussed in Kenton, Mulryne and Thomas, [2], in collaboration with my supervisors, Steven Thomas and David Mulryne. It aims to explain the observed CMB power asymmetry through using a multiple-field inflation model. Previous work explaining the asymmetry with a multiple-field inflation model had a zero value for the local trispectrum, $g_{\rm NL}$, and a non-zero value for the local bispectrum, $f_{\rm NL}$, which was too large to be consistent with observations.

In this work, we consider a higher-order term in the δN expansion for the CMB power asymmetry generated by a superhorizon isocurvature field fluctuation. The term can generate the asymmetry without requiring a large value of $f_{\rm NL}$. Instead it produces a non-zero value of $g_{\rm NL}$. A combination of constraints leads to an allowed region in $f_{\rm NL} - g_{\rm NL}$ space. To produce the asymmetry with this term without a large value of $f_{\rm NL}$ we find that the isocurvature field needs to contribute less than the inflaton towards the power spectrum of the curvature perturbation.

This work has been used and built upon in the recent work of [213, 214], where the authors allowed for a scale-dependent non-Gaussianity to describe the asymmetry - which was also recently shown to be scale-dependent [215] (see also earlier work on scale-dependence, e.g. [216]).

5.1 Introduction

Inflation is widely accepted as the likely origin for structure in our universe. Its generic predictions of a nearly scale invariant and close to Gaussian primordial curvature perturbation, ζ, have been confirmed with increasing precision by successive Cosmic Microwave Background (CMB) experiments. There are, however, also observational anomalies which are harder to explain within the standard inflationary paradigm. One such anomaly is the hemispherical power asymmetry – the observation that for scales with $l \leq 60$ there is more power in CMB temperature fluctuations in one half

of the sky than the other. First identified in the Wilkinson Microwave Anisotropy Probe data [217–220], it was later confirmed by the Planck collaboration [221] and others [222–224], with around a 3-σ significance on large scales, although its significance remains disputed [225]. It's an anomaly in the sense that it isn't expected to occur in a ΛCDM model, and the reported p-value (i.e. the probability to find an asymmetry at least as strong as the one measured in our CMB) is $\lesssim 0.01$ [221, 223]. In this work we treat the asymmetry as a real effect which requires a primordial origin. So far, CMB data has been fitted to a template which models the asymmetry as a spatially linear modulation.

The leading primordial explanation for this asymmetry is the Erickcek-Kamionkowski-Carroll (EKC) mechanism [226, 227], in which a long-wavelength isocurvature perturbation modulates the power on shorter scales. Further work investigating this effect includes Refs. [228–236]. The origin of the long wavelength mode may be explicitly realised in the open inflation scenario of [229] or due to a domain wall, as in, for example, [237, 238].

The δN formalism provides a convenient expression for the modulation of power by a super-horizon mode, as reviewed below. In principle many terms in this δN expansion can contribute to the observed asymmetry. Until now, however, most theoretical work has focused on the leading term, which can have the form of a spatially linear modulation.

If the leading term in δN is responsible for the asymmetry then a further consequence is that the local bispectrum parameter must satisfy the constraint $f_{\rm NL} \gtrsim 30\beta$ [228][9] on the scales that are modulated, where β is an order one constant depending on assumptions of the model. A value of $\beta < 1$ can be achieved but only if our observable universe is located at a fine-tuned region within the long-wavelength perturbation [228], and otherwise can be much larger than one. Combined temperature and polarization data bounds a purely scale-independent local bispectrum as $f_{\rm NL} = 0.8 \pm 5.0$ at 68%CL [85], while we work with $|f_{\rm NL}| \lesssim 10$ as a rough 95%CL. The asymmetry appears to be scale dependent [239], and hence the non-Gaussianity produced must also be, but there are no direct constraints on such a strongly scale dependent non-Gaussianity. A new parametrisation of the scale-dependence of the non-Gaussianity and its application to the scale-dependence of the asymmetry was given in [240], which includes an accompanying $g_{\rm NL}$. It is, however, perhaps unlikely that a very large value of $f_{\rm NL}$ could be accommodated by current observations, even if $f_{\rm NL}$ decays with scale.

In this short chapter, therefore, we investigate whether the next term in the δN expression for the asymmetry could instead be responsible. We find it can, without violating any other observational or self-consistency constraints. It contributes a more

[9] Without considering our position within the modulation, and with slightly different numerical values [235] earlier found $f_{\rm NL} \gtrsim 66$.

general modulation of the power, leading to an asymmetry, which does not necessarily only involve a spatially linear modulation[10]. Using this higher-order term requires a non-zero value of $g_{\rm NL}$, but allows for a smaller value of f_{NL} than when the linear term alone contributes. If this higher-order term is responsible for the asymmetry, then the allowed parameter space indicates the modulating isocurvature field must contribute less than the inflaton towards the total power spectrum of the curvature perturbation on scales which are modulated, and this may be considered a fine-tuning of the model. Related to this, we find that if this higher-order term is dominant in our observable patch, then in certain neighbouring patches the linear term will instead be dominant.

In this work, as a first step we only focus on one of the higher-order terms, but the idea is more general and could be applied to a combination of higher-order terms. Satisfying the constraints in that case might be more complicated than the simple use of exclusion plots that we employ here.

5.2 Generating the Asymmetry

The δN Formalism

Our calculation is performed within the δN formalism [22, 37, 40, 41, 241] which states that ζ can be associated with the difference in the number of e-folds undergone by neighbouring positions in the universe from an initial flat hypersurface at horizon crossing to a final uniform density one when the dynamics have become adiabatic: $\zeta = \delta N$. On the flat hypersurface the inflationary fields are not constant, and by writing N as a function of the fields, δN can be written as a Taylor expansion in the horizon crossing field fluctuations.

We consider two scalar fields, though our work easily generalises for more than two fields, and we take both our fields to have canonical kinetic terms. We choose the inflaton field, denoted ϕ, to be the direction in field space aligned with the inflationary trajectory at horizon exit, t_*, so that $\epsilon^* = \epsilon^*_\phi$ and this implies the derivative of N with respect to the inflaton is a constant

$$N_{,\phi} = (2\epsilon^*)^{-1/2}. \tag{5.1}$$

The isocurvature field orthogonal to ϕ is denoted χ, and the curvature perturbation has contributions from both fields

$$\zeta = N_{,\phi}\delta\phi + N_{,\chi}\delta\chi + \frac{1}{2}N_{,\chi\chi}\delta\chi^2 + \frac{1}{6}N_{,\chi\chi\chi}\delta\chi^3 + ... \tag{5.2}$$

[10] To the best of our knowledge, no current data analysis has been performed using a template involving these more general modulation terms.

where we have neglected terms with higher-order ϕ derivatives since they are negligible. The arguments of N and its derivatives are usually taken to be the average values of the fields within our observable universe, denoted ϕ_0 and χ_0, while $\delta\phi$ and $\delta\chi$ contain all fluctuations in ϕ and χ with wavelengths of order the size of our observable universe or less.

The power spectrum of the curvature perturbation is then given by

$$\mathcal{P}_\zeta = N_{,I} N_{,I} \left(\frac{H}{2\pi}\right)^2 \tag{5.3}$$

where I runs over $\{\phi, \chi\}$, the summation convention has been used, and we have neglected higher-order $\delta\phi$ and $\delta\chi$ correlators.

Non-Gaussianities in ζ are generated because of the non-linear relationship between ζ and $\delta\chi$ in (5.2). In particular, one finds for the local bispectrum, f_{NL}, and trispectrum, g_{NL}, parameters that [242, 243]

$$f_{NL} = \frac{5}{6} \frac{N_{,\chi\chi} N_{,\chi}^2}{(N_{,I} N_{,I})^2} \tag{5.4}$$

$$g_{NL} = \frac{25}{54} \frac{N_{,\chi\chi\chi} N_{,\chi}^3}{(N_{,I} N_{,I})^3} \,. \tag{5.5}$$

In what follows we will only be concerned with the magnitude of f_{NL} and g_{NL} , $|f_{NL}|$ and $|g_{NL}|$, but to avoid clutter we will drop the absolute symbols. We will also use the expression for the tensor-to-scalar ratio

$$r = \frac{8}{N_{,I} N_{,I}} \tag{5.6}$$

and we will find it convenient to define the contribution of χ to the total power spectrum

$$x \equiv \frac{P_\chi}{P_\zeta} = \frac{N_{,\chi}^2}{N_{,I} N_{,I}} = 1 - \frac{r}{16\epsilon^*}. \tag{5.7}$$

Superhorizon Fluctuation

In addition to the background value of the fields inside our observable universe, $\{\phi_0, \chi_0\}$ and their fluctuations with wavelength inside our observable universe, $\{\delta\phi, \delta\chi\}$, the EKC mechanism works by postulating a superhorizon field fluctuation in χ, denoted $\Delta\chi(\mathbf{x})$, with wavelength, k_L^{-1}, much larger than the size of our observable universe, this size given by the distance to the last scattering surface, x_d, such that $k_L x_d \ll 1$. We assume the leading order behaviour $\Delta\chi(\mathbf{x}) = \overline{\Delta\chi}(\hat{\mathbf{n}} \cdot \hat{\mathbf{k}}_\mathbf{L})$ for $\mathbf{x}$ within our observable universe, where $\hat{\mathbf{n}} = \mathbf{x}/|\mathbf{x}|$ and $\hat{\mathbf{k}}_\mathbf{L} = \mathbf{k}_\mathbf{L}/|\mathbf{k}_\mathbf{L}|$, and we don't assume any particular form for the fluctuation outside of our observable patch. Note that in this paper we take

$\overline{\Delta\chi}$ to be the maximum variation in χ across our patch about our observable universe's average field value χ_0 as seen in the left panel of Fig 7 [11].

Superhorizon fluctuations source multipole moments in the CMB, upon which there are constraints from the observed homogeneity of the universe [226,227]. Using the non-linear results of [228], together with the multipole constraints from [227], we have the following homogeneity constraints from the quadrupole and octupole respectively [12]

$$|N_{,\chi\chi}\left(\overline{\Delta\chi}\right)^2| < 1.1 \times 10^{-4} \tag{5.8}$$

$$|N_{,\chi\chi\chi}\left(\overline{\Delta\chi}\right)^3| < 8.6 \times 10^{-4} \tag{5.9}$$

where we have assumed no cancellation between δN terms. We also take the following constraint

$$|N_{,\chi}\overline{\Delta\chi}| < aP_\zeta^{1/2} \tag{5.10}$$

where $P_\zeta = 2.2 \times 10^{-9}$ [244] and a is some threshold parameter.

Asymmetry

The superhorizon fluctuation modulates the power spectrum on shorter scales, and so it depends on the direction $\hat{\mathbf{n}}$ through

$$P_\zeta[\hat{\mathbf{n}}] = P_\zeta[\chi_0 + \Delta\chi(\hat{\mathbf{n}})]. \tag{5.11}$$

Since $\Delta\chi(\hat{\mathbf{n}}) < \overline{\Delta\chi}$ in our patch, and $\overline{\Delta\chi}$ is small, we can Taylor expand P_ζ in (5.11) in powers of $\Delta\chi(\hat{\mathbf{n}})$ giving

$$P_\zeta[\hat{\mathbf{n}}] = P_\zeta\left(1 + 2\sum_{m=1}^{\infty} A_m(\hat{\mathbf{n}}\cdot\hat{\mathbf{k}}_\mathbf{L})^m\right) \tag{5.12}$$

where the round brackets indicate multiplication,

$$A_m \equiv \frac{1}{2P_\zeta}\frac{(\overline{\Delta\chi})^m}{m!}\frac{\partial^m P_\zeta}{\partial\chi^m} \tag{5.13}$$

[11] These properties are in contrast to the $\Delta\sigma(\mathbf{x})$ of Ref. [228] which is a long wavelength fluctuation around the background field value, σ_{bg}, of the entire universe which is much larger than our observable patch. Our results can be matched to the results of their section 6, with our χ_0 replacing their $\sigma_{bg} + \Delta\tilde{\sigma}\cos\theta$, and our $\overline{\Delta\chi}$ replacing their $k_L x_d \Delta\tilde{\sigma}\sin\theta$. One might demand $|N_{,\chi\chi\chi}\left(\Delta\tilde{\sigma}\right)^3| < 1$ which is in fact satisfied by (5.9) for $k_L x_d \approx 0.1$.

[12] The hexadecapole will also receive contributions from $N_{,\chi\chi\chi}$ though it appears suppressed by powers of $k_L x_d$ meaning if it satisfies the octupole constraint it will also satisfy the hexadecapole, and similarly for higher derivatives and multipoles.

and we have used the shorthand that when P_ζ and its derivatives appear without an argument they are taken to be evaluated at the average field values of the observable universe. Observations indicate a power asymmetry, with the power along the preferred direction $\hat{\mathbf{n}} = \hat{\mathbf{k}}_\mathbf{L}$ being greater than the power on the opposite side of the sky $\hat{\mathbf{n}} = -\hat{\mathbf{k}}_\mathbf{L}$. We note that only the odd m terms in (5.12) can contribute towards an asymmetry of this sort, with the even terms contributing only towards general anisotropy.

Usually only the $m = 1$ term is kept, and the data has been fitted to this with the result that [221] $A_1 = 0.07$. The $m = 1$ and $m = 2$ terms were considered in [240] [13]. Here we consider instead the $m = 3$ term, since this can contribute towards asymmetry [14]. Ideally a fit to the data with $m = 1, 2, 3$ terms should be done to constrain the parameters A_1, A_2 and A_3. In the absence of this, we will look at the simplest case involving only the $m = 3$ term and take [15] $A_3 \gtrsim 0.07$.

Linear Term Asymmetry

It has been noted in e.g [228, 231, 235] that a large f_{NL} accompanies the asymmetry when only the $m = 1$ term is considered, and we briefly review this now. Differentiating (5.3) gives

$$A_1 = \frac{N_{,\chi\chi} N_{,\chi} \overline{\Delta\chi}}{N_{,I} N_{,I}}. \tag{5.14}$$

We now combine this with constraint (5.8) giving

$$f_{NL} \approx \frac{5 N_{,\chi\chi} N_{,\chi}^2}{6 (N_{,I} N_{,I})^2} \gtrsim 37 \left(\frac{A_1}{0.07} \right)^2, \tag{5.15}$$

which is outside of the observational bounds for a local-type non-Gaussianity [16].

Cubic Term Asymmetry

The asymmetry may be due to multiple odd m terms in (5.12). We will now show that postulating the cubic $m = 3$ term is dominant over the linear $m = 1$ term, and is responsible for the asymmetry, allows the constraint on f_{NL} to be relaxed, but

[13] Although the authors of [240] claim the limit $2A_2 = 0.002 \pm 0.016$, which they inferred from [245], we think [245] only constrains a term in Fourier rather than real space $(\hat{\mathbf{k}} \cdot \hat{\mathbf{E}}_{\rm cl})^2$, and so to the best of our knowledge there is no direct bound on A_2.

[14] One might worry that the second and third order terms in (5.2) become of comparable size for asymmetry generated by the $m = 3$ term and so loop corrections to $f_{\rm NL}$ may be important, changing the expression for $f_{\rm NL}$ in (5.4). However one can check these loop corrections to $f_{\rm NL}$ are subdominant to the tree level term for $\overline{\Delta\chi} > \delta\chi$.

[15] We expect this to be $\gtrsim 0.07$ since the area under a cubic curve is less than the area under a linear curve if they share the same endpoints.

[16] Different authors have used slightly different values for the quadrupole and octupole, and the value of A, leading to other numbers appearing in (5.15) ranging from $30 - 70$.

introduces new ones on g_{NL}. Later we will check the self-consistency of ignoring the $m = 1$ term compared to the $m = 3$ one.

Differentiating (5.3) three times gives

$$\frac{P_{\zeta,\chi\chi\chi}}{P_\zeta} = \frac{6N_{,\chi\chi\chi}N_{,\chi\chi} + 2N_{,\chi\chi\chi\chi}N_{,\chi}}{N_{,I}N_{,I}}. \tag{5.16}$$

We will be interested in the case where the asymmetry is generated by the $N_{,\chi\chi\chi}N_{,\chi\chi}$ term, and we neglect $N_{,\chi\chi\chi\chi}$, so that our asymmetry is given by [17]

$$A_3 = \frac{N_{,\chi\chi\chi}N_{,\chi\chi}(\overline{\Delta\chi})^3}{2N_{,I}N_{,I}}. \tag{5.17}$$

In this case, we now show there is still a lower bound on f_{NL}, but this time it depends on x defined in (5.7). Using (5.17) together with the octupole constraint (5.9), we find

$$f_{NL} \approx \frac{5N_{,\chi\chi}N_{,\chi}^2}{6(N_{,I}N_{,I})^2} \gtrsim 9.5\left(\frac{A_3}{0.07}\right)\left(\frac{x}{0.07}\right). \tag{5.18}$$

We see that if x is sufficiently small, we can have an acceptably small f_{NL} in this scenario. We will later show that there is a lower bound $x \gtrsim A_3$, and so 9.5 is the smallest value of f_{NL} allowed from this cubic term alone [18], which is an improvement compared to the contribution from the linear term alone.

Consistency Checks

For simplicity we assumed that the asymmetry is only due to the $m = 3$ term in (5.12), which then must be larger than the $m = 1$ term. We therefore require

$$\frac{N_{,\chi\chi\chi}N_{,\chi\chi}(\overline{\Delta\chi})^2}{2N_{,\chi\chi}N_{,\chi}} > 1. \tag{5.19}$$

Even powers of $\overline{\Delta\chi}$ don't contribute towards the asymmetry but they do still cause more general anisotropy of the power spectrum. Since these anisotropies have not been observed, we also demand the following

$$\frac{N_{,\chi\chi\chi}N_{,\chi\chi}\overline{\Delta\chi}}{N_{,\chi\chi\chi}N_{,\chi}} > b \tag{5.20}$$

$$\text{and } \frac{N_{,\chi\chi\chi}N_{,\chi\chi}\overline{\Delta\chi}}{N_{,\chi\chi}^2} > c \tag{5.21}$$

where b, c are some threshold parameters.

[17] We consider the $N_{,\chi\chi\chi\chi}N_{,\chi}$ term in the conclusion, noting that this term may avoid a large $f_{\rm NL}$, introducing a non-zero $h_{\rm NL}$ instead.

[18] Although one can get a value of 7 if both $m = 1, 3$ terms contribute equally $A_1 = A_3 = 0.035$.

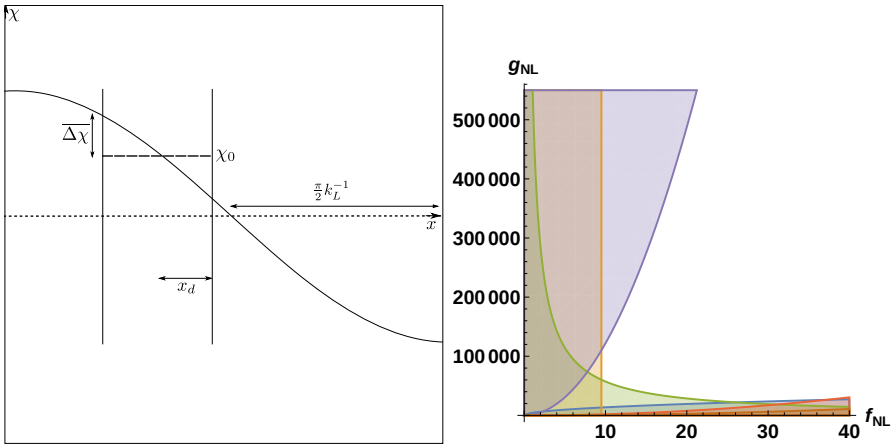

Figure 7: *Left*: The value of χ varies by an amount $\overline{\Delta\chi}$ from its average value, χ_0, within our observable universe (the interior of the two vertical lines), due to the long-wavelength fluctuation (solid wave). The average within our observable universe (long-dashed line) is not necessarily the same as the background value over the entire universe (dotted horizontal line). *Right*: Exclusion plot for (5.22)-dark-blue, (5.23)-orange, (5.24)-green, (5.25)-red, (5.26)-purple, (5.27)-brown, with $x = 0.07$, $a = 10$, $b = 0.25$ and $c = 1$. The red and brown lines are hard to see on this scale at the bottom of the plot. The allowed region is left white.

There is a lower limit on $x = x(\chi_0)$ coming from $x(\chi_0 - \overline{\Delta\chi}) > 0$, by definition (5.7). Expanding out $x(\chi_0 - \overline{\Delta\chi})$ to cubic order and neglecting the linear term, we find $x(\chi_0) \gtrsim A_3$ for $b, c \sim \mathcal{O}(1)$.

Allowed Parameters

We have six constraints to simultaneously satisfy: (5.8), (5.9), (5.10), (5.19), (5.20) and (5.21). Using (5.17) to substitute for $\overline{\Delta\chi}$, and using (5.4), (7.55) and (5.6) the six constraints become, respectively,

$$g_{NL} > \left(\frac{x}{0.07}\right)\left(\frac{A_3}{0.07}\right) 4.3\times 10^3 f_{NL}^{1/2} \tag{5.22}$$

$$f_{NL} > \left(\frac{x}{0.07}\right)\left(\frac{A_3}{0.07}\right) 9.5 \tag{5.23}$$

$$g_{NL} > \left(\frac{x}{0.07}\right)^4\left(\frac{A_3}{0.07}\right) 1.8\times 10^7 a^{-3/2} f_{NL}^{-1} \tag{5.24}$$

$$g_{NL} > \left(\frac{x}{0.07}\right)\left(\frac{A_3}{0.07}\right)^{-2} 19 f_{NL}^2 \tag{5.25}$$

$$g_{NL} < \left(\frac{x}{0.07}\right)^{-2}\left(\frac{A_3}{0.07}\right) 19 b^{-3} f_{NL}^2 \tag{5.26}$$

$$g_{NL} > \left(\frac{x}{0.07}\right)^{-1/2}\left(\frac{A_3}{0.07}\right)^{-1/2} 6.7 c^{3/2} f_{NL}^2. \tag{5.27}$$

In the right panel of Fig 7 we plot the allowed region, left in white, for (5.22)-(5.27),

with $x = A_3 = 0.07$, $a = 10$, $b = 0.25$ and $c = 1$. We chose these values for the parameters so as the highlight that values of around $f_{\rm NL} \approx 10$ and $g_{\rm NL} \approx 10^5$ are possible with these constraints. Other values are also possible, though not shown here. We find that the cubic term can generate the required asymmetry with a lower value of f_{NL} than from the linear term alone. Moreover it requires a non-zero value of $g_{NL} \gtrsim 5 \times 10^4$ for the smallest allowed values of $f_{\rm NL}$. Note that if x is much bigger than 0.07 then this pushes the allowed values of $f_{\rm NL}$ and $g_{\rm NL}$ up. The small value of $x = 0.07$ may be considered a fine-tuning required when only the $m = 3$ term generates the asymmetry.

Outside Our Observable Patch

In the above we neglected the first order $m = 1$ term in (5.12), assuming that this term is small in our observable universe. However, since we are considering a scenario in which $N_{,\chi\chi}$ and $N_{,\chi\chi\chi}$ are non-zero, neighbouring regions of the universe with a different background field value may have a larger first order term. This is closely related to a similar effect in inhomogeneous non-Gaussianity [246–250]. If this term is larger in neighbouring patches this would not violate observational bounds, but would imply that our position within neighbouring regions was finely tuned – in the sense that neighbouring regions would instead see a dominant first order term. Although not invalidating the proposed scenario, it would make it less appealing. The biggest change in the average value of χ is in a neighbouring patch along the direction of the long wavelength mode, where its average value is of order $\chi_0 + \overline{\Delta\chi}$, since $\overline{\Delta\chi} > \delta\chi$. The first order term in these patches is then of order

$$\begin{aligned} N_{,\chi\chi}N_{,\chi}\Big|_{\chi_0+\overline{\Delta\chi}} =& N_{,\chi\chi}N_{,\chi}\Big|_{\chi_0} \\ &+ \overline{\Delta\chi}(N_{,\chi\chi}^2 + N_{,\chi\chi\chi}N_{,\chi})\Big|_{\chi_0} \\ &+ \frac{3}{2}(\overline{\Delta\chi})^2 N_{,\chi\chi\chi}N_{,\chi\chi}\Big|_{\chi_0} + ... \end{aligned} \tag{5.28}$$

where we have neglected fourth and higher derivatives of N. The order $\overline{\Delta\chi}$ term in (5.28) is related to the zeroth order term by

$$\frac{\overline{\Delta\chi}(N_{,\chi\chi}^2 + N_{,\chi\chi\chi}N_{,\chi})}{N_{,\chi\chi}N_{,\chi}}\Big|_{\chi_0} > (b + c) \tag{5.29}$$

and so these terms are of comparable order for $b, c = \mathcal{O}(1)$ and if (5.20) and (5.21) are not hierarchical inequalities. The order $(\overline{\Delta\chi})^2$ term in (5.28) is related to the zeroth

order term using (5.19)

$$\frac{3(\overline{\Delta\chi})^2 N_{,\chi\chi\chi} N_{,\chi\chi}}{2N_{,\chi\chi} N_{,\chi}}\Big|_{\chi_0} > 3 \tag{5.30}$$

so we see that the first order term in $\overline{\Delta\chi}$ in (5.12) in these neighbouring patches will actually be of the same order or larger than the cubic one in our own patch which we consider to be responsible for the asymmetry. This then implies that in these neighbouring patches the value of f_{NL} is necessarily larger than in our own patch. This agrees with the result of [251] that if $g_{NL} \gg f_{NL}$ in our observable patch, then neighbouring patches will generically have a larger value of f_{NL} than in our own. If the asymmetry in our patch is due to the third order term rather than the linear term, then our patch should be considered fine-tuned compared to its neighbours along the direction of the long wavelength mode.

5.3 Conclusion

We have presented a mechanism involving a modulating isocurvature field which can produce the required hemispherical power asymmetry while satisfying the homogeneity constraints, and which produces non-Gaussianity within observational bounds. A novel feature is the non-zero value of g_{NL} required to generate this asymmetry. We note that there are models with a large g_{NL} and small f_{NL}, for example, [252] and [253]. A requirement on the model is that the isocurvature field contributes a small amount towards the power spectrum of the curvature perturbation, which could be considered a fine tuning. We also note that the large minimal value of g_{NL} required implies our observable patch of the universe has a significantly smaller value of $f_{\rm NL}$ than our neighbours. The observed asymmetry is scale dependent, with a smaller asymmetry on small scales, which this model does not account for.

Moreover, if asymmetry is third order rather than first order, it is considered a fine-tuned situation since one would normally expect the first order term in a Taylor series to contribute more than a third order term if the series is to be applicable.

If the observed asymmetry is due to the higher-order term considered in this work, then this will put strong bounds on f_{NL} and g_{NL}. Measurements of f_{NL} and g_{NL} outside of our allowed region would falsify models which use this cubic term to generate the asymmetry.

The cubic term has a different $\hat{\mathbf{n}}$-dependence compared to the first order term. For this paper we assumed $A_3 \gtrsim 0.07$, but we would like to see a fit to the data with the $m = 1, 2, 3$ terms, in order to properly constrain the parameters A_1, A_2 and A_3.

This study has shown that a higher-order term can generate the required asymmetry, relaxing the constraint on $f_{\rm NL}$ compared to that generated only by the first

order. Perhaps the other cubic order term in (5.16), $N_{,\chi\chi\chi\chi}N_{,\chi}$, may also contribute – although the bound on the non-linear parameter, h_{NL} [254], associated to this term is considerably weaker than that on g_{NL}, and so this term is not as easily falsifiable. Indeed, since the third order term can have a large contribution, other higher-order terms (and combinations of them) may also be significant. Our work prompts investigation of the case where δN can't be Taylor expanded.

Chapter 6

The Squeezed Limit of the Bispectrum in Multi-Field Inflation

This chapter contains material discussed in [3] in collaboration with my supervisor, David Mulryne.

The aim of the chapter is to provide the first calculation of the squeezed limit of the bispectrum produced by inflation with multiple light fields. In the next chapter, Chapter 7, we generalize these results to calculate soft limits of higher-point correlators. To calculate the squeezed limit of the bispectrum from multi-field inflation we allow for different horizon exit times for each mode and calculate the intrinsic field-space three-point function in the squeezed limit using soft-limit techniques. We then use the δN formalism from the time the last mode exits the horizon to calculate the bispectrum of the primordial curvature perturbation. We apply our results to calculate the spectral index of the halo bias, $n_{\delta b}$, an important observational probe of the squeezed limit of the primordial bispectrum and compare our results with previous formulae. We give an example of a curvaton model with $n_{\delta b} \sim \mathcal{O}(n_s - 1)$ for which we find a 20% correction to observable parameters for squeezings relevant to future experiments. For completeness, we also calculate the squeezed limit of three-point correlation functions involving gravitons for multiple field models.

6.1 Introduction

Reliable calculations of the N-point correlation functions of the primordial curvature perturbation, ζ, are essential to confront models of inflation with present and future observational constraints. Since inflation can occur at energies as high as 10^{14}GeV, these correlation functions provide an unparalleled observational window into high en-

ergy physics, providing information about the fields and their interactions active in the early universe. In this chapter we consider the three-point correlation function, and discuss how it can be calculated in a particular limit, known as the 'squeezed limit'. Our primary aim is to provide clarity on how to accurately confront models of inflation with more than one light field against observations sensitive to this limit. This includes models in which more than one field supports inflation, as well as spectator models such as the curvaton scenario and modulated reheating models – we refer to such models as multi-field models, and exclude cases in which additional heavy fields play a role.

The three-point function, parametrised by the bispectrum, is a function of three wave vectors which sum to zero as a result of momentum conservation, forming a triangle in momentum space. The squeezed limit refers to the case where one of the associated wave numbers is much smaller than the other two, such that the triangle looks 'squeezed'. Calculations of the three-point function are now extremely mature, yet for technical reasons previous multiple field calculations have only been been performed explicitly for the case of a mild hierarchy between wave numbers, as we will see. The highly squeezed limit is, however, very important both from an observational and a theoretical point of view.

The squeezed limit of the the bispectrum is the simplest possible example of a more general class of limits of correlation functions, referred to as soft limits. Soft limits occur when there exists a separation of scales in a physical problem. In the inflationary context, soft limits of correlation functions of the primordial curvature perturbation offer an exciting opportunity to confront theory with observations. For example, in the case of a single slow-roll field with canonical kinetic terms, Maldacena [36] found that the bispectrum of the curvature perturbation in the squeezed limit is purely determined by the tilt of the power spectrum, with the assumption of a Bunch-Davies initial state. The relation is: $12f_{\rm NL}^{\rm sq} = -5(n_s - 1)$, where $f_{\rm NL}^{\rm sq}$ is the squeezed limit of the reduced bispectrum, and $n_s - 1 = -0.032 \pm 0.006$ [65] is the spectral tilt. Creminelli & Zaldarriaga [84] (see also Ref. [255]), showed that Maldacena's result holds even without the assumption of slow-roll[19] in all models with a Bunch-Davies initial state and where the classical solution is a dynamical attractor – the proof of which was later formalized by Cheung *et al.* [83]. Thus a detection of $f_{\rm NL}^{\rm sq} \gtrsim \mathcal{O}(0.01)$ would rule out all single field models with a Bunch-Davies initial state and where the classical solution is a dynamical attractor[20]. For single field inflation, considerable work has also gone into studying more general soft limit results and providing further consistency relations amongst correlation functions [30, 61, 258, 260–279]. Moreover, soft limits can be used to provide information about other fields present during inflation [280–287].

[19] See, for example, [256, 257] for single field, but non-slow-roll models which obey Maldacena's relation.

[20] See [258] (and e.g. [259]) where more general initial states are considered, and see [260] (and references therein) where non-attractor models are considered.

In the case of inflation with multiple light fields, in contrast to the single field case, *model independent* results such as the Maldacena consistency relation are not possible. However, many observables which constrain non-Gaussianity produced by multiple field inflation are particularly sensitive to soft limits. Examples include[21] the spectral index of the halo bias [291] and CMB μ-distortions [292]. This is why explicit calculations of soft limits in the multiple field context are important when comparing *model dependent* predictions against observation.

In this chapter, as a starting point to more general studies of soft limits in multiple field inflation, we explore the simplest case of the squeezed limit of the bispectrum. In most previous studies, the path to the bispectrum for multiple field models has been to first use the in-in formalism to calculate the three-point function of scalar field perturbations at a time soon after all modes have left the horizon, as was first done by Seery & Lidsey [43]. Next the δN formalism [37, 40] is applied to convert the field-space correlations to correlations of ζ [41]. The result of Seery & Lidsey for the three-point function, however, requires that there is not a large hierarchy between the three wavenumbers involved in the bispectrum, and thus that the modes of the bispectrum must cross the horizon during inflation at roughly the same time. As is clearly stated in their paper, therefore, their result is not valid in the highly squeezed limit where there is an appreciable difference in the exit times of different modes. Moreover, on using δN to convert from field-space fluctuations to ζ, one finds that the three-point function of the curvature perturbation involves copies of the two-point function of field fluctuations evaluated after all modes have exited the horizon. At this point in the procedure, previous explicit calculations have considered at most a mild hierarchy between the scales at which these two-point functions are evaluated [45, 293], with $|\log(k_1/k_3)| \sim \mathcal{O}(1)$, where k_1 is the long-wavelength mode, and k_3 is the short-wavelength mode.

Future experiments, together with the expected amount of squeezing they will be sensitive to, are shown in Table 5 [293]. These experiments will probe a hierarchy much larger than that allowed by previous theoretical calculations. Therefore, it is very important to have theoretical predictions for multiple field models valid in the highly squeezed limit, to be able to compare with observations.

Experiment	Dark Energy Survey	CMB	Euclid	μ-distortions
Squeezing, $\log(k_1/k_3) \sim$	-2	-7	-8	-19

Table 5: Experiment/experiment type and their observable range of scales.

[21] One might naively think that the long-wavelength fluctuations used to model the observed CMB power asymmetry (see e.g. [2, 240, 288–290]) may also be an observational probe of soft limits – however, to describe the asymmetry, the long wavelength mode is required to be superhorizon, and so won't be suitable as a soft momentum in the correlation functions considered in this chapter.

In our study, therefore, we wish to relax the requirement of a mild hierarchy, and study models explicitly in the highly squeezed limit. To do so we will use a similar soft limit argument to Cheung *et al.* [83], but applied to calculate the three-point function of the scalar field perturbations. This result reduces to that of Seery & Lidsey for mild squeezing, but is valid in the highly squeezed limit and does not rely on slow-roll. In analogy with the single field case, where the three-point function depends on the tilt of the power spectrum, we find that the three-point function of the scalar field perturbations depends on derivatives of the field space two-point function with respect to the background value of the fields. Armed with this result, we further relax the usual assumption that the copies of the two-point function of the field perturbations, which appear in the three-point function for ζ, involve only a mild hierarchy of scales. This can easily be achieved by accounting for the evolution between horizon crossing times. We find that for any model in which previous applications of the δN formalism give rise to analytic results, analytic expressions for the highly squeezed limit are also possible. We finish by considering a specific curvaton model and compare our new squeezed limit formulae with previous expressions. We find significant differences for cases in which non-Gaussianity depends on scale.

The outline of this chapter is as follows: in §6.2 we conveniently parametrise the evolution of the superhorizon field perturbations between exit times in terms of a 'Γ-matrix', and calculate the three-point function of the scalar field perturbations at the time the last mode exits the horizon using soft-limit arguments. Putting these elements into the δN formalism we calculate the highly squeezed limit of the bispectrum of the curvature perturbation. In §6.3 we calculate the scale dependence of the squeezed limit of the reduced bispectrum, focussing on the spectral index of the halo bias. In §6.4 we provide explicit formulae for the Γ matrix, and investigate the concrete example of the mixed inflaton-curvaton scenario [294] with self-interactions [240].

Throughout this chapter we work in units where $\hbar = c = 1$ and we set the reduced Planck mass $M_p = 1$. For a review of the δN formalism and the notation we use in this chapter, see Section 2.2.6.

6.2 The squeezed limit of the bispectrum with δN

In this chapter we wish to extend previous work to explicitly calculate the bispectrum at the late time, t_u, on a uniform-density slice, in the case of a truly squeezed momentum configuration, $k_1 \ll k_2 \approx k_3$, which will involve (perhaps very) different horizon exit times $t_1 \ll t_2 \approx t_3$. To do so we will employ expression (2.66), setting $T = t_3$, but will fully account for the different horizon crossing times, and also show how to calculate $\alpha^{(3)}_{ijk}$ for highly squeezed configurations. In contrast to Section 2.2.6, the new objects we need to calculate are $\Sigma^{(3)}_{ij}(k_1)$, the field perturbation two-point function for modes

which cross the horizon at time t_1 evaluated at the later time t_3, and $\alpha^{(3)}_{ijk}(k_1, k_2, k_3)$ for the $k_1 \ll k_2 \approx k_3$ configuration. Many authors have discussed how to propagate the field-space two-point correlation function past horizon crossing [20, 21, 42], but to the best of our knowledge no one has then employed these techniques to explicitly investigate the bispectrum of ζ beyond cases of mild squeezing. Moreover, to the best of our knowledge we are the first to attempt a calculation of $\alpha^{(3)}_{ijk}(k_1, k_2, k_3)$ in the squeeeezed limit using a background wave method[22] which generalizes most easily to a result which is independent of a slow-roll assumption.

We proceed to discuss how to calculate each of these objects now, and then combine them to compute the bispectrum of ζ in the squeezed limit for multiple field models.

6.2.1 Field evolution between different crossing times

The first task is to calculate $\Sigma^{(3)}_{ij}(k_1)$. To do this we need to account for the evolution of the field-space perturbations on a flat hypersurface with wavenumber k_1 between the time this wavenumber crosses the horizon and the later time t_3. We choose to approach this problem in a manner closely connected with the δN framework, and which therefore provides a unified treatment of the overall problem. It will also make transparent the cases in which analytic progress can be made.

Returning to the separate universe picture, perturbations at time t_3 are defined by

$$\delta\phi^{(3)}_i(\mathbf{x}) \equiv \phi^{(3)}_i(\mathbf{x}) - \phi^{(3)}_i \tag{6.1}$$

where $\phi^{(3)}_i(\mathbf{x})$ is the true value, and $\phi^{(3)}_i$ without an $\mathbf{x}$ argument is the homogeneous background value. In general, for a given i, $\phi^{(3)}_i(\mathbf{x})$ will depend on the value of all the fields and field velocities at the earlier time t_1. Assuming, however, slow-roll between t_1 and t_3, the fields velocities become functions of the fields. One can write therefore

$$\delta\phi^{(3)}_i(\mathbf{x}) = \phi^{(3)}_i(\phi^{(1)}_j(\mathbf{x})) - \phi^{(3)}_i \tag{6.2}$$

$$= \phi^{(3)}_i(\phi^{(1)}_j + \delta\phi^{(1)}_j(\mathbf{x})) - \phi^{(3)}_i. \tag{6.3}$$

In analogy with the δN expression, one can Taylor expand this in the perturbation $\delta\phi^{(1)}_j(\mathbf{x})$ to give

$$\delta\phi^{(3)}_i(\mathbf{x}) = \delta\phi^{(1)}_j(\mathbf{x})\frac{\partial\phi^{(3)}_i}{\partial\phi^{(1)}_j} + ... \tag{6.4}$$

[22] Although similar results can be found in [262] using a Hamiltonian method and [295] using a second-order perturbation theory method. See also [296, 297] where α in the squeezed limit was given in terms of OPE coefficients. .

In this chapter we won't need the higher order terms. We use the shorthand

$$\Gamma_{ij}^{(3,1)} \equiv \frac{\partial \phi_i^{(3)}}{\partial \phi_j^{(1)}} \tag{6.5}$$

which we will often refer to as the 'Γ-matrix'. We would like to emphasise that the 'Γ-matrix' used here is constructed using the background cosmology and is analogous to $N_i^{(T)}$ in (2.61). In Fourier space we have

$$\delta\phi_{i,\mathbf{k}}^{(3)} = \Gamma_{ij}^{(3,1)} \delta\phi_{j,\mathbf{k}}^{(1)} + \dots \quad . \tag{6.6}$$

Objects like the Γ matrices have been used by a number of authors in the past[23] [38, 55, 56, 298–302], and we note the properties: $\Gamma_{ij}^{(a,a)} = \delta_{ij}$, $\Gamma_{ki}^{(c,b)}\Gamma_{ij}^{(b,a)} = \Gamma_{kj}^{(c,a)}$ and so $\Gamma_{ki}^{(c,a)}\Gamma_{ij}^{(a,c)} = \delta_{kj}$ for arbitrary times t_a, t_b, t_c. Moreover since ζ in (2.60) is independent of T, at first order we find that

$$N_i^{(b)} \delta\phi_{i,\mathbf{k}}^{(b)} = N_i^{(a)} \delta\phi_{i,\mathbf{k}}^{(a)} \tag{6.7}$$

and so we must have

$$N_i^{(b)} = N_j^{(a)} \Gamma_{ji}^{(a,b)}. \tag{6.8}$$

We can now use the Γ matrices to relate correlation functions at different times, and in particular using Eq. (2.67) we find

$$\boxed{\Sigma_{ij}^{(3)}(k_1) = \Gamma_{ik}^{(3,1)}\Gamma_{jk}^{(3,1)}\Sigma_{ij}^{(1)}(k_1) = \Gamma_{ik}^{(3,1)}\Gamma_{jk}^{(3,1)}\frac{{H^{(1)}}^2}{2k_1^3}} \tag{6.9}$$

While at one level Eq. (6.9) has simply swapped the unknown correlation matrix $\Sigma_{ij}^{(3)}(k_1)$ for the unknown $\Gamma_{ik}^{(3,1)}$ matrix, the point is that the problem has been reduced to a matter of solving the background cosmology, which must be done anyway to apply the δN formalism. Moreover, in all models where the derivatives of N can be calculated analytically, analytic expressions should also exist for the required Γ matrix, as we will see in an explicit example below. On the other hand, if numerical tools are needed to calculate the derivatives of N, similar tools can be applied to calculate $\Gamma_{ik}^{(3,1)}$. The formulation in terms of Γ is therefore very convenient for explicitly studying the squeezed limit.

[23] Γ can also be generalised to be k-dependent, as in [57].

6.2.2 The field-space bispectrum in the squeezed limit

The next step is to calculate $\alpha^{(3)}_{ijk}(k_1, k_2, k_3)$ in the squeezed limit. To do so we can adapt an idea used by Maldacena [36] and subsequently other authors [83, 84] in the single field context. The calculation relies on the following simplifying assumption: the long wavelength mode k_1 which exits the horizon at the first exit time, t_1, can only affect the much shorter wavelength modes, which at that time are still deep inside the horizon, through its effect on the background cosmology. The k_1 mode shifts the background field configuration, and hence changes the background cosmology which is felt by the two modes which exit later – producing a correlation between the k_1 mode and the two-point function of the k_2, k_3 modes in the shifted background.

In the single field case the calculation is performed directly with the modes of ζ in the comoving gauge, and the shift in background cosmology induced by the long wavelength mode exiting the horizon can be thought of as a *shift in the time* at which the short modes exit. This leads to the three-point correlation function of ζ being related to the tilt of the two-point function of the short modes, and to the famous consistency relation of Maldacena[24].

In the multiple field case we are calculating the three-point function of field perturbations in the flat gauge, and the shift in the background cosmology induced by the long wavelength mode exiting the horizon can be thought of as a *shift in the background field values*. This won't result in a simple consistency relation for ζ, but does allow analytic progress to be made in calculating α in the highly squeezed limit.

To calculate α we follow a similar calculation to that in Cheung *et al.* [83] for $\langle\zeta\zeta\zeta\rangle$ in the single field case. We show a derivation of the squeezed limit of α which relies on slow-roll - though this derivation can be easily generalised to relax the assumption of slow-roll. In the end the final result we get for the squeezed limit of $\langle\zeta\zeta\zeta\rangle$ must rely on a slow-roll approximation at the time of the last horizon crossing, t_3, because we will be using the δN formalism at that time.

We begin our calculation in position space, denoting short-wavelength perturbations with a superscript S, and long-wavelength perturbations with a superscript L. We ask how a short-wavelength two-point function $\langle\delta\phi^{S(3)}_{\ j}(\mathbf{x_2})\delta\phi^{S(3)}_{\ k}(\mathbf{x_3})\rangle$ at t_3 is affected by a further long-wavelength perturbation $\delta\phi^{L(3)}_{\ i}(\mathbf{x})$. To proceed, we evaluate the long-wavelength fluctuation $\delta\phi^{L(3)}_{\ i}(\mathbf{x})$ at the midpoint $\mathbf{x} = \mathbf{x_+} \equiv (\mathbf{x_2} + \mathbf{x_3})/2$. Then we Taylor expand the short-wavelength two-point function around the value it would have in the absence of the long-wavelength perturbation, denoting this value by a subscript

[24] Note that the consistency relation holds for all single field models with a Bunch-Davies initial state and where the classical solution is a dynamical attractor.

0. One finds

$$\langle \delta\phi^{S\,(3)}_{\ j}(\mathbf{x_2})\delta\phi^{S\,(3)}_{\ k}(\mathbf{x_3})\rangle\Big|_{\delta\phi^{L\,(3)}_{\ m}(\mathbf{x_+})} = \langle \delta\phi^{S\,(3)}_{\ j}(\mathbf{x_2})\delta\phi^{S\,(3)}_{\ k}(\mathbf{x_3})\rangle\Big|_0 + \delta\phi^{L\,(3)}_{\ m}(\mathbf{x_+})\langle \delta\phi^{S\,(3)}_{\ j}(\mathbf{x_2})\delta\phi^{S\,(3)}_{\ k}(\mathbf{x_3})\rangle_{,m}\Big|_0 + ... \tag{6.10}$$

where the subscript $,m$ denotes the partial derivative with respect to the background field $\phi^{(3)}_m$. At this stage we employ the simple soft limit argument discussed above and assume that in the squeezed limit the three-point function in momentum space will receive its largest contribution from the correlation between the long-wavelength mode, which effectively shifts the background cosmology, and the short-wavelength two-point function in the shifted background. This leads to

$$\langle \delta\phi^{L\,(3)}_{\ i}(\mathbf{x_1})\delta\phi^{S\,(3)}_{\ j}(\mathbf{x_2})\delta\phi^{S\,(3)}_{\ k}(\mathbf{x_3})\rangle \approx \langle \delta\phi^{L\,(3)}_{\ i}(\mathbf{x_1})\langle \delta\phi^{S\,(3)}_{\ j}(\mathbf{x_2})\delta\phi^{S\,(3)}_{\ k}(\mathbf{x_3})\rangle\Big|_{\delta\phi^{L\,(3)}_{\ m}(\mathbf{x_+})}\rangle \tag{6.11}$$

$$\approx \langle \delta\phi^{L\,(3)}_{\ i}(\mathbf{x_1})\delta\phi^{L\,(3)}_{\ m}(\mathbf{x_+})\langle \delta\phi^{S\,(3)}_{\ j}(\mathbf{x_2})\delta\phi^{S\,(3)}_{\ k}(\mathbf{x_3})\rangle_{,m}\Big|_0\rangle \tag{6.12}$$

$$\approx \langle \delta\phi^{L\,(3)}_{\ i}(\mathbf{x_1})\delta\phi^{L\,(3)}_{\ m}(\mathbf{x_+})\rangle\langle \delta\phi^{S\,(3)}_{\ j}(\mathbf{x_2})\delta\phi^{S\,(3)}_{\ k}(\mathbf{x_3})\rangle_{,m}\Big|_0 \tag{6.13}$$

$$\approx \int \frac{d^3\mathbf{p}}{(2\pi)^3}\frac{d^3\mathbf{q}}{(2\pi)^3} e^{i\mathbf{p}\cdot(\mathbf{x_1}-\mathbf{x_+})+i\mathbf{q}\cdot(\mathbf{x_2}-\mathbf{x_3})}\Sigma^{(3)}_{im}(p)\Sigma^{(3)}_{jk,m}(q)\Big|_0 . \tag{6.14}$$

In what follows we will drop the subscript $|_0$ for notational ease. Now we insert $1 = \int d^3\mathbf{k_1}\delta(\mathbf{k_1}+\mathbf{p})$ to get

$$\begin{aligned}&\langle \delta\phi^{L\,(3)}_{\ i}(\mathbf{x_1})\delta\phi^{S\,(3)}_{\ j}(\mathbf{x_2})\delta\phi^{S\,(3)}_{\ k}(\mathbf{x_3})\rangle \\ &\approx \int \frac{d^3\mathbf{k_1}}{(2\pi)^3}\frac{d^3\mathbf{p}}{(2\pi)^3}\frac{d^3\mathbf{q}}{(2\pi)^3} e^{-i\mathbf{k_1}\cdot\mathbf{x_1}-i\mathbf{p}\cdot\mathbf{x_+}+i\mathbf{q}\cdot(\mathbf{x_2}-\mathbf{x_3})}(2\pi)^3\delta(\mathbf{k_1}+\mathbf{p})\Sigma^{(3)}_{im}(p)\Sigma^{(3)}_{jk,m}(q).\end{aligned} \tag{6.15}$$

Changing the integration variables from $\mathbf{p}, \mathbf{q}$ to $\mathbf{k_2} = \frac{1}{2}\mathbf{p} - \mathbf{q}$ and $\mathbf{k_3} = \frac{1}{2}\mathbf{p} + \mathbf{q}$ we find

$$\begin{aligned}&\langle \delta\phi^{L\,(3)}_{\ i}(\mathbf{x_1})\delta\phi^{S\,(3)}_{\ j}(\mathbf{x_2})\delta\phi^{S\,(3)}_{\ k}(\mathbf{x_3})\rangle \\ &\approx \int \frac{d^3\mathbf{k_1}}{(2\pi)^3}\frac{d^3\mathbf{k_2}}{(2\pi)^3}\frac{d^3\mathbf{k_3}}{(2\pi)^3} e^{-i\mathbf{k_1}\cdot\mathbf{x_1}-i\mathbf{k_2}\cdot\mathbf{x_2}-i\mathbf{k_3}\cdot\mathbf{x_3}}(2\pi)^3\delta(\mathbf{k_1}+\mathbf{k_2}+\mathbf{k_3})\Sigma^{(3)}_{im}(k_1)\Sigma^{(3)}_{jk,m}(k_3),\end{aligned} \tag{6.16}$$

where we have used the relation $\mathbf{q} = \mathbf{k_3}(1 + \mathcal{O}(k_1/k_3))$. From (6.16) we can now read off the squeezed limit of the momentum space three-point function of the field

perturbations

$$\lim_{k_1 \ll k_3, k_2} \langle \delta\phi^{(3)}_{i,\mathbf{k_1}} \delta\phi^{(3)}_{j,\mathbf{k_2}} \delta\phi^{(3)}_{k,\mathbf{k_3}} \rangle \approx (2\pi)^3 \delta(\mathbf{k_1} + \mathbf{k_2} + \mathbf{k_3}) \Sigma^{(3)}_{im}(k_1) \Sigma^{(3)}_{jk,m}(k_3) \tag{6.17}$$

and so

$$\boxed{\lim_{k_1 \ll k_3, k_2} \alpha^{(3)}_{ijk}(k_1, k_2, k_3) \approx \Sigma^{(3)}_{im}(k_1) \Sigma^{(3)}_{jk,m}(k_3)} \tag{6.18}$$

This is a very general expression for the squeezed limit of α, independent of the multiple field model, relating the squeezed limit of the three-point function of the field perturbations to the two-point function of the field perturbations and its derivatives with respect to the background fields. It is one of the principal results of this chapter. It only relied on slow-roll at time t_3 in (6.10) where the Taylor expansion was done only in terms of the field, rather than both the field and its velocity. If one promoted the indices i to run over both fields and field velocities, then (6.18) with this more general index notation would still hold, independent of whether slow-roll was valid at time t_3.

At this stage we can make our result more explicit in the case where slow-roll is valid between the horizon exit times t_1 and t_3. In this case, we can use the Γ evolution between crossing times, which by (6.9) and (2.67) gives

$$\begin{aligned} \alpha^{(3)}_{ijk}(k_1, k_2, k_3) &\approx \Gamma^{(3,1)}_{il} \Gamma^{(3,1)}_{mn} \Sigma^{(1)}_{ln}(k_1) \Sigma^{(3)}_{jk,m}(k_3) \approx \Gamma^{(3,1)}_{il} \Gamma^{(3,1)}_{ml} \delta_{jk} \frac{{H^{(1)}}^2}{2k_1^3} \frac{\left[{H^{(3)}}^2\right]_{,m}}{2k_3^3} \\ &\approx -\Gamma^{(3,1)}_{il} \Gamma^{(3,1)}_{ml} \delta_{jk} \frac{{H^{(1)}}^2}{2k_1^3} \frac{{H^{(3)}}^2}{2k_3^3} \frac{d\phi^{(3)}_m}{dN}. \end{aligned} \tag{6.19}$$

where the final line uses the slow-roll equations of motion for the background fields, and for clarity we note that $dN \equiv d\log a$ is the local measure of e-folding time (and is not related to the δN formula).

6.2.3 The squeezed limit of the bispectrum of ζ

We now have all the ingredients we need to calculate the bispectrum of ζ (2.66) in the squeezed limit for multiple field inflation, and since we now use the δN formalism, the results which follow in this and subsequent sections are only valid in slow-roll models. The schematic picture of our approach is shown in Figure 8.

Putting $\alpha^{(3)}_{ijk}(k_1, k_2, k_3)$ from (6.19) and $\Sigma^{(3)}_{ij}(k_1)$ from (6.9) into (2.66), with $T \mapsto t_3$,

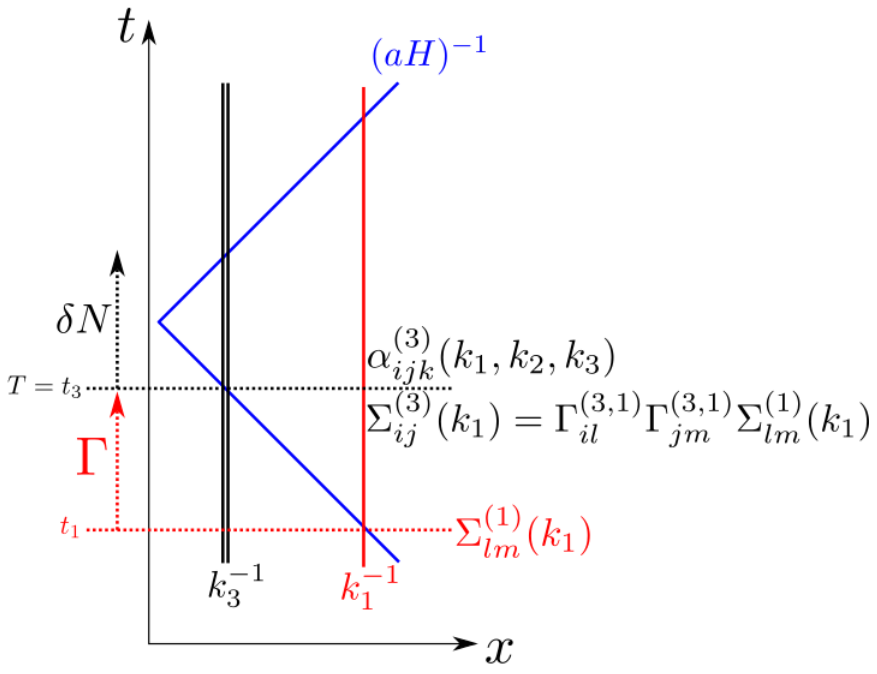

Figure 8: Schematic picture of δN evolution from time $T = t_3$ onwards, using $\Sigma^{(3)}_{ij}(k_1)$ from Subsection 6.2.1 and $\alpha^{(3)}_{ijk}(k_1, k_2, k_3)$ from Subsection 6.2.2. The Γ-evolution of field perturbations occurs between t_1 and t_3. The blue line is the comoving Hubble radius, the solid red line is the inverse of the squeezed wavenumber, k_1, while the solid black lines are the inverses of the other wavenumbers, k_2 and k_3.

gives

$$\lim_{k_1 \ll k_2, k_3} B_\zeta(k_1, k_2, k_3) \approx -N_i^{(3)} N_j^{(3)} N_j^{(3)} \Gamma^{(3,1)}_{ik} \Gamma^{(3,1)}_{mk} \frac{H^{(1)^2}}{2k_1^3} \frac{H^{(3)^2}}{2k_3^3} \frac{d\phi_m^{(3)}}{dN} + N_i^{(3)} N_{jk}^{(3)} N_k^{(3)} \left[2\Gamma^{(3,1)}_{im} \Gamma^{(3,1)}_{jm} \frac{H^{(1)^2}}{2k_1^3} \frac{H^{(3)^2}}{2k_3^3} + \delta^{ij} \left(\frac{H^{(3)^2}}{2k_3^3} \right)^2 \right] \tag{6.20}$$

and since $k_1 \ll k_3$ this can be simplified to

$$\boxed{\lim_{k_1 \ll k_2, k_3} B_\zeta(k_1, k_2, k_3) \approx -N_i^{(3)} N_j^{(3)} N_j^{(3)} \Gamma^{(3,1)}_{ik} \Gamma^{(3,1)}_{mk} \frac{H^{(1)^2}}{2k_1^3} \frac{H^{(3)^2}}{2k_3^3} \frac{d\phi_m^{(3)}}{dN} + 2N_i^{(3)} N_{jk}^{(3)} N_k^{(3)} \Gamma^{(3,1)}_{im} \Gamma^{(3,1)}_{jm} \frac{H^{(1)^2}}{2k_1^3} \frac{H^{(3)^2}}{2k_3^3}} \tag{6.21}$$

which is one of the main results of this chapter. In Appendix B.1 we check that it reduces to the Maldacena result [36] in the single field limit. In Appendix B.2 we check

that our result for α in (6.19) agrees with the result of Seery & Lidsey [43] if we take a near-equilateral limit.

We can then form the reduced bispectrum in the squeezed limit

$$\lim_{k_1 \ll k_2, k_3} \frac{6}{5} f_{\rm NL}(k_1, k_2, k_3) \approx -\frac{N_i^{(3)} \Gamma_{ik}^{(3,1)} \Gamma_{mk}^{(3,1)}}{2 N_l^{(3)} N_n^{(3)} \Gamma_{lq}^{(3,1)} \Gamma_{nq}^{(3,1)}} \frac{d\phi_m^{(3)}}{dN} + \frac{N_i^{(3)} N_{jk}^{(3)} N_k^{(3)} \Gamma_{im}^{(3,1)} \Gamma_{jm}^{(3,1)}}{N_l^{(3)} N_n^{(3)} N_p^{(3)} N_p^{(3)} \Gamma_{lq}^{(3,1)} \Gamma_{nq}^{(3,1)}}. \tag{6.22}$$

For convenience we define

$$B^{[\alpha]}(k_1, k_2, k_3) \equiv -N_i^{(3)} N_j^{(3)} N_j^{(3)} \Gamma_{ik}^{(3,1)} \Gamma_{mk}^{(3,1)} \frac{{H^{(1)}}^2}{2k_1^3} \frac{{H^{(3)}}^2}{2k_3^3} \frac{d\phi_m^{(3)}}{dN} \tag{6.23}$$

$$\frac{6}{5} f_{\rm NL}^{[\alpha]}(k_1, k_2, k_3) \equiv -\frac{N_i^{(3)} \Gamma_{ik}^{(3,1)} \Gamma_{mk}^{(3,1)}}{2 N_l^{(3)} N_n^{(3)} \Gamma_{lq}^{(3,1)} \Gamma_{nq}^{(3,1)}} \frac{d\phi_m^{(3)}}{dN} \tag{6.24}$$

so that superscript $[\alpha]$ labels the contribution from the term involving α.

As we noted in Section 2.2.6 for the near-equilateral configuration, the term coming from α can only be of order slow-roll [43], and so if the reduced bispectrum of ζ is to be sufficiently large to be observable by present or next generation experiments, it will be dominated by the second line of Eq. (2.66) [44].

For our highly squeezed case it's not immediately clear whether the contribution of $f_{\rm NL}^{[\alpha]}(k_1, k_2, k_3)$ must be of order ϵ. One might think that because at least one component of the vector N_i is of order $\epsilon^{-1/2}$, and because as many Γ matrices appear in the numerator as in the denominator, that the likely order is indeed ϵ. However, while this is likely the most common outcome, because $\Gamma_{ij}^{(3,1)}$ is a matrix and appears with different contractions in the numerator compared with the demoninator, it is not impossible that the contractions may conspire to make $f_{\rm NL}^{[\alpha]}(k_1, k_2, k_3)$ larger than $\mathcal{O}(\epsilon)$. In this chapter we do not perform a general study, but armed with this explicit expression for $f_{\rm NL}^{[\alpha]}(k_1, k_2, k_3)$ we can consider the amplitude of this term on a case by case basis.

Finally, for completeness, we note that in addition to purely scalar correlations, it is possible to calculate the three-point functions involving both the scalar curvature perturbation and gravitons in the squeezed limit. In Appendix B.3 we use similar techniques to those employed above to find the scalar-graviton three-point functions for multiple field models, noting that the graviton-only three-point function will be the same as for the single field case, as given in [36].

6.3 Scale dependence

6.3.1 Spectral index of the halo bias

An important quantity for large scale structure surveys is the *scale-dependent halo bias*, $\delta b(k_1)$ [291]. In Chapter 2 we introduced the concept of halo bias in Eq. (2.77). At lowest order it linearly relates the dark matter density contrast $\delta = \delta\rho/\rho$, to the halo/galaxy density contrast δ_g, on large scales via a local *halo bias* factor $b(z)$

$$\delta(z, \vec{x}) = b(z)\delta_g(z, \vec{x}). \tag{6.25}$$

We don't observe the dark matter directly but only the correlations of the halo density tracers. Corrections to the bias come from higher order correlations of the underlying dark matter density, and give a non-linear relation. The leading correction induces a scale-dependent shift in the bias, $b(z) \mapsto b(z) + \delta b(z, k)$, and we refer to $\delta b(z, k)$ as the scale-dependent halo bias.

The scale-dependent halo bias is sensitive to how the ratio of the bispectrum to the power spectrum, $B_\zeta(k_1, k_2, k_3)/P_\zeta(k_1)$, scales with the squeezed momentum k_1, where $k_1 \ll k_2 \approx k_3$. This is captured by the *spectral index of the halo bias*, $n_{\delta b} \equiv n_{\rm sq} - (n_s - 1)$, where $n_{\rm sq}$ is the tilt of the squeezed limit of the bispectrum with respect to its squeezed momentum k_1:

$$\lim_{k_1 \ll k_2, k_3} B_\zeta(k_1, k_2, k_3) \sim \frac{\mathcal{B}_\zeta}{k_1^3 k_3^3} \left(\frac{k_1}{k_s}\right)^{n_{\rm sq}} \tag{6.26}$$

with k_s some arbitrary scale and $\mathcal{B}_\zeta$ roughly constant. Dias *et al.* [293] investigated $n_{\delta b}$ in multiple field inflation in the case where $|\log(k_1/k_3)|$ is of order a few, as discussed further in Appendix B.5. Here we would like to explore the highly squeezed case, and find if there are significant differences.

Our results of §6.2 for the bispectrum in the highly squeezed limit can be applied to calculate $n_{\delta b}$ for large values of $|\log(k_1/k_3)|$. Differentiating $\log(k_1^3 B_\zeta)$ in (7.49) with respect to $\log k_1$ we find

$$n_{\rm sq} = -\frac{\left[N_i^{(3)} N_q^{(3)} (N_q^{(3)} V_{,j}^{(3)} + 6 N_{qj}^{(3)} H^{(3)2})\right]}{\left[N_m^{(3)} N_r^{(3)} (N_r^{(3)} V_{,n}^{(3)} + 6 N_{rn}^{(3)} H^{(3)2})\right]} \frac{\left[2\epsilon^{(1)} L_{ij}^{(3,1)} - P_{ij,1}^{(3,1)}\right]}{L_{mn}^{(3,1)}} \tag{6.27}$$

where we have defined

$$L_{ij}^{(3,1)} \equiv \Gamma_{im}^{(3,1)} \Gamma_{jm}^{(3,1)} \tag{6.28}$$

$$P_{ij,1}^{(3,1)} \equiv \frac{dL_{ij}^{(3,1)}}{d\log k_1} = -\frac{V_{,l}^{(1)}}{V^{(1)}} \left(\Gamma_{ik,l}^{(3,1)} \Gamma_{jk}^{(3,1)} + \Gamma_{ik}^{(3,1)} \Gamma_{jk,l}^{(3,1)}\right) \tag{6.29}$$

$$\Gamma^{(3,1)}_{ik,l} \equiv \frac{\partial}{\partial \phi^{(1)}_l}\Gamma^{(3,1)}_{ik} \tag{6.30}$$

and we have used the slow-roll equations to relate $\dot{\phi}_i$ to $V_{,i}$ in (6.29).

The spectral index of the halo bias requires also the tilt of the power spectrum at k_1

$$n_s - 1 = \frac{d\log(k_1^3 P_\zeta(k_1))}{d\log k_1} = -2\frac{N^{(3)}_i N^{(3)}_j \Gamma^{(3,1)}_{ik}\Gamma^{(3,1)}_{jl} M^{(1)}_{kl}}{N^{(3)}_m N^{(3)}_n L^{(3,1)}_{mp}} \tag{6.31}$$

where

$$M^{(1)}_{ij} \equiv \epsilon^{(1)}\delta_{ij} + u^{(1)}_{ij} \tag{6.32}$$

$$\text{and } u^{(1)}_{ij} \equiv \frac{V^{(1)}_{,i}V^{(1)}_{,j}}{{V^{(1)}}^2} - \frac{V^{(1)}_{,ij}}{V^{(1)}}. \tag{6.33}$$

This leads to the expression for the spectral index of the halo bias

$$\boxed{\begin{aligned} n_{\delta b} = &- \frac{\left[N^{(3)}_i N^{(3)}_q (N^{(3)}_q V^{(3)}_{,j} + 6N^{(3)}_{qj} {H^{(3)}}^2)\right]}{\left[N^{(3)}_m N^{(3)}_r (N^{(3)}_r V^{(3)}_{,n} + 6N^{(3)}_{rn} {H^{(3)}}^2)\right]} \frac{\left[2\epsilon^{(1)} L^{(3,1)}_{ij} - P^{(3,1)}_{ij,1}\right]}{L^{(3,1)}_{mn}} \\ &+ 2\frac{N^{(3)}_i N^{(3)}_j \Gamma^{(3,1)}_{ik}\Gamma^{(3,1)}_{jl} M^{(1)}_{kl}}{N^{(3)}_m N^{(3)}_n L^{(3,1)}_{mn}} \end{aligned}} \tag{6.34}$$

valid for large values of $|\log(k_1/k_3)|$, and is another key result of this chapter. In Appendix B.5 we show that when we take our exit times to be roughly equal (6.34) reduces to the same form of (17) of [293], given in the appendix as (B.19), and in §6.4.3 we compare approaches for a concrete model.

We note that if $f^{[\alpha]}_{\rm NL}(k_1, k_2, k_3)$ is negligible, then our expression simplifies to

$$n_{\delta b} = -\frac{N^{(3)}_i N^{(3)}_q N^{(3)}_{qj}}{N^{(3)}_m N^{(3)}_r N^{(3)}_{rn}} \frac{\left(2\epsilon^{(1)} L^{(3,1)}_{ij} - P^{(3,1)}_{ij,1}\right)}{L^{(3,1)}_{mn}} + 2\frac{N^{(3)}_i N^{(3)}_j \Gamma^{(3,1)}_{ik}\Gamma^{(3,1)}_{jl} M^{(1)}_{kl}}{N^{(3)}_m N^{(3)}_n L^{(3,1)}_{mp}}. \tag{6.35}$$

6.3.2 Tilts of the reduced bispectrum in the squeezed limit

In a similar manner to Refs. [45, 303–305], one can study the scaling of the squeezed limit of the reduced bispectrum (6.22) with respect to k_1 and k_3. In the squeezed limit $k_2 \approx k_3$, so one can parametrize how this depends on scale by differentiating with respect to k_1 or k_3 leading to the tilts

$$n^X_{f_{\rm NL}} \equiv \frac{\partial \log |f_{\rm NL}(k_1, k_2, k_3)|}{\partial \log X} \tag{6.36}$$

where $X = k_1$ or k_3, with the other momenta held fixed in the derivative. Note that $n^{k_1}_{f_{\rm NL}} = n_{\delta b}$ since the k_1 dependence of $f_{\rm NL}$ is captured by the scaling of the ratio $B_\zeta(k_1, k_2, k_3)/P_\zeta(k_1)$ with k_1. We calculate $n^{k_3}_{f_{\rm NL}}$ in (B.30) of Appendix B.6. We note that each of these results are different to the scale dependence of the equilateral configuration of Byrnes *et al.* [45] given in Eq. (2.71), since we are working only in the squeezed limit. These authors also considered the scale dependence of near-equilateral triangles, writing the wavenumbers as $k_a = \alpha_a \tilde{k}$, and varying with respect to $\tilde{k}$, keeping the α_a constant. Their near-equilateral result has the same form as (2.71), with all $*$'s replaced by the exit time of a pivot scale k_p not too different from the k's. Their calculation relies on an expansion to first order in $|\log(k_1/k_3)|$ and as a result is only valid for a small squeezing. We calculate the $\tilde{k}$ tilt using our approach in Eq (B.35) of Appendix B.6, where more details on the expansion of [45] can also be found. We emphasise again that all of our expressions can be employed for a large hierarchy of scales.

6.4 Employing the Γ formalism in concrete models

In this chapter we have advocated the use of the Γ matrices to allow the bispectrum of ζ to be calculated in the highly squeezed limit for multiple field models. These matrices allow us to account for the evolution of the inflationary fields between horizon crossing times, and help provide compact expressions for the bispectrum and its scale dependence, including the contribution from the field-space three-point function. To be of use, however, we must be able to calculate the Γ matrices in concrete settings.

In any given model, we could solve for $\Gamma^{(3,1)}_{ij}$ numerically. Either by solving the equation of motion it satisfies [38] from the initial conditions at t_1 of $\Gamma^{(3,1)}_{ij} = \delta_{ij}$, which follow from its definition, or by solving the background equations and implying finite differences as was done for the derivatives of N in, for example, Refs. [38, 306, 307]. However, what makes this parametrisation particularly useful is that in any model for which the derivatives of N can be calculated analytically, the Γ matrices also admit analytic solutions. This allows us to compute the amplitude of the highly squeezed limit of the bispectrum in such models and to compare this against previous squeezed limit expressions, as well as against the amplitude of the bispectrum for near-equilateral triangles.

We therefore calculate Γ analytically in §6.4.1 for sum-separable potentials. Then we consider the importance of Γ in specific settings. In §6.4.2 we show that in all single-source models, where only one field (which need not be the inflaton) contributes towards the curvature perturbation, the effect of the Γ matrices is to cause the reduced bispectrum in the squeezed limit to become independent of the squeezed momentum k_1, and that because the bispectrum scales with k_1 in exactly the same way as the power

spectrum, the spectral index of the halo bias will be zero, and so not observable. Then in §6.4.3 we consider a specific multiple-source model where more interesting results are possible. In particular, we examine a mixed curvaton-inflaton model [15, 240, 308–314] allowing for self-interaction terms for the curvaton. For this specific model with our given parameter choices, we find that in highly squeezed cases relevant for future observations, the bispectrum is suppressed by the Γ matrices at a level of 20% when compared to using the existing expressions of Byrnes *et al.* [45] and Dias *et al.* [293] for this model. In addition, we find that the spectral index of the halo bias is enhanced at a level of 20% in this model compared with the results that would be obtained with previous expressions which assume a mild hierarchy of scales.

6.4.1 Calculating Γ: sum-separable potential

In the δN framework, all models which are analytically tractable have a common feature. This is that the inflationary potentials are of separable form, either sum or product separable [306, 315, 316], or of the generalised sum-separable form of Ref [317]. This is true not only for models in which the evolution is tracked during inflation, but also for models in which the post inflationary evolution is important such as the curvaton model. In this work we will focus on sum-separable potentials and confirm that we can derive analytic formulae for the Γ matrices, using similar techniques as those originally used for derivatives of N in Ref. [306].

We will initially work with the simple case of a two field model: ϕ, χ and write the potential as $W(\phi, \chi) = U(\phi) + V(\chi)$. The slow-roll equations are then

$$3H\dot{\phi} = -U_{,\phi} \,, \qquad 3H\dot{\chi} = -V_{,\chi} \,, \qquad 3H^2 = W. \tag{6.37}$$

Using these slow-roll equations we have

$$\frac{d\phi}{d\chi} = \frac{\dot{\phi}}{\dot{\chi}} = \frac{U_{,\phi}}{V_{,\chi}} \,. \tag{6.38}$$

The number of e-folds between a flat hypersurface at time t_1 and another flat hypersurface at time t_3 is

$$\Delta N \equiv \int_{t_1}^{t_3} H dt = \int_{\phi^{(1)}}^{\phi^{(3)}} \frac{H}{\dot{\phi}} d\phi = -\int_{\phi^{(1)}}^{\phi^{(3)}} \frac{W}{U_{,\phi}} d\phi \tag{6.39}$$

and using (6.38) this gives

$$\Delta N = -\int_{\phi^{(1)}}^{\phi^{(3)}} \frac{U}{U_{,\phi}} d\phi - \int_{\chi^{(1)}}^{\chi^{(3)}} \frac{V}{V_{,\chi}} d\chi. \tag{6.40}$$

We also have, by (6.38), that

$$\int_{\phi^{(1)}}^{\phi^{(3)}} \frac{1}{U_{,\phi}} d\phi = \int_{\chi^{(1)}}^{\chi^{(3)}} \frac{1}{V_{,\chi}} d\chi. \tag{6.41}$$

To determine $\Gamma_{ij}^{(3,1)}$ we need to find the following four derivatives of flat hypersurface fields

$$\Gamma_{ij}^{(3,1)} = \begin{pmatrix} \frac{\partial\phi^{(3)}}{\partial\phi^{(1)}} & \frac{\partial\phi^{(3)}}{\partial\chi^{(1)}} \\ \frac{\partial\chi^{(3)}}{\partial\phi^{(1)}} & \frac{\partial\chi^{(3)}}{\partial\chi^{(1)}} \end{pmatrix}. \tag{6.42}$$

For flat hypersurfaces, by definition, if we vary our position on the initial slice, then ΔN does not alter. This implies that the derivative of ΔN with respect to field values on the initial flat hypersurface satisfies: $\Delta N_{,\phi^{(1)}} = 0 = \Delta N_{,\chi^{(1)}}$. Employing (6.40) then leads to two independent equations relating the derivatives. Moreover, differentiating (6.41) with respect to the field values on the initial flat hypersurface yields two further independent equations relating the derivatives. Between these four equations we can then solve for each derivative and hence determine $\Gamma_{ij}^{(3,1)}$.

We begin with $\Delta N_{,\phi^{(1)}} = 0$ and $\Delta N_{,\chi^{(1)}} = 0$ giving respectively

$$-\frac{U^{(3)}}{U_{,\phi}^{(3)}}\frac{\partial\phi^{(3)}}{\partial\phi^{(1)}} - \frac{V^{(3)}}{V_{,\chi}^{(3)}}\frac{\partial\chi^{(3)}}{\partial\phi^{(1)}} = -\frac{U^{(1)}}{U_{,\phi}^{(1)}} \tag{6.43}$$

$$-\frac{U^{(3)}}{U_{,\phi}^{(3)}}\frac{\partial\phi^{(3)}}{\partial\chi^{(1)}} - \frac{V^{(3)}}{V_{,\chi}^{(3)}}\frac{\partial\chi^{(3)}}{\partial\chi^{(1)}} = -\frac{V^{(1)}}{V_{,\chi}^{(1)}}. \tag{6.44}$$

Next differentiating (6.41) with respect to $\phi^{(1)}$ and $\chi^{(1)}$ gives respectively

$$\frac{1}{U_{,\phi}^{(3)}}\frac{\partial\phi^{(3)}}{\partial\phi^{(1)}} - \frac{1}{V_{,\chi}^{(3)}}\frac{\partial\chi^{(3)}}{\partial\phi^{(1)}} = \frac{1}{U_{,\phi}^{(1)}} \tag{6.45}$$

$$\frac{1}{U_{,\phi}^{(3)}}\frac{\partial\phi^{(3)}}{\partial\chi^{(1)}} - \frac{1}{V_{,\chi}^{(3)}}\frac{\partial\chi^{(3)}}{\partial\chi^{(1)}} = -\frac{1}{V_{,\chi}^{(1)}}. \tag{6.46}$$

Solving, we find

$$\Gamma_{ij}^{(3,1)} = \begin{pmatrix} \frac{\partial\phi^{(3)}}{\partial\phi^{(1)}} & \frac{\partial\phi^{(3)}}{\partial\chi^{(1)}} \\ \frac{\partial\chi^{(3)}}{\partial\phi^{(1)}} & \frac{\partial\chi^{(3)}}{\partial\chi^{(1)}} \end{pmatrix} = \begin{pmatrix} \frac{U_{,\phi}^{(3)}}{U_{,\phi}^{(1)}}\frac{(U^{(1)}+V^{(3)})}{W^{(3)}} & \frac{U_{,\phi}^{(3)}}{V_{,\chi}^{(1)}}\frac{(V^{(1)}-V^{(3)})}{W^{(3)}} \\ \frac{V_{,\chi}^{(3)}}{U_{,\phi}^{(1)}}\frac{(U^{(1)}-U^{(3)})}{W^{(3)}} & \frac{V_{,\chi}^{(3)}}{V_{,\chi}^{(1)}}\frac{(V^{(1)}+U^{(3)})}{W^{(3)}} \end{pmatrix}, \tag{6.47}$$

which is the analytic calculation of Γ for two-field sum-separable potentials we required. Note that i labels the rows and j labels the columns.

For a model with n fields one can calculate the Γ matrix by generalizing the two-field

case. In what follows we will suspend the summation convention of repeated indices, and where a sum should be taken we explicitly state this. We take the sum-separable potential $W(\phi_1, \phi_2, ..., \phi_n) = \sum_l W_l(\phi_l)$. We have, in analogy with (6.40),

$$\Delta N = -\sum_l \int_{\phi_l^{(1)}}^{\phi_l^{(3)}} \frac{W_l}{W_l'} d\phi_l \tag{6.48}$$

where $W_l' \equiv \partial W_l / \partial \phi_l$ for which we can write the equations $\Delta N_{,\phi_j^{(1)}} = 0$ in analogy to (6.43) and (6.44). We also have the relations, in analogy to (6.41), for all l, i

$$\int_{\phi_l^{(1)}}^{\phi_l^{(3)}} \frac{d\phi_l}{W_{,\phi_l}} = \int_{\phi_i^{(1)}}^{\phi_i^{(3)}} \frac{d\phi_i}{W_{i,\phi_i}} \tag{6.49}$$

for which we can take derivatives with respect to $\phi_j^{(1)}$ giving equations analogous to (6.45) and (6.46). Combining these equations with those from $\Delta N_{,\phi_j^{(1)}} = 0$, after some algebra we arrive at

$$\Gamma_{ij}^{(3,1)} = \frac{\partial \phi_i^{(3)}}{\partial \phi_j^{(1)}} = \frac{W_i'^{(3)}}{W_j'^{(1)}} \frac{(W_j^{(1)} - W_j^{(3)})}{W^{(3)}} + \delta_{ij} \frac{W_i'^{(3)}}{W_i'^{(1)}} \tag{6.50}$$

which reduces to (6.47) in the two-field case.

6.4.2 Single-source models

In what follows we will assume for now that in the highly squeezed limit we can neglect $B_\zeta^{[\alpha]}(k_1, k_2, k_3)$, the contribution to the bispectrum from intrinsic field-space three-point function. This needs to be checked on a case by case basis.

In the single-source case where only one field, which we denote χ, contributes to ζ, the bispectrum (7.49) (without $B_\zeta^{[\alpha]}(k_1, k_2, k_3)$) simplifies to

$$\lim_{k_1 \ll k_2, k_3} B_\zeta(k_1, k_2, k_3) \approx 2 N_\chi^{(3)} N_{\chi\chi}^{(3)} N_\chi^{(3)} \Gamma_{\chi m}^{(3,1)} \Gamma_{\chi m}^{(3,1)} \frac{{H^{(1)}}^2}{2k_1^3} \frac{{H^{(3)}}^2}{2k_3^3}. \tag{6.51}$$

Now we can use (7.43) to relate $N_\chi^{(3)}$ to $N_i^{(1)}$ through the Γ's to give the bispectrum and reduced bispectrum as

$$\lim_{k_1 \ll k_2, k_3} B_\zeta(k_1, k_2, k_3) \approx 2 N_m^{(1)} N_{\chi\chi}^{(3)} N_m^{(1)} \frac{{H^{(1)}}^2}{2k_1^3} \frac{{H^{(3)}}^2}{2k_3^3} \tag{6.52}$$

$$\approx 2 P_\zeta(k_1) P_\zeta(k_3) \frac{N_{\chi\chi}^{(3)}}{{N_\chi^{(3)}}^2} \tag{6.53}$$

$$\lim_{k_1 \ll k_2, k_3} \frac{6}{5} f_{\rm NL}(k_1, k_2, k_3) \approx \frac{N^{(3)}_{\chi\chi}}{{N^{(3)}_{\chi}}^2}. \tag{6.54}$$

We note that the effect of the Γ matrices has been to make the bispectrum proportional to $2P_\zeta(k_1)P_\zeta(k_3)$, so that the reduced bispectrum is independent of k_1, and coincidentally of the same form as would be derived in the near-equilateral regime assuming $t_* \approx t_3$. Because the bispectrum scales with k_1 in exactly the same way as the power spectrum, the spectral index of the halo bias will be zero, and so will not be observable unless the intrinsic contribution we have neglected is important.

Note that the results of this subsection did not rely on assuming a sum-separable potential – all single source models satisfy (6.54). In the next subsection we will look at a specific multiple-source model which does rely on the assumption of a sum-separable potential.

6.4.3 Multiple-source models: the mixed curvaton-inflaton model

We now consider multiple-source models, and will consider the concrete example of a curvaton model for which both the inflaton, ϕ, and curvaton, χ, contribute towards ζ. In order to make analytic progress we will need expressions for the derivatives of N in this multiple-source model to combine with our analytic expression for Γ, valid for sum-separable potentials.

More detailed studies of the curvaton scenario can be found in the literature, see e.g. [15, 308–312]. Here we just give a very brief account outlining our parameter choices and quote the results for the N derivatives. Our main focus will instead be on the differences between our new expressions compared to existing formulae in the literature. We will show these diffences graphically, where the plots are produced using the expressions for the N derivatives that follow, together with the Γ matrix for sum-separable potentials.

For the inflaton and curvaton, we take the potential

$$W(\phi, \chi) = \frac{1}{2} m_\phi^2 \phi^2 + \frac{1}{2} m_\chi^2 \chi^2 + \lambda \chi^n, \tag{6.55}$$

where the curvaton is given a self-interaction with coupling λ, and $n > 2$. If we are to see a difference between the bispectrum in the highly squeezed limit and the near-equilateral limit, it is natural to expect that we will need the field configuration to differ significantly between different exit times, otherwise the $\delta\phi_i$ would not evolve between t_1 and t_3 and we would just get $\Gamma^{(3,1)}_{ij} = \delta_{ij}$. This means that we expect to see interesting effects for models which generate a significantly scale-dependent non-Gaussianity. In the present model, this means that the curvaton field, while light, cannot be completely frozen. To achieve this we take the mass of the curvaton and inflaton to be the same

$m_\chi = m_\phi$.

The self-interacting curvaton model can give significant scale dependence of $f_{\rm NL}$, [240, 318], and analytic expressions for the derivatives of N are available in the limit of weak self-interaction $s_k \equiv 2\lambda\chi_k^{n-2}/m_\chi^2 \ll 1$ [240]. Here, and in what follows, a subscript k indicates the result is a function of the value of the curvaton and/or inflaton fields at the time, t_k, when a given k-mode exits.

The relevant N derivatives are given by [41, 240, 294]

$$N_\phi = \frac{1}{\sqrt{2\epsilon_\phi}|_k} \tag{6.56}$$

$$N_\chi = \frac{2r_{\rm dec}}{3}\frac{\sigma'_{\rm osc}}{\sigma_{\rm osc}}\Big|_k \tag{6.57}$$

$$N_{\chi\chi} = \frac{r_{\rm dec}}{3}\left[\frac{\sigma''_{\rm osc}}{\sigma_{\rm osc}} + \left(\frac{\sigma'_{\rm osc}}{\sigma_{\rm osc}}\right)^2\right]\Big|_k \tag{6.58}$$

$$\text{where } \sigma_{\rm osc}(\chi_k) \propto \chi_k\left(1+\frac{n}{2}s_k\right)^{-1/(n-2)}. \tag{6.59}$$

The parameter $r_{\rm dec}$ denotes the value of $3\rho_\chi/(3\rho_\chi + 4\rho_\gamma)$ at the time of curvaton decay, where ρ is the energy density and the subscript labels the species, with γ denoting radiation. In the example which follows we take to be $r_{\rm dec} = 0.02$. We have neglected $N_{\phi\phi}, N_{\phi\chi}$ which are much smaller than $N_{\chi\chi}$ for the parameter choices considered.

We take the initial condition[25] $\phi_0 = 16$ which leads to 63.5 e-folds of inflation and assume that all scales which exit the horizon after this time are within the horizon today and potentially observable. We will also take $\chi_0 = 2\times10^{-3}$ to generate a significant non-Gaussianity. To see a significantly scale-dependent non-Gaussianity we take the self-interaction with $n = 6$ and $\lambda = 0.2$, which gives $s_k \approx 0.07$.

The power spectrum for this model is shown in Figure 9a, and the tilt of the power spectrum is shown in Figure 9b. In order to see a large scale dependence of $f_{\rm NL}$ for this simple model, we took the curvaton mass to be as large as the inflaton mass[26]. However this has the adverse effect of making the tilt of the power spectrum to not be as red (negative) as observations suggest. This could be fixed by beginning with a more complicated model, and not requiring the curvaton mass to be as large, but this is not our focus here, and instead we focus on the results for the bispectrum.

We can now compare our new expressions with Γ's against existing expressions in the literature. In the 3d plots, the near-equilateral limit $\log(k_1/k_3) \approx 0$ is on the far right of each plot, and the squeezing increases as you move away from this corner. The highly squeezed limit, where $\log(k_1/k_3) \sim -20$ is on the far left of each plot.

[25] Note we are still working in units where the reduced Planck mass is set to one.

[26] A potential issue for the mixed curvaton-inflaton model with equal masses is that since both fields begin oscillating at exactly the same time, the curvaton energy density remains subdominant for a long time – see [319] for a discussion on this.

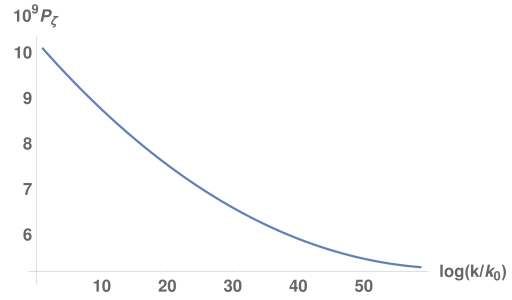

(a) Power spectrum

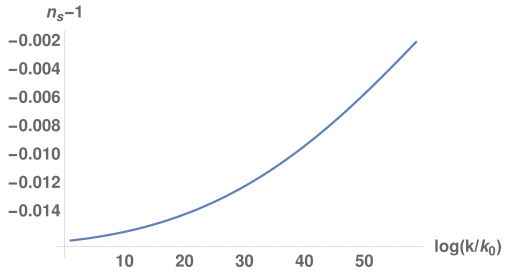

(b) Tilt of the power spectrum

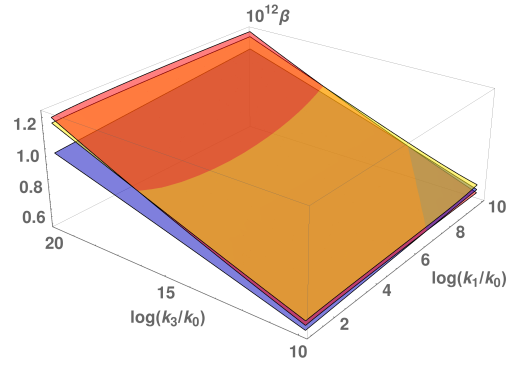

(c) Bispectrum $\beta = 4k_1^3 k_3^3 B_\zeta$ in (7.49)

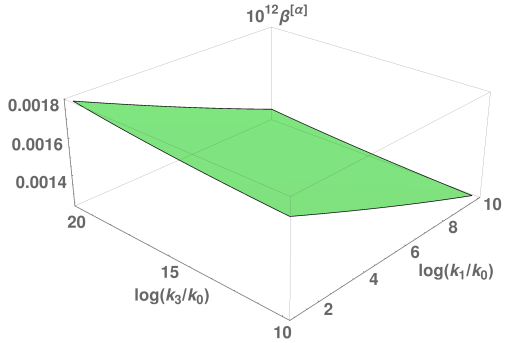

(d) $\beta^{[\alpha]} = 4k_1^3 k_3^3 B_\zeta^{[\alpha]}$ from first line of (7.49)

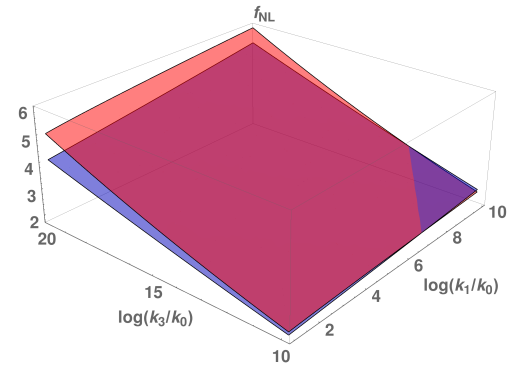

(e) Reduced bispectrum $f_{\rm NL}$, (5.4)

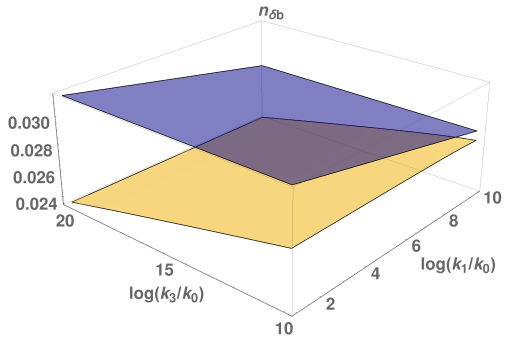

(f) Spectral index of the halo bias, (6.35)

Figure 9: In the 3d plots, the blue surfaces are our expressions with Γ's. Red surfaces are Byrnes *et al.* [45] expressions. Yellow surfaces are the Dias *et al.* [293] expressions. The near-equilateral regime is on the far right of each plot. The highly squeezed limit is on the far left of each plot. The green surface shows the $[\alpha]$ contribution is negligible for this model.

In Figure 9c we plot the bispectrum $\beta \equiv 4k_1^3 k_3^3 B_\zeta$ to show how the bispectrum scales with $\log(k_1/k_0)$ and $\log(k_3/k_0)$ where $k_0 = H^{(0)}$ at the initial time t_0, where we have set $a_0 = 1$. The blue surface uses our new expression (7.49), the red surface uses (96) of Byrnes *et al.* [45] given in (B.13), and the yellow surface uses (14) of Dias *et al.* [293], given in (B.18). In the highly squeezed limit we see a percentage difference of about 20%. The near-equilateral results are within a few percent of each other for

each of the three expressions – the small difference is because previous authors have included an additional constant term which appears at next order in slow-roll in their expression for Σ at horizon crossing discussed in Footnote 2 and Appendix B.4.

In Figure 9d we plot the contribution to the bispectrum from the field-space three-point function $\beta^{[\alpha]} = 4k_1^3 k_3^3 B_\zeta^{[\alpha]}$ where $B_\zeta^{[\alpha]}$ is the first line of (7.49). We see that this is a factor of 10^3 smaller than the total bispectrum for all scales considered, and so all the $[\alpha]$ terms in observables can be neglected for this model.

In Figure 9e we plot the reduced bispectrum, where the blue surface is our new expression (6.22) and the red surface is (96) of [45] divided by the factor $2P_\zeta(k_1)P_\zeta(k_3)$, i.e. the curly brackets of (B.13). Dias *et al.* don't give an explicit expression for the reduced bispectrum, so we don't plot this here. Again, in the highly squeezed limit we see a percentage difference of about 20%, and close agreement in the near-equilateral configuration.

Finally, in Figure 9f we plot the spectral index of the halo bias. Blue is our new expression (6.35), and the yellow surface is (17) of [293], given in (B.19). Byrnes *et al.* [45] don't give an expression for the spectral index of the halo bias so we don't plot this here. Similarly to the other observables we see a percentage difference of about 20% in the highly squeezed limit. We see agreement to within a few percent in the near-equilateral limit, the small discrepancy being due to the Dias *et al.* expression being evaluated at the exit time of $k_t \equiv k_1 + k_2 + k_3$ compared to ours being evaluated at t_3.

The 20% level difference for all these observables for a squeezing of $|\log(k_1/k_3)| \sim \mathcal{O}(20)$ can be estimated heuristically as arising from a scale-dependence of the reduced bispectrum of $\mathcal{O}(0.01)$, multiplied by the squeezing. We thus expect similar levels of discrepancy for any model where the scale-dependence of the reduced bispectrum is of similar order to the scale-dependence of the power spectrum, when considering a squeezing of $|\log(k_1/k_3)| \sim \mathcal{O}(20)$, and that the percentage difference will scale linearly with the scale-dependence of the bispectrum.

The expected levels of squeezing for three future experiments were shown in Table 5 of the introduction. The results of this section show that inclusion of the effects of field evolution can be important when computing the theoretical predictions of a model for comparison against observations for large squeezing, even for this simple model.

6.5 Conclusion

In this work we calculated the squeezed limit of the bispectrum of the curvature perturbation for multiple field inflation. Different scales involved in one triangle of the bispectrum will exit the horizon at different times, and previous analytic expressions have been limited to a mild squeezing where the exit times are roughly equal. Observa-

tions can at present probe only a mildly squeezed limit, but future large-scale structure surveys and observations of CMB μ-distortions will be able to probe a highly squeezed limit. It is important, therefore, to have accurate theoretical predictions for this highly squeezed limit in order to ensure the uncertainty in the prediction is less than the uncertainty in the data. For certain models, our results give a correction at a level of 20% in the highly squeezed limit compared to extrapolating existing expressions, valid only in the mildly squeezed limit, to the highly squeezed limit.

In order to study this highly squeezed limit, we suggested using the elegant Γ matrix formalism to account for the evolution on superhorizon scales of the perturbations between exit times. We also calculated the intrinsic three-point function of the field perturbations, α, in the highly squeezed limit for the first time. We did so by appealing to a soft limit argument, previously used in the single field context for the curvature perturbation. Together these elements allowed us to extend δN expressions for the bispectrum of ζ to account for multiple crossing times. From this expression, we then obtained the reduced bispectrum and the spectral index of the halo bias. Working with a specific model, the mixed inflaton-curvaton scenario with a self-interacting curvaton, we checked the difference in our theoretical prediction, valid for a large squeezing, against existing predictions, valid for a mild squeezing. As would be expected we found significant differences, especially in the highly squeezed limit for the cases in which there is significant scale dependence in the reduced bispectrum.

The overall aim of this chapter was to provide clarity in how to confront models of inflation against observations sensitive to the squeezed limit of the bispectrum. Our results however, could also be useful to check numerical methods in the squeezed limit. From a theoretical and observational point of view, soft-limits – of which the squeezed limit is the simplest example – are of considerable interest. In the next chapter we consider soft limits of higher n-point correlation functions for multiple field inflation, using a similar approach. For $n > 3$, the story can be more interesting than for the bispectrum, where the only soft limit is when a single external momenta becomes small. Firstly, one can consider multiple-soft limits, where more than one momentum becomes smaller than the others. Moreover, one can also consider the collapsed limit, when an internal momentum becomes soft. Observing these higher-point functions may be even harder than for the bispectrum, but it is still important to have theoretical predictions for multiple field inflation to constrain models using observational limits, in particular to search for deviations from single field inflation.

Finally, we mention that the intrinsic term in the bispectrum coming from α was negligible compared to the other term in the case study presented. Calculating this expression explicitly allowed us to determine this, but more work is required to investigate whether this term can ever be as large as, or even dominate over, the other contribution.

Chapter 7

The Separate Universe Approach to Soft Limits

This chapter is based on the work [4], *The Separate Universe Approach to Soft Limits*, undertaken with my supervisor, David Mulryne.

In this chapter we develop a formalism for calculating soft limits of n-point inflationary correlation functions using separate universe techniques. Our method naturally allows for multiple fields and leads to an elegant diagrammatic approach. As an application we focus on the trispectrum produced by inflation with multiple light fields, giving explicit formulae for all possible single- and double-soft limits. We also investigate consistency relations and present an infinite tower of inequalities between soft correlation functions which generalise the Suyama-Yamaguchi inequality.

7.1 Introduction

Observational cosmology constrains the correlations of primordial perturbations that we believe were produced during inflation. Soft limits of cosmological correlation functions occur when there is a large hierarchy between scales involved in the correlation (here soft means a longer wavelength perturbation) and are interesting both observationally and theoretically. From the observational point of view, future experiments will be able to probe a much larger range of scales than is currently available [291,292]. We therefore need to be able to calculate correlations between perturbations on very different scales in order to compare theories against these observations. On the theoretical side, soft limits represent an important simplification to the calculation of correlation functions, leading to elegant analytic expressions and to consistency relations which apply for broad classes of models.

Soft limits come in two types: *squeezed* - where an external wavevector becomes soft, or *collapsed* where an internal wavevector (i.e. a sum of external wavevectors)

becomes soft.

In Maldacena's seminal work [36] he found that the squeezed limit of the bispectrum in single-field slow-roll inflation was determined by the tilt of the power spectrum, providing a consistency relation between these observables. The result was found to hold more generally for all single-field models with a Bunch-Davies initial state and where the classical solution is an attractor [83, 84]. More general single-field soft limits have subsequently been studied, providing further consistency relations amongst correlation functions [30, 61, 255–267, 270–279, 320]. Multiple-soft limits (involving more than one soft mode) were considered for single-field inflation in [268, 269].

Soft limits have also been shown to be sensitive to additional fields present during inflation [280–287]. In our earlier work [3], presented in Chapter 6, we considered the case of inflation driven by multiple light fields. Employing separate universe techniques [39, 40] including the δN expansion [22, 37], we gave explicit analytic expressions for the squeezed limit of the bispectrum in multi-field inflation for the first time. We found that our expression for the reduced bispectrum in a squeezed configuration can be significantly different to the standard expression for the reduced bispectrum in a close to equilateral configuration [41] (contrast Eq. (7.51) with Eq. (7.52)). Shortly thereafter, Byrnes et al. [321,322] applied a similar approach to study the hemispherical asymmetry (see e.g. [2, 240, 288–290]) and its relation to the squeezed bispectrum and collapsed limit of the trispectrum.

In this chapter our aim is to extend our earlier results and to investigate general soft limits in multi-field inflation utilising expansions similar to the δN expansion.

In particular, we show how to produce soft limit diagrams with associated rules that lead to compact expressions for soft limits of the correlation functions of ζ. Our approach can be applied very generally to multiple-soft limits of squeezed (external) and collapsed (internal) momenta of arbitrary n-point cosmological correlation functions for models of inflation with any number of fields. In this sense, this chapter can be viewed as an extension to the multiple-soft limit results of [268, 269]. As applications, we apply our approach to explore all the single- and multiple-soft limits of the trispectrum, and to derive an infinite tower of inequalities between soft limits of correlation functions, generalizing the Suyama-Yamaguchi inequality [280, 286, 287, 323] to higher point correlation functions.

The compact expressions obtained from using the Soft Limit Expansion Eq. (7.10) provide analytic insight, but are not easy to evaluate explicitly. This is because the coefficients they contain can only easily be calculated in certain circumstances, such as for inflation with multiple light scalar fields. Moreover, they contain field-space correlations of soft perturbations evaluated at a later time than the horizon exit time of the soft perturbations. On the other hand the objects which are more easily calculated

are these correlations evaluated at the horizon exit time[27]. We therefore introduce one further separate universe expansion – the Γ expansion [55–57, 298, 299] – which allows these later correlations to be calculated in terms of the horizon crossing correlations, and then present explicit expressions for the soft limits of inflation with multiple light scalar fields.

At present, observations can only probe a mildly soft limit, but future large scale structure surveys, and more distant future spectral distortion experiments may probe a larger range of scales. Even for the bispectrum, the squeezed limit is not well constrained by current experiments, and higher-order soft limits of higher-point function also remain out of reach of current experiments. However, in principle, there may be a large signal in a double-soft limit of a certain higher-point function which future experiments may be sensitive to, even if the squeezed limit of the bispectrum remains rather unconstrained.

The results of this paper only hold to lowest order in the gradient expansion - if the hierarchy of the scales involved is not large enough then contributions from higher order gradient terms will become important.

This chapter is laid out as follows. In §7.2 we consider soft limits. We introduce a new Soft Limit Expansion in §7.2.1, which is a form of background wave method used by other authors. As a simple example we calculate formal expressions for the squeezed bispectrum and collapsed trispectrum in §7.2.2, showing how the Suyama-Yamaguchi inequality arises in our approach. In §7.2.3 we introduce the soft limit diagrams. We then use them to quickly calculate all other soft limits of the trispectrum in §7.2.4, and to find an infinite tower of inequalities in §7.2.5 which generalise the Suyama-Yamaguchi inequality to higher-point correlation functions. In §7.3 we give more explicit expressions. We introduce the Γ expansion in §7.3.1 applying it to correlation functions in §7.3.2 and provide explicit examples for multiple light fields in §7.3.3. We conclude in §7.4. In Appendix C.1 we give more details on the background wave method. In Appendix C.2 we show how our multi-field double-soft limit reduces to the consistency relation of the single field case. In Appendix C.3 we present a diagrammatic approach for the Γ expansion.

A few notational comments are in order for this chapter. We use the upper case Roman indices, $A, B, ...$, to denote multiple-light scalar fields allowing for this to be extened to include other degrees of freedom too. These extra degrees of freedom may include field velocities if these were important or vector or tensorial perturbations for example. At a formal level these extensions are always possible, though the explicit calculation of the coefficients (the derivatives of N) becomes less clear. Going beyond a

[27]These are far from trivial to calculate, but the statistics are expected to be close to Gaussian for canonical models with light fields, and known expressions exist for the two-point [20, 21], three-point [324, 325] and four point correlation functions [243, 264] in many circumstances.

separate universe approximation we could even include the sensitivity of ζ at the later time to gradient terms at the earlier time – moving therefore to a gradient expansion [25, 326, 327]. To keep the notation clean throughout this chapter, and because our primary concern is models with multiple light fields, we will indicate a summation over only field space indices using upper case Roman indices, $A, B, ...$ We will always bear in mind, however, that this set of variables can be formally extended to all relevant degrees of freedom, and so the results, such as our consistency relations, are rather general.

7.1.1 Correlations of the Curvature Perturbation

The objects of primary interest for observations are the $n-$point correlation functions of ζ evaluated at some late time relevant to observations t_f. We introduce arbitrary external momenta, $\mathbf{k_1}, \mathbf{k_2}, ..., \mathbf{k_n}$ which we will order, without loss of generality, by their magnitudes $k_1 \leq k_2 \leq ... \leq k_n$, where $k = |\mathbf{k}|$. These scales exit the horizon, $k = aH(t)$, at times $t_1, t_2, ..., t_n$ respectively, where $t_1 \leq t_2 \leq ... \leq t_n$. From now on if we drop the time superscript *on any object other than* ζ, it is to be understood that the evaluation time should be the exit time of the hardest mode, (shortest wavelength), t_n, for example $N \equiv N^{(n)}$ and $\delta\phi_A \equiv \delta\phi_A^{(n)}$. This avoids unnecessary clutter of our expressions.

We introduce notation for $n-$point ζ correlation functions such that

$$\langle \zeta(\mathbf{k_1}) \cdots \zeta(\mathbf{k_n}) \rangle = G_n(\mathbf{k_1}, ..., \mathbf{k_n})(2\pi)^3 \delta(\mathbf{k_1} + \cdots + \mathbf{k_n}) \tag{7.1}$$

so that, for example, G_2, G_3 and G_4 represent the power spectrum, bispectrum and trispectrum respectively

$$G_2(\mathbf{k_1}, -\mathbf{k_1}) = P_\zeta(k_1) \tag{7.2}$$

$$G_3(\mathbf{k_1}, \mathbf{k_2}, \mathbf{k_3}) = B_\zeta(k_1, k_2, k_3) \tag{7.3}$$

$$G_4(\mathbf{k_1}, \mathbf{k_2}, \mathbf{k_3}, \mathbf{k_4}) = T_\zeta(\mathbf{k_1}, \mathbf{k_2}, \mathbf{k_3}, \mathbf{k_4}). \tag{7.4}$$

And in a similar manner for $n-$point field space correlation functions we have

$$\langle \delta\phi_{A_1}(\mathbf{k_1}) \cdots \delta\phi_{A_p}(\mathbf{k_p}) \rangle = F_{A_1 \cdots A_p}(\mathbf{k_1}, ..., \mathbf{k_p})(2\pi)^3 \delta(\mathbf{k_1} + \cdots + \mathbf{k_p}) \,. \tag{7.5}$$

For the two, three and four point we also employ the conventional symbols

$$F_{AB}(\mathbf{k_1}, -\mathbf{k_1}) = \Sigma_{AB}(k_1) \tag{7.6}$$

$$F_{ABC}(\mathbf{k_1}, \mathbf{k_2}, \mathbf{k_3}) = \alpha_{ABC}(k_1, k_2, k_3) \tag{7.7}$$

$$F_{ABCD}(\mathbf{k_1}, \mathbf{k_2}, \mathbf{k_3}, \mathbf{k_4}) = T_{ABCD}(\mathbf{k_1}, \mathbf{k_2}, \mathbf{k_3}, \mathbf{k_4}). \tag{7.8}$$

The δN expansion then allows us to write the ζ correlators in terms of the $\delta\phi_A$ correlators. The result for the power spectrum of ζ was first given in [37], the bispectrum in [41] and the trispectrum in [242, 243, 264, 328]. Higher point ζ correlators are related to field-space correlators and can be nicely calculated using the diagrammatic presentation of [329].

7.2 Soft Limits

7.2.1 Soft Limit Expansion

Soft limits occur when there is a hierarchical separation of scales involved in a correlation. For any real-space perturbation, Y, (for example, Y can stand for ζ or for $\delta\phi_A$) we can consider two contributions to this perturbation. One contains only Fourier modes clustered around some hard mode $1/k_{\rm h}$ (subscript h for hard), and the other contains only long modes around some arbitrary soft mode, $1/k_{\rm s}$ (subscript s for soft), leading to

$$\begin{aligned} Y(\mathbf{x}) &\subset Y^{\rm h}(\mathbf{x}) + Y^{\rm s}(\mathbf{x}) \\ Y^{\rm h}(\mathbf{x}) &= \int_{k_{\rm h}-\Delta k_{\rm h}}^{k_{\rm h}+\Delta k_{\rm h}} \frac{{\rm d}^3\mathbf{k}}{(2\pi)^3} e^{i\mathbf{k}.\mathbf{x}} Y_{\mathbf{k}} \\ Y^{\rm s}(\mathbf{x}) &= \int_{k_{\rm s}-\Delta k_{\rm s}}^{k_{\rm s}+\Delta k_{\rm s}} \frac{{\rm d}^3\mathbf{k}}{(2\pi)^3} e^{i\mathbf{k}.\mathbf{x}} Y_{\mathbf{k}} \end{aligned} \tag{7.9}$$

where the ranges $\Delta k_{\rm h}$ and $\Delta k_{\rm s}$ are arbitrary, but small. This means that the Fourier components of $Y^{\rm h}$ only have support on $[k_{\rm h}-\Delta k_{\rm h}, k_{\rm h}+\Delta k_{\rm h}]$ and similarly for $Y^{\rm s}$ whose Fourier components only have support on $[k_{\rm s}-\Delta k_{\rm s}, k_{\rm s}+\Delta k_{\rm s}]$.

For soft limits it can be argued that the dominant contribution to correlations between hard and soft modes comes from how the soft modes, which exit the horizon at much earlier times, correlate with the shifts that the soft modes cause in the background cosmology felt by the hard modes. This is a form of the background wave assumption, which is discussed at length in Appexdix C.1. It can be used for any set of scales, but becomes accurate only when the hierarchy is large. In this work we implement this assumption by Taylor expanding the value the hard contribution to ζ takes in the background of the soft contribution to the scalar fields, which we denote $\zeta^{\rm h}(\mathbf{x})\big|_{\rm s}$, about the value it would have taken in the absence of soft scalar field modes, denoted $\zeta^{\rm h}$. The expansion then, in Fourier space for some hard wavevector $\mathbf{k}$, is

$$\zeta^{\rm h}_{\mathbf{k}}\Big|_{\rm s} = \zeta^{\rm h}_{\mathbf{k}} + \left[\zeta^{\rm h}_{,A} \star \delta\phi^{\rm s}_A\right]_{\mathbf{k}} + \frac{1}{2}\left[\frac{\partial^2\zeta^{\rm h}}{\partial\phi_A\partial\phi_B} \star \delta\phi^{\rm s}_A \star \delta\phi^{\rm s}_B\right]_{\mathbf{k}} + \dots \tag{7.10}$$

(see Appexdix C.1 for a fuller discussion). We call Eq. (7.10) the Soft Limit Expansion.

It can be seen as a form of separate universe expansion, in which the soft modes alter the background cosmology in which hard modes exit and subsequently evolve. The hard modes effectively feel a different background in different spatial locations. The derivatives in the Taylor expansion are taken with respect to *the background fields*, $\phi_A(t)$, a consequence of the separate universe approximation. The time of evaluation of $\delta\phi_A^{\rm s}$ and $\partial/\partial\phi_A$ is arbitrary, as long as they are the same as each other. We will always take it to be the last exit time of the modes under consideration within a correlation.

In writing Eq. (7.10), we have again assumed that the perturbed cosmology can be fully defined at some given time just in terms of field fluctuations on flat hypersurfaces, which is the case during slow roll, for example. As for the δN expression, however, there is nothing to stop us, at least at a formal level, from extending this to include any other degrees of freedom that may be important. The expansion Eq. (7.10) could be generalised to include spatial gradients to get subleading soft behaviour - this would be the analogy to the gradient expansion [25,326,327] which extends the usual δN. We leave this for future work.

In the following sections we will consider soft limits of correlations. We will insert the expansion Eq. (7.10) for all modes considered hard, and assume that the dominant contributions will come from Wick contractions amongst soft modes themselves, and Wick contractions amongst hard modes themselves, but not between soft and hard modes. This is the mathematical version of the assumption that the main contribution to the correlations come from how the soft modes correlate with the shifts they cause to the background cosmology which the hard modes experience. This leads to the factorization of the soft limits of correlations into hard sub-processes.

7.2.2 Simple Examples

Before presenting general rules which allow us to generate expressions for arbitrary soft limits let us consider two simple examples: the squeezed limit of the bispectrum and the single-soft collapsed limit of the trispectrum.

The Squeezed Limit of the Bispectum

As a first simple example of the use of the expansions presented above we revisit the squeezed limit of the bispectrum, considered in our earlier work [330]. We take $\langle\zeta_{\mathbf{k_1}}\zeta_{\mathbf{k_2}}\zeta_{\mathbf{k_3}}\rangle$, with $k_1 \ll k_2 \sim k_3$, and employ Eq. (7.10) to expand $\zeta^{\rm h}_{\mathbf{k_2}}\big|_{\rm s}$ and $\zeta^{\rm h}_{\mathbf{k_3}}\big|_{\rm s}$ in terms of long field perturbations, and insert these into the correlator

$$\lim_{k_1\ \rm soft}\langle\zeta_{\mathbf{k_1}}\zeta_{\mathbf{k_2}}\zeta_{\mathbf{k_3}}\rangle \approx \langle\zeta^{\rm s}_{\mathbf{k_1}}\zeta^{\rm h}_{\mathbf{k_2}}\big|_{\rm s}\zeta^{\rm h}_{\mathbf{k_3}}\big|_{\rm s}\rangle \tag{7.11}$$

$$\approx \langle \zeta^{\rm s}_{\mathbf{k_1}} \left(\zeta^{\rm h}_{\mathbf{k_2}} + \left[\frac{\partial \zeta^{\rm h}}{\partial \phi_A} \star \delta\phi^{\rm s}_A \right]_{\mathbf{k_2}} + \dots \right) \left(\zeta^{\rm h}_{\mathbf{k_3}} + \left[\frac{\partial \zeta^{\rm h}}{\partial \phi_B} \star \delta\phi^{\rm s}_B \right]_{\mathbf{k_3}} + \dots \right) \rangle \tag{7.12}$$

$$\approx (2\pi)^3 \delta(\mathbf{k_1} + \mathbf{k_2} + \mathbf{k_3}) \langle \zeta^{\rm s}_{\mathbf{k_1}} \delta\phi^{\rm s}_{B\,-\mathbf{k_1}} \rangle' \frac{\partial}{\partial \phi_B} \left(\frac{1}{2} P_\zeta(k_2) + \frac{1}{2} P_\zeta(k_3) \right) \tag{7.13}$$

where the primed correlator denotes the correlator stripped of the delta function and the factor of $(2\pi)^3$. In the first line we make the soft limit assumption that the dominant contribution in the soft limit comes from the correlation between the soft modes and the change that the soft modes cause in the hard modes. This allows us to replace $\zeta_{\mathbf{k_1}}$ with $\zeta^{\rm s}_{\mathbf{k_1}}$, and to replace $\zeta_{\mathbf{k_2}}$ with $\zeta^{\rm h}_{\mathbf{k_2}}\big|_{\rm s}$ within the correlator (and similarly for $\zeta_{\mathbf{k_3}}$). In the final line we use Wick's theorem and the soft limit assumption that only soft modes correlate with soft modes, and only hard modes correlate with hard modes.

Now, in the soft limit to leading order $k_2 \approx k_3$, we have that the final line simplifies to

$$\lim_{k_1 \text{ soft}} \langle \zeta_{\mathbf{k_1}} \zeta_{\mathbf{k_2}} \zeta_{\mathbf{k_3}} \rangle \approx (2\pi)^3 \delta(\mathbf{k_1} + \mathbf{k_2} + \mathbf{k_3}) N_A \Sigma_{AB}(k_1) P_{\zeta,B}(k_3) \tag{7.14}$$

where we also used the first order δN expansion Eq. (2.60) for the soft ζ, and the notation $Y_{,B} \equiv \frac{\partial Y}{\partial \phi_B}$, for any function Y, together with Eq. (7.6) for the definition of $\Sigma_{AB}(k_1)$.

The expression Eq. (7.14) is quite formal, but very compact. In §7.3 we will see how to turn it into a more explicit expression which can be evaluated to gain model specific predictions.

The Collapsed Limit of the Trispectum

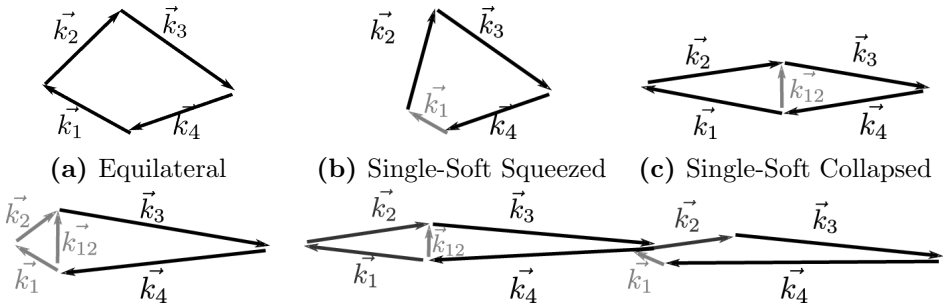

(a) Equilateral **(b)** Single-Soft Squeezed **(c)** Single-Soft Collapsed

(d) Double-Soft Kite **(e)** Double-Soft Squished **(f)** Double-Soft Wonky

Figure 10: Possible soft shapes of the trispectrum. For illustration we have drawn the quadrilaterals here as planar, but in general they can be three-dimensional. The greyscale adds emphasis, with lighter grey being more soft, while darker grey is more hard.

The possible soft limit shapes for the trispectrum are shown in Fig. 10. As a second example we consider the single-soft collapsed limit of the trispectrum, $k_{12} \ll k_1 \approx k_2 \sim k_3 \approx k_4$, where $\mathbf{k_{12}} = \mathbf{k_1} + \mathbf{k_2}$, illustrated in Fig. 10(c). We consider the four point function, $\langle \zeta_{\mathbf{k_1}} \zeta_{\mathbf{k_2}} \zeta_{\mathbf{k_3}} \zeta_{\mathbf{k_4}} \rangle$ with all the external ζ's taken to be hard with respect to the soft collapsed mode k_{12}. We use Eq. (7.10) on each of the four ζ's and insert these into the correlator

$$\lim_{k_{12}\ \text{soft}} \langle \zeta_{\mathbf{k_1}} \zeta_{\mathbf{k_2}} \zeta_{\mathbf{k_3}} \zeta_{\mathbf{k_4}} \rangle \approx \langle \zeta^{\rm h}_{\mathbf{k_1}}\big|_{\rm s} \zeta^{\rm h}_{\mathbf{k_2}}\big|_{\rm s} \zeta^{\rm h}_{\mathbf{k_3}}\big|_{\rm s} \zeta^{\rm h}_{\mathbf{k_4}}\big|_{\rm s} \rangle \tag{7.15}$$

$$\begin{aligned} &\approx \langle \left(\zeta^{\rm h}_{\mathbf{k_1}} + \left[\zeta^{\rm h}_{,A} \star \delta\phi^{\rm s}_A \right]_{\mathbf{k_1}} + \dots \right) \left(\zeta^{\rm h}_{\mathbf{k_2}} + \left[\zeta^{\rm h}_{,B} \star \delta\phi^{\rm s}_B \right]_{\mathbf{k_2}} + \dots \right) \times \\ &\qquad \left(\zeta^{\rm h}_{\mathbf{k_3}} + \left[\zeta^{\rm h}_{,C} \star \delta\phi^{\rm s}_C \right]_{\mathbf{k_3}} + \dots \right) \left(\zeta^{\rm h}_{\mathbf{k_4}} + \left[\zeta^{\rm h}_{,D} \star \delta\phi^{\rm s}_D \right]_{\mathbf{k_4}} + \dots \right) \rangle. \end{aligned} \tag{7.16}$$

There are lots of possible terms that can now appear when we Wick contract. In what follows we only show the terms that contribute at leading order in the soft limit. These are the terms that contain $\Sigma_{AB}(k_{12})$, which occur either when $\zeta^{\rm h}_{\mathbf{k_1}}$ gets contracted with the $\zeta^{\rm h}_{,B}$ inside the convolution $\left[\zeta^{\rm h}_{,B} \star \delta\phi^{\rm s}_B \right]_{\mathbf{k_2}}$, or similarly, when $\zeta^{\rm h}_{\mathbf{k_2}}$ gets contracted with the $\zeta^{\rm h}_{,A}$ inside the convolution $\left[\zeta^{\rm h}_{,A} \star \delta\phi^{\rm s}_A \right]_{\mathbf{k_1}}$. This is because the delta function that accompanies these contractions then forces the integrated momentum in the convolution, (which is the momentum of $\delta\phi^{\rm s}_B$ or $\delta\phi^{\rm s}_A$ respectively) to have magnitude k_{12} – which then appears in $\Sigma_{AB}(k_{12})$. There are four possible such terms giving the following contribution to the correlator

$$\begin{aligned} &\lim_{k_{12}\ \text{soft}} \langle \zeta_{\mathbf{k_1}} \zeta_{\mathbf{k_2}} \zeta_{\mathbf{k_3}} \zeta_{\mathbf{k_4}} \rangle \\ &\approx \int_{\mathbf{p}} \int_{\mathbf{q}} \left(\langle \zeta^{\rm h}_{\mathbf{k_1}} \zeta^{\rm h}_{,A\mathbf{k_2}-\mathbf{p}} \rangle + \langle \zeta^{\rm h}_{,A\mathbf{k_1}-\mathbf{p}} \zeta^{\rm h}_{\mathbf{k_2}} \rangle \right) \langle \delta\phi^{\rm s}_{A\mathbf{p}} \delta\phi^{\rm s}_{B\mathbf{q}} \rangle \left(\langle \zeta^{\rm h}_{\mathbf{k_3}} \zeta^{\rm h}_{,B\mathbf{k_4}-\mathbf{q}} \rangle + \langle \zeta^{\rm h}_{,B\mathbf{k_3}-\mathbf{q}} \zeta^{\rm h}_{\mathbf{k_4}} \rangle \right). \end{aligned} \tag{7.17}$$

Now using $\langle \zeta^{\rm h}_{\mathbf{k_1}} \zeta^{\rm h}_{,A\mathbf{k_2}-\mathbf{p}} \rangle = (2\pi)^3 \delta(\mathbf{k_1} + \mathbf{k_2} - \mathbf{p}) \frac{1}{2} P_\zeta(k_1)_{,A}$, and similarly for the other three two-point functions, we get

$$\begin{aligned} &\lim_{k_{12}\ \text{soft}} \langle \zeta_{\mathbf{k_1}} \zeta_{\mathbf{k_2}} \zeta_{\mathbf{k_3}} \zeta_{\mathbf{k_4}} \rangle \\ &\approx (2\pi)^3 \delta(\mathbf{k_1} + \mathbf{k_2} + \mathbf{k_3} + \mathbf{k_4}) \frac{1}{2} \left[P_\zeta(k_1) + P_\zeta(k_2) \right]_{,A} \Sigma_{AB}(k_{12}) \frac{1}{2} \left[P_\zeta(k_3) + P_\zeta(k_4) \right]_{,B}. \end{aligned} \tag{7.18}$$

Now, since in the soft limit to leading order $k_1 \approx k_2$ and $k_3 \approx k_4$, we can replace $P_\zeta(k_2)$

with $P_\zeta(k_1)$ and $P_\zeta(k_4)$ with $P_\zeta(k_3)$ to get our final expression

$$\begin{aligned}&\lim_{k_{12}\ \text{soft}} \langle \zeta_{\mathbf{k_1}} \zeta_{\mathbf{k_2}} \zeta_{\mathbf{k_3}} \zeta_{\mathbf{k_4}} \rangle \\ &\approx (2\pi)^3 \delta(\mathbf{k_1}+\mathbf{k_2}+\mathbf{k_3}+\mathbf{k_4}) P_\zeta(k_1)_{,A} \Sigma_{AB}(k_{12}) P_\zeta(k_3)_{,B}.\end{aligned} \tag{7.19}$$

We note that, though presented in a different manner, this agrees with the calculation of Byrnes et al. [322] for the collapsed limit.

Suyama-Yamaguchi Inequality

We can use Eq. (7.19) and Eq. (7.14) to directly prove the soft limit version of the Suyama-Yamaguchi inequality [287] relating the single-soft collapsed limit of the trispectrum to the squeezed limit of the bispectrum [280, 323, 331]. We begin by defining the dimensionless parameters

$$\tilde{f}_{\rm NL}(k_{12},k_1,k_2) \equiv \frac{5}{12}\frac{\lim_{k_{12}\ \text{soft}} B_\zeta(k_{12},k_1,k_2)}{P_\zeta(k_{12})P_\zeta(k_1)} = \frac{5}{12}\frac{N_A \Sigma_{AB}(k_{12}) P_\zeta(k_1)_{,B}}{P_\zeta(k_{12})P_\zeta(k_1)}\,, \tag{7.20}$$

$$\tilde{\tau}_{\rm NL}(\mathbf{k_1},\mathbf{k_2},\mathbf{k_3},\mathbf{k_4}) \equiv \frac{1}{4}\frac{\lim_{k_{12}\ \text{soft}} T_\zeta(\mathbf{k_1},\mathbf{k_2},\mathbf{k_3},\mathbf{k_4})}{P_\zeta(k_{12})P_\zeta(k_1)P_\zeta(k_3)} = \frac{1}{4}\frac{P_{\zeta,A}(k_1)\Sigma_{AB}(k_{12})P_{\zeta,B}(k_3)}{P_\zeta(k_{12})P_\zeta(k_1)P_\zeta(k_3)}. \tag{7.21}$$

The equalities that follow the definitions use Eq. (7.14) and Eq. (7.19) respectively.

The soft version of the Suyama-Yamaguchi inequality follows in the special case where $k_3 = k_1$. In this case the numerator of Eq. (7.21) becomes $P_\zeta(k_1)_{,A}\Sigma_{AB}(k_{12})P_\zeta(k_1)_{,B}$, which can be viewed as the inner product, with respect to the metric $\Sigma_{AB}(k_{12})$, of a vector with components $P_\zeta(k_1)_{,A}$. The numerator of Eq. (7.20) is $N_A\Sigma_{AB}(k_{12})P_\zeta(k_1)_{,B}$ which is the inner product of a different vector, N_A, with the original vector $P_\zeta(k_1)_{,B}$. The Cauchy-Schwarz inequality then gives

$$[P_\zeta(k_1)_{,A}\Sigma_{AB}(k_{12})P_\zeta(k_1)_{,B}][N_C\Sigma_{CD}(k_{12})N_D] \geq [N_E\Sigma_{EF}(k_{12})P_\zeta(k_1)_{,F}]^2. \tag{7.22}$$

We can now use the $k_3 = k_1$ version of Eq. (7.21) to replace the the first term in the left hand side of Eq. (7.22) in terms of $\tilde{\tau}_{\rm NL}$, and rewrite the second term using the δN expression $P_\zeta(k_{12}) = N_C\Sigma_{CD}(k_{12})N_D$. Finally using Eq. (7.20) to replace the RHS in terms of $\tilde{f}_{\rm NL}$, we arrive at

$$\tilde{\tau}_{\rm NL} \geq \left(\frac{6}{5}\tilde{f}_{\rm NL}\right)^2. \tag{7.23}$$

This is a rather direct proof of this soft limit relation, which to our knowledge hasn't appeared before, but which recovers the results of [280, 323, 331]. In §7.2.5 we will

see how this inequality can be generalised to provide relations between higher point functions.

7.2.3 Soft Limit Diagrams

The examples given so far were sufficiently simple that we could easily take a direct approach using the expansion Eq. (7.10) and then Wick contracting, using some algebra to get simple final expressions such as Eq. (7.14) and Eq. (7.19). For soft limits of higher-point correlation functions, however, this approach becomes cumbersome. It proves useful to generate a set of rules which lead to compact final expressions of the form given above. This can be readily achieved since for any soft limit the procedure is simply to insert the Soft Limit Expansion Eq. (7.10) for every hard ζ perturbation that is present. Wick contractions then occur amongst the soft modes themselves, and between the hard modes themselves, but not between soft and hard modes. Soft and hard modes are correlated only through the derivatives of the Soft Limit Expansion, Eq. (7.10). If there are N soft momenta of the same size, we need to Taylor expand to N-th order consistently in both the Soft Limit Expansion, Eq. (7.10), and in the δN expansion of the soft ζ

$$\zeta^{\rm s}_{\mathbf{k}} = N_A \delta\phi^{\rm s}_{A\mathbf{k}} + \frac{1}{2} N_{AB} \left[\delta\phi^{\rm s}_A \star \delta\phi^{\rm s}_B\right]_{\mathbf{k}} + \cdots . \tag{7.24}$$

We can then organise the result in terms of diagrams, which we call Soft Limit Diagrams. These diagrams are analogous to the δN graphs [329] which represent the Taylor expansion of standard δN. For simplicity we focus here only on tree level[28] contributions and capture only leading order behaviour in the soft limit and gradient expansion.

We now give rules for how to calculate a correlation in which all of the soft momenta are the same hierarchical size. It may be helpful to read these rules in combination with the examples which follow, in order to clarify the proceedure.

1. Identify all soft squeezed (soft external) momenta and put a box around each one. Identify *all* soft collapsed (internal) momenta built from a group of hard external momenta and put a box around each group. At this stage all external momenta should now be in a box. Draw a black vertex on each box.

2. Connect the black vertices by drawing a connected tree diagram with dashed lines. Each dashed line must connect on one end to a black vertex and on the other end to a white vertex. At a black vertex (possibly multiple) dashed lines can connect to a box. At a white vertex dashed lines connect to other dashed lines.

[28] Although we note that loops could easily be included in our diagrammatic approach.

3. Label each dashed line with a distinct field index $A_1, A_2, ...$

4. Ensure momentum conservation at every vertex, which determines the momentum of each dashed line.

5. The two vertex types are assigned the following factors:

   (a) Assign a factor $[G_Q(\{\mathbf{k}\})]_{,A_1\cdots A_m}$ to each black vertex which connects a box containing $Q \geq 1$ external momenta, $\{\mathbf{k}\}$, to m dashed lines with field indices $A_1 \cdots A_m$, where $m \geq 1$. Note that for $Q = 1$, we have $[G_1(\mathbf{k})]_{,A_1\cdots A_m} = N_{A_1\cdots A_m}$.

   (b) Assign a factor $F_{A_1\cdots A_s}(\mathbf{p_1}, ..., \mathbf{p_s})$ to each white vertex with s dashed lines with incoming momenta $\mathbf{p_1}, ..., \mathbf{p_s}$ and field index $A_1 \cdots A_s$, where $s \geq 2$.

6. Each diagram is associated with the mathematical expression obtained by multiplying together all vertex factors. Repeat the above process from stage 2 onwards to generate all distinct connected tree diagrams. $G_n(\mathbf{k_1}, ..., \mathbf{k_n})$ is then obtained by summing over all these diagrams.

If there are consecutive soft momenta, where there are hierarchies amongst the soft momenta, then follow the rules above for the softest in the hierarchy. Then recursively repeat the same rules for the next level up in the hierarchy, to calculate soft limits of correlators sitting within the hard sub-process box(es).

7.2.4 Examples Using Diagrams

We now show some examples of soft limits calculated using the diagrammatic approach. First we revisit the calculations of §7.2.2 using the rules presented above to check they reproduce the same answers. Then we consider other soft limits of the trispectrum, such as single-soft squeezed and various double-soft limits.

Simple Examples Revisited

In Fig. 11 we show the diagram one gets for the squeezed limit of the bispectrum. Multiplying the vertex factors together, one can check that this diagram reproduces the soft bispectrum of Eq. (7.14).

In Fig. 12 we show the diagram one gets for the single-soft collapsed limit of the trispectrum. Multiplying the vertex factors together, one can check that this diagram reproduces the single-soft collapsed result of Eq. (7.19).

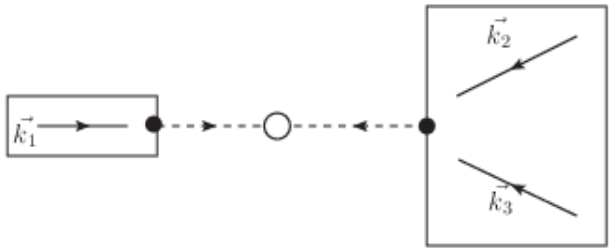

Figure 11: The only tree-level connected soft diagram for the squeezed limit of the bispectrum.

Figure 12: The only tree-level connected soft diagram for the single-soft collapsed limit of the trispectrum.

Other Examples

We now look at the single-soft squeezed limit of the trispectrum, $k_1 \ll k_2 \approx k_3 \approx k_4$. This has a very similar diagram to the squeezed limit of the bispectrum, and is shown in Fig. 13, giving the result

$$\lim_{k_1 \ll k_2 \approx k_3 \approx k_4} T_\zeta(\mathbf{k_1}, \mathbf{k_2}, \mathbf{k_3}, \mathbf{k_4}) = N_A \Sigma_{AB}(k_1) \left[B_\zeta(k_2, k_3, k_4)\right]_{,B} . \tag{7.25}$$

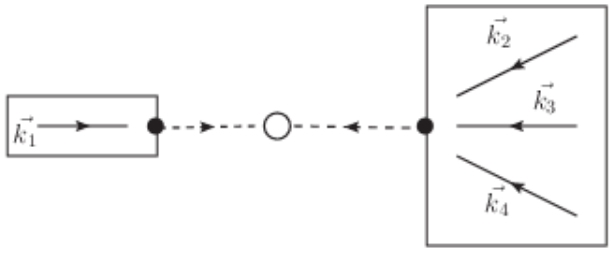

Figure 13: The only tree-level connected soft diagram for the single-soft squeezed limit of the trispectrum.

Next we consider the double-soft limits of the trispectrum, which in general is given by taking both $k_1 \ll k_3 \approx k_4$ and $k_2 \ll k_3 \approx k_4$. In this double-soft limit we have three choices for how k_1, k_2 and k_{12} are related, shown in Fig. 10, which we name

$$k_1 \approx k_2 \approx k_{12} \ll k_3 \approx k_4 \qquad \text{(kite)} \tag{7.26}$$

$$k_{12} \ll k_1 \approx k_2 \ll k_3 \approx k_4 \qquad \text{(squished)} \tag{7.27}$$

$$k_1 \ll k_2 \ll k_3 \approx k_4 \qquad \text{(wonky)}. \tag{7.28}$$

1. Double-Soft Kite: $k_1 \approx k_2 \approx k_{12} \ll k_3 \approx k_4$

For the kite shape there are four diagrams which can be drawn, shown in Fig. 10(d). The sum of the diagrams gives the expression (appearing in relative locations in the expression below)

$$\begin{aligned}&\lim_{\text{kite}} T_\zeta(\mathbf{k_1}, \mathbf{k_2}, \mathbf{k_3}, \mathbf{k_4}) \\ =&N_A N_B P_\zeta(k_3)_{,C} \alpha_{ABC}(k_1, k_2, k_{12}) + N_A N_B P_\zeta(k_3)_{,CD} \Sigma_{AC}(k_1) \Sigma_{BD}(k_2) \\ +&N_A N_{BC} P_\zeta(k_3)_{,D} \Sigma_{AB}(k_1) \Sigma_{CD}(k_{12}) + N_A N_{BC} P_\zeta(k_3)_{,D} \Sigma_{AB}(k_2) \Sigma_{CD}(k_{12}).\end{aligned} \tag{7.29}$$

Note that in order to get the bottom line of Eq. (7.29) we had to expand $\zeta^{\rm s}_{\mathbf{k_1}}$ and $\zeta^{\rm s}_{\mathbf{k_2}}$ to second order in δN expansion, using Eq. (7.24), so as to work to second order consistently throughout the calculation, i.e. we need to work to second order in both the δN expansion and the Soft Limit Expansion.

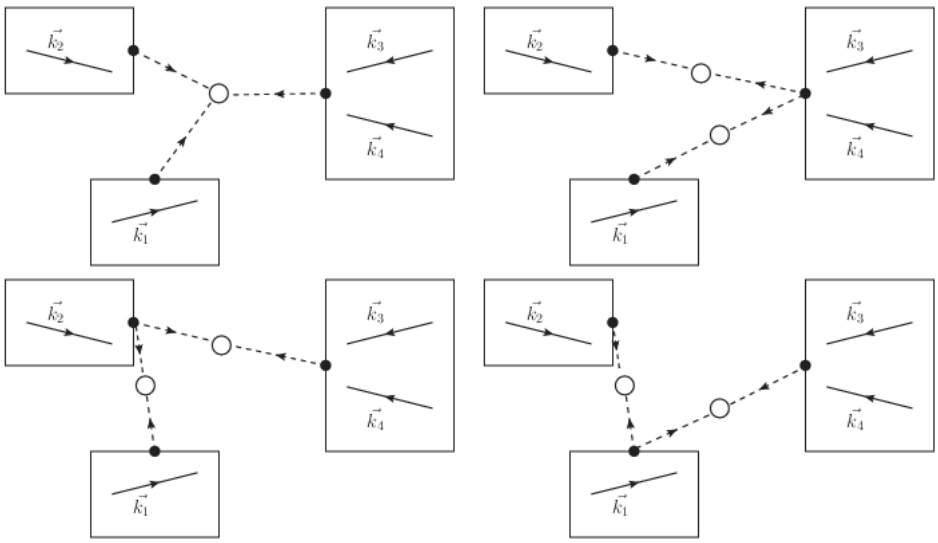

Figure 14: The four distinct tree-level connected soft diagrams for the double-soft limit of the trispectrum for the kite shape.

2. Double-Soft Squished: $k_{12} \ll k_1 \approx k_2 \ll k_3 \approx k_4$
For the squished shape we have the same diagram as in Fig. 12, leading to the same expression as Eq. (7.19)

$$\begin{aligned}&\lim_{k_{12}\ \text{soft}} \langle \zeta_{\mathbf{k_1}} \zeta_{\mathbf{k_2}} \zeta_{\mathbf{k_3}} \zeta_{\mathbf{k_4}} \rangle \\ &\approx (2\pi)^3 \delta(\mathbf{k_1} + \mathbf{k_2} + \mathbf{k_3} + \mathbf{k_4}) P_\zeta(k_1)_{,A} \Sigma_{AB}(k_{12}) P_\zeta(k_3)_{,B}.\end{aligned} \tag{7.30}$$

3. Double-Soft Wonky: $k_1 \ll k_2 \ll k_3 \approx k_4$
For the wonky shape we have to use the soft diagram rules recursively. The soft diagram is shown in Fig. 10(f). The diagram is constructed in two steps. First one draws a box around k_1, which is the softest momentum, and another box around the other three momenta. The second step, inside the box containing the other three momenta, is to draw a sub box around k_2, which is the next softest momenta, and another around the remaining two momenta. The resulting expression is

$$\lim_{\text{wonky}} T_\zeta(\mathbf{k_1}, \mathbf{k_2}, \mathbf{k_3}, \mathbf{k_4}) = N_A \Sigma_{AB}(k_1) \left[N_C \Sigma_{CD}(k_2) \left[P_\zeta(k_3) \right]_{,D} \right]_{,B}. \tag{7.31}$$

Note that we could expand out the derivatives here, and obtain three terms corresponding to the first three terms of Eq. (7.29), but with $\alpha_{ABC}(k_1, k_2, k_{12})$ replaced by its soft limit counterpart $\lim_{k_1 \ll k_2} \alpha_{ABC}(k_1, k_2, k_{12}) \approx \Sigma_{AD}(k_1) \Sigma_{BC,D}(k_2)$ [330]. The fourth term in Eq. (7.29), corresponding to the bottom right diagram of Fig. 14, is not present in the wonky limit, as it will be subdominant in the wonky limit compared to the other terms.

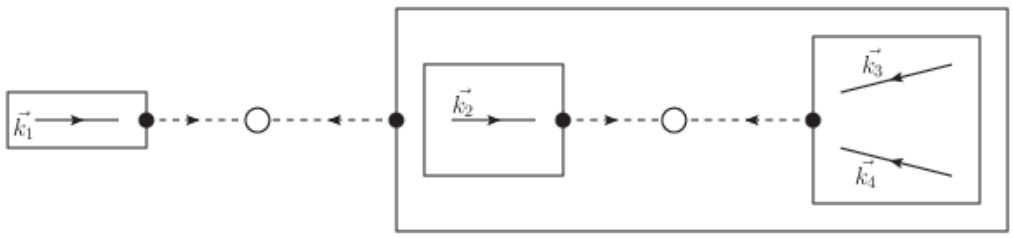

Figure 15: The tree-level connected soft diagram for the wonky shape double-soft limit of the trispectrum.

In this section we only considered examples up to the trispectrum for simplicity, but the rules can be applied to higher n-point function examples. We note that this procedure goes beyond what is available in the current literature, and in particular it allows for multiple fields. The resulting expressions provide relations between soft

limits of n-point ζ correlation functions and derivatives of lower-point ζ correlation functions, contracted with soft field-space correlation functions.

7.2.5 Inequalities Between Soft Correlation Functions

Following our considerations in §7.2.2 of the Suyama-Yamaguchi inequality [287], Eq. (7.23), we will now show how to generalise this inequality to higher-point functions. In the equilateral limit, and for Gaussian fields, [332] found inequalities amongst higher-point functions using the Cauchy-Schwarz inequality. Here we find inequalities for soft limit higher-point functions and without assuming Gaussian fields.

Consider a single-soft limit of an n-point function, with momenta ordered such that $k_1 \leq ... \leq k_n$. We take the soft momentum to be $\mathbf{p} \equiv \sum_{i=1}^{r} \mathbf{k_i}$, where $r = 1$ corresponds to a squeezed soft limit, while $2 \leq r \leq n-1$ corresponds to a collapsed soft limit. We will take the hard momenta to have wavenumbers all approximately of the size k_*. We then apply the soft diagram rules to find

$$\lim_{p \text{ soft}} G_n(\mathbf{k_1}, ..., \mathbf{k_r}, \mathbf{k_{r+1}}, ..., \mathbf{k_n}) \approx \left[G_r(\mathbf{k_1}, ..., \mathbf{k_r})\right]_{,A} \Sigma_{AB}(p) \left[G_{n-r}(\mathbf{k_{r+1}}, ..., \mathbf{k_n})\right]_{,B} . \tag{7.32}$$

Next we identify the following two vectors

$$X_A \equiv \left[G_r(\mathbf{k_1}, ..., \mathbf{k_r})\right]_{,A} \tag{7.33}$$

$$Y_B \equiv \left[G_{n-r}(\mathbf{k_{r+1}}, ..., \mathbf{k_n})\right]_{,B} . \tag{7.34}$$

We note that since $\Sigma_{AB}(p)$ is a real symmetric matrix it provides an inner product on the vector space in which X and Y live, which means we can utilise the Cauchy-Schwarz inequality for X and Y

$$\left[X_A \Sigma_{AB}(p) Y_B\right]^2 \leq \left[X_C \Sigma_{CD}(p) X_D\right] \left[Y_E \Sigma_{EF}(p) Y_F\right] . \tag{7.35}$$

The LHS of Eq. (7.35) gives Eq. (7.32), and since $G_r(\mathbf{k_1}, ..., \mathbf{k_r}) = G_r(-\mathbf{k_1}, ..., -\mathbf{k_r})$, the RHS of Eq. (7.35) can be written as the product of two other soft limits

$$\lim_{p \text{ soft}} G_{2r}(\mathbf{k_1}, ..., \mathbf{k_r}, -\mathbf{k_1}, ..., -\mathbf{k_r}) \approx \left[G_r(\mathbf{k_1}, ..., \mathbf{k_r})\right]_{,A} \Sigma_{AB}(p) \left[G_r(-\mathbf{k_1}, ..., -\mathbf{k_r})\right]_{,B} \tag{7.36}$$

$$\lim_{p \text{ soft}} G_{2(n-r)}(\mathbf{k_{r+1}}, ..., \mathbf{k_n}, -\mathbf{k_{r+1}}, ..., -\mathbf{k_n}) \approx \left[G_n(\mathbf{k_{r+1}}, ..., \mathbf{k_n})\right]_{,A} \Sigma_{AB}(p) \times \left[G_r(-\mathbf{k_{r+1}}, ..., -\mathbf{k_n})\right]_{,B} \tag{7.37}$$

which yields

$$\left[\lim_{p\ \text{soft}} G_n(\mathbf{k_1},...,\mathbf{k_r},\mathbf{k_{r+1}},...,\mathbf{k_n})\right]^2 \leq \left[\lim_{p\ \text{soft}} G_{2r}(\mathbf{k_1},...,\mathbf{k_r},-\mathbf{k_1},...,-\mathbf{k_r})\right] \times \left[\lim_{p\ \text{soft}} G_{2(n-r)}(\mathbf{k_{r+1}},...,\mathbf{k_n},-\mathbf{k_{r+1}},...,-\mathbf{k_n})\right]. \tag{7.38}$$

This can be written in terms of soft limit dimensionless parameters

$$f_n(\mathbf{k_1},...,\mathbf{k_r},\mathbf{k_{r+1}},...,\mathbf{k_n}) \equiv \lim_{p\ \text{soft}} \frac{G_n(\mathbf{k_1},...,\mathbf{k_r},\mathbf{k_{r+1}},...,\mathbf{k_n})}{P_\zeta(p)[P_\zeta(k_*)]^{n-2}} \tag{7.39}$$

as

$$[f_n(\mathbf{k_1},...,\mathbf{k_r},\mathbf{k_{r+1}},...,\mathbf{k_n})]^2 \leq [f_{2r}(\mathbf{k_1},...,\mathbf{k_r},-\mathbf{k_1},...,-\mathbf{k_r})] \times \left[f_{2(n-r)}(\mathbf{k_{r+1}},...,\mathbf{k_n},-\mathbf{k_{r+1}},...,-\mathbf{k_n})\right] \tag{7.40}$$

or, suppressing the momentum dependence for brevity,

$$f_n^2 \leq f_{2r} f_{2(n-r)}. \tag{7.41}$$

We note that $f_2 = 1$ by definition, while $f_3 = \frac{12}{5}\tilde{f}_{\rm NL}$ and $f_4 = 4\tilde{\tau}_{\rm NL}$. If we fix $n = 3$ and $r = 1$, one recovers the soft limit Suyama-Yamaguchi inequality, $\left(6\tilde{f}_{\rm NL}/5\right)^2 \leq \tilde{\tau}_{\rm NL}$ [280, 287, 323, 331].

Novel, yet similar, relations exist between the single-soft squeezed (external) limit of an n-point correlator and the single-soft collapsed (internal) limit of a $2n-2$ correlation function, which follows by fixing $r = 1$ and $n > 3$.

For $1 < r < n - 1$, a qualitatively different kind of relation emerges between the single-soft collapsed limit of an n-point correlator and the product of a single-soft collapsed limit of a $2r$-point correlator and a single-soft collapsed limit of a $2(n-r)$-point correlator, i.e. all the soft limits in this case are collapsed ones. The first non-trival example of this type of inequality occurs for $n = 5$, $r = 2$, which relates the collapsed 5-point function to the collapsed 6-point function and collapsed 4 point function.

Note that in the case of single-source inflation, all of the inequalities are saturated, since the Cauchy-Schwarz inequality becomes an equality in a vector space of only one dimension.

7.3 Explicit Expressions

7.3.1 The Γ expansion

The soft limit expressions we generated in §7.2, while compact, are not fully explicit. This is because these soft limit expressions involve field-space s-point correlation functions of the soft momenta, $F_{A_1,...,A_s}(\mathbf{p_1},...,\mathbf{p_s})$, (for the definition see Eq. (7.5)) corresponding to the white vertices in the diagrams. These s-point functions need to be evaluated at the time the last mode exits, t_n. However, explicit analytic expressions for field-space correlation functions are usually calculated when the evaluation time matches the earlier exit time of the $\mathbf{p_1},...,\mathbf{p_s}$.

In this section we will calculate $F_{A_1,...,A_s}(\mathbf{p_1},...,\mathbf{p_s})$ in terms of correlation functions evaluated at the earlier time at which the soft modes exit, for which there are analytic expressions available. To do so we will need to account for the evolution of field space perturbations themselves between successive flat hypersurfaces. This can be achieved by use of a separate universe expansion, analogous to the δN expansion, which allows us to account for the evolution of field fluctuations between horizon crossing times, given by the Γ expansion

$$\begin{aligned}\delta\phi^{(l)}_{A,\mathbf{k}} &= \Gamma^{(le)}_{A,B}\delta\phi^{(e)}_{B,\mathbf{k}} + \frac{1}{2}\Gamma^{(lee)}_{A,BC}\left[\delta\phi^{(e)}_{B}\star\delta\phi^{(e)}_{C}\right]_{\mathbf{k}} + \dots\,,\\ \text{where}\quad \Gamma^{(le)}_{A,B} &\equiv \frac{\partial\phi^{(l)}_{A}}{\partial\phi^{(e)}_{B}}\,,\quad \Gamma^{(lee)}_{A,BC} \equiv \frac{\partial^2\phi^{(l)}_{A}}{\partial\phi^{(e)}_{B}\partial\phi^{(e)}_{C}}\,,\end{aligned} \tag{7.42}$$

which expresses the perturbations on flat hypersurfaces at some later time t_l in terms of the perturbation at some earlier time t_e. This was used at first-order in [330] and to second-order in [322], and objects similar to the Γ matrices have been used by a number of authors in the past[29] [38,55,56,298–302]. We note that formally this expansion could be extended to include other degrees of freedom, just as we argued for the δN and Soft Limit Expansion presented in earlier sections, though here we will only consider field perturbations.

The real power of the Γ matrix expansion is that following a separate universe approach, they can be calculated with knowledge only of the background cosmology, in the same way that the δN coefficients can also be calculated using just the background cosmology. This is what allows the correlations generated in specific models to be explicitly calculated. In Ref. [330], for example, we gave explicit expressions for $\Gamma_{A,B}$ in canonical slow-roll models with sum-separable potentials, and these can easily be extended to second order. Finally, we note that for the bispectrum and trispectrum, it will be sufficient to keep terms in the expansion up to first- and second-order, respectively, while we note that for s-point field-space correlation functions, the $(s-1)$th

[29] One can generalise the Γ matrices to be k-dependent, as in [57].

order contributions are required.

In following sections we will make use of the result

$$N_B^{(e)} = N_A^{(l)} \Gamma_{A,B}^{(l,e)} \tag{7.43}$$

which relates the earlier derivative of N to the later one.

7.3.2 Field-Space Correlation Functions

We can insert Eq. (7.42) into the field-space correlation functions $F_{A_1,...,A_s}(\mathbf{p_1}, ..., \mathbf{p_s})$ to express them in terms of correlation functions evaluated instead at the earlier times at which the soft modes exit the horizon, for which there are analytic expressions available.

We first consider the two-point function, evaluated at the late time t_n, for some soft momentum $\mathbf{p_1}$ which exits at an earlier time $t_1 < t_n$. Inserting the expansion Eq. (7.42) and taking the two-point function gives the tree level contribution (here, for clarity, we explicitly state the time label (n), which was suppressed in previous sections)

$$\Sigma_{AB}^{(n)}(p_1) = \Gamma_{A,C}^{(n,1)} \Gamma_{B,D}^{(n,1)} \Sigma_{CD}^{(1)}(p_1). \tag{7.44}$$

Note that the LHS of Eq. (7.44) was the object that appeared in the expressions of the previous section, such as Eq. (7.14), Eq. (7.19), Eq. (7.25), Eq. (7.29), Eq. (7.30) and Eq. (7.31). The RHS of Eq. (7.44) involves the Γ matrices – set by the background cosmology – and the field-space two-point function of the soft momentum at the time of horizon exit, t_1, which, specialising to canonical light fields, has the well known expression[30] [20, 21]

$$\Sigma_{CD}^{(1)}(p_1) = \frac{{H^{(1)}}^2}{2p_1^3} \delta_{CD}. \tag{7.45}$$

For the trispectrum in the double-soft-kite limit, Eq. (7.29), we also need the field space three-point function of soft momenta $\mathbf{p_1}, \mathbf{p_2}, \mathbf{p_3}$, evaluated at the later time t_n. Inserting three copies of Eq. (7.42) into the three-point function gives the tree level contribution [55, 56]

$$\begin{aligned} \alpha_{ABC}^{(n)}(p_1, p_2, p_3) =& \Gamma_{A,D}^{(n,1)} \Gamma_{B,E}^{(n,1)} \Gamma_{C,F}^{(n,1)} \alpha_{DEF}^{(1)}(p_1, p_2, p_3) \\ &+ \left[\Gamma_{A,DE}^{(n,11)} \Gamma_{B,F}^{(n,1)} \Gamma_{C,G}^{(n,1)} \Sigma_{DF}^{(1)}(p_2) \Sigma_{EG}^{(1)}(p_3) + (A, p_1 \to B, p_2 \to C, p_3) \right] \end{aligned} \tag{7.46}$$

where the three permutations in the second line are formed by cycling through $A \to$

[30] Strictly, this is the result that the two-point function takes after the decaying mode, present at horizon crossing, has decayed, written in terms of horizon crossing parameters.

$B \to C$ whilst simultaneously cycling the momenta $p_1 \to p_2 \to p_3$. The LHS of Eq. (7.46) appears in Eq. (7.29) with $p_1 = k_1, p_2 = k_2$ and $p_3 = k_{12}$. The RHS of Eq. (7.46) involves the first and second order Γ matrices – set by the background cosmology – as well as the two- and three-point functions of the soft momenta at the time of horizon exit of the soft momenta t_1. The two-point function is given by Eq. (7.45) and the three-point function, again for canonical light fields, is given by [324]

$$\begin{aligned}&\alpha^{(1)}_{DEF}(p_1,p_2,p_3)\\&= \frac{4\pi^4}{p_1^3 p_2^3 p_3^3}\left(\frac{H^{(1)}}{2\pi}\right)^4 \sum_{6\text{ perms}} \frac{\dot\phi^{(1)}_D \delta_{EF}}{4H^{(1)}}\left(-3\frac{p_2^2 p_3^2}{p_t} - \frac{p_2^2 p_3^2}{p_t^2}(p_1+2p_3) + \frac{1}{2}p_1^2 - p_1 p_2^2\right)\end{aligned} \tag{7.47}$$

for $p_t \equiv p_1 + p_2 + p_3$, and where the sum is over the six permutations of (DEF) while simultaneously rearranging the momenta p_1, p_2, p_3 such that the relative positioning of the p's is respected.

We could proceed to consider s-point functions rewritten in terms of correlations at horizon crossing in a similar way, keeping terms in the Γ expansion up to the $(s-1)$th order, but for now we have what is required for the bispectrum and trispectrum. We give the method for calculating the s-point functions using diagrams in App. C.3.

7.3.3 Explicit Examples

Continuing to consider models with canonical light fields, we will now give our final expressions for the examples considered in §7.2, using the results of §7.3.2. The results given in this section can be used to compare a given multi-field model against data. We will show results for dimensionless versions of the correlation functions.

Bispectrum

The bispectrum can be parametrized in terms of the dimensionless quantity,

$$f_{\rm NL}(k_1,k_2,k_3) \equiv \frac{5}{6}\frac{B_\zeta(k_1,k_2,k_3)}{[P_\zeta(k_1)P_\zeta(k_2) + P_\zeta(k_2)P_\zeta(k_3) + P_\zeta(k_3)P_\zeta(k_1)]} \tag{7.48}$$

known as the reduced bispectrum.

For the squeezed limit of the bispectrum, the result Eq. (7.14) becomes

$$\begin{aligned}\lim_{k_1 \ll k_2, k_3} B_\zeta(k_1,k_2,k_3) \approx\ & - N^{(3)}_A N^{(3)}_E N^{(3)}_E \Gamma^{(3,1)}_{A,C}\Gamma^{(3,1)}_{B,C}\frac{d\phi^{(3)}_B}{dN}\frac{H^{(1)^2}}{2k_1^3}\frac{H^{(3)^2}}{2k_3^3}\\ & + 2N^{(3)}_A N^{(3)}_{EB} N^{(3)}_E \Gamma^{(3,1)}_{A,C}\Gamma^{(3,1)}_{B,C}\frac{H^{(1)^2}}{2k_1^3}\frac{H^{(3)^2}}{2k_3^3}\end{aligned} \tag{7.49}$$

where we used Eq. (7.44) and Eq. (7.45) for $\Sigma_{AB}(k_1)$, and we differentiated the δN expression for $P_\zeta(k_3)$.

If the bispectrum is large enough to be observed by present or near future probes, the second term in Eq. (7.49) must be dominant, and we can then form the dimensionless reduced bispectrum

$$\lim_{k_1 \ll k_2, k_3} f_{\rm NL} \equiv \frac{5}{12} \frac{\lim\limits_{k_1 \ll k_2, k_3} B_\zeta(k_1, k_2, k_3)}{P_\zeta(k_1) P_\zeta(k_3)} \approx \frac{5}{6} \frac{N^{(3)}_A N^{(3)}_{EB} N^{(3)}_E \Gamma^{(3,1)}_{A,C} \Gamma^{(3,1)}_{B,C}}{N^{(3)}_D N^{(3)}_D N^{(3)}_F N^{(3)}_G \Gamma^{(3,1)}_{F,H} \Gamma^{(3,1)}_{G,H}} \,, \tag{7.50}$$

which is dependent on the two scales k_1 and k_3 through the two horizon crossing times.

We could use Eq. (7.43) to write this more succinctly as

$$\lim_{k_1 \ll k_2, k_3} f_{\rm NL} \approx \frac{5}{6} \frac{N^{(1)}_A N^{(3)}_{BC} N^{(3)}_B \Gamma^{(3,1)}_{C,A}}{N^{(3)}_D N^{(3)}_D N^{(1)}_E N^{(1)}_E} \,, \tag{7.51}$$

which can be contrasted with the usual δN formula for the reduced bispectrum, valid for close to equilateral configurations (under the same assumptions)

$$\lim_{k_1 \approx k_2 \approx k_3} f_{\rm NL} \equiv \frac{5}{6} \frac{\lim\limits_{k_1 \approx k_2 \approx k_3} B_\zeta(k_1, k_2, k_3)}{[P_\zeta(k_1) P_\zeta(k_2) + 2 \text{ perms}]} = \frac{5}{6} \frac{N^{(3)}_A N^{(3)}_{AB} N^{(3)}_B}{N^{(3)}_C N^{(3)}_C N^{(3)}_D N^{(3)}_D} \,, \tag{7.52}$$

which retains dependence on only a single horizon crossing time. In [330] we found that the difference between Eq. (7.51) and Eq. (7.52) can be very important for models with significant scale dependence. For this we looked at a simple two-field example of a mixed inflaton-curvaton model with curvaton self-interactions. For that model it was possible to derive analytic expressions for the derivatives of N and the first-order Γ matrices. We expect it to be possible to calculate higher-order Γ matrices in this model as well, but we leave this for future work.

Trispectrum

Turning to the trispectrum, let us first review results for the case in which all modes cross the horizon at close to the same time, if the trispectrum is observable by present or near future observations then in this case it is given by [242, 328]

$$\begin{aligned} T_\zeta(\mathbf{k_1}, \mathbf{k_2}, \mathbf{k_3}, \mathbf{k_4}) =& \tau_{\rm NL} \left[P_\zeta(k_{13}) P_\zeta(k_3) P_\zeta(k_4) + \ 11\text{perms} \right] \\ &+ g_{\rm NL} \left[P_\zeta(k_2) P_\zeta(k_3) P_\zeta(k_4) + 4 \text{ perms} \right] \end{aligned} \tag{7.53}$$

where

$$\tau_{\rm NL} \equiv \frac{N^{(3)}_{AB} N^{(3)}_B N^{(3)}_{AC} N^{(3)}_C}{(N^{(3)}_D N^{(3)}_D)^3} \tag{7.54}$$

$$g_{\rm NL} \equiv \frac{N^{(3)}_{ABC} N^{(3)}_{A} N^{(3)}_{B} N^{(3)}_{C}}{(N^{(3)}_{D} N^{(3)}_{D})^3} \tag{7.55}$$

are dimensionless parameters which represent the amplitude of two distinct shapes.

This decomposition into two shapes is only useful for close to equilateral configurations. This is because, in soft limits, the square brackets have the same k-dependence as each other at leading order in the soft limit - that is, there isn't a unique decomposition into different shapes between them.

This is regardless of whether $\tau_{\rm NL}$ and $g_{\rm NL}$ are constants, since the split requires different configuration dependence. In the case where $\tau_{\rm NL}$ and $g_{\rm NL}$ are constants, they can, and in general will, be different to the dimensionless expressions we present in the next few pages, because the terms that appear in these new dimensionless expressions are different - since they depend on Γ matrices for example, which are not constrained to be constants if $\tau_{\rm NL}$ and $g_{\rm NL}$ are constants.

For soft limits one can, however, form dimensionless versions of the trispectrum. In the case of the single-soft limit of the trispectrum, we will form the single-soft dimensionless trispectrum by dividing the trispectrum by one power spectrum evaluated on the soft momentum, and two copies of the power spectrum evaluated on the hard momentum. For the double-soft limit, we will form the double-soft dimensionless trispectrum by dividing the trispectrum by two copies of the power spectrum evaluated on the soft momentum, and one power spectrum evaluated on the hard momentum.

Single-Soft Squeezed Trispectrum

For the single-soft squeezed limit of the trispectrum, we obtained the result Eq. (7.25), which contains the derivative of the near-equilateral bispectrum, $B_\zeta(k_2, k_3, k_4)$. The standard δN expression in near equilateral configurations can be used to give an expression for this piece, which we then need to differentiate. Focusing again on the case in which the bispectrum and trispectrum are observably large, and using Eq. (7.44) to write $\Sigma_{AB}(k_1)$ in terms of known quantities and Γ matrices we find

$$f_4^{\rm ext}(\mathbf{k_1}, \mathbf{k_2}, \mathbf{k_3}, \mathbf{k_4}) \equiv \frac{\lim\limits_{k_1 \ll k_2 \approx k_3 \approx k_4} T_\zeta(\mathbf{k_1}, \mathbf{k_2}, \mathbf{k_3}, \mathbf{k_4})}{3 P_\zeta(k_1) \left[P_\zeta(k_4)\right]^2} \tag{7.56}$$

$$\approx \frac{N^{(4)}_{A} \Gamma^{(4,1)}_{A,E} \Gamma^{(4,1)}_{B,E} N^{(4)}_{CDB} N^{(4)}_{C} N^{(4)}_{D}}{N^{(4)}_{G} N^{(4)}_{H} \Gamma^{(4,1)}_{G,F} \Gamma^{(4,1)}_{H,F} (N^{(4)}_{I} N^{(4)}_{I})^2} + \frac{N^{(4)}_{A} \Gamma^{(4,1)}_{A,E} \Gamma^{(4,1)}_{B,E} N^{(4)}_{CD} N^{(4)}_{CB} N^{(4)}_{D}}{N^{(4)}_{G} N^{(4)}_{H} \Gamma^{(4,1)}_{G,F} \Gamma^{(4,1)}_{H,F} (N^{(4)}_{I} N^{(4)}_{I})^2}. \tag{7.57}$$

We can again use Eq. (7.43) to write this more succinctly as

$$f_4^{\rm ext}(\mathbf{k_1},\mathbf{k_2},\mathbf{k_3},\mathbf{k_4}) \approx \frac{N_A^{(1)}\Gamma^{(4,1)}_{B,A}N^{(4)}_{CDB}N^{(4)}_C N^{(4)}_D}{N^{(1)}_E N^{(1)}_E (N^{(4)}_F N^{(4)}_F)^2} + \frac{N_A^{(1)}\Gamma^{(4,1)}_{B,A}N^{(4)}_{CD}N^{(4)}_{CB} N^{(4)}_D}{N^{(1)}_E N^{(1)}_E (N^{(4)}_F N^{(4)}_F)^2}. \quad (7.58)$$

If we had taken the near-equilateral configuration, Eq. (7.53), and formed the analogous reduced trispectrum and pushed this expression towards the single-soft squeezed limit, we would have found a contribution both from the $\tau_{\rm NL}$ and the $g_{\rm NL}$ shape in this limit, and we would have arrived at a similar expression to Eq. (7.58) but with all the N derivatives appearing with the same superscript and $\Gamma^{(4,1)}_{A,B}$ replaced with δ_{AB}. Our expression can be significantly different from this naive one.

Single-Soft Internal Trispectrum

We now proceed to produce similar expressions for the other soft limits. For the single-soft collapsed limit of the trispectrum, we obtained the result Eq. (7.19). The derivative of the power spectrum gives

$$P_\zeta(k_1)_{,A} = 2N_{BA}N_C\Sigma_{BC}(k_1) + N_B N_C \Sigma_{BC,A}(k_1)\,. \quad (7.59)$$

Utilising this expression, keeping only the first term, we find

$$f_4^{\rm int}(\mathbf{k_1},\mathbf{k_2},\mathbf{k_3},\mathbf{k_4}) \equiv \frac{\lim\limits_{k_{12}\ll k_1\approx k_2\approx k_3\approx k_4} T_\zeta(\mathbf{k_1},\mathbf{k_2},\mathbf{k_3},\mathbf{k_4})}{4P_\zeta(k_{12})\left[P_\zeta(k_4)\right]^2} \approx \frac{N^{(4)}_{AB}N^{(4)}_A\Gamma^{(4,12)}_{B,C}\Gamma^{(4,12)}_{D,C}N^{(4)}_{ED}N^{(4)}_E}{N^{(12)}_F N^{(12)}_F (N^{(4)}_G N^{(4)}_G)^2}. \quad (7.60)$$

Considering Eq. (7.53) for close to equilateral configurations and pushing this expression towards the collapsed limit, we could have found a contribution from the $\tau_{\rm NL}$ shape alone, and a similar expression to Eq. (7.60), but with all the N derivatives appearing with the same superscript and $\Gamma^{(4,12)}_{A,B}$ replaced with δ_{AB}. Once again our new expression can be significantly altered from this naive expression.

Double-Soft Trispectrum

1. Kite

We had Eq. (7.29) from the soft diagrams, so here we can once again use Eq. (7.44) and Eq. (7.45) to write $\Sigma_{AB}(k_1)$ and $\Sigma_{AB}(k_2)$ in terms of known quantities and Γ matrices, and now we also need to use Eq. (7.46) with Eq. (7.47) and Eq. (7.45) to write $\alpha^{(4)}_{ABC}(k_1,k_2,k_{12})$, in terms of horizon crossing expressions and Γ matrices – in this case the second order Γ coefficient is necessary. We note that there is nothing to

stop $\alpha_{ABC}(k_1, k_2, k_{12})$ from becoming large even in canonical models, because it has evolved from time t_1 to time t_4.

Keeping all the terms that can be significant and taking $k_s \approx k_1 \approx k_2 \approx k_{12}$ and $k_h \approx k_3 \approx k_4$ with $k_s \ll k_h$ to define the kite limit, then the dimensionless quantity appropriate here is

$$f_4^{\rm kite}(\mathbf{k_1}, \mathbf{k_2}, \mathbf{k_3}, \mathbf{k_4}) \equiv \frac{\lim_{\rm kite} T_\zeta(\mathbf{k_1}, \mathbf{k_2}, \mathbf{k_3}, \mathbf{k_4})}{2\left[P_\zeta(k_s)\right]^2 P_\zeta(k_h)} \tag{7.61}$$

$$\begin{aligned} &\approx \frac{N_A^{(h)} N_B^{(h)} N_{FC}^{(h)} N_F^{(h)} \Gamma_{A,DE}^{(h,s)} \Gamma_{B,D}^{(h,s)} \Gamma_{C,E}^{(h,s)}}{\left(N_G^{(s)} N_G^{(s)}\right)^2 N_H^{(h)} N_H^{(h)}} \\ &+ \frac{N_A^{(h)} N_B^{(h)} \left(N_{ECD}^{(h)} N_E^{(h)} + N_{EC}^{(h)} N_{DE}^{(h)}\right) \Gamma_{A,F}^{(h,s)} \Gamma_{C,F}^{(h,s)} \Gamma_{B,I}^{(h,s)} \Gamma_{D,I}^{(h,s)}}{\left(N_G^{(s)} N_G^{(s)}\right)^2 N_H^{(h)} N_H^{(h)}} \\ &+ \frac{2 N_A^{(h)} N_{BC}^{(h)} N_E^{(h)} N_{ED}^{(h)} \Gamma_{A,F}^{(h,s)} \Gamma_{B,F}^{(h,s)} \Gamma_{C,I}^{(h,s)} \Gamma_{D,I}^{(h,s)}}{\left(N_G^{(s)} N_G^{(s)}\right)^2 N_H^{(h)} N_H^{(h)}} \end{aligned} \tag{7.62}$$

We note once again that considering Eq. (7.53) for close to equilateral configurations and pushing this towards the kite limit, both the $\tau_{\rm NL}$ and $g_{\rm NL}$ shapes would have contributed in this limit and we would have found similar terms to the last two lines of Eq. (7.62). The term in the first line of Eq. (7.62), however, is qualitatively different, and we believe is a new form of possibly significant contribution to the trispectrum, which could be large, even in models where the equilateral $g_{\rm NL}$ and $\tau_{\rm NL}$ are small. We hope to investigate this further in future work.

2. Squished

The squished limit gave the same expression Eq. (7.30) as the single-soft collapsed limit Eq. (7.19). We refer to the corresponding result Eq. (7.60) for the explicit form of the reduced trispectrum in this case.

3. Wonky

For this limit we had Eq. (7.31). The dimensionless trispectrum relevant here is

$$f_4^{\rm wonky}(\mathbf{k_1}, \mathbf{k_2}, \mathbf{k_3}, \mathbf{k_4}) \equiv \frac{\lim_{k_1 \ll k_2 \ll k_3 \approx k_4} T_\zeta(\mathbf{k_1}, \mathbf{k_2}, \mathbf{k_3}, \mathbf{k_4})}{2 P_\zeta(k_1) P_\zeta(k_2) P_\zeta(k_4)} \tag{7.63}$$

$$\approx \frac{N_A^{(4)} \Gamma_{A,E}^{(4,1)} \Gamma_{B,E}^{(4,1)} \left(N_C^{(4)} \Gamma_{C,F}^{(4,2)} \Gamma_{D,F}^{(4,2)} N_{GD}^{(4)} N_G^{(4)}\right)_{,B}}{N_F^{(4)} N_F^{(4)} N_G^{(1)} N_G^{(1)} N_H^{(2)} N_H^{(2)}} \tag{7.64}$$

where we have again neglected both first and second derivatives of $\Sigma_{AB}^{(s)}(k_s)$. Note the

comments concerning the kite limit, and a new contribution to the trispectrum, also apply here.

7.4 Conclusion

In this chapter we developed a formalism for calculating soft limits of n-point inflationary correlation functions for multiple light fields. This formalism allows for squeezed (external) or collapsed (internal) soft modes and for multiple soft modes either of the same size or with a hierarchy amongst the soft modes. We used a diagrammatic approach to organise the separate universe Soft Limit Expansion Eq. (7.10) to allow for explicit computation of any n-point ζ correlators in soft limit polygon shapes.

We applied our results to derive new, explicit expressions for the single- and double-soft limits of the trispectrum for a variety of quadrilateral shapes. A highlight of this section was the identification of possibly large contributions to the trispectrum in canonical models which are missed by the usual analysis. We also gave a new, direct proof of the soft limit version of the Suyama-Yamaguchi inequality and generalized this to give an infinite tower of new inequalities between soft limits of n-point correlators which are constrained by products of $2r$- and $2(n-r)$-point equilateral correlators, with $1 \leq r \leq n-2$. The case of $n = 3, r = 2$ is the well-known Suyama-Yamaguchi inequality – with other choices of n and r representing new inequalities. All of these are saturated in single-source models, and their violation may signify a breakdown of the inflationary paradigm.

We emphasize that these results are important for future observations which can probe a larger range of scales. Accurate theoretical predictions may be necessary, even for the trispectrum, and we may hope to rule out large classes of inflationary models by observations of these soft limits. For example, DES, Euclid may provide new constraints in the near future, and μ-distortion experiments such as PIXIE may be able to give sensitivity three orders of magnitude better than the current limits on spectral distortion, giving us access to an even wider range of scales, though this may occur later in the future.

Chapter 8

Conclusion

In this thesis we have pushed forward our understanding of the early universe, developing the connection between inflationary theory and observables. We will now recapitulate the original motivation for this thesis, then summarise our findings and present a critique of the studies before suggesting future directions for research on this topic. We begin with the motivation for this thesis.

The broad motivation for this thesis was to further our knowledge on the precise microphysics of inflation, the phase necessary for resolving the *horizon problem*. More specifically, the work presented here falls into the area of inflationary observables - providing theoretical predictions of these observables from inflationary models. The hope is that this work will help towards discerning the true nature of the physics of inflation by comparing future observations against the theoretical predictions made in this thesis.

Our choice of inflationary models was motivated in two ways: from the top-down and from the bottom-up. In the top-down approach one begins with a well-motivated UV complete theory, such as string theory, and derives from it the specific predictions of the inflationary observables. In the bottom-up approach one begins with a generic low energy effective theory (or classes of theories), such as multi-field inflation, and derives correspondingly general predictions of observables from this class of models.

This thesis is in no way a complete description of the study of inflationary observables. Instead we hope that it has advanced the current knowledge of inflationary predictions for the models we considered. Below we summarise the findings of this thesis, providing also a critique of the studies.

In Part I we took the top-down approach by selecting our model of inflation from string theory. In Chapter 4 we investigated a model of natural inflation derived from a string theory compactification in the warped resolved conifold geometry, using a D-brane position modulus as our inflaton candidate. The novelty of this work was two-fold. First, we applied knowledge of the analytic solutions to the Laplace equation on the

resolved conifold to allow us to investigate D-brane inflation near the tip – this was not possible in previous work using the deformed conifold, where analytic solutions to the Laplace equation are not known. Second, we took advantage of this near-tip parameter space to give a natural inflation model containing an observably-large value of the tensor-to-scalar ratio – this wasn't achieved in previous D-brane models of inflation and is also hard to arrange in simple closed-string models of natural inflation.

In critique of the work of Chapter 4, we note a few shortcomings. Firstly, moduli stabilization of the warped resolved conifold throat was not addressed in detail, under the assumption that there were other warped throats in which moduli stabilization, uplifting to a de Sitter vacuum and links to standard model physics occur. However, this assumption is not entirely satisfactory if one wants to understand a complete model. This shortcoming can be seen as a specific example of a wider problem of string inflation models - that is, the tension between working locally, in an area of the compactification in which the metric is known, and global effects of the compactification, which can't be probed locally. In order to overcome this more general problem, other approaches are needed. One may be a numerical relativity approach, where Ricci-flat geometries are built and then probed numerically, without writing down a global metric.

A second shortcoming is that the presented model of natural inflation with an observably-large value of the tensor-to-scalar ratio was contrived in its setup, requiring large amounts of warping, wrapping, flux, and specific initial conditions as well as fine-tuned choices for coefficients in the potential. One should rightly ask why nature would choose this setup over other possibilities. This is also part of a larger problem faced by string theory models of inflation, which is that although the models occur in UV complete theories, they still have problems that inflation theories outside of string theory suffer from: the problem of initial conditions, the measure problem and associated problems. Perhaps a better understanding of string theory will shed light on these problems, but for now the field doesn't suggest any universally accepted solutions to these difficulties. Future research projects in this area could investigate more systematically why it is hard to produce a large tensor-to-scalar ratio in D-brane models, and the relation of this to the weak gravity conjecture.

In Part II we took the bottom-up approach beginning with a general class of low energy effective multi-field inflation models and deriving observables from these models. In particular we focussed on the effects of primordial non-Gaussianity. The overarching theme of this part of the thesis is that multi-field inflation models can produce primordial non-Gaussianity which couples long-wavelength modes to short-wavelength modes, leading to a variety of observable effects.

In Chapter 5 we gave a new explanation for the observed CMB power asymmetry using a long-wavelength mode of a second light field to modulate the short-wavelength scalar power spectrum. By using higher-order terms in the δN expansion, we allowed

for a novel non-zero trispectrum, giving a cubic-term asymmetry. This meant the requirements on the bispectrum were relaxed compared to previous work, with the model allowing for an observably-allowed value for $f_{\rm NL}$, which wasn't possible in previous work neglecting the trispectrum.

However, this explanation comes with its own problems related to fine-tuning. Having a large trispectrum compared to the bispectrum implied that our observable patch was fine-tuned compared to others. Moreover, a necessary condition for the explanation was that the isocurvature field contributed a small amount towards the power spectrum of the curvature perturbation - perhaps another fine-tuning. Also, the directional dependence of the cubic term used is different to one constrained by data and as such a more complete data analysis may turn out to require different constraints on the model parameters. While these are all problems with the presented model, they don't conflict with the proof-of-concept nature of this work, which is that including higher-order terms, in particular involving the trispectrum, can help relieve tension between observations of asymmetry and the non-observation of the bispectrum. Future research is needed to construct realistic models which produce the required asymmetry and give suitably small levels of non-Gaussianity. Also, the strong scale dependence of the asymmetry needs to be addressed.

Chapter 6 reviewed our study of the squeezed limit of the bispectrum in multi-field inflation, where one long-wavelength mode acts as a background for the two shorter-wavelength modes. This work was the first calculation of its kind, generalizing calculations of the squeezed limit of the bispectrum from single-field models to multi-field models. This is the observationally interesting case, since single-field models predict a vanishingly-small squeezed limit of the bispectrum, so in order to compare with future (hopefully non-zero) observations of the squeezed limit of the bispectrum, these multi-field predictions are necessary. The result was very general, not relying on the specifics of the multi-field model, relating the squeezed bispectrum to the field-space power spectra and their field derivatives. We made use of a separate-universe type Γ-expansion relating field perturbations at late horizon exit time to those at the earlier horizon exit time, with coefficients determined by the background cosmology. Applying our general results to a mixed inflaton-curvaton model with curvaton self-interactions, gave us an example in which using our results gave a prediction which was 20% more accurate in the highly squeezed limit.

One criticism of the above work is that observations may not be able to probe such highly-squeezed limits, in which this work is more accurate than previous studies. We point to future large-scale structure surveys, such as Euclid, and experiments to detect CMB μ-distortion as examples where a highly-squeezed limit is probed, in which case these results will be important. Future work could be done here to allow for heavy fields and non-canonical kinetic terms, though we expect the results to be similar in

spirit to those presented in this thesis. Moreover, one could extend to next-order in the soft limit, keeping higher-order terms in k_1/k_3. This is necessary to use these analytic results to compare against theoretical numerical work, which can't efficiently probe the highly squeezed limit, and more importantly, to compare against observations which are not in such a highly squeezed limit.

In Chapter 7 we generalized the work on the squeezed limit of the bispectrum to include any soft limit of any higher-point inflationary correlation function for multi-field models. The soft limits occur when the long wavelength modes act as a background in which the shorter wavelength modes interact. We again used separate universe techniques to perform the calculations. In doing so, we gave an even simpler form for the squeezed limit of the bispectrum, repackaging separate terms that appeared in Chapter 6. We used a Feynman-diagram type method to organise the soft limit expansion. We focussed primarily on the trispectrum, giving explicit formulae for all possible single- and double-soft limits for general multi-field models. We required higher-order terms in the Γ-expansion introduced in Chapter 6 and noted these terms could lead to novel shapes, for example in the trispectrum. We also presented an infinite tower of inequalities between soft limits of correlation functions, generalizing the soft Suyama-Yamaguchi inequality.

A potential criticism of this work is that the higher-order correlators, such as the trispectrum, are not well constrained by current data. However, we note that the current constraints from the data only apply across a limited range of CMB scales. It might be that it's possible to constrain the higher-point correlators in soft polygon configurations using future large-scale structure surveys and CMB μ-distortion experiments, as noted above for the squeezed limit of the bispectrum. Future work could investigate the new contribution to the kite-double-soft trispectrum shape, which can be large even in models where the equilateral configuration trispectrum is small. Furthermore, one could explore to what extent double-soft limits probe the underlying symmetries of the multi-field model, which may be sensitive to a non-linearly realized non-Abelian symmetry of which the multiple fields may be Goldstone bosons. It is also possible the double-soft limits are sensitive to the curvature of the field space, and may provide information of the underlying metric on field space.

In the above paragraphs we discussed potential future research projects inspired by the work presented in this thesis. We now give some other future research ideas inspired more broadly by the general area of research related to connecting theory to observables in inflation.

A key task for future research could utilise recent progress in numerical calculations of inflationary observables, linking this to data pipelines to more strongly constrain models with non-Gaussian signatures. This could potentially be done in such a way as to avoid using the shape templates, such as the local, equilateral and orthogonal

shapes for the bispectrum. This would provide a more robust way to check parameter constraints on models and avoid the data loss associated to fitting to these shape templates.

This thesis motivates studying multi-field models from the top-down perspective, as the phenomenology of them is more likely to be detected by future experiments than single-field inflation models. Most existence proofs in string theory however have focussed on arranging just single-field inflation. Thus, it would be interesting to survey the multi-field models from string compactifications and see how to categorize them and what observables they predict which have a specifically stringy, multi-field nature.

A better understanding of time-dependent solutions in the top-down and bottom-up approaches may be necessary for a more systematic study of string theory and inflationary cosmology. This requires extending string theory beyond the adiabatic approximation and would be most relevant for geometries with string-scale curvature. Both of these seem out of reach of our current understanding of string theory solutions.

More broadly, the reheating stage in the early universe requires a more detailed treatment, and future research could link inflationary theories more solidly to reheating phenomenology. In particular, it would be interesting to know precisely how to link multi-field models to the standard model sector.

It's difficult to predict what direction future research in this area will take. In the post-Planck era, inflationary cosmology needs to find new ways of distinguishing between competing scenarios if inflation is to remain predictive. Theoretical studies should have in mind particular observational consequences and special attention should be paid to scenarios which we might be able to confirm/rule out with the next wave of experiments.

Exciting, elementary questions remain unanswered. What fields drive inflation? What sets the initial conditions for inflation? What observational signatures are inevitable? Can inflation be embedded in a UV-complete theory? How do we link inflation robustly to reheating and the standard model? Is string theory the correct UV completion of gravity and does it have cosmological consequences, in particular for inflation? What new astronomical observations will help us to probe the very early universe?

Answering these questions will be one of the greatest scientific achievements of our time, allowing us to look back to the earliest period in the history of the universe. It's amazing to think that everything we've ever seen, from galaxies to planets and even humans, could have originated from quantum fluctuations stretched during inflation.

Appendix A

Appendices for D-branes in the Warped Resolved Conifold

A.1 D-brane Backreaction

The D5-brane can backreact on both the warp factor and the internal geometry, so we need to estimate the size of each. Our strategy will be to first assume the backreaction on the internal geometry is small, so that we have an ISD solution with warp factor $\mathcal{H}$. We then compute the backreaction on this warp factor. In finding that this is small, we use the non-backreaction of the warp factor to compute the possible backreaction on the internal geometry. We will find that this is small too, making our approach self-consistent.

We should begin with the full action for the SUGRA background and include terms in the action for all localized sources, which include the stack of N D3-branes located at the north pole of the finite S^2, with no fluxes turned on, as well as the mobile probe wrapped D5-brane with flux. The full action is then

$$\begin{aligned} S = &\frac{1}{2\kappa_{10}^2}\tilde{S} - NT_3\int_{M_4} d^4\chi\sqrt{-\det(P_4[g_{MN}])} + NT_3\int_{M_4} P_4[C_4] \\ &- T_5\int_{M_4\times\Sigma_2} d^6\xi\sqrt{-\det(P_6[g_{MN}+\mathcal{F}_{MN}])} + T_5\int_{M_4\times\Sigma_2} P_6\left[C_6 + C_4\wedge\mathcal{F}_2\right] \end{aligned} \tag{A.1}$$

where $\tilde{S}$ is given by (**??**). In our WRC geometry, $C_6 = 0$, $B_2 = 0$ and we've turned on the flux $F_2 = \frac{q}{2}\sin\theta_1 d\theta_1\wedge d\phi_1$ on the D5-brane.

We now need to promote the worldvolume integrals to integrals over the full M_{10} space, in order to vary this action and get the equations of motion. To do this we introduce the following D3 charge densities

$$\rho_3^{ND3} = \frac{N}{\sqrt{g_6}}\delta(r)\delta(\psi)\delta(\theta_2)\delta(\phi_2)\delta(\theta_1)\delta(\phi_1) \tag{A.2}$$

$$\rho_3^{pD5} = \frac{p}{\sqrt{h_4}}\delta(r-r^*)\delta(\psi-\psi^*)\delta(\theta_2-\theta_2^*)\delta(\phi_2-\phi_2^*) \tag{A.3}$$

$$\rho_3^{pqD5} = \frac{p}{\sqrt{g_6}}(2\pi\alpha')\left(\frac{q}{2}\sin\theta_1\right)\delta(r-r^*)\delta(\psi-\psi^*)\delta(\theta_2-\theta_2^*)\delta(\phi_2-\phi_2^*) \tag{A.4}$$

so that the stack of N D3's are at the tip, $y=0$, and the p-wrapped probe D5 is at $(r^*,\psi^*,\theta_2^*,\phi_2^*)$. The metric h_4 is the warped metric on the 4D space transverse to the brane in the extra 6 dimensions. We then define the 6D unwarped densities (with a tilde) via

$$\tilde{\rho}_3^{ND3} = \mathcal{H}^{3/2}\rho_3^{ND3} \qquad \tilde{\rho}_3^{pqD5} = \mathcal{H}^{3/2}\rho_3^{pqD5}. \qquad \text{since } \sqrt{g_6} = \mathcal{H}^{3/2}\sqrt{\tilde{g}_6}. \tag{A.5}$$

For the 4D density, we have

$$\tilde{\rho}_3^{pD5} = \mathcal{H}\rho_3^{pD5} \text{ since } \sqrt{h_4} = \mathcal{H}\sqrt{\tilde{h}_4}. \tag{A.6}$$

Note that the Hodge dual $\star_6$ of the warped 6D metric g_6 acts on a 6D warped density ρ as

$$\star_6\rho = \rho\sqrt{g_6}\; dr\wedge d\psi\wedge d\theta_1\wedge d\phi_1\wedge d\theta_2\wedge d\phi_2. \tag{A.7}$$

We then have the full 10D action

$$\begin{aligned} S = {} & \frac{1}{2\kappa_{10}^2}\tilde{S} - T_3\int_{M_{10}} d^{10}x\sqrt{-\det(P_4[g_{MN}])}\sqrt{g_6}\rho_3^{ND3} + T_3\int_{M_{10}} C_4\wedge\star_6\rho_3^{ND3} \\ & - T_5\int_{M_{10}} d^{10}x\sqrt{-\det(P_6[g_{MN}+\mathcal{F}_{MN}])}\sqrt{h_4}\rho_3^{pD5} + T_5\int_{M_{10}} C_4\wedge\star_6\rho_3^{pqD5}. \end{aligned} \tag{A.8}$$

We obtain the stress tensors from the DBI part of each local brane action. For the stack of N D3-branes we get the following non-zero components for the stress-energy tensor

$$T_0^0 = T_1^1 = T_2^2 = T_3^3 = -T_3\rho_3^{ND3}, \tag{A.9}$$

so that

$$\left(T_m^m - T_\mu^\mu\right)_{ND3} = 4T_3\rho_3^{ND3} \tag{A.10}$$

where we've used the shorthand

$$T_m^m - T_\mu^\mu \equiv \sum_{M=4}^{9} T_M{}^M - \sum_{M=0}^{3} T_M{}^M. \tag{A.11}$$

Now we do a similar calculation for the p-wrapped D5-brane. Neglecting the $\mathcal{O}(\alpha'^2q^2)$

flux contribution, we get the following non-zero components for the stress-energy tensor

$$T^0_0 = T^1_1 = T^2_2 = T^3_3 = T^{\theta_1}_{\theta_1} = T^{\phi_1}_{\phi_1} = -T_5\rho_3^{pD5} \tag{A.12}$$

$$\text{so that } \left(T^m_m - T^\mu_\mu\right)_{pD5} = 2T_5\rho_3^{pD5}. \tag{A.13}$$

Varying the full 10D action with respect to C_4 gives the Bianchi identity

$$d\tilde{F}_5 = H_3 \wedge F_3 + 2\kappa_{10}^2\left(T_3 \star_6 \rho_3^{ND3} + T_5 \star_6 \rho_3^{pqD5}\right). \tag{A.14}$$

Using the warped background ansatz, this becomes

$$\tilde{\nabla}^2\alpha = ie^{2A}\frac{G_{mnp}\star_6\overline{G}^{mnp}}{12\text{Im}\tau} + 2e^{-6A}\bullet_m\alpha\bullet^m e^{4A} + 2\kappa_{10}^2e^{2A}\left(T_3\rho_3^{ND3} + T_5\rho_3^{pqD5}\right). \tag{A.15}$$

The trace of the Einstein equations can be written [109]

$$\begin{aligned}\tilde{\nabla}^2e^{4A} = {}& \frac{\kappa_{10}^2}{2}e^{2A}\left[\frac{1}{4}(T^m_m - T^\mu_\mu)_{ND3} + \frac{1}{4}(T^m_m - T^\mu_\mu)_{pD5}\right] \\ & + e^{2A}\frac{G_{mnp}\overline{G}^{mnp}}{12\text{Im}\tau} + e^{-6A}(\bullet_m\alpha\bullet^m\alpha + \bullet_m e^{4A}\bullet^m e^{4A}).\end{aligned} \tag{A.16}$$

Combining (A.15) and (A.16) gives

$$\begin{aligned}\tilde{\nabla}^2(e^{4A} - \alpha) = {}& \frac{e^{2A}}{24\text{Im}\tau}|iG_3 - \star_6 G_3|^2 + e^{-6A}|\bullet(e^{4A} - \alpha)|^2 \\ & + 2\kappa_{10}^2e^{2A}\left(\frac{1}{4}(T^m_m - T^\mu_\mu)_{ND3} - T_3\rho_3^{ND3}\right) \\ & + 2\kappa_{10}^2e^{2A}\left(\frac{1}{4}(T^m_m - T^\mu_\mu)_{pD5} - T_5\rho_3^{pqD5}\right).\end{aligned} \tag{A.17}$$

The first two terms on the RHS are non-negative. The third term actually vanishes by (A.9), but note that this is a special result for D3-branes. The fourth term for the D5-brane doesn't vanish, so we need to work out its size. It can be written in terms of the warp factor as

$$2\kappa_{10}^2\mathcal{H}^{-1/2}\left(\frac{1}{4}(T^m_m - T^\mu_\mu)_{pD5} - T_5\rho_3^{pqD5}\right). \tag{A.18}$$

In order to estimate its size we need the warp factor. For the moment let's assume (A.18) is small so that we can ignore it. We'll come back to the size of this term after we have computed the backreaction on the warp factor. This allows us to begin with the usual ISD solution $G_- = 0 = \Phi_-$.

Backreaction on the Warp Factor

We now compute the backreaction on the warp factor. We write the trace of Einstein's equations (A.16) in the form

$$-\tilde{\nabla}^2 e^{-4A} = 2\kappa_{10}^2 T_3 \tilde{\rho}_3^{ND3} + \kappa_{10}^2 T_5 \mathcal{H}^{1/2} \tilde{\rho}_3^{pD5}. \tag{A.19}$$

We begin with the warp factor arising as the Green's function on the WRC for a stack of N D3's placed at the north pole $\theta_2 = 0$ of the S^2 at $r = 0$ to get $\mathcal{H}$. The result near the tip $r = r_{\min}$, but away from the north pole, is given by

$$\mathcal{H} = \frac{4\pi g_s N l_s^4}{r_{\min}^4}. \tag{A.20}$$

We now consider corrections to this from modifying the Green's function equation to (A.19). We will compute the size of each term on the RHS of (A.19), and find that the dominant one is from the stack.

We want to compare factors in front of dimensionless delta functions, and since r has dimensions of length, we should look at dimensionless ρ, and use the scaling property of delta functions $\delta(r) = \frac{1}{3u}\delta(\rho)$. Let's define the following combinations of dimensionless delta functions

$$\delta(M_6) \equiv \delta(\rho)\delta(\psi)\delta(\theta_2)\delta(\phi_2)\delta(\theta_1)\delta(\phi_1) \tag{A.21}$$

$$\delta(M_4^*) \equiv \delta(\rho - \rho^*)\delta(\psi - \psi^*)\delta(\theta_2 - \theta_2^*)\delta(\phi_2 - \phi_2^*). \tag{A.22}$$

Then the first term on the RHS of (A.19) coming from the stack is

$$2\kappa_{10}^2 T_3 \tilde{\rho}_3^{ND3} = 3(2\pi)^5 \frac{N g_s l_s^4}{r_{\min}^3 u^3 \sin\theta_1 \sin\theta_2} \delta(M_6). \tag{A.23}$$

The second term in (A.19) coming from the p-wrapped D5-brane probe, evaluated at $r \approx r_{\min} \ll u$ is

$$\kappa_{10}^2 T_5 \mathcal{H}^{1/2} \tilde{\rho}_3^{pD5} = \frac{(2\pi)^3}{16} \frac{25 N g_s l_s^4}{r_{\min} u^5 \sin\theta_2} \delta(M_4^*), \tag{A.24}$$

using $T_5 = [(2\pi)^5 g_s l_s^6]^{-1}$. We see that the probe D5-brane source term for the warp factor is much smaller than that sourced by the stack of N D3-branes, as long as

$$\left(\frac{r_{\min}}{u}\right)^2 \ll \frac{48}{25}(2\pi)^2 \frac{1}{\sin\theta_1} \approx \frac{76}{\sin\theta_1}, \tag{A.25}$$

and since $\sin\theta_1 \leq 1$, the RHS of (A.25) is greater than 76. So our p-wrapped D5-brane can be neglected in the warp factor equation since we have $r_{\min} \ll u$.

Backreaction on the internal geometry

Now that we've shown that the probe approximation for the warp factor is self-consistent, we can go back to the equation for the internal geometry to check the validity of assuming (A.18) is small.

Using the trace of the energy momentum tensor for the D5-brane given in (A.13) and the unwarped density in (A.5) gives (A.18) to be

$$2\kappa_{10}^2 T_5 \mathcal{H}^{-1/2}\left(\frac{1}{2}\mathcal{H}^{-1}\tilde{\rho}_3^{pD5} - \mathcal{H}^{-3/2}\tilde{\rho}_3^{pqD5}\right). \tag{A.26}$$

Now that we have the warp factor, we can now check the size of each term individually, and check that they are small relative to the LHS of (A.17), which scales as $\tilde{\nabla}^2\Phi_- = \mathcal{O}(\delta/r_{\min}^2)$ in the small r region, and with $\Phi_- = e^{4A} - \alpha = \delta$ which is small. The first part of (A.26) is

$$\kappa_{10}^2 T_5 \mathcal{H}^{-3/2}\tilde{\rho}_3^{pD5} = \frac{25\pi}{32}\frac{1}{Ng_s l_s^4}\frac{r_{\min}^7}{u^5\sin\theta_2}\delta(M_4^*). \tag{A.27}$$

For this term to be negligable, we need to impose

$$\gamma \ll 1 \tag{A.28}$$

$$\text{where } \gamma \equiv \frac{\beta}{\delta}, \qquad \beta \equiv \frac{25\pi}{32}\frac{1}{Ng_s l_s^4}\frac{r_{\min}^9}{u^5\sin\theta_2}. \tag{A.29}$$

This may be possible to arrange for given values of $r_{\min} \ll u$ in the SUGRA limit of large N. Note that $l_s \ll u$ is required for the curvature of the WRC geometry to not be too large - necessary for the SUGRA approximation. We also work in the perturbative regime of small g_s. There is no restriction on the size of $r_{\min}/l_s$, as $r_{\min}$ isn't a curvature term, it's just a coordinate distance in the WRC, and is set by the minimum of the potential. We see that as long as we stay away from $\theta_2 = 0$, (A.28) can be satisfied for a suitable potential. Note that this condition (A.28) is more stringent than the condition from the backreaction on the warp factor.

The data from Table 4, together with the values of p in (4.61) and q in (4.71) gives

$$\gamma = \frac{25\pi}{32\delta}\frac{1}{Ng_s l_s^4}\frac{r_{\min}^9}{u^5\sin\theta_2} \tag{A.30}$$

$$\approx 8\times 10^{-8} \ll 1 \tag{A.31}$$

as required.

The second term in (A.26) is

$$-2\kappa_{10}^2 T_5 \mathcal{H}^{-2}\tilde{\rho}_3^{pqD5} = -\frac{25\pi}{32}\frac{1}{Ng_s l_s^4}\frac{r_{\min}^7}{u^5\sin\theta_2}\left[48\pi^{1/2}\frac{q}{\sqrt{Ng_s}}\right]\delta(M_4^*) \tag{A.32}$$

which is small compared to $\delta/r_{\min}^2$ if

$$q \ll 10^{-2}\gamma^{-1}\sqrt{Ng_s}, \tag{A.33}$$

which for the q in (4.71) requires

$$1.2\times 10^{-15}\frac{N^{3/2}}{g_s^{1/2}\delta B}\left(\frac{u}{l_s}\right)^4\left(\frac{u}{r_{\min}}\right)^2 \ll 10^{-2}\gamma^{-1}\sqrt{Ng_s}. \tag{A.34}$$

Substituing $\gamma = \beta/\delta$ and tidying up means we require

$$\frac{1}{Bg_s^2\delta^2\sin^2\theta_2}\frac{u}{l_s}\left(\frac{r_{\min}}{l_s}\right)^7 \ll 3.4\times 10^{12} \tag{A.35}$$

which is independent of N. Putting in the data from Table 4 gives

$$\frac{1}{Bg_s^2\delta^2\sin^2\theta_2}\frac{u}{l_s}\left(\frac{r_{\min}}{l_s}\right)^7 \sim 5\times 10^6 \ll 3.4\times 10^{12}. \tag{A.36}$$

It's interesting to note that this condition on q from backreaction is less restrictive than that coming from our approximation for $\mathcal{F}$ in (4.57), which we used to get a Planckian decay constant. This was shown to be satisfied for our data in (4.74). It seems that setting a Planck scale decay constant together with a hierarchically smaller GUT scale of inflation is a more delicate procedure than maintaining control over the backreaction from the flux of a wrapped brane.

A.2 Corrections from the 4D Ricci Scalar

We now consider the effect of a non-negligible 4D Ricci scalar $\mathcal{R}_4$. The solution to the full Poisson equation (4.10) is denoted Φ_-. For a 4D quasi-de Sitter spacetime, we have that

$$\tilde{\nabla}^2\Phi_- = \mathcal{R}_4 \approx 12H^2 \approx \frac{4V}{M_p^2} \approx \varphi(y) + \lambda\Phi_-. \tag{A.37}$$

By the Friedmann equation, $H^2 = V/(3M_p^2)$, where we have seperated the Φ_- dependence from the rest of the potential. The potential V, and hence $\varphi(y)$ and λ, depend on the choice of probe D-brane.

For a probe D3-brane, we have $\varphi(y) = V_0$, a constant and $\lambda = 4T_3/M_p^2$. This can

be solved exactly, in the region $r_{\min} \ll r \ll r_{\rm UV}$, in which case the geometry of the SC is relevant [110]. The solutions are modified Bessel functions with argument $x \equiv \sqrt{\lambda} r$. When these are expanded for small x, a mass term appears as the leading curvature correction, leading to the eta problem as seen from the 10D supergravity perspective.

Note that in [170] the Ricci scalar term was omitted from the equation of motion for Φ_-. However, it was argued that a mass term should be added to the final potential. The origin of this mass term is this curvature.

We now consider the case of a probe D5-brane moving in the WRC throat, in which case $\varphi(y)$ is not constant. The solution to (A.37) in this case can be derived using the expansion method developed in [110], which was originally used for the case where the perturbations to Φ_- come from fluxes and curvature at leading order. The expansion takes the form

$$\Phi_- = \sum_{n=0}^{\infty} \Phi_-^{[n]} \tag{A.38}$$

$$\text{where } \Phi_-^{[0]}(y) = \overline{\Phi}_-(y) + \Phi_h(y) \tag{A.39}$$

$$\text{and } \Phi_-^{[n]}(y) = \lambda \int \sqrt{\tilde{g}_6'} d^6y' G(y;y') \Phi_-^{[n-1]}(y'), \tag{A.40}$$

where $\Phi_h(y)$ is the solution to the homogeneous Laplace equation, and $\overline{\Phi}_-(y)$ is sourced by $\varphi(y)$ via

$$\overline{\Phi}_-(y) \equiv \int \sqrt{\tilde{g}_6'} d^6y' G(y;y') \varphi(y'). \tag{A.41}$$

In the above, G is the Green's function satisfying

$$\tilde{\nabla}_y^2 G(y;y') = \frac{\delta(y-y')}{\sqrt{\tilde{g}_6'}}. \tag{A.42}$$

The expansion (A.38) can be truncated if $\lambda r^2 < 1$, in which case the leading order term is from $\Phi_-^{[0]}$. We will now calculate the $\overline{\Phi}_-(y)$ term for a D5-brane in the WRC. We will find that the leading correction from the Ricci scalar is subdominant to $\varphi(y)$ in the small ρ limit, contributing a term of only at order ρ^4, which is small.

Using our chosen p and q we get

$$\varphi(y) = \frac{4}{M_p^2} 4\pi u^2 p T_5 \mathcal{H}^{-1/2} \approx \frac{180}{u^2} \rho^2 \tag{A.43}$$

$$\lambda = \frac{4}{M_p^2} 4\pi^2 l_s^2 T_5 pq \approx 4 \frac{M_{\rm GUT}^4}{\delta M_p^2} \approx \frac{0.2}{\delta u^2} \approx \frac{20}{u^2} \tag{A.44}$$

where we've used that $M_{\rm GUT} = 4 \times 10^{-3} M_p$, and

$$M_p^2 = \frac{N u^2}{2(2\pi)^4 g_s l_s^4} \approx \frac{2 \times 10^8}{u^2} \tag{A.45}$$

for our data. Then we have

$$\lambda M_p^2/4 \approx 100 M_{\rm GUT}^4. \tag{A.46}$$

We note that in the potential there is the term

$$\frac{M_p^2}{4}\varphi(\rho) \approx M_{\rm GUT}^4 880 \rho^2 \tag{A.47}$$

coming from the non-cancellation of DBI and CS terms.

The expansion of $\Phi_-(y)$ in (A.38) can be truncated if $\lambda r^2 \ll 1$. In our case, we are interested in probing the $r \sim r_{\rm min} \sim u/50$ region, in which case $\lambda r^2 \approx 20/2500 \approx 8 \times 10^{-3} \ll 1$. Then the leading order term is $\Phi_-^{[0]}$. We have chosen Φ_h, and so now we need to calculate $\overline{\Phi}_-$. To compute this we need to calculate the Green's function and integrate (A.41) to find the leading order small ρ behaviour of $\overline{\Phi}_-$.

We can calculate the Green's function using the eigenfunctions, $Y_L(Z)$, of the Laplacian on $T^{1,1}$. The delta function on the RC splits into a radial delta function and the delta function on $T^{1,1}$,

$$\delta(y - y') = \delta(r - r') \prod_{i=1}^{i=5} \delta(Z_i - Z_i'). \tag{A.48}$$

The delta function on the angular parts can be expanded in the $Y_L(Z)$

$$\frac{\prod_{i=1}^{i=5} \delta(Z_i - Z_i')}{\sqrt{\tilde{g}_5}} = \sum_L Y_L(Z_i) Y_L^*(Z_i') \tag{A.49}$$

which have the conventional normalisation

$$\int d^5 Z_i \sqrt{\tilde{g}_5} Y_L^*(Z_i) Y_{L'}(Z_i) = \delta_{LL'} \tag{A.50}$$

where

$$\sqrt{\tilde{g}_5} \equiv \frac{\sqrt{\tilde{g}_6}}{\sqrt{\tilde{g}_r}} = \frac{r^3(r^2 + 6u^2)}{\sqrt{\tilde{g}_r}} \frac{\sin\theta_1 \sin\theta_2}{108} = \frac{\sin\theta_1 \sin\theta_2}{108}. \tag{A.51}$$

The Y_L are given by

$$Y_L(Z_i) = J_{l_1,m_1,R}(\theta_1) J_{l_2,m_2,R}(\theta_2) e^{i(m_1\phi_1 + m_2\phi_2 + R\psi/2)} \tag{A.52}$$

$$\text{where } J^{\Upsilon}_{l_i,m_i,R}(\theta_i) = N_{\Upsilon}(\sin\theta_i)^{m_i}\left(\cot\left(\frac{\theta_i}{2}\right)\right)^{R/2} \times {}_2F_1\left(-l_i+m_i, 1+l_i+m_i; 1+m_i-R/2; \sin^2\left(\frac{\theta_i}{2}\right)\right) \tag{A.53}$$

$$\text{and } J^{\Omega}_{l_i,m_i,R}(\theta_i) = N_{\Omega}(\sin\theta_i)^{R/2}\left(\cot\left(\frac{\theta_i}{2}\right)\right)^{m_i} \times {}_2F_1\left(-l_i+R/2, 1+l_i+R/2; 1+R/2-m_i; \sin^2\left(\frac{\theta_i}{2}\right)\right). \tag{A.54}$$

The Υ solution is regular for $m_i \geq R/2$, while Ω is regular for $m_i \leq R/2$. N_{Υ} and N_{Ω} impose the normalisation (A.50).

In order to obtain single-valued regular functions, the charges must satisfy

- l_1 & l_2 both integers or both half-integers
- $m_1 \in \{-l_1, ..., l_1\}$ and $m_2 \in \{-l_2, ..., l_2\}$
- $R \in \mathbb{Z}$ and $\frac{R}{2} \in \{-l_1, ..., l_1\}$ and $\frac{R}{2} \in \{-l_2, ..., l_2\}$.

The Green's function can be expanded in these Y_L, as

$$G(y;y') = \sum_L G_L(r;r')Y_L(Z_i)Y_L^*(Z_i'). \tag{A.55}$$

Then the $\overline{\Phi}_-(y)$ term is

$$\overline{\Phi}_-(y) = \sum_L Y_L(Z_i)\int d^5Z_i' \frac{\sin\theta_1'\sin\theta_2'}{108} Y_L^*(Z_i')\int \sqrt{\tilde{g_r}'}dr' G_L(r;r')\varphi(r'). \tag{A.56}$$

We now prove that if $\varphi(y)$ has no angular dependence, then $\overline{\Phi}_-(y)$ only has a contribution from the singlet $L = (0,0,0,0,0)$, due to the vanishing of the angular integral

$$\int d^5Z_i' \frac{\sin\theta_1'\sin\theta_2'}{108} Y_L^*(Z_i') \tag{A.57}$$

for other L.

To see this, note that because $0 \leq \psi < 4\pi$, we must have $R = 0$, for $\int_0^{4\pi} e^{iR\psi/2} \neq 0$. For $R = 0$, we must have that l_1, l_2 are both integers. Hence m_1, m_2 must both be integers.

Similarly, in order for $\int_0^{2\pi} e^{im_i\phi_i} \neq 0$, for m_i integers, we must have $m_1 = 0 = m_2$. For $m_i = R = 0$, the Υ and Ω solutions coincide, so we drop these labels. The form of the θ_i dependence will simplify to the Legendre polynomials P_{l_i}

$$J_{l_i,0,0} = N\,{}_2F_1\left(-l_i, 1+l_i; 1; \sin^2\left(\frac{\theta_i}{2}\right)\right) \tag{A.58}$$

$$= NP_{l_i}(\cos\theta_i). \tag{A.59}$$

To see this, note that the Jacobi Polynomials $P_n^{(\alpha,\beta)}(x)$ are defined in terms of the hypergeometric function by

$$P_n^{(\alpha,\beta)}(z) = \frac{(\alpha+1)_n}{n!}{}_2F_1\left(-n, 1+n+\alpha+\beta; 1+\alpha; \frac{1}{2}(1-z)\right) \tag{A.60}$$

where $(\alpha+1)_n$ is the rising Pochhammer symbol. We have the special case $n = l_i, \alpha = 0 = \beta$, and $z = \cos\theta_i$, for which the Jacobi polynmials reduce to the Legendre polynomials

$$P_n^{(0,0)}(z) = P_n(z) \tag{A.61}$$

and the Pochhammer symbol is $(1)_n = n!$, so that

$$J_{l_i,0,0} = NP_{l_i}(\cos\theta_i). \tag{A.62}$$

We then evaluate the integral using the orthogonality of Legendre polynomials, noting that $P_0(z) = 1$, and making the substitution $z = \cos\theta_i$

$$\int_0^\pi d\theta_i \sin\theta_i P_{l_i}(\cos\theta_i) = \int_{-1}^1 P_{l_i}(z)dz \tag{A.63}$$

$$= \delta_{0l_i} \tag{A.64}$$

which vanishes unless $l_i = 0$. Thus the only contribution to (A.57) is from the singlet $L = (0,0,0,0,0)$. This has a constant eigenfunction $Y_{\{0\}}(Z_i) = \alpha$, where α is set by the normalization (A.50), giving

$$\int d^5 Z_i \frac{\sin\theta_1 \sin\theta_2}{108}|\alpha|^2 = 1 \tag{A.65}$$

$$\Rightarrow |\alpha| = \sqrt{\frac{27}{16\pi^3}}. \tag{A.66}$$

Now looking at (A.56), the only non-vanishing contribution comes from the $L = \{0\}$ term, which has angular part

$$Y_{\{0\}}(Z_i)\int d^5 Z_i' \frac{\sin\theta_1' \sin\theta_2'}{108} Y^*_{\{0\}}(Z_i') = |\alpha|^2 * |\alpha|^{-2} = 1. \tag{A.67}$$

We then just need to work out the radial integral

$$\overline{\Phi}_-(y) = \int \sqrt{\tilde{g_r}'} dr' G_{\{0\}}(r;r')\varphi(r'). \tag{A.68}$$

$$= (3u)^6 \int \sqrt{\tilde{g_\rho}'} d\rho' G_{\{0\}}(\rho;\rho')\varphi(\rho'). \tag{A.69}$$

For each $G_L(r;r')$ in (A.55), we have the radial equation on the RC

$$\begin{aligned} &\frac{1}{r^3(r^2+6u^2)} \bullet_r \left(r^3(r^2+9u^2) \bullet_r G_L\right) \\ &- \left[\frac{6(l_1(l_1+1)-R^2/4)}{r^2} + \frac{6(l_2(l_2+1)-R^2/4)}{r^2+6u^2} + \frac{9R^2/4}{\kappa r^2}\right] G_L = \frac{\delta(r-r')}{r^3(r^2+6u^2)} \end{aligned} \tag{A.70}$$

which for dimensionless ρ becomes

$$\begin{aligned} &\frac{1}{\rho^3(\rho^2+2/3)} \bullet_\rho \left(\rho^3(\rho^2+1) \bullet_\rho G_L\right) \\ &- \left[\frac{6(l_1(l_1+1)-R^2/4)}{\rho^2} + \frac{6(l_2(l_2+1)-R^2/4)}{\rho^2+2/3} + \frac{9R^2/4}{\kappa\rho^2}\right] G_L = \frac{\delta(\rho-x)}{(3u)^4\rho^3(\rho^2+2/3)}. \end{aligned} \tag{A.71}$$

Here we've written ρ' as x, for clarity of variables in the following. The good news about (A.71) is that we can solve it exactly for $L = \{0\}$ on the whole of the RC, including the region of small ρ. For $L = \{0\}$ we just have

$$\bullet_\rho^2 G_{\{0\}} + \left(\frac{5\rho + 3\rho^{-1}}{\rho^2+1}\right) \bullet_\rho G_{\{0\}} = \frac{\delta(\rho-x)}{(3u)^4}. \tag{A.72}$$

The solution is

$$G_{\{0\}}(\rho;x) = \frac{1}{(3u)^4} \begin{cases} -(2x^2)^{-1} - \log x + \frac{1}{2}\log(x^2+1) & \text{if } \rho \le x \\ -(2\rho^2)^{-1} - \log\rho + \frac{1}{2}\log(\rho^2+1) & \text{if } \rho \ge x. \end{cases} \tag{A.73}$$

Viewed as a function of ρ, the $\rho \le x$ part of the solution is just a constant, fixed by continuity of $G_{\{0\}}$, while the $\rho \ge x$ part is the non-constant solution to the homogeneous equation, regular at infinity.

Now we do the Green's function integral for the $L = \{0\}$ mode. The integral is done in two pieces, the first is for $x \le \rho$

$$\begin{aligned} &\int_0^\rho x^5 \left(x^2 + \frac{2}{3}\right)\left(-\frac{1}{2\rho^2} + \frac{1}{2}\log\left(\rho^2+1\right) - \log\rho\right) dx \\ &= -\frac{1}{144}\rho^4\left(9\rho^2+8\right)\left[2\rho^2\log\rho - \rho^2\log\left(\rho^2+1\right) + 1\right] \end{aligned} \tag{A.74}$$

the second is for $x \geq \rho$

$$\begin{aligned}&\int_{\rho}^{1/3} x^5 \left(x^2+\frac{2}{3}\right)\left(-\frac{1}{2x^2}+\frac{1}{2}\log\left(x^2+1\right)-\log x\right) dx \\ =&\frac{1}{23328}\Big[162\log\left(9\left(\rho^2+1\right)\right)+162\left(9\rho^2+8\right)\rho^6\left(2\log\rho-\log\left(\rho^2+1\right)\right) \\ &+81\left(18\rho^4+25\rho^2-2\right)\rho^2-9-160\log(10)\Big].\end{aligned} \tag{A.75}$$

Putting these together gives the exact result

$$\begin{aligned}\overline{\Phi}_-(y) = (3u)^6\int\sqrt{\tilde{g_\rho}'}dx G_{\{0\}}(\rho;x)\frac{180}{u^2}x^2 = \frac{5}{72}\Big[&81\left(9\rho^2-2\right)\rho^2+162\log\left(9\left(\rho^2+1\right)\right) \\ &-9-160\log(10)\Big]\end{aligned} \tag{A.76}$$

which, for small ρ has leading order behaviour

$$\overline{\Phi}_-(y) \approx -1.4905+45\rho^4+\frac{15}{4}\rho^6+\mathcal{O}(\rho^8). \tag{A.77}$$

Using (A.46), we see that in the potential will appear the term $100M_{GUT}^4 45\rho^4 = M_{GUT}^4 4500\rho^4$, as in (4.81). This doesn't contribute quantitatively in the small ρ limit.

The result that only the $L=\{0\}$ mode contributes to $\overline{\Phi}_-(y)$ means that $\overline{\Phi}_-(y) = \overline{\Phi}_-(r)$ is purely radial. If the homogeneous solution $\Phi_h(y)$ is also purely radial, then $\Phi_-^{[0]}(y)$ is also purely radial. The results of the above can then be applied so that we would have all $\Phi_-^{[n]}(y)$ purely radial since the integrals over the Y_L would vanish for $L \neq \{0\}$.

However, in our case, we have angular dependence in $\Phi_h(y)$ for the form of the Natural Inflation potential, which would induce angular dependence in $\Phi_-^{[n]}(y)$ for higher n.

A.3 Wrapped D5-branes and the b-Axion

Wrapped D5-branes can source a potential for the NS-NS axion, b, which arises from the integral of the 2-form field B_2 over a 2-cycle in a type IIB compactification. The application of this to inflation was investigated in the original axion monodromy models, for example in [200], where the couplings of the axion are generated just from the DBI part of the D5-brane action. Our model of natural inflation involves a wrapped D5-brane giving rise to a potential for this field, and so we should consider whether these b-axions are relevant to inflation.

In our case, we can choose to turn on a worldvolume B_2 flux of strength b along the

wrapped 2-cycle so that its pullback has the following non-zero components $P_6[B_2]_{\theta_1\phi_1} = \frac{b}{2}\sin\theta_1$. Then a potential for b enters via the function $\mathcal{F}$ in (4.42), with $2\pi\alpha' q$ shifted to $2\pi\alpha' q + b$. The same analysis leading to natural inflation with a Planckian decay constant follows as long as we make the choice $b \lesssim 2\pi\alpha' q$, together with the upper bound on q coming from (4.57). In contrast, models of axion monodromy inflation assume that $b \gg l$ initially, where l is the size of the wrapped S^2. In this way the b-axion acquires a linear potential effectively from expanding the $\mathcal{F}$ term leading to large field inflation. In our model this would mean taking the $2\pi\alpha' q + b$ term to be the dominant factor inside $\mathcal{F}$ which is the opposite of what we have assumed. Ultimately this is a choice of initial condition on the value of b. Our choice of initial condition is that $b \leq 2\pi\alpha' q$ so that $2\pi\alpha' q + b$ is still sub-dominant to the warp factor term in $\mathcal{F}$ when the brane is near the tip. As such b will not play a role in generating significant inflation and we may ignore it.

Finally, in more recent axion monodromy models [175] the monodromy is induced not by the DBI part of the wrapped D5-brane action, instead through background 3-form fluxes coupling to the b-axion associated with B_2 in the CS part of the action. However, our model is constructed using the WRC in which SUSY preserving 3-form fluxes are absent and so no such monodromy is induced either. Turning on such fluxes may be of interest in discussing moduli stabilisation mechanisms within the WRC which is something that we would like to investigate further.

The conclusion of this appendix is that although the inclusion of wrapped D5-branes in our model could source potentials for b-axions, and hence complicate the inflationary picture, our assumed initial conditions on the size of b ensure that it will not contribute towards the inflationary dynamics. However, more complicated models could relax these initial conditions.

Appendix B

Appendix for the Squeezed Limit of the Bispectrum

B.1 Reduction to single field case

We should check that our expression (7.49) for B_ζ reduces to the Maldacena single field squeezed limit result [36] in the case of one slowly rolling scalar field, given by

$$\lim_{k_1 \ll k_2, k_3} B_\zeta(k_1, k_2, k_3) \approx -(n_s^{(3)} - 1) P_\zeta(k_1) P_\zeta(k_3) \tag{B.1}$$

with $n_s - 1 = 2\eta_V - 6\epsilon_V$, and the superscript (3) denoting evaluation at time t_3 when k_3 exits. Here $\epsilon_V \equiv \frac{1}{2}(V'/V)^2$ and $\eta_V \equiv V''/V$ are the potential slow-roll parameters.

Thus we begin with a slowly rolling single field ϕ. In this case we have

$$N_\phi = -\frac{H}{\dot{\phi}} = \frac{1}{\sqrt{2\epsilon_V}}\,, \qquad \frac{N_{\phi\phi}}{N_\phi^2} = 2\epsilon_V - \eta_V\,, \qquad \frac{d}{d\phi^{(3)}} = \frac{1}{\dot{\phi}^{(3)}}\frac{d}{dt_3} \tag{B.2}$$

and the Γ matrix is just the number $N_\phi^{(1)}/N_\phi^{(3)}$. Then (7.49) simplifies to

$$\begin{aligned}
&\lim_{k_1 \ll k_2, k_3} B_\zeta(k_1, k_2, k_3) \\
\approx &\frac{(N_\phi^{(1)})^2 {H^{(1)}}^2}{2k_1^3} \frac{(N_\phi^{(3)})^2 {H^{(3)}}^2}{2k_3^3} \left(-\frac{\dot{\phi^{(3)}}}{H^{(3)}}\right) \frac{2}{H^{(3)}} \left(\frac{1}{\dot{\phi^{(3)}}} \frac{dH^{(3)}}{dt_3}\right) \\
&+ 2\frac{(N_\phi^{(1)})^2 {H^{(1)}}^2}{2k_1^3} \frac{(N_\phi^{(3)})^2 {H^{(3)}}^2}{2k_3^3} \frac{N_{\phi\phi}^{(3)}}{(N_\phi^{(3)})^2} \\
\approx &[2\epsilon_V^{(3)} + 2(2\epsilon_V^{(3)} - \eta_V^{(3)})] P_\zeta(k_1) P_\zeta(k_3) \\
\approx &-(n_s^{(3)} - 1) P_\zeta(k_1) P_\zeta(k_3)
\end{aligned} \tag{B.3}$$

as required.

B.2 Recovering Seery & Lidsey result in near-equilateral limit

A further important check is that the near-equilateral limit of our result for α, (6.19) goes over to the result of Seery & Lidsey [43], given earlier in (7.47), valid when k_1 is small, but not so small as to change the exit times appreciably. That is, we want to check that

$$\lim_{t_1\to t_3} N_i^{(3)}N_j^{(3)}N_k^{(3)}\alpha_{ijk}^{(3)}(k_1,k_2,k_3) = \lim_{k_1\ll k_2,k_3}\frac{4\pi^4}{k_1^3k_2^3k_3^3}\left(\frac{H^{(3)}}{2\pi}\right)^4 N_i^{(3)}N_j^{(3)}N_k^{(3)} \times \sum_{6\text{ perms}}\frac{\dot\phi_i^{(3)}}{4H^{(3)}}\delta_{jk}\left(-3\frac{k_2^2k_3^2}{k_t}-\frac{k_2^2k_3^2}{k_t^2}(k_1+2k_3)+\frac{1}{2}k_1^2-k_1k_2^2\right). \tag{B.4}$$

Beginning with the RHS, one can do the sum over all six permutations, then take the slightly squeezed limit to get the RHS equal to

$$-N_i^{(3)}N_j^{(3)}N_j^{(3)}\frac{{H^{(3)}}^4}{4k_1^3k_3^3}\frac{d\phi_i^{(3)}}{dN} \tag{B.5}$$

which is exactly the $t_1\to t_3$ limit of $\alpha_{ijk}^{(3)}$ in (6.19), in which $\Gamma_{ij}^{(3,1)}\to\delta_{ij}$, contracted with $N_i^{(3)}N_j^{(3)}N_k^{(3)}$.

B.3 Squeezed limits of graviton correlators

Three-point functions involving gravitons (tensors) are likely significantly harder to detect observationally than those just involving scalars. Nonetheless they are interesting to calculate with a view to observations in the more distant future, and from a theoretical perspective.

Maldacena found squeezed limits of scalar-graviton and graviton-graviton three-point functions in the case of a single scalar field [36][31]. Here we use our soft-limit argument to calculate these in the multiple field case.

First order graviton perturbations, denoted by γ, are gauge invariant in contrast to scalar perturbations. They are defined as the transverse traceless perturbations of the spatial metric, h_{IJ}, such that

$$h_{IJ} = a^2(t)\left[(1+2\zeta)\delta_{IJ}+\gamma_{IJ}\right] \tag{B.6}$$

[31] Maldacena and Pimentel [333] found graviton-graviton correlators for gravity theories not restricted to Einstein gravity, using a de Sitter approximation. Squeezed limits of correlation functions involving gravitons in models of quasi single field inflation were considered in [334]

where $\gamma_{II} = 0 = \partial_I \gamma_{IJ}$. We can Fourier expand γ as

$$\gamma_{IJ} = \int \frac{d^3k}{(2\pi)^3} \sum_{s=\pm} \epsilon^s_{IJ}(k) \gamma^s_{\mathbf{k}}(t) e^{i\mathbf{k}\cdot\mathbf{x}} \tag{B.7}$$

where s, r indices label the polarization of the graviton, and the polarization tensors $\epsilon^s_{IJ}(k)$ satisfy $\epsilon^s_{II}(k) = 0 = k_I \epsilon^s_{IJ}(k)$ and $\epsilon^s_{IJ}(k)\epsilon^r_{IJ}(k) = 2\delta_{sr}$. The two-point function of the graviton is given by

$$\langle \gamma^s_{\mathbf{k_1}} \gamma^r_{\mathbf{k_2}} \rangle = (2\pi)^3 \delta(\mathbf{k_1} + \mathbf{k_2}) P^{sr(1)}_\gamma(k_1) \tag{B.8}$$

$$P^{sr(1)}_\gamma(k_1) = \delta_{sr} \frac{2{H^{(1)}}^2}{2k_1^3}. \tag{B.9}$$

We now consider the squeezed limit of three-point correlation functions involving gravitons. When the soft mode k_1 is that of a ζ, there will be a correlation between $\zeta_{\mathbf{k_1}}$ and two γ's by way of a similar soft limit argument applied now to a $\zeta\gamma\gamma$ correlator, giving the result

$$\lim_{k_1 \ll k_2, k_3} \langle \zeta_{\mathbf{k_1}} \gamma^s_{\mathbf{k_2}} \gamma^r_{\mathbf{k_3}} \rangle = (2\pi)^3 \delta(\mathbf{k_1} + \mathbf{k_2} + \mathbf{k_3}) N^{(3)}_i \Gamma^{(3,1)}_{in} \Gamma^{(3,1)}_{ml} \Sigma^{(1)}_{nl}(k_1) P^{sr(3)}_{\gamma,m}(k_3) \tag{B.10}$$

which can be contrasted with the corresponding single field result given in [36]. In the single field case, the result is proportional to the tilt of the graviton power spectrum, providing another consistency relation between observables. Now in the multiple field case, this consistency relation no longer holds, but instead the squeezed limit three-point function is related to how the two-point γ correlator depends on the background scalar fields ϕ_i.

When the soft mode is instead a graviton, we can refer to Maldacena's argument that when the $\zeta_{\mathbf{k_2}}, \zeta_{\mathbf{k_3}}$ modes exit, the graviton with momentum k_1 exited much earlier and is already frozen, so that fluctuations of ζ at time t_3 will be those in the deformed geometry of the background $\gamma_{\mathbf{k_1}}$ mode. The main effect of the deformation of the background geometry is to change the $\delta_{IJ} k_3^I k_3^J \to \delta_{IJ} k_3^I k_3^J - \gamma_{IJ} k_3^I k_3^J$ inside the correlation function of the two ζ's (equivalently in the second order action for ζ_{k_3}). Putting this into a soft limit type argument gives

$$\lim_{k_1 \ll k_2, k_3} \langle \gamma^s_{\mathbf{k_1}} \zeta_{\mathbf{k_2}} \zeta_{\mathbf{k_3}} \rangle \approx -(2\pi)^3 \delta(\mathbf{k_1} + \mathbf{k_2} + \mathbf{k_3}) P^{sr(1)}_\gamma(k_1) \epsilon^r_{IJ}(k_1) k_3^I k_3^J \frac{d}{dk_3^2} P_\zeta(k_3). \tag{B.11}$$

Similarly, the squeezed limit of the three-point correlator is exactly as given by Malda-

cena [36]

$$\lim_{k_1 \ll k_2, k_3} \langle \gamma^s_{\mathbf{k_1}} \gamma^r_{\mathbf{k_2}} \gamma^t_{\mathbf{k_3}} \rangle \approx -(2\pi)^3 \delta(\mathbf{k_1} + \mathbf{k_2} + \mathbf{k_3}) P_\gamma^{sq(1)}(k_1) \epsilon^q_{IJ}(k_1) k_3^I k_3^J \frac{d}{dk_3^2} P_\gamma^{rt(3)}(k_3). \tag{B.12}$$

We highlight that the result (B.10) may lead to new shape dependence compared to the single field results.

B.4 Reduction to Byrnes *et al.*

It is also important to check our expressions match those which have previously appeared in the literature in the near-equilateral, midly-squeezed configuration, which is the overlapping regime of validity. A result for the squeezed limit of the bispectrum was given by Byrnes *et al.* in Eq. (96) of Ref [45]

$$B_\zeta(k_1, k_2, k_3) = \left\{ \frac{N_i^{(1)} N_j^{(1)} N_{lm}^{(3)} \left[\delta_{il} + \left(2c + \log \frac{k_3}{k_1}\right) u_{il}\right] \left[\delta_{jm} + \left(2c + \log \frac{k_3}{k_2}\right) u_{jm}\right]}{N_r^{(1)} N_s^{(1)} N_t^{(3)} N_z^{(3)} \left(\delta_{rs} + 2c u_{rs}\right) \left(\delta_{tz} + 2c u_{tz}\right)} \right\} \times P_\zeta(k_1) P_\zeta(k_2) + 2 \text{ perms} \tag{B.13}$$

where $c = 2 - \log 2 - \gamma$, with γ the Euler-Masheroni constant, and u_{ij} is given by (6.33), and since u_{ij} is of order slow-roll, it can be evaluated at any time. Their result is valid for small $\log(k_3/k_1) u_{ij}$ with the intrinsic contribution from the three-point function of field perturbations neglected. It was derived by considering the two-point correlation at unequal times, calculated using the expression

$$\delta\phi^{(3)}_{i,\mathbf{k}} = \left[\delta_{ij} + \log \frac{k_3}{k_1} u_{ij}\right] \delta\phi^{(1)}_{j,\mathbf{k}} \tag{B.14}$$

which is valid for small $\log(k_3/k_1) u_{ij}$. However, for a large squeezing, $\log(k_3/k_1) u_{ij}$ may not be small, even though u_{ij} is of order slow-roll, and one will instead need the full Γ expression (6.6) for the evolution of the field perturbations. The Γ matrix can be written formally as a time-ordered exponential [38, 55, 56, 298–300]

$$\Gamma^{(3,1)}_{ij} = T \exp\left[\int_{N_1}^{N_3} u_{ij}(N) dN\right] \tag{B.15}$$

where N_1 is the number of e-folds corresponding to time t_1 and similarly for N_3. Note that in the limit of small $\log(k_3/k_1)u_{ij}$, we have, at leading order in $\log(k_3/k_1)u_{ij}$

$$\Gamma_{ij}^{(3,1)} \approx \delta_{ij} + \log\left(\frac{k_3}{k_1}\right) u_{ij}^{(1)} + ... \tag{B.16}$$

As discussed in Footnote 2, these authors used a next-order in slow-roll expression for Σ,

$$\Sigma_{ij}^{(*)}(k_1) \approx \frac{{H^{(*)}}^2}{2k_1^3}(\delta_{ij} + 2cu_{ij}). \tag{B.17}$$

Taking our expression for the squeezed limit of the bispectrum (6.20), and substituting the RHS of (B.16) for Γ, and replacing ${H^{(*)}}^2\delta_{ij}/2k_1^3$ with the RHS of (B.17), we recover (B.13).

The reason we didn't need to use (B.17) in the main part of this work was because we were throughout working to leading order in slow-roll, rather than next to leading order in slow-roll. The only time we needed to consider slow-roll terms, such as u_{ij}, are when they appear multiplied by $\log(k_3/k_1)$, which can be as large as $\mathcal{O}(20)$, in which case $|\log(k_3/k_1)u_{ij}| \sim 1$. Note that the expansion in Eq (B.16) cannot be truncated for $|\log(k_3/k_1)u_{ij}| \sim 1$. In the highly squeezed limit this is why the full expression for Γ given in Eq (6.5) needs to be used instead of Eq (B.16), even though we can safely neglect the slow-roll correction to the power spectrum in Eq (B.17).

B.5 Reduction to Dias *et al.*

Dias *et al.* [293] used a next-to-leading order expression for the bispectrum [42]

$$\lim_{k_1 \ll k_2, k_3} B_\zeta(k_1, k_2, k_3) \approx 2N_{ij}N_lN_m\left[\Sigma_{il}(k_1)\Sigma_{jm}(k_2) + \Sigma_{il}(k_2)\Sigma_{jm}(k_3) + \Sigma_{il}(k_3)\Sigma_{jm}(k_1)\right] \tag{B.18}$$

to calculate the spectral index of the halo bias as

$$n_{\delta b} \equiv \frac{d\log B_\zeta}{d\log k_1} = -2\frac{N_iN_jN_kM_{im}\alpha^{\rm LO}_{mjk} + N_{ij}N_kN_l(M_{im}\Sigma_{mk} + M_{km}\Sigma_{im})\Sigma_{jl}}{N_nN_pN_q\alpha^{\rm LO}_{npq} + 2N_nN_pN_{qr}\Sigma_{nq}\Sigma_{pr}} + 2\frac{N_iN_jM_{ij}}{N_lN_l} \tag{B.19}$$

where the right hand sides of both expressions are evaluated at the time t_t when $k_t \equiv k_1 + k_2 + k_3$ crosses the horizon, and where

$$\alpha^{\rm LO}_{ijk} = -H^4\frac{\dot\phi_i}{H}\delta_{jk} = -H^4\frac{V_{,i}}{V}\delta_{jk} \tag{B.20}$$

$$\Sigma_{ij}(k_a) = H^{(t_t)^2}\left[\delta_{ij} + 2r_{ij} - 2M_{ij}\log\left(\frac{2k_a}{k_t}\right)\right] \tag{B.21}$$

$$\text{with } M_{ij} \equiv \epsilon\delta_{ij} + u_{ij} \tag{B.22}$$

$$\text{and } r_{ij} \equiv \epsilon\delta_{ij}(1-\gamma) + u_{ij}(2-\gamma) \tag{B.23}$$

$$\text{where } u_{ij} \equiv \frac{V_{,i}V_{,j}}{V^2} - \frac{V_{,ij}}{V} \tag{B.24}$$

in which all quantities on the right hand side are again evaluated at t_t, and γ is the Euler-Masheroni constant. These results can be trusted for a mild hierarchy of scales, where $|\log(k_1/k_3)|$ is of order a few. We now check that our expression for $n_{\delta b}$, (6.34), can recover the Dias *et al.* result, (B.19), in the limit where the exit times are very close. To do so we begin with the expressions

$$\frac{V^{(1)}_{,l}}{V^{(1)}}\Gamma^{(3,1)}_{ik,l} = -\frac{\dot{\phi}^{(1)}_{l}}{H^{(1)}}\Gamma^{(3,1)}_{ik,l} = -\frac{1}{H^{(1)}}\frac{d}{dt_1}\Gamma^{(3,1)}_{ik} = -\frac{d}{d\log k_1}\Gamma^{(3,1)}_{ik}. \tag{B.25}$$

Now assuming we can swap the limit of differentiation with respect to k_1 and the limit of taking $t_1 \to t_3$, and using (B.16) we get

$$\lim_{t_1\to t_3}\left(\frac{V^{(1)}_{,l}}{V^{(1)}}\Gamma^{(3,1)}_{ik,l}\right) = -\frac{d}{d\log k_1}\left(\delta_{ik} + \log\left(\frac{k_3}{k_1}\right)u^{(1)}_{ik} + ...\right) = u^{(1)}_{ik}. \tag{B.26}$$

Substituting this into $n_{\delta b}$ of (6.34) and setting $\Gamma^{(3,1)}_{ij} \to \delta_{ij}$ we get

$$\lim_{t_1\to t_3} n_{\delta b} = -2\frac{N^{(3)}_i N^{(3)}_q (N^{(3)}_q V^{(3)}_{,j} + 6N^{(3)}_{qj}H^{(3)^2})M^{(1)}_{ij}}{N^{(3)}_m N^{(3)}_r (N^{(3)}_r V^{(3)}_{,m} + 6N^{(3)}_{rm}H^{(3)^2})} + 2\frac{N^{(3)}_i N^{(3)}_j M^{(1)}_{ij}}{N^{(3)}_m N^{(3)}_m} \tag{B.27}$$

which is the of the same form as (B.19) when (B.20) and (B.21) are substituted in. Note that in their expression everything on the RHS is instead evaluated at exit time of $k_t = k_1 + k_2 + k_3$, rather than t_3, but in the limit where the exit times are very close, this won't affect the result significantly, and we recover their result.

B.6 Tilt of reduced bispectrum in the squeezed limit

As discussed in §6.3.2 one can study the tilts of the reduced bispectrum, $f_{\rm NL}$, in the squeezed configuration with respect to any combination of the k-modes which it involves. In particular, one can calculate how $f_{\rm NL}$ of (6.22) varies with respect to $k_1 \approx k_2$ or k_3, or some combination of them. The dependence can be parametrized by

$$n^X_{f_{\rm NL}} \equiv \frac{d\log|f_{\rm NL}|}{d\log X} \tag{B.28}$$

for $X = k_1, k_3$. In §6.3.2 we found $n^{k_1}_{f_{\rm NL}} = n_{\delta b}$, where $n_{\delta b}$ was calculated in §6.3.1 in (6.34). To find $n^{k_3}_{f_{\rm NL}}$ we write (6.22) in a form where the second square bracket contains all the k_3 dependence

$$\lim_{k_1 \ll k_2, k_3} \frac{6}{5} f_{\rm NL}(k_1, k_2, k_3) \approx \left[\frac{1}{N_q^{(1)} N_q^{(1)}}\right] \left[L_{ij}^{(3,1)} \left(N_i^{(3)} [\log H^{(3)}]_{,j} + \frac{N_i^{(3)} N_{jk}^{(3)} N_k^{(3)}}{N_p^{(3)} N_p^{(3)}}\right)\right] \tag{B.29}$$

so that

$$n^{k_3}_{f_{\rm NL}} \approx \frac{1}{f_{\rm NL}} \left[P_{ij,3}^{(3,1)} \left(N_i^{(3)} [\log H^{(3)}]_{,j} + \frac{N_i^{(3)} N_{jk}^{(3)} N_k^{(3)}}{N_p^{(3)} N_p^{(3)}}\right) + L_{ij}^{(3,1)} Q_{ij}^{(3)}\right] \tag{B.30}$$

$$\begin{aligned} \text{where } Q_{ij}^{(3)} \equiv{}& \frac{1}{2} N_i^{(3)} u_{jk}^{(3)} \frac{V_{,k3}}{V^{(3)}} - \frac{1}{2} N_k^{(3)} u_{ik}^{(3)} \frac{V_{,j}}{V^{(3)}} - \frac{N_i^{(3)} N_{jk}^{(3)} N_k^{(3)} N_m^{(3)} N_n^{(3)} u_{mn}^{(3)}}{(N_p^{(3)} N_p^{(3)})^2} \\ & - \frac{1}{N_p^{(3)} N_p^{(3)}} \left(N_i^{(3)} N_k^{(3)} N_{jkl}^{(3)} \frac{V_{,l}^{(3)}}{V^{(3)}} + N_k^{(3)} N_l^{(3)} N_{jk}^{(3)} u_{il}^{(3)} + N_i^{(3)} N_l^{(3)} N_{jk}^{(3)} u_{kl}^{(3)}\right) \end{aligned} \tag{B.31}$$

$$\text{and } P_{ij,3}^{(3,1)} \equiv \frac{dL_{ij}^{(3,1)}}{d \log k_3} = -\frac{V_{,l}^{(3)}}{V^{(3)}} \Gamma_{ml}^{(1,3)} \left(\Gamma_{ik,m}^{(3,1)} \Gamma_{jk}^{(3,1)} + \Gamma_{ik}^{(3,1)} \Gamma_{jk,m}^{(3,1)}\right). \tag{B.32}$$

Note that we have neglected the intrinsic contribution in Eq. (6.22) for simplicity.

To compare with observations, one might wish to use the variables in [335], given by $\tilde{k}, \tilde{\alpha}, \tilde{\beta}$, defined as

$$\tilde{k} = \frac{1}{2} k_1 + \frac{1}{2} k_2 + \frac{1}{2} k_3, \qquad \tilde{\alpha} = \frac{k_2 - k_3}{\tilde{k}}, \qquad \tilde{\beta} = \frac{\tilde{k} - k_1}{\tilde{k}} \tag{B.33}$$

which in the squeezed limit are related to k_1, k_3 by

$$k_1 = \tilde{k} \frac{1 - \tilde{\beta}}{3 - \tilde{\beta}}, \qquad k_3 = \frac{\tilde{k}}{3 - \tilde{\beta}} \tag{B.34}$$

with $\tilde{\alpha} \approx 0$. We can use the chain rule to calculate

$$n^{\tilde{k}}_{f_{\rm NL}} = \frac{\partial \log f_{\rm NL}}{\partial \log \tilde{k}} = \frac{\partial \log f_{\rm NL}}{\partial \log k_1} \frac{\partial \log k_1}{\partial \log \tilde{k}} + \frac{\partial \log f_{\rm NL}}{\partial \log k_3} \frac{\partial \log k_3}{\partial \log \tilde{k}} = n^{k_1}_{f_{\rm NL}} + n^{k_3}_{f_{\rm NL}} \tag{B.35}$$

$$n^{\tilde{\beta}}_{f_{\rm NL}} = \frac{\partial \log f_{\rm NL}}{\partial \log \tilde{\beta}} = \frac{\partial \log f_{\rm NL}}{\partial \log k_1} \frac{\partial \log k_1}{\partial \log \tilde{\beta}} + \frac{\partial \log f_{\rm NL}}{\partial \log k_3} \frac{\partial \log k_3}{\partial \log \tilde{\beta}} = \frac{-2\tilde{\beta} n^{k_1}_{f_{\rm NL}}}{(1 - \tilde{\beta})(3 - \tilde{\beta})} + \frac{\tilde{\beta} n^{k_3}_{f_{\rm NL}}}{(3 - \tilde{\beta})}. \tag{B.36}$$

Note that in the squeezed limit $\tilde{\beta} \approx 1$, and so if we use our expression for the squeezed

limit of $f_{\rm NL}$ in (6.22), we shouldn't vary $\tilde{\beta}$ significantly away from 1.

Appendix C

Appendix for the Separate Universe Approach to Soft Limits

C.1 The background wave method

In this appendix we review the background wave method as used previously for models of single-field inflation (see e.g. [36, 83, 84, 271]) and then show how this generalises to models of multi-field inflation. In summary, for single-field inflation, the background wave method allows the effect of a soft mode to be traded for a change of spatial coordinates. In multi-field inflation however, one can't trade for a change in spatial coordinates, but instead one can trade for a change in field-space background values.

We begin with how soft ζ modes can be set to zero, if one performs a suitable change of spatial coordinates. Since ζ appears in the perturbed spatial metric as $g_{ij}(t,\mathbf{x})dx^i dx^j = a^2(t)e^{2\zeta(t,\mathbf{x})}\delta_{ij}dx^i dx^j$, a soft mode $\zeta^{\rm s}(t,\mathbf{x})$ can be recast as a change in coordinates, i.e. one can set $\zeta^{\rm s}(t,\mathbf{x}) \mapsto 0$ as long as one performs the coordinate transformation [83]

$$\mathbf{x} \mapsto \mathbf{x}' \equiv e^{\zeta^{\rm s}(t,\mathbf{x})}\mathbf{x} \tag{C.1}$$

everywhere. This statement is true of both single- and muti-field inflation. However, its utility for application to soft limits depends on whether one works with a single- or multi-field inflation model.

For single-field inflation, the method runs as follows: in single-field inflation, one assumes that the hard ζ mode[32] in the presence of soft modes, denoted $\zeta^{\rm h}(\mathbf{x})\Big|_{\rm s}$, feels the effect of the soft modes *only* through dependence on the soft ζ modes

$$\zeta^{\rm h}(\mathbf{x})\Big|_{\rm s} = \zeta^{\rm h}(\mathbf{x})\Big|_{\zeta^{\rm s}}. \tag{C.2}$$

[32] or correlation functions of hard ζ modes

Note that equation Eq. (C.2) holds only for single-field inflation since in this case there are no isocurvature modes, χ_α, and hence no dependence on soft isocurvature modes, $\chi^{\rm s}_\alpha$. The relation Eq. (C.1) means that $\zeta^{\rm h}(\mathbf{x})\Big|_{\zeta^{\rm s}} = \zeta^{\rm h}(\mathbf{x}')\Big|_0$, where the subscript zero indicates the value the hard modes take in the absence of any soft modes. This can then be inserted into Eq. (C.2) to give, for single-field inflation,

$$\zeta^{\rm h}(\mathbf{x})\Big|_{\rm s} = \zeta^{\rm h}(\mathbf{x}')\Big|_0. \tag{C.3}$$

The interpretation of this is that for single-field models, the effect of soft modes on the hard ζ can be accounted for by just rescaling the spatial coordinates and evaluating the hard mode in the absence of any soft modes. One can then Taylor expand the RHS of Eq. (C.3), for small $\zeta^{\rm s}$, to get (see e.g. [83, 84])

$$\zeta^{\rm h}(\mathbf{x}')\Big|_0 = \zeta^{\rm h}(\mathbf{x})\Big|_0 + \zeta^{\rm s}\ \mathbf{x}\cdot\nabla\zeta^{\rm h}(\mathbf{x})\Big|_0 + \cdots \tag{C.4}$$

which holds for single-field models. This can then be inserted into soft correlation functions to derive single-field consistency relations.

For multi-field models, Eq. (C.1) still holds, but Eq. (C.2) does not. This means one doesn't have Eq. (C.3) or Eq. (C.4). Instead of Eq. (C.2), for multi-field models we assume

$$\zeta^{\rm h}(\mathbf{x})\Big|_{\rm s} = \zeta^{\rm h}(\mathbf{x})\Big|_{\zeta^{\rm s},\chi^{\rm s}_\alpha} \tag{C.5}$$

where the $\chi^{\rm s}_\alpha$ are soft isocurvature modes. Equivalently, since ζ and χ_α can be recast in terms of fluctuations of the multiple scalar fields, we have

$$\zeta^{\rm h}(\mathbf{x})\Big|_{\rm s} = \zeta^{\rm h}(\mathbf{x})\Big|_{\delta\phi^{\rm s}_A}. \tag{C.6}$$

The interpretation of Eq. (C.6) is that for multi-field inflation, the effect of soft modes on the hard ζ is not just a local rescaling of coordinates (which was the single-field case), but is instead a more general transformation in the background values of the multiple scalar field values.

When inserted into soft limits of correlation functions, Eq. (C.6) implies that we are assuming that the main contribution to correlations between hard and soft modes comes from how the soft modes, which exit the horizon at much earlier times, alter the background cosmology in which hard modes exit. This assumption can be used for any set of scales, but becomes accurate only when the hierarchy is large. We then can Taylor expand the RHS of Eq. (C.6) in powers of $\delta\phi^{\rm s}_A$ around the value it would have taken in the absence of any soft scale modes $\zeta^{\rm h}(\mathbf{x})\Big|_0 \equiv \zeta^{\rm h}(\mathbf{x})$ to get Eq. (7.10).

C.2 Reduction to Single Field Result

We would like to recover the single-field result (5) of [268] (which agrees with the results of [269]) for the double-soft kite limit, with their N set to $N = 2$

$$\lim_{\mathrm{k}_1\approx\mathrm{k}_2\ll\mathrm{k}_3\approx\mathrm{k}_4} T_\zeta(\mathbf{k_1},\mathbf{k_2},\mathbf{k_3},\mathbf{k_4}) = B_\zeta(k_1,k_2,k_{12})\delta_{\mathcal{D}}P_\zeta(k_3) + P_\zeta(k_1)P_\zeta(k_2)\delta^2_{\mathcal{D}}P_\zeta(k_3) \tag{C.7}$$

$$\text{where } \delta_{\mathcal{D}} = -3 - \frac{d}{d\log k_3}. \tag{C.8}$$

In the single field case, our expression Eq. (7.29) reduces to

$$\begin{aligned}&\lim_{\mathrm{k}_1\approx\mathrm{k}_2\ll\mathrm{k}_3\approx\mathrm{k}_4} T_\zeta(\mathbf{k_1},\mathbf{k_2},\mathbf{k_3},\mathbf{k_4})\\ =&N_\phi^2 P_\zeta(k_3)_{,\phi}\alpha_{\phi\phi\phi}(k_1,k_2,k_{12}) + N_\phi^2 P_\zeta(k_3)_{,\phi\phi}\Sigma_{\phi\phi}(k_1)\Sigma_{\phi\phi}(k_2)\\ +&N_\phi N_{\phi\phi}P_\zeta(k_3)_{,\phi}\Sigma_{\phi\phi}(k_1)\Sigma_{\phi\phi}(k_{12}) + N_\phi N_{\phi\phi}P_\zeta(k_3)_{,\phi}\Sigma_{\phi\phi}(k_2)\Sigma_{\phi\phi}(k_{12}).\end{aligned} \tag{C.9}$$

We will use the standard single-field slow-roll expressions $N_\phi = -H/\dot\phi = 1/\sqrt{2\epsilon_V}$ and $N_{\phi\phi} = 1 - \eta_V/(2\epsilon_V)$ where $\epsilon_V \equiv \frac{1}{2}\left(V'/V\right)^2$ and $\eta_V \equiv V''/V$ are the potential slow roll parameters for slow-roll potential V. We will also use $\Sigma(k_3)_{\phi\phi} = H^2/2k_3^3$. Note that the scalar spectral index is

$$n_s - 1 = 2\eta_V - 6\epsilon_V = -\frac{(1+2N_{\phi\phi})}{N_\phi^2} \tag{C.10}$$

and in terms of the dilatation operator we have

$$n_s - 1 = -\frac{1}{P_\zeta(k_3)}\delta_{\mathcal{D}}P_\zeta(k_3). \tag{C.11}$$

The scalar tilt is given by

$$\alpha_s \equiv \frac{d\log(n_s-1)}{d\log k} = -\frac{(n_s-1)_{,\phi}}{N_\phi(n_s-1)} \tag{C.12}$$

where we've used $k = aH$ at horizon exit and $N_\phi = -H/\dot\phi$.

We would like to have expressions for $P_\zeta(k_3)_{,\phi}$ and $P_\zeta(k_3)_{,\phi\phi}$. Firstly

$$P_\zeta(k_3)_{,\phi} = \left(N_\phi^2\frac{H^2}{2k_3^3}\right)_{,\phi} = \frac{P_\zeta(k_3)}{N_\phi}(1+2N_{\phi\phi}) = -N_\phi(n_s-1)P_\zeta(k_3) = N_\phi\delta_{\mathcal{D}}P_\zeta(k_3) \tag{C.13}$$

where in the second equality we have used the slow-roll result $\left(H^2\right)_{,\phi} = H^2/N_\phi$, in the third equality we have used Eq. (C.10) and in the final equality we used Eq. (C.11).

Next, the second derivative is

$$P_\zeta(k_3)_{,\phi\phi} = \left(-N_\phi(n_s-1)P_\zeta(k_3)\right)_{,\phi} \tag{C.14}$$

$$= -N_{\phi\phi}(n_s-1)P_\zeta(k_3) + N_\phi\left[\alpha_s + N_\phi(n_s-1)\right](n_s-1)P_\zeta(k_3) \tag{C.15}$$

$$= N_{\phi\phi}\delta_{\mathcal{D}}P_\zeta(k_3) + N_\phi\left[-3 - \frac{d}{d\log k_3}\right]\left(-(n_s-1)P_\zeta(k_3)\right) \tag{C.16}$$

$$= N_{\phi\phi}\delta_{\mathcal{D}}P_\zeta(k_3) + N_\phi\delta^2_{\mathcal{D}}P_\zeta(k_3) \tag{C.17}$$

where we've made repeated use of Eq. (C.13), together with Eq. (C.12) in the second line. We can now substitute Eq. (C.13) and Eq. (C.17) into Eq. (C.9) and factor out $\delta_{\mathcal{D}}P_\zeta$ and $\delta^2_{\mathcal{D}}P_\zeta$ terms to give

$$\begin{aligned}&\lim_{\mathrm{k_1}\approx\mathrm{k_2}\ll\mathrm{k_3}\approx\mathrm{k_4}} T_\zeta(\mathbf{k_1},\mathbf{k_2},\mathbf{k_3},\mathbf{k_4})\\ =&\left\{N^3_\phi\alpha_{\phi\phi\phi}(k_1,k_2,k_{12}) + N^2_\phi N_{\phi\phi}\left[\Sigma_{\phi\phi}(k_1)\Sigma_{\phi\phi}(k_2) + (k_1\to k_2\to k_{12})\right]\right\}\delta_{\mathcal{D}}P_\zeta(k_3)\\ &+ N^4_\phi\Sigma_{\phi\phi}(k_1)\Sigma_{\phi\phi}(k_2)\delta^2_{\mathcal{D}}P_\zeta(k_3)\end{aligned} \tag{C.18}$$

$$= B_\zeta(k_1,k_2,k_{12})\delta_{\mathcal{D}}P_\zeta(k_3) + P_\zeta(k_1)P_\zeta(k_2)\delta^2_{\mathcal{D}}P_\zeta(k_3) \tag{C.19}$$

which is the desired single field result.

C.3 Γ Diagrams

In §7.3 we made the Γ expansion Eq. (7.42) expressing perturbation on flat hypersurfaces at some later time in terms of the perturbations on an earlier flat hypersurface. Then in §7.3.2 we inserted this expansion into the late time field-space two- and three-point functions. In this appendix, we consider the more general case of the field-space s-point function $F^{(n)}_{A_1\cdots A_s}(\mathbf{p_1},...,\mathbf{p_s})$, defined in Eq. (7.5), writing it in terms of field-space correlation functions whose evaluation time matches the exit time of the soft modes. We must expand up to $(s-1)$-th order to be consistent. Wick contractions then occur between the terms. Again, we can organise the result in terms of diagrams, which we call the Γ diagrams, which are analogous to both the δN Diagrams and the Soft Limit Diagrams. As before, we focus on tree-level, and keep only leading order terms in the gradient expansion.

Γ Diagram Rules:

1. Draw s-external dashed lines, labelled with incoming momenta $\mathbf{p_a}$ and field index A_a for $a = 1,...,s$. Draw a cross vertex at the end of each dashed line.

2. Connect the cross vertices by drawing a connected tree diagram with wavy lines. Each wavy line must connect on one end to a cross vertex and on the other end to a square vertex. At a cross vertex, (possibly multiple) wavy lines can connect to a dashed line. At a square vertex wavy lines connect to other wavy lines.

3. Label each wavy line with a distinct field index $B_1, B_2, ...$

4. Ensure momentum conservation at every vertex, which determines the momentum of each wavy line.

5. The two vertex types are assigned the following factors

   (a) Assign a factor $\Gamma^{(n,1\dots1)}_{A_a,B1\cdots B_m}$ to each cross vertex with one external dashed line with index A_a and m wavy lines with field indices $B_1, \cdots, B_m$, where $1 \leq m \leq s-1$.

   (b) Assign a factor $F^{(1)}_{B_1\cdots B_r}(\mathbf{q_1}, ..., \mathbf{q_r})$ to each square vertex with no dashed external lines and r wavy lines with incoming momenta $\mathbf{q_1}, ..., \mathbf{q_s}$ and field indices $B_1 \cdots B_r$, where $2 \leq r \leq s$.

6. Each diagram is associated with the mathematical expression obtained by multiplying together all vertex factors. Repeat the above process from stage 2 onwards to generate all distinct connected tree diagrams. $F^{(n)}_{A_1\cdots A_s}(\mathbf{p_1}, ..., \mathbf{p_s})$ is then obtained by summing over all these diagrams.

As an example, in Fig. 16, we show the Γ diagrams for the late-time field-space three-point function, corresponding to the expression Eq. (7.46) [322], which we repeat here for convenience

$$\begin{aligned}\alpha^{(n)}_{ABC}(p_1,p_2,p_3) =&\Gamma^{(n,1)}_{A,D}\Gamma^{(n,1)}_{B,E}\Gamma^{(n,1)}_{C,F}\alpha^{(1)}_{DEF}(p_1,p_2,p_3)\\ &+\left[\Gamma^{(n,11)}_{A,DE}\Gamma^{(n,1)}_{B,F}\Gamma^{(n,1)}_{C,G}\Sigma^{(1)}_{DF}(p_2)\Sigma^{(1)}_{EG}(p_3)+(A,p_1\to B,p_2\to C,p_3)\right].\end{aligned} \tag{C.20}$$

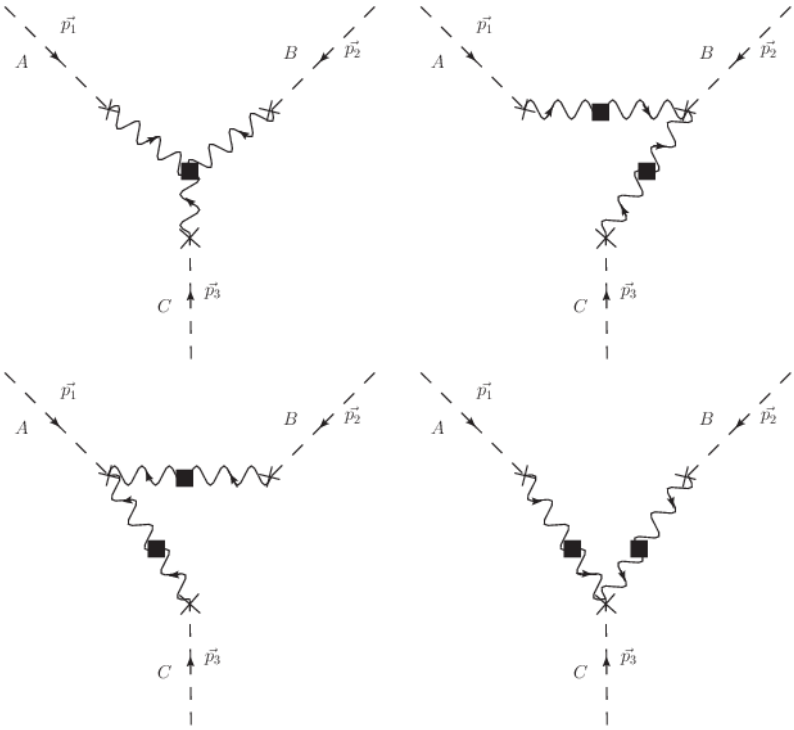

Figure 16: Distinct tree-level connected Γ Diagrams for the field space three-point function

Bibliography

[1] Z. Kenton and S. Thomas, *D-brane Potentials in the Warped Resolved Conifold and Natural Inflation*, *JHEP* **02** (2015) 127, [arXiv:1409.1221].

[2] Z. Kenton, D. J. Mulryne, and S. Thomas, *Generating the cosmic microwave background power asymmetry with g_{NL}*, *Phys. Rev.* **D92** (2015), no. 2 023505, [arXiv:1504.0573].

[3] Z. Kenton and D. J. Mulryne, *The squeezed limit of the bispectrum in multi-field inflation*, *JCAP* **1510** (2015), no. 10 018, [arXiv:1507.0862].

[4] Z. Kenton and D. J. Mulryne, *The Separate Universe Approach to Soft Limits*, *JCAP* **1610** (2016), no. 10 035, [arXiv:1605.0343].

[5] A. H. Guth, *The Inflationary Universe: A Possible Solution to the Horizon and Flatness Problems*, *Phys. Rev.* **D23** (1981) 347–356.

[6] D. H. Lyth and A. R. Liddle, *The primordial density perturbation: Cosmology, inflation and the origin of structure*. 2009.

[7] A. D. Linde, *Chaotic inflation*, *Physics Letters B* **129** (Sept., 1983) 177–181.

[8] K. Freese, J. Frieman, and A. Olinto, *Natural inflation with pseudo nambu-goldstone bosons*, *Physical Review Letters* **65** (1990) 3233–3236.

[9] C. Armendariz-Picon, T. Damour, and V. F. Mukhanov, *k - inflation*, *Phys. Lett.* **B458** (1999) 209–218, [hep-th/9904075].

[10] M. Alishahiha, E. Silverstein, and D. Tong, *DBI in the sky*, *Phys. Rev.* **D70** (2004) 123505, [hep-th/0404084].

[11] D. Wands, *Multiple field inflation*, *Lect. Notes Phys.* **738** (2008) 275–304, [astro-ph/0702187].

[12] A. R. Liddle, A. Mazumdar, and F. E. Schunck, *Assisted inflation*, *Phys. Rev.* **D58** (1998) 061301, [astro-ph/9804177].

[13] A. D. Linde, *Hybrid inflation*, *Phys. Rev.* **D49** (1994) 748–754, [astro-ph/9307002].

[14] K. Enqvist and M. S. Sloth, *Adiabatic CMB perturbations in pre - big bang string cosmology*, *Nucl. Phys.* **B626** (2002) 395–409, [hep-ph/0109214].

[15] D. H. Lyth and D. Wands, *Generating the curvature perturbation without an inflaton*, *Phys.Lett.* **B524** (2002) 5–14, [hep-ph/0110002].

[16] T. Moroi and T. Takahashi, *Effects of cosmological moduli fields on cosmic microwave background*, *Phys. Lett.* **B522** (2001) 215–221, [hep-ph/0110096]. [Erratum: Phys. Lett.B539,303(2002)].

[17] S. Mollerach, *Isocurvature Baryon Perturbations and Inflation*, *Phys. Rev.* **D42** (1990) 313–325.

[18] A. Linde and V. Mukhanov, *Non-gaussian isocurvature perturbations from inflation*, *Phys. Rev. D* **56** (Jul, 1997) R535–R539.

[19] D. Baumann, *TASI Lectures on Inflation*, 0907.5424.

[20] E. D. Stewart and D. H. Lyth, *A More accurate analytic calculation of the spectrum of cosmological perturbations produced during inflation*, *Phys.Lett.* **B302** (1993) 171–175, [gr-qc/9302019].

[21] T. T. Nakamura and E. D. Stewart, *The Spectrum of cosmological perturbations produced by a multicomponent inflaton to second order in the slow roll approximation*, *Phys.Lett.* **B381** (1996) 413–419, [astro-ph/9604103].

[22] D. H. Lyth, K. A. Malik, and M. Sasaki, *A General proof of the conservation of the curvature perturbation*, *JCAP* **0505** (2005) 004, [astro-ph/0411220].

[23] G. Rigopoulos and E. Shellard, *The separate universe approach and the evolution of nonlinear superhorizon cosmological perturbations*, *Phys.Rev.* **D68** (2003) 123518, [astro-ph/0306620].

[24] D. H. Lyth and Y. Rodriguez, *Non-Gaussianity from the second-order cosmological perturbation*, *Phys.Rev.* **D71** (2005) 123508, [astro-ph/0502578].

[25] D. S. Salopek and J. R. Bond, *Nonlinear evolution of long-wavelength metric fluctuations in inflationary models*, *Phys. Rev. D* **42** (Dec, 1990) 3936–3962.

[26] J. Garriga and V. F. Mukhanov, *Perturbations in k-inflation*, *Phys. Lett.* **B458** (1999) 219–225, [hep-th/9904176].

[27] D. Lyth, *A bound on inflationary energy density from the isotropy of the microwave background*, *Physics Letters B* **147** (1984), no. 6 403 – 404.

[28] D. H. Lyth, *What would we learn by detecting a gravitational wave signal in the cosmic microwave background anisotropy?*, *Phys. Rev. Lett.* **78** (Mar, 1997) 1861–1863.

[29] D. Baumann and L. McAllister, *Inflation and String Theory*. Cambridge University Press, 2015.

[30] S. Weinberg, *Quantum contributions to cosmological correlations*, *Phys. Rev.* **D72** (2005) 043514, [hep-th/0506236].

[31] S. Weinberg, *Quantum contributions to cosmological correlations. II. Can these corrections become large?*, *Phys. Rev.* **D74** (2006) 023508, [hep-th/0605244].

[32] J. Schwinger, *Brownian motion of a quantum oscillator*, *Journal of Mathematical Physics* **2** (1961), no. 3.

[33] P. M. Bakshi and K. T. Mahanthappa, *Expectation value formalism in quantum field theory. i*, *Journal of Mathematical Physics* **4** (1963), no. 1.

[34] P. M. Bakshi and K. T. Mahanthappa, *Expectation value formalism in quantum field theory. ii*, *Journal of Mathematical Physics* **4** (1963), no. 1.

[35] L. V. Keldysh, *Diagram technique for nonequilibrium processes*, *Zh. Eksp. Teor. Fiz.* **47** (1964) 1515–1527. [Sov. Phys. JETP20,1018(1965)].

[36] J. M. Maldacena, *Non-Gaussian features of primordial fluctuations in single field inflationary models*, *JHEP* **0305** (2003) 013, [astro-ph/0210603].

[37] M. Sasaki and E. D. Stewart, *A General analytic formula for the spectral index of the density perturbations produced during inflation*, *Prog. Theor. Phys.* **95** (1996) 71–78, [astro-ph/9507001].

[38] J. Elliston, D. J. Mulryne, D. Seery, and R. Tavakol, *Evolution of f_{NL} to the adiabatic limit*, *JCAP* **11** (Nov., 2011) 5, [arXiv:1106.2153].

[39] D. Lyth, *Large Scale Energy Density Perturbations and Inflation*, *Phys.Rev.* **D31** (1985) 1792–1798.

[40] D. Wands, K. A. Malik, D. H. Lyth, and A. R. Liddle, *A New approach to the evolution of cosmological perturbations on large scales*, *Phys. Rev.* **D62** (2000) 043527, [astro-ph/0003278].

[41] D. H. Lyth and Y. Rodriguez, *The Inflationary prediction for primordial non-Gaussianity*, *Phys.Rev.Lett.* **95** (2005) 121302, [astro-ph/0504045].

[42] M. Dias, R. H. Ribeiro, and D. Seery, *The δN formula is the dynamical renormalization group*, *JCAP* **10** (Oct., 2013) 62, [arXiv:1210.7800].

[43] D. Seery and J. E. Lidsey, *Primordial non-Gaussianities from multiple-field inflation*, *JCAP* **0509** (2005) 011, [astro-ph/0506056].

[44] D. H. Lyth and I. Zaballa, *A Bound concerning primordial non-Gaussianity*, *JCAP* **0510** (2005) 005, [astro-ph/0507608].

[45] C. T. Byrnes, S. Nurmi, G. Tasinato, and D. Wands, *Scale dependence of local f_{NL}*, *JCAP* **2** (Feb., 2010) 34, [arXiv:0911.2780].

[46] X. Chen, R. Easther, and E. A. Lim, *Large Non-Gaussianities in Single Field Inflation*, *JCAP* **0706** (2007) 023, [astro-ph/0611645].

[47] X. Chen, R. Easther, and E. A. Lim, *Generation and Characterization of Large Non-Gaussianities in Single Field Inflation*, *JCAP* **0804** (2008) 010, [arXiv:0801.3295].

[48] D. K. Hazra, L. Sriramkumar, and J. Martin, *BINGO: A code for the efficient computation of the scalar bi-spectrum*, *JCAP* **1305** (2013) 026, [arXiv:1201.0926].

[49] H. Funakoshi and S. Renaux-Petel, *A Modal Approach to the Numerical Calculation of Primordial non-Gaussianities*, *JCAP* **1302** (2013) 002, [arXiv:1211.3086].

[50] M. Dias, J. Frazer, D. J. Mulryne, and D. Seery, *Numerical evaluation of the bispectrum in multiple field inflation*, arXiv:1609.0037.

[51] D. J. Mulryne, *PyTransport: A Python package for the calculation of inflationary correlation functions*, arXiv:1609.0038.

[52] D. Seery, *CppTransport: a platform to automate calculation of inflationary correlation functions*, arXiv:1609.0038.

[53] D. J. Mulryne, D. Seery, and D. Wesley, *Moment transport equations for non-Gaussianity*, *JCAP* **1001** (2010) 024, [arXiv:0909.2256].

[54] D. J. Mulryne, D. Seery, and D. Wesley, *Moment transport equations for the primordial curvature perturbation*, *JCAP* **1104** (2011) 030, [arXiv:1008.3159].

[55] D. Seery, D. J. Mulryne, J. Frazer, and R. H. Ribeiro, *Inflationary perturbation theory is geometrical optics in phase space*, *JCAP* **1209** (2012) 010, [arXiv:1203.2635].

[56] G. J. Anderson, D. J. Mulryne, and D. Seery, *Transport equations for the inflationary trispectrum*, *JCAP* **1210** (2012) 019, [arXiv:1205.0024].

[57] D. J. Mulryne, *Transporting non-Gaussianity from sub to super-horizon scales*, *JCAP* **1309** (2013) 010, [arXiv:1302.3842].

[58] I. Huston and A. J. Christopherson, *Calculating Non-adiabatic Pressure Perturbations during Multi-field Inflation*, *Phys. Rev.* **D85** (2012) 063507, [arXiv:1111.6919].

[59] L. C. Price, J. Frazer, J. Xu, H. V. Peiris, and R. Easther, *MultiModeCode: An efficient numerical solver for multifield inflation*, *JCAP* **1503** (2015), no. 03 005, [arXiv:1410.0685].

[60] M. Dias, J. Frazer, and D. Seery, *Computing observables in curved multifield models of inflation—A guide (with code) to the transport method*, *JCAP* **1512** (2015), no. 12 030, [arXiv:1502.0312].

[61] S. Weinberg, *Adiabatic modes in cosmology*, *Phys. Rev.* **D67** (2003) 123504, [astro-ph/0302326].

[62] U. Seljak and M. Zaldarriaga, *A Line of sight integration approach to cosmic microwave background anisotropies*, *Astrophys. J.* **469** (1996) 437–444, [astro-ph/9603033].

[63] A. Lewis, A. Challinor, and A. Lasenby, *Efficient computation of CMB anisotropies in closed FRW models*, *Astrophys. J.* **538** (2000) 473–476, [astro-ph/9911177].

[64] D. Blas, J. Lesgourgues, and T. Tram, *The Cosmic Linear Anisotropy Solving System (CLASS). Part II: Approximation schemes*, *JCAP* **7** (July, 2011) 034, [arXiv:1104.2933].

[65] **Planck** Collaboration, P. Ade et al., *Planck 2015 results. XX. Constraints on inflation*, arXiv:1502.0211.

[66] S. Dodelson, *Coherent phase argument for inflation*, *AIP Conf. Proc.* **689** (2003) 184–196, [hep-ph/0309057]. [,184(2003)].

[67] F. Bernardeau, S. Colombi, E. Gaztanaga, and R. Scoccimarro, *Large scale structure of the universe and cosmological perturbation theory*, *Phys. Rept.* **367** (2002) 1–248, [astro-ph/0112551].

[68] V. Springel, *The Cosmological simulation code GADGET-2*, *Mon. Not. Roy. Astron. Soc.* **364** (2005) 1105–1134, [astro-ph/0505010].

[69] R. Hlozek, J. Dunkley, G. Addison, J. W. Appel, J. R. Bond, C. Sofia Carvalho, S. Das, M. J. Devlin, R. Dünner, T. Essinger-Hileman, J. W. Fowler, P. Gallardo, A. Hajian, M. Halpern, M. Hasselfield, M. Hilton, A. D. Hincks, J. P. Hughes, K. D. Irwin, J. Klein, A. Kosowsky, T. A. Marriage, D. Marsden, F. Menanteau, K. Moodley, M. D. Niemack, M. R. Nolta, L. A. Page, L. Parker, B. Partridge, F. Rojas, N. Sehgal, B. Sherwin, J. Sievers, D. N. Spergel, S. T. Staggs, D. S. Swetz, E. R. Switzer, R. Thornton, and E. Wollack, *The Atacama Cosmology Telescope: A Measurement of the Primordial Power Spectrum*, *APJ* **749** (Apr., 2012) 90, [arXiv:1105.4887].

[70] N. Dalal, O. Dore, D. Huterer, and A. Shirokov, *The imprints of primordial non-gaussianities on large-scale structure: scale dependent bias and abundance of virialized objects*, *Phys. Rev.* **D77** (2008) 123514, [arXiv:0710.4560].

[71] S. Matarrese and L. Verde, *The effect of primordial non-Gaussianity on halo bias*, *Astrophys. J.* **677** (2008) L77–L80, [arXiv:0801.4826].

[72] **Planck** Collaboration, P. A. R. Ade et al., *Planck 2015 results. XIII. Cosmological parameters*, *Astron. Astrophys.* **594** (2016) A13, [arXiv:1502.0158].

[73] **BICEP2, Planck** Collaboration, P. A. R. Ade et al., *Joint Analysis of BICEP2/KeckArray and Planck Data*, *Phys. Rev. Lett.* **114** (2015) 101301, [arXiv:1502.0061].

[74] **BICEP2** Collaboration, P. A. R. Ade et al., *Detection of B-Mode Polarization at Degree Angular Scales by BICEP2*, *Phys. Rev. Lett.* **112** (2014), no. 24 241101, [arXiv:1403.3985].

[75] B. Reichborn-Kjennerud et al., *EBEX: a balloon-borne CMB polarization experiment*, *Proc. SPIE* **7741** (July, 2010) 77411C, [arXiv:1007.3672].

[76] **BICEP3** Collaboration, Z. Ahmed et al., *BICEP3: a 95GHz refracting telescope for degree-scale CMB polarization*, *Proc. SPIE Int. Soc. Opt. Eng.* **9153** (2014) 91531N, [arXiv:1407.5928].

[77] T. Essinger-Hileman et al., *The Atacama B-Mode Search: CMB Polarimetry with Transition-Edge-Sensor Bolometers*, *ArXiv e-prints* (Aug., 2010) [arXiv:1008.3915].

[78] A. A. Fraisse et al., *SPIDER: probing the early Universe with a suborbital polarimeter*, *JCAP* **4** (Apr., 2013) 047, [arXiv:1106.3087].

[79] J. R. Eimer, C. L. Bennett, D. T. Chuss, T. Marriage, E. J. Wollack, and L. Zeng, *The cosmology large angular scale surveyor (CLASS): 40 GHz optical design*, in *Millimeter, Submillimeter, and Far-Infrared Detectors and Instrumentation for Astronomy VI*, vol. 8452, p. 845220, Sept., 2012. arXiv:1211.0041.

[80] J. E. Austermann et al., *SPTpol: an instrument for CMB polarization measurements with the South Pole Telescope*, in *Millimeter, Submillimeter, and Far-Infrared Detectors and Instrumentation for Astronomy VI*, vol. 8452, p. 84521E, Sept., 2012. arXiv:1210.4970.

[81] Z. D. Kermish et al., *The POLARBEAR experiment*, in *Millimeter, Submillimeter, and Far-Infrared Detectors and Instrumentation for Astronomy VI*, vol. 8452, p. 84521C, Sept., 2012. arXiv:1210.7768.

[82] M. D. Niemack et al., *ACTPol: a polarization-sensitive receiver for the Atacama Cosmology Telescope*, in *Millimeter, Submillimeter, and Far-Infrared Detectors and Instrumentation for Astronomy V*, vol. 7741, p. 77411S, July, 2010. arXiv:1006.5049.

[83] C. Cheung, A. L. Fitzpatrick, J. Kaplan, and L. Senatore, *On the consistency relation of the 3-point function in single field inflation*, *JCAP* **0802** (2008) 021, [arXiv:0709.0295].

[84] P. Creminelli and M. Zaldarriaga, *Single field consistency relation for the 3-point function*, *JCAP* **0410** (2004) 006, [astro-ph/0407059].

[85] **Planck** Collaboration, P. Ade et al., *Planck 2015 results. XVII. Constraints on primordial non-Gaussianity*, arXiv:1502.0159.

[86] V. Assassi, D. Baumann, D. Green, and M. Zaldarriaga, *Renormalized Halo Bias*, *JCAP* **1408** (2014) 056, [arXiv:1402.5916].

[87] V. Assassi, D. Baumann, and F. Schmidt, *Galaxy Bias and Primordial Non-Gaussianity*, *JCAP* **1512** (2015), no. 12 043, [arXiv:1510.0372].

[88] V. Assassi, D. Baumann, E. Pajer, Y. Welling, and D. van der Woude, *Effective theory of large-scale structure with primordial non-Gaussianity*, *JCAP* **1511** (2015) 024, [arXiv:1505.0666].

[89] Y. Welling, D. van der Woude, and E. Pajer, *Lifting Primordial Non-Gaussianity Above the Noise*, *JCAP* **1608** (2016), no. 08 044, [arXiv:1605.0642].

[90] D. Baumann, A. Nicolis, L. Senatore, and M. Zaldarriaga, *Cosmological Non-Linearities as an Effective Fluid*, *JCAP* **1207** (2012) 051, [arXiv:1004.2488].

[91] J. J. M. Carrasco, M. P. Hertzberg, and L. Senatore, *The Effective Field Theory of Cosmological Large Scale Structures*, *JHEP* **09** (2012) 082, [arXiv:1206.2926].

[92] J. J. M. Carrasco, S. Foreman, D. Green, and L. Senatore, *The Effective Field Theory of Large Scale Structures at Two Loops*, *JCAP* **1407** (2014) 057, [arXiv:1310.0464].

[93] R. A. Porto, L. Senatore, and M. Zaldarriaga, *The Lagrangian-space Effective Field Theory of Large Scale Structures*, *JCAP* **1405** (2014) 022, [arXiv:1311.2168].

[94] S. M. Carroll, S. Leichenauer, and J. Pollack, *Consistent effective theory of long-wavelength cosmological perturbations*, *Phys. Rev.* **D90** (2014), no. 2 023518, [arXiv:1310.2920].

[95] L. Mercolli and E. Pajer, *On the velocity in the Effective Field Theory of Large Scale Structures*, *JCAP* **1403** (2014) 006, [arXiv:1307.3220].

[96] E. Pajer and M. Zaldarriaga, *On the Renormalization of the Effective Field Theory of Large Scale Structures*, *JCAP* **1308** (2013) 037, [arXiv:1301.7182].

[97] M. P. Hertzberg, *Effective field theory of dark matter and structure formation: Semianalytical results*, *Phys. Rev.* **D89** (2014), no. 4 043521, [arXiv:1208.0839].

[98] E. Pajer and M. Zaldarriaga, *A New Window on Primordial non-Gaussianity*, *Phys. Rev. Lett.* **109** (2012) 021302, [arXiv:1201.5375].

[99] E. Dimastrogiovanni and R. Emami, *Correlating CMB Spectral Distortions with Temperature: what do we learn on Inflation?*, arXiv:1606.0428.

[100] A. Kogut, D. J. Fixsen, D. T. Chuss, J. Dotson, E. Dwek, M. Halpern, G. F. Hinshaw, S. M. Meyer, S. H. Moseley, M. D. Seiffert, D. N. Spergel, and E. J. Wollack, *The Primordial Inflation Explorer (PIXIE): a nulling polarimeter for cosmic microwave background observations*, *JCAP* **7** (July, 2011) 025, [arXiv:1105.2044].

[101] **PRISM** Collaboration, P. Andre et al., *PRISM (Polarized Radiation Imaging and Spectroscopy Mission): A White Paper on the Ultimate Polarimetric Spectro-Imaging of the Microwave and Far-Infrared Sky*, arXiv:1306.2259.

[102] J.-L. Lehners, *Ekpyrotic Non-Gaussianity: A Review*, *Adv. Astron.* **2010** (2010) 903907, [arXiv:1001.3125].

[103] M. Green, J. Schwarz, and E. Witten, *Superstring Theory: Volume 1, Introduction*. Cambridge Monographs on Mathematical Physics. Cambridge University Press, 1988.

[104] J. Polchinski, *String Theory: Volume 1, An Introduction to the Bosonic String*. Cambridge Monographs on Mathematical Physics. Cambridge University Press, 1998.

[105] B. Zwiebach, *A First Course in String Theory*. A First Course in String Theory. Cambridge University Press, 2004.

[106] K. Becker, M. Becker, and J. H. Schwarz, *String theory and M-theory: A modern introduction*. Cambridge University Press, 2006.

[107] L. Randall and R. Sundrum, *A Large mass hierarchy from a small extra dimension*, *Phys. Rev. Lett.* **83** (1999) 3370–3373, [hep-ph/9905221].

[108] M. Nakahara, *Geometry, topology, and physics*. Graduate student series in physics. Institute of Physics Publishing, Bristol, Philadelphia, 2003.

[109] S. B. Giddings, S. Kachru, and J. Polchinski, *Hierarchies from fluxes in string compactifications*, *Phys. Rev. D* **66** (Nov., 2002) 106006, [0105097].

[110] D. Baumann, A. Dymarsky, S. Kachru, I. R. Klebanov, and L. McAllister, *D3-brane potentials from fluxes in AdS/CFT*, *J. High Energy Phys.* **6** (June, 2010) 72, [arXiv:1001.5028].

[111] S. Gukov, C. Vafa, and E. Witten, *CFT's from Calabi-Yau four-folds*, *Nucl. Phys. B* **584** (Sept., 2000) 69–108.

[112] D. J. Gross and E. Witten, *Superstring modifications of einstein's equations*, *Nuclear Physics B* **277** (1986) 1 – 10.

[113] K. Becker, M. Becker, M. Haack, and J. Louis, *Supersymmetry breaking and alpha-prime corrections to flux induced potentials*, *JHEP* **06** (2002) 060, [hep-th/0204254].

[114] M. Shifman and A. Vainshtein, *On gluino condensation in supersymmetric gauge theories with su(n) and o(n) groups*, *Nuclear Physics B* **296** (1988), no. 2 445 – 461.

[115] V. Novikov, M. Shifman, A. Vainshtein, and V. Zakharov, *Instanton effects in supersymmetric theories*, *Nuclear Physics B* **229** (1983), no. 2 407 – 420.

[116] V. Novikov, M. Shifman, A. Vainshtein, V. Voloshin, and V. Zakharov, *Supersymmetry transformations of instantons*, *Nuclear Physics B* **229** (1983), no. 2 394 – 406.

[117] S. Ferrara, L. Girardello, and H. Nilles, *Breakdown of local supersymmetry through gauge fermion condensates*, *Physics Letters B* **125** (1983), no. 6 457 – 460.

[118] M. Dine, R. Rohm, N. Seiberg, and E. Witten, *Gluino condensation in superstring models*, *Physics Letters B* **156** (1985), no. 1 55 – 60.

[119] J. Derendinger, L. Ibáñez, and H. Nilles, *On the low energy d = 4, n = 1 supergravity theory extracted from the d = 10, n = 1 superstring*, *Physics Letters B* **155** (1985), no. 1 65 – 70.

[120] S. Kachru, R. Kallosh, A. Linde, and S. P. Trivedi, *de sitter vacua in string theory*, *Phys. Rev. D* **68** (Aug, 2003) 046005.

[121] V. Balasubramanian, P. Berglund, J. P. Conlon, and F. Quevedo, *Systematics of moduli stabilisation in calabi-yau flux compactifications*, *Journal of High Energy Physics* **2005** (2005), no. 03 007.

[122] M. Headrick and T. Wiseman, *Numerical Ricci-flat metrics on K3*, *Class.Quant.Grav.* **22** (2005) 4931–4960, [hep-th/0506129].

[123] M. Headrick and A. Nassar, *Energy functionals for Calabi-Yau metrics*, *Adv.Theor.Math.Phys.* **17** (2013) 867–902, [arXiv:0908.2635].

[124] M. Reid, *The moduli space of 3-folds withk=0 may nevertheless be irreducible*, *Mathematische Annalen* **278** (1987), no. 1 329–334.

[125] P. Candelas, A. Dale, C. Lütken, and R. Schimmrigk, *Complete intersection calabi-yau manifolds*, *Nuclear Physics B* **298** (1988), no. 3 493 – 525.

[126] P. S. Green and T. Hübsch, *Connecting moduli spaces of calabi-yau threefolds*, *Communications in Mathematical Physics* **119** (1988), no. 3 431–441.

[127] P. Candelas, P. S. Green, and T. Hübsch, *Rolling among calabi-yau vacua*, *Nuclear Physics B* **330** (1990), no. 1 49 – 102.

[128] P. Candelas and X. C. de la Ossa, *Comments on Conifolds*, *Nucl. Phys.* **B342** (1990) 246–268.

[129] I. R. Klebanov and M. J. Strassler, *Supergravity and a confining gauge theory: Duality cascades and chi SB resolution of naked singularities*, *JHEP* **08** (2000) 052, [hep-th/0007191].

[130] I. R. Klebanov and A. Murugan, *Gauge/Gravity Duality and Warped Resolved Conifold*, *JHEP* **03** (2007) 042, [hep-th/0701064].

[131] L. A. Pando Zayas and A. A. Tseytlin, *3-branes on resolved conifold*, *JHEP* **11** (2000) 028, [hep-th/0010088].

[132] J. M. Maldacena, *The Large N limit of superconformal field theories and supergravity*, *Int. J. Theor. Phys.* **38** (1999) 1113–1133, [hep-th/9711200]. [Adv. Theor. Math. Phys.2,231(1998)].

[133] I. R. Klebanov and E. Witten, *Superconformal field theory on three-branes at a Calabi-Yau singularity*, *Nucl. Phys.* **B536** (1998) 199–218, [hep-th/9807080].

[134] I. R. Klebanov and E. Witten, *AdS / CFT correspondence and symmetry breaking*, *Nucl. Phys.* **B556** (1999) 89–114, [hep-th/9905104].

[135] N. Arkani-Hamed, L. Motl, A. Nicolis, and C. Vafa, *The String landscape, black holes and gravity as the weakest force*, *JHEP* **06** (2007) 060, [hep-th/0601001].

[136] T. Banks, M. Dine, P. J. Fox, and E. Gorbatov, *On the possibility of large axion decay constants*, *JCAP* **0306** (2003) 001, [hep-th/0303252].

[137] P. Svrcek and E. Witten, *Axions In String Theory*, *JHEP* **06** (2006) 051, [hep-th/0605206].

[138] K. Kooner, S. Parameswaran, and I. Zavala, *Warping the Weak Gravity Conjecture*, *Phys. Lett.* **B759** (2016) 402–409, [arXiv:1509.0704].

[139] F. C. Adams, J. R. Bond, K. Freese, J. A. Frieman, and A. V. Olinto, *Natural inflation: Particle physics models, power-law spectra for large-scale structure, and constraints from the cosmic background explorer*, *Phys. Rev. D* **47** (Jan, 1993) 426–455.

[140] K. Freese and W. H. Kinney, *On: Natural inflation*, *Phys.Rev.* **D70** (2004) 083512, [hep-ph/0404012].

[141] K. Freese and W. H. Kinney, *Natural Inflation: Consistency with Cosmic Microwave Background Observations of Planck and BICEP2*, arXiv:1403.5277.

[142] S. Kachru, R. Kallosh, A. D. Linde, J. M. Maldacena, L. P. McAllister, et al., *Towards inflation in string theory*, *JCAP* **0310** (2003) 013, [hep-th/0308055].

[143] S. Kachru, R. Kallosh, A. D. Linde, and S. P. Trivedi, *De Sitter vacua in string theory*, *Phys. Rev. D* **68** (2003) 046005, [hep-th/0301240].

[144] G. Dvali and S.-H. H. Tye, *Brane inflation*, *Phys. Lett. B* **450** (Mar., 1999) 72–82.

[145] P. Candelas and X. C. de la Ossa, *Comments on conifolds*, *Nucl. Phys. B* **342** (Sept., 1990) 246–268.

[146] R. Minasian and D. Tsimpis, *On the geometry of nontrivially embedded branes*, *Nucl.Phys.* **B572** (2000) 499–513, [hep-th/9911042].

[147] K. Ohta and T. Yokono, *Deformation of conifold and intersecting branes*, *JHEP* **0002** (2000) 023, [hep-th/9912266].

[148] I. R. Klebanov and A. A. Tseytlin, *Gravity duals of supersymmetric SU(N) x SU(N+M) gauge theories*, *Nucl.Phys.* **B578** (2000) 123–138, [hep-th/0002159].

[149] I. R. Klebanov and M. J. Strassler, *Supergravity and a confining gauge theory: duality cascades and $\{\chi\}$SB-resolution of naked singularities*, *J. High Energy Phys.* **8** (Aug., 2000) 52.

[150] L. A. P. Zayas and A. A. Tseytlin, *3-branes on resolved conifold*, *J. High Energy Phys.* **2000** (Nov., 2000) 028, [0010088].

[151] K. Dasgupta, P. Franche, A. Knauf, and J. Sully, *D-terms on the resolved conifold*, *JHEP* **0904** (2009) 027, [arXiv:0802.0202].

[152] A. Dymarsky, I. R. Klebanov, and N. Seiberg, *On the moduli space of the cascading SU (M + p) SU (p) gauge theory*, *J. High Energy Phys.* **2006** (Jan., 2006) 155, [0511254].

[153] A. Butti, M. Graña, R. Minasian, M. Petrini, and A. Zaffaroni, *The Baryonic Branch of Klebanov-Strassler Solution: a Supersymmetric Family of SU(3) Structure Backgrounds*, *J. High Energy Phys.* **2005** (Mar., 2005) 069, [0412187].

[154] G. Papadopoulos and A. A. Tseytlin, *Complex geometry of conifolds and five-brane wrapped on two sphere*, *Class.Quant.Grav.* **18** (2001) 1333–1354, [hep-th/0012034].

[155] I. R. Klebanov and A. Murugan, *Gauge/gravity duality and warped resolved conifold*, *J. High Energy Phys.* **2007** (Mar., 2007) 042, [0701064].

[156] X. Chen, *Multi-throat brane inflation*, *Phys.Rev.* **D71** (2005) 063506, [hep-th/0408084].

[157] Y.-F. Cai and W. Xue, *N-flation from multiple DBI type actions*, *Phys.Lett.* **B680** (2009) 395–398, [arXiv:0809.4134].

[158] Y.-F. Cai and H.-Y. Xia, *Inflation with multiple sound speeds: a model of multiple DBI type actions and non-Gaussianities*, *Phys.Lett.* **B677** (2009) 226–234, [arXiv:0904.0062].

[159] J. Emery, G. Tasinato, and D. Wands, *Local non-Gaussianity from rapidly varying sound speeds*, *JCAP* **1208** (2012) 005, [arXiv:1203.6625].

[160] J. Emery, G. Tasinato, and D. Wands, *Mixed non-Gaussianity in multiple-DBI inflation*, *JCAP* **1305** (2013) 021, [arXiv:1303.3975].

[161] D. Baumann and L. McAllister, *A Microscopic Limit on Gravitational Waves from D-brane Inflation*, *Phys.Rev.* **D75** (2007) 123508, [hep-th/0610285].

[162] D. Baumann, A. Dymarsky, I. R. Klebanov, J. Maldacena, L. McAllister, and A. Murugan, *On D3-brane potentials in compactifications with fluxes and wrapped D-branes*, *J. High Energy Phys.* **11** (Nov., 2006) 31.

[163] D. Baumann, A. Dymarsky, I. R. Klebanov, L. McAllister, and P. J. Steinhardt, *A Delicate Universe: Compactification Obstacles to D-brane Inflation*, *Phys. Rev. Lett.* **99** (Oct., 2007) 141601, [arXiv:0705.3837].

[164] D. Baumann, A. Dymarsky, S. Kachru, I. R. Klebanov, and L. McAllister, *Holographic systematics of D-brane inflation*, *J. High Energy Phys.* **3** (Mar., 2009) 93, [arXiv:0808.2811].

[165] S. Gandhi, L. McAllister, and S. Sjors, *A Toolkit for Perturbing Flux Compactifications*, *JHEP* **1112** (2011) 053, [arXiv:1106.0002].

[166] E. Pajer, *Inflation at the Tip*, *JCAP* **0804** (2008) 031, [arXiv:0802.2916].

[167] I. R. Klebanov and E. Witten, *Superconformal field theory on threebranes at a Calabi-Yau singularity*, *Nucl. Phys. B* **536** (Dec., 1998) 199–218.

[168] C. Krishnan and S. Kuperstein, *Gauge theory RG flows from a warped resolved orbifold*, *J. High Energy Phys.* **2008** (Apr., 2008) 009, [arXiv:0801.1053].

[169] C. Krishnan and S. Kuperstein, *The mesonic branch of the deformed conifold*, *J. High Energy Phys.* **2008** (May, 2008) 072, [arXiv:0802.3674].

[170] R. Gregory and D. Kaviani, *Spinflation with Angular Potentials*, *JHEP* **1201** (2012) 037, [arXiv:1107.5522].

[171] N. Agarwal, R. Bean, L. McAllister, and G. Xu, *Universality in D-brane Inflation*, *JCAP* **9** (2011) 002, [arXiv:1103.2775].

[172] M. Dias, J. Frazer, and A. R. Liddle, *Multifield consequences for D-brane inflation*, *JCAP* **6** (June, 2012) 20, [arXiv:1203.3792].

[173] L. McAllister, S. Renaux-Petel, and G. Xu, *A statistical approach to multifield inflation: many-field perturbations beyond slow roll*, *JCAP* **10** (Oct., 2012) 46, [arXiv:1207.0317].

[174] M. Aganagic, A. Karch, D. Lust, and A. Miemiec, *Mirror symmetries for brane configurations and branes at singularities*, *Nucl.Phys.* **B569** (2000) 277–302, [hep-th/9903093].

[175] F. Marchesano, G. Shiu, and A. M. Uranga, *F-term Axion Monodromy Inflation*, arXiv:1404.3040.

[176] D. Langlois, S. Renaux-Petel, and D. A. Steer, *Multi-field DBI inflation: Introducing bulk forms and revisiting the gravitational wave constraints*, *JCAP* **0904** (2009) 021, [arXiv:0902.2941].

[177] D. Easson, R. Gregory, I. Zavala, and G. Tasinato, *Cycling in the throat*, *J. High Energy Phys.* **4** (Apr., 2007) 26.

[178] D. A. Easson, R. Gregory, D. F. Mota, G. Tasinato, and I. Zavala, *Spinflation*, *JCAP* **0802** (2008) 010, [arXiv:0709.2666].

[179] D. Kaviani, *Spinflation with backreaction*, *Int.J.Mod.Phys.* **D22** (2013) 1350062, [arXiv:1212.5831].

[180] T. Kidani and K. Koyama, *Non-Gaussianities in DBI inflation with angular motion*, *Phys. Rev. D* **90** (July, 2014) 023515, [arXiv:1403.6687].

[181] D. Langlois, S. Renaux-Petel, D. A. Steer, and T. Tanaka, *Primordial fluctuations and non-Gaussianities in multi-field DBI inflation*, *Phys.Rev.Lett.* **101** (2008) 061301, [arXiv:0804.3139].

[182] D. Langlois, S. Renaux-Petel, D. A. Steer, and T. Tanaka, *Primordial perturbations and non-Gaussianities in DBI and general multi-field inflation*, *Phys.Rev.* **D78** (2008) 063523, [arXiv:0806.0336].

[183] L. McAllister, E. Silverstein, and A. Westphal, *Gravity Waves and Linear Inflation from Axion Monodromy*, *Phys.Rev.* **D82** (2010) 046003, [arXiv:0808.0706].

[184] R. Kappl, S. Krippendorf, and H. P. Nilles, *Aligned Natural Inflation: Monodromies of two Axions*, arXiv:1404.7127.

[185] J. E. Kim, H. P. Nilles, and M. Peloso, *Completing natural inflation*, *JCAP* **0501** (2005) 005, [hep-ph/0409138].

[186] K. Choi, H. Kim, and S. Yun, *Natural Inflation with Multiple Sub-Planckian Axions*, arXiv:1404.6209.

[187] C. Long, L. McAllister, and P. McGuirk, *Aligned Natural Inflation in String Theory*, *Phys.Rev.* **D90** (2014) 023501, [arXiv:1404.7852].

[188] I. Ben-Dayan, F. G. Pedro, and A. Westphal, *Towards Natural Inflation in String Theory*, arXiv:1407.2562.

[189] I. Ben-Dayan, F. G. Pedro, and A. Westphal, *Hierarchical Axion Inflation*, arXiv:1404.7773.

[190] X. Gao, T. Li, and P. Shukla, *Combining Universal and Odd RR Axions for Aligned Natural Inflation*, arXiv:1406.0341.

[191] S. Dimopoulos, S. Kachru, J. McGreevy, and J. G. Wacker, *N-flation*, *JCAP* **0808** (2008) 003, [hep-th/0507205].

[192] A. Ashoorioon, H. Firouzjahi, and M. Sheikh-Jabbari, *M-flation: Inflation From Matrix Valued Scalar Fields*, *JCAP* **0906** (2009) 018, [arXiv:0903.1481].

[193] A. Ashoorioon and M. Sheikh-Jabbari, *Gauged M-flation, its UV sensitivity and Spectator Species*, *JCAP* **1106** (2011) 014, [arXiv:1101.0048].

[194] A. Ashoorioon and M. Sheikh-Jabbari, *Gauged M-flation After BICEP2*, arXiv:1405.1685.

[195] M. Cicoli, K. Dutta, and A. Maharana, *N-flation with Hierarchically Light Axions in String Compactifications*, arXiv:1401.2579.

[196] S. A. Kim and A. R. Liddle, *Nflation: multi-field inflationary dynamics and perturbations*, *Phys.Rev.* **D74** (2006) 023513, [astro-ph/0605604].

[197] T. C. Bachlechner, M. Dias, J. Frazer, and L. McAllister, *A New Angle on Chaotic Inflation*, arXiv:1404.7496.

[198] K. Choi, H. Kim, and S. Yun, *Natural Inflation with Multiple Sub-Planckian Axions*, *Phys.Rev.* **D90** (2014) 023545, [arXiv:1404.6209].

[199] M. Czerny, T. Higaki, and F. Takahashi, *Multi-Natural Inflation in Supergravity and BICEP2*, arXiv:1403.5883.

[200] E. Silverstein and A. Westphal, *Monodromy in the CMB: Gravity Waves and String Inflation*, *Phys.Rev.* **D78** (2008) 106003, [arXiv:0803.3085].

[201] R. H. Brandenberger, A. Knauf, and L. C. Lorenz, *Reheating in a brane monodromy inflation model*, *J. High Energy Phys.* **10** (Oct., 2008) 110, [arXiv:0808.3936].

[202] H. Peiris, R. Easther, and R. Flauger, *Constraining Monodromy Inflation*, *JCAP* **1309** (2013) 018, [arXiv:1303.2616].

[203] S. Franco, D. Galloni, A. Retolaza, and A. Uranga, *Axion Monodromy Inflation on Warped Throats*, arXiv:1405.7044.

[204] R. Flauger, L. McAllister, E. Pajer, A. Westphal, and G. Xu, *Oscillations in the CMB from Axion Monodromy Inflation*, *JCAP* **1006** (2010) 009, [arXiv:0907.2916].

[205] R. Blumenhagen and E. Plauschinn, *Towards Universal Axion Inflation and Reheating in String Theory*, arXiv:1404.3542.

[206] J. P. Conlon, *Brane-Antibrane Backreaction in Axion Monodromy Inflation*, *JCAP* **1201** (2012) 033, [arXiv:1110.6454].

[207] M. Berg, E. Pajer, and S. Sjors, *Dante's Inferno*, *Phys.Rev.* **D81** (2010) 103535, [arXiv:0912.1341].

[208] A. Hebecker, S. C. Kraus, and L. T. Witkowski, *D7-Brane Chaotic Inflation*, arXiv:1404.3711.

[209] N. Kaloper, A. Lawrence, and L. Sorbo, *An Ignoble Approach to Large Field Inflation*, *JCAP* **1103** (2011) 023, [arXiv:1101.0026].

[210] R. Kallosh, A. Linde, and B. Vercnocke, *Natural Inflation in Supergravity and Beyond*, arXiv:1404.6244.

[211] E. Pajer and M. Peloso, *A review of axion inflation in the era of Planck*, *Class. Quantum Gravity* **30** (Nov., 2013) 214002, [arXiv:1305.3557].

[212] M. Becker, L. Leblond, and S. Shandera, *Inflation from wrapped branes*, *Phys. Rev. D* **76** (Dec., 2007) 123516, [arXiv:0709.1170].

[213] C. T. Byrnes, D. Regan, D. Seery, and E. R. M. Tarrant, *The hemispherical asymmetry from a scale-dependent inflationary bispectrum*, *JCAP* **1606** (2016), no. 06 025, [arXiv:1511.0312].

[214] C. T. Byrnes, D. Regan, D. Seery, and E. R. M. Tarrant, *Implications of the cosmic microwave background power asymmetry for the early universe*, *Phys. Rev.* **D93** (2016), no. 12 123003, [arXiv:1601.0197].

[215] S. Aiola, B. Wang, A. Kosowsky, T. Kahniashvili, and H. Firouzjahi, *Microwave Background Correlations from Dipole Anisotropy Modulation*, *Phys. Rev.* **D92** (2015) 063008, [arXiv:1506.0440].

[216] D. Hanson and A. Lewis, *Estimators for CMB statistical anisotropy*, *PRD* **80** (Sept., 2009) 063004, [arXiv:0908.0963].

[217] H. Eriksen, F. Hansen, A. Banday, K. Gorski, and P. Lilje, *Asymmetries in the Cosmic Microwave Background anisotropy field*, *Astrophys.J.* **605** (2004) 14–20, [astro-ph/0307507].

[218] H. K. Eriksen, A. Banday, K. Gorski, F. Hansen, and P. Lilje, *Hemispherical power asymmetry in the three-year Wilkinson Microwave Anisotropy Probe sky maps*, *Astrophys.J.* **660** (2007) L81–L84, [astro-ph/0701089].

[219] F. K. Hansen, A. Banday, and K. Gorski, *Testing the cosmological principle of isotropy: Local power spectrum estimates of the WMAP data*, *Mon.Not.Roy.Astron.Soc.* **354** (2004) 641–665, [astro-ph/0404206].

[220] J. Hoftuft, H. K. Eriksen, A. J. Banday, K. M. Górski, F. K. Hansen, and P. B. Lilje, *Increasing Evidence for Hemispherical Power Asymmetry in the Five-Year WMAP Data*, *APJ* **699** (July, 2009) 985–989, [arXiv:0903.1229].

[221] **Planck** Collaboration, P. Ade et al., *Planck 2013 results. XXIII. Isotropy and statistics of the CMB*, *Astron.Astrophys.* **571** (2014) A23, [arXiv:1303.5083].

[222] F. Paci, A. Gruppuso, F. Finelli, A. De Rosa, N. Mandolesi, et al., *Hemispherical power asymmetries in the WMAP 7-year low-resolution temperature and polarization maps*, *Mon.Not.Roy.Astron.Soc.* **434** (2013) 3071, [arXiv:1301.5195].

[223] S. Flender and S. Hotchkiss, *The small scale power asymmetry in the cosmic microwave background*, *JCAP* **1309** (2013) 033, [arXiv:1307.6069].

[224] Y. Akrami, Y. Fantaye, A. Shafieloo, H. Eriksen, F. Hansen, et al., *Power asymmetry in WMAP and Planck temperature sky maps as measured by a local variance estimator*, *Astrophys.J.* **784** (2014) L42, [arXiv:1402.0870].

[225] C. L. Bennett, R. S. Hill, G. Hinshaw, D. Larson, K. M. Smith, J. Dunkley, B. Gold, M. Halpern, N. Jarosik, A. Kogut, E. Komatsu, M. Limon, S. S. Meyer, M. R. Nolta, N. Odegard, L. Page, D. N. Spergel, G. S. Tucker, J. L. Weiland, E. Wollack, and E. L. Wright, *Seven-year Wilkinson Microwave Anisotropy Probe (WMAP) Observations: Are There Cosmic Microwave Background Anomalies?*, *Astrophys. J. Suppl.* **192** (Feb., 2011) 17, [arXiv:1001.4758].

[226] A. L. Erickcek, M. Kamionkowski, and S. M. Carroll, *A Hemispherical Power Asymmetry from Inflation*, *Phys.Rev.* **D78** (2008) 123520, [arXiv:0806.0377].

[227] A. L. Erickcek, S. M. Carroll, and M. Kamionkowski, *Superhorizon Perturbations and the Cosmic Microwave Background*, *Phys.Rev.* **D78** (2008) 083012, [arXiv:0808.1570].

[228] T. Kobayashi, M. Cortes, and A. R. Liddle, *A separate universe view of the asymmetric sky*, arXiv:1501.0586.

[229] A. R. Liddle and M. Cortes, *Cosmic microwave background anomalies in an open universe*, *Phys.Rev.Lett.* **111** (2013), no. 11 111302, [arXiv:1306.5698].

[230] L. Dai, D. Jeong, M. Kamionkowski, and J. Chluba, *The Pesky Power Asymmetry*, *Phys.Rev.* **D87** (2013), no. 12 123005, [arXiv:1303.6949].

[231] D. H. Lyth, *The CMB modulation from inflation*, *JCAP* **1308** (2013) 007, [arXiv:1304.1270].

[232] M. H. Namjoo, S. Baghram, and H. Firouzjahi, *Hemispherical Asymmetry and Local non-Gaussianity: a Consistency Condition*, *Phys.Rev.* **D88** (2013) 083527, [arXiv:1305.0813].

[233] M. H. Namjoo, A. A. Abolhasani, S. Baghram, and H. Firouzjahi, *CMB Hemispherical Asymmetry: Long Mode Modulation and non-Gaussianity*, *JCAP* **1408** (2014) 002, [arXiv:1405.7317].

[234] D. H. Lyth, *Generating f_{NL} at $l \sim 60$*, *JCAP* **1504** (2015), no. 04 039, [arXiv:1405.3562].

[235] S. Kanno, M. Sasaki, and T. Tanaka, *A viable explanation of the CMB dipolar statistical anisotropy*, *PTEP* **2013** (2013) 111E01, [arXiv:1309.1350].

[236] A. A. Abolhasani, S. Baghram, H. Firouzjahi, and M. H. Namjoo, *Asymmetric Sky from the Long Mode Modulations*, *Phys.Rev.* **D89** (2014), no. 6 063511, [arXiv:1306.6932].

[237] S. Jazayeri, Y. Akrami, H. Firouzjahi, A. R. Solomon, and Y. Wang, *Inflationary power asymmetry from primordial domain walls*, *JCAP* **1411** (2014) 044, [arXiv:1408.3057].

[238] K. Kohri, C.-M. Lin, and T. Matsuda, *Scale-dependent CMB asymmetry from primordial configuration*, *JCAP* **1408** (2014) 026, [arXiv:1308.5790].

[239] C. M. Hirata, *Constraints on cosmic hemispherical power anomalies from quasars*, *JCAP* **9** (Sept., 2009) 11, [arXiv:0907.0703].

[240] C. T. Byrnes and E. R. M. Tarrant, *Scale-dependent non-Gaussianity and the CMB Power Asymmetry*, *JCAP* **1507** (2015), no. 07 007, [arXiv:1502.0733].

[241] M. Sasaki and T. Tanaka, *Super-Horizon Scale Dynamics of Multi-Scalar Inflation*, 9801017.

[242] C. T. Byrnes, M. Sasaki, and D. Wands, *The primordial trispectrum from inflation*, *Phys.Rev.* **D74** (2006) 123519, [astro-ph/0611075].

[243] D. Seery and J. E. Lidsey, *Non-Gaussianity from the inflationary trispectrum*, *JCAP* **0701** (2007) 008, [astro-ph/0611034].

[244] **Planck** Collaboration, P. Ade et al., *Planck 2013 results. XVI. Cosmological parameters*, *Astron.Astrophys.* **571** (2014) A16, [arXiv:1303.5076].

[245] J. Kim and E. Komatsu, *Limits on anisotropic inflation from the Planck data*, *Phys.Rev.* **D88** (2013) 101301, [arXiv:1310.1605].

[246] C. T. Byrnes, S. Nurmi, G. Tasinato, and D. Wands, *Inhomogeneous non-gaussianity*, *JCAP* **3** (Mar., 2012) 12, [arXiv:1111.2721].

[247] E. Nelson and S. Shandera, *Statistical Naturalness and Non-Gaussianity in a Finite Universe*, *Physical Review Letters* **110** (Mar., 2013) 131301, [arXiv:1212.4550].

[248] S. Nurmi, C. T. Byrnes, and G. Tasinato, *A non-Gaussian landscape*, *JCAP* **1306** (2013) 004, [arXiv:1301.3128].

[249] M. LoVerde, E. Nelson, and S. Shandera, *Non-Gaussian Mode Coupling and the Statistical Cosmological Principle*, *JCAP* **1306** (2013) 024, [arXiv:1303.3549].

[250] B. Baytas, A. Kesavan, E. Nelson, S. Park, and S. Shandera, *Non-local bispectra from super cosmic variance*, arXiv:1502.0100.

[251] C. T. Byrnes, S. Nurmi, G. Tasinato, and D. Wands, *Implications of the Planck bispectrum constraints for the primordial trispectrum*, *Europhys.Lett.* **103** (2013) 19001, [arXiv:1306.2370].

[252] J. Elliston, L. Alabidi, I. Huston, D. Mulryne, and R. Tavakol, *Large trispectrum in two-field slow-roll inflation*, *JCAP* **1209** (2012) 001, [arXiv:1203.6844].

[253] K. Enqvist, D. J. Mulryne, and S. Nurmi, *Resolving primordial physics through correlated signatures*, arXiv:1412.5973.

[254] T. Suyama and S. Yokoyama, *Extension of local-type inequality for the higher order correlation functions*, *JCAP* **7** (July, 2011) 33, [arXiv:1105.5851].

[255] P. Creminelli, G. D'Amico, M. Musso, and J. Noreña, *The (not so) squeezed limit of the primordial 3-point function*, *JCAP* **11** (Nov., 2011) 38, [arXiv:1106.1462].

[256] J. Khoury and F. Piazza, *Rapidly-Varying Speed of Sound, Scale Invariance and Non-Gaussian Signatures*, *JCAP* **0907** (2009) 026, [arXiv:0811.3633].

[257] R. H. Ribeiro, *Inflationary signatures of single-field models beyond slow-roll*, *JCAP* **5** (May, 2012) 37, [arXiv:1202.4453].

[258] L. Berezhiani and J. Khoury, *On the Initial State and Consistency Relations*, *JCAP* **1409** (2014) 018, [arXiv:1406.2689].

[259] A. Ashoorioon, K. Dimopoulos, M. Sheikh-Jabbari, and G. Shiu, *Reconciliation of High Energy Scale Models of Inflation with Planck*, *JCAP* **1402** (2014) 025, [arXiv:1306.4914].

[260] S. Mooij, G. A. Palma, and A. E. Romano, *Consistently violating the non-Gaussian consistency relation*, arXiv:1502.0345.

[261] M.-x. Huang and G. Shiu, *Inflationary trispectrum for models with large non-gaussianities*, *Phys. Rev. D* **74** (Dec, 2006) 121301.

[262] M. Li and Y. Wang, *Consistency Relations for Non-Gaussianity*, *JCAP* **0809** (2008) 018, [arXiv:0807.3058].

[263] L. Leblond and E. Pajer, *Resonant Trispectrum and a Dozen More Primordial N-point functions*, *JCAP* **1101** (2011) 035, [arXiv:1010.4565].

[264] D. Seery, M. S. Sloth, and F. Vernizzi, *Inflationary trispectrum from graviton exchange*, *JCAP* **0903** (2009) 018, [arXiv:0811.3934].

[265] K. Hinterbichler, L. Hui, and J. Khoury, *Conformal Symmetries of Adiabatic Modes in Cosmology*, *JCAP* **1208** (2012) 017, [arXiv:1203.6351].

[266] P. Creminelli, J. Norena, and M. Simonovic, *Conformal consistency relations for single-field inflation*, *JCAP* **1207** (2012) 052, [arXiv:1203.4595].

[267] P. McFadden, *Soft limits in holographic cosmology*, *JHEP* **1502** (2015) 053, [arXiv:1412.1874].

[268] A. Joyce, J. Khoury, and M. Simonovic, *Multiple Soft Limits of Cosmological Correlation Functions*, *JCAP* **1501** (2015), no. 01 012, [arXiv:1409.6318].

[269] M. Mirbabayi and M. Zaldarriaga, *Double Soft Limits of Cosmological Correlations*, *JCAP* **1503** (2015), no. 03 025, [arXiv:1409.6317].

[270] K. Hinterbichler, L. Hui, and J. Khoury, *An Infinite Set of Ward Identities for Adiabatic Modes in Cosmology*, *JCAP* **1401** (2014) 039, [arXiv:1304.5527].

[271] L. Senatore and M. Zaldarriaga, *A Note on the Consistency Condition of Primordial Fluctuations*, *JCAP* **1208** (2012) 001, [arXiv:1203.6884].

[272] W. D. Goldberger, L. Hui, and A. Nicolis, *One-particle-irreducible consistency relations for cosmological perturbations*, *Phys.Rev.* **D87** (2013), no. 10 103520, [arXiv:1303.1193].

[273] L. Senatore and M. Zaldarriaga, *On Loops in Inflation*, *JHEP* **1012** (2010) 008, [arXiv:0912.2734].

[274] R. Flauger, D. Green, and R. A. Porto, *On squeezed limits in single-field inflation. Part I*, *JCAP* **1308** (2013) 032, [arXiv:1303.1430].

[275] G. L. Pimentel, *Inflationary Consistency Conditions from a Wavefunctional Perspective*, *JHEP* **1402** (2014) 124, [arXiv:1309.1793].

[276] L. Berezhiani, J. Khoury, and J. Wang, *Non-Trivial Checks of Novel Consistency Relations*, *JCAP* **1406** (2014) 056, [arXiv:1401.7991].

[277] T. Tanaka and Y. Urakawa, *Dominance of gauge artifact in the consistency relation for the primordial bispectrum*, *JCAP* **1105** (2011) 014, [arXiv:1103.1251].

[278] E. Pajer, F. Schmidt, and M. Zaldarriaga, *The Observed Squeezed Limit of Cosmological Three-Point Functions*, *Phys.Rev.* **D88** (2013), no. 8 083502, [arXiv:1305.0824].

[279] P. Creminelli, C. Pitrou, and F. Vernizzi, *The CMB bispectrum in the squeezed limit*, *JCAP* **1111** (2011) 025, [arXiv:1109.1822].

[280] V. Assassi, D. Baumann, and D. Green, *On Soft Limits of Inflationary Correlation Functions*, *JCAP* **1211** (2012) 047, [arXiv:1204.4207].

[281] A. Kehagias and A. Riotto, *High Energy Physics Signatures from Inflation and Conformal Symmetry of de Sitter*, *Fortsch. Phys.* **63** (2015) 531–542, [arXiv:1501.0351].

[282] N. Arkani-Hamed and J. Maldacena, *Cosmological Collider Physics*, arXiv:1503.0804.

[283] M. Mirbabayi and M. Simonovic, *Effective Theory of Squeezed Correlation Functions*, arXiv:1507.0475.

[284] N. S. Sugiyama, E. Komatsu, and T. Futamase, *Non-Gaussianity Consistency Relation for Multi-field Inflation*, *Phys.Rev.Lett.* **106** (2011) 251301, [arXiv:1101.3636].

[285] N. S. Sugiyama, *Consistency Relation for multifield inflation scenario with all loop contributions*, *JCAP* **1205** (2012) 032, [arXiv:1201.4048].

[286] K. M. Smith, M. LoVerde, and M. Zaldarriaga, *Universal bound on n-point correlations from inflation*, *Phys. Rev. Lett.* **107** (Nov, 2011) 191301.

[287] T. Suyama and M. Yamaguchi, *Non-gaussianity in the modulated reheating scenario*, *Phys. Rev. D* **77** (Jan, 2008) 023505.

[288] A. L. Erickcek, M. Kamionkowski, and S. M. Carroll, *A Hemispherical Power Asymmetry from Inflation*, *Phys. Rev.* **D78** (2008) 123520, [arXiv:0806.0377].

[289] A. L. Erickcek, S. M. Carroll, and M. Kamionkowski, *Superhorizon Perturbations and the Cosmic Microwave Background*, *Phys. Rev.* **D78** (2008) 083012, [arXiv:0808.1570].

[290] T. Kobayashi, M. Cortes, and A. R. Liddle, *A separate universe view of the asymmetric sky*, *JCAP* **1505** (2015), no. 05 029, [arXiv:1501.0586].

[291] N. Dalal, O. Doré, D. Huterer, and A. Shirokov, *Imprints of primordial non-gaussianities on large-scale structure: Scale-dependent bias and abundance of virialized objects*, *Phys. Rev. D* **77** (Jun, 2008) 123514.

[292] E. Pajer and M. Zaldarriaga, *New Window on Primordial Non-Gaussianity*, *Physical Review Letters* **109** (July, 2012) 021302, [arXiv:1201.5375].

[293] M. Dias, R. H. Ribeiro, and D. Seery, *Scale-dependent bias from multiple-field inflation*, *Phys.Rev.* **D87** (2013), no. 10 107301, [arXiv:1303.6000].

[294] J. Fonseca and D. Wands, *Primordial non-Gaussianity from mixed inflaton-curvaton perturbations*, *JCAP* **6** (June, 2012) 28, [arXiv:1204.3443].

[295] L. E. Allen, S. Gupta, and D. Wands, *Non-gaussian perturbations from multi-field inflation*, *JCAP* **0601** (2006) 006, [astro-ph/0509719].

[296] A. Kehagias and A. Riotto, *Operator Product Expansion of Inflationary Correlators and Conformal Symmetry of de Sitter*, *Nucl.Phys.* **B864** (2012) 492–529, [arXiv:1205.1523].

[297] A. Kehagias and A. Riotto, *The Four-point Correlator in Multifield Inflation, the Operator Product Expansion and the Symmetries of de Sitter*, *Nucl.Phys.* **B868** (2013) 577–595, [arXiv:1210.1918].

[298] S. Yokoyama, T. Suyama, and T. Tanaka, *Primordial Non-Gaussianity in Multi-Scalar Slow-Roll Inflation*, *JCAP* **0707** (2007) 013, [arXiv:0705.3178].

[299] S. Yokoyama, T. Suyama, and T. Tanaka, *Primordial Non-Gaussianity in Multi-Scalar Inflation*, *Phys.Rev.* **D77** (2008) 083511, [arXiv:0711.2920].

[300] S. Yokoyama, T. Suyama, and T. Tanaka, *Efficient diagrammatic computation method for higher order correlation functions of local type primordial curvature perturbations*, *JCAP* **0902** (2009) 012, [arXiv:0810.3053].

[301] A. Avgoustidis, S. Cremonini, A.-C. Davis, R. H. Ribeiro, K. Turzynski, and S. Watson, *The Importance of Slow-roll Corrections During Multi-field Inflation*, *JCAP* **1202** (2012) 038, [arXiv:1110.4081].

[302] J. Elliston, D. Seery, and R. Tavakol, *The inflationary bispectrum with curved field-space*, *JCAP* **1211** (2012) 060, [arXiv:1208.6011].

[303] C. T. Byrnes, K.-Y. Choi, and L. M. Hall, *Large non-Gaussianity from two-component hybrid inflation*, *JCAP* **0902** (2009) 017, [arXiv:0812.0807].

[304] E. Sefusatti, M. Liguori, A. P. Yadav, M. G. Jackson, and E. Pajer, *Constraining Running Non-Gaussianity*, *JCAP* **0912** (2009) 022, [arXiv:0906.0232].

[305] C. T. Byrnes and G. Tasinato, *Non-Gaussianity beyond slow roll in multi-field inflation*, *JCAP* **0908** (2009) 016, [arXiv:0906.0767].

[306] F. Vernizzi and D. Wands, *Non-gaussianities in two-field inflation*, *JCAP* **0605** (2006) 019, [astro-ph/0603799].

[307] G. Leung, E. R. M. Tarrant, C. T. Byrnes, and E. J. Copeland, *Reheating, multifield inflation and the fate of the primordial observables*, *JCAP* **9** (Sept., 2012) 8, [arXiv:1206.5196].

[308] D. H. Lyth, C. Ungarelli, and D. Wands, *The Primordial density perturbation in the curvaton scenario*, *Phys.Rev.* **D67** (2003) 023503, [astro-ph/0208055].

[309] D. Langlois and F. Vernizzi, *Mixed inflaton and curvaton perturbations*, *Phys.Rev.* **D70** (2004) 063522, [astro-ph/0403258].

[310] M. Sasaki, J. Valiviita, and D. Wands, *Non-Gaussianity of the primordial perturbation in the curvaton model*, *Phys.Rev.* **D74** (2006) 103003, [astro-ph/0607627].

[311] J. Fonseca and D. Wands, *Non-Gaussianity and Gravitational Waves from Quadratic and Self-interacting Curvaton*, *Phys.Rev.* **D83** (2011) 064025, [arXiv:1101.1254].

[312] J. Fonseca and D. Wands, *Primordial non-Gaussianity from mixed inflaton-curvaton perturbations*, *JCAP* **1206** (2012) 028, [arXiv:1204.3443].

[313] J. Meyers and E. R. M. Tarrant, *Perturbative Reheating After Multiple-Field Inflation: The Impact on Primordial Observables*, *Phys.Rev.* **D89** (2014), no. 6 063535, [arXiv:1311.3972].

[314] J. Elliston, S. Orani, and D. J. Mulryne, *General analytic predictions of two-field inflation and perturbative reheating*, *Phys.Rev.* **D89** (2014), no. 10 103532, [arXiv:1402.4800].

[315] T. Battefeld and R. Easther, *Non-Gaussianities in Multi-field Inflation*, *JCAP* **0703** (2007) 020, [astro-ph/0610296].

[316] K.-Y. Choi, L. M. Hall, and C. van de Bruck, *Spectral Running and Non-Gaussianity from Slow-Roll Inflation in Generalised Two-Field Models*, *JCAP* **0702** (2007) 029, [astro-ph/0701247].

[317] T. Wang, *Note on non-Gaussianities in two-field inflation*, *PRD* **82** (Dec., 2010) 123515, [arXiv:1008.3198].

[318] C. T. Byrnes, K. Enqvist, S. Nurmi, and T. Takahashi, *Strongly scale-dependent polyspectra from curvaton self-interactions*, *JCAP* **1111** (2011) 011, [arXiv:1108.2708].

[319] R. J. Hardwick and C. T. Byrnes, *Bayesian evidence of the post-Planck curvaton*, arXiv:1502.0695.

[320] D. Binosi and A. Quadri, *The Cosmological Slavnov-Taylor Identity from BRST Symmetry in Single-Field Inflation*, *JCAP* **1603** (2016), no. 03 045, [arXiv:1511.0930].

[321] C. T. Byrnes, D. Regan, D. Seery, and E. R. M. Tarrant, *Implications of the CMB power asymmetry for the early universe*, arXiv:1601.0197.

[322] C. T. Byrnes, D. Regan, D. Seery, and E. R. M. Tarrant, *The hemispherical asymmetry from a scale-dependent inflationary bispectrum*, arXiv:1511.0312.

[323] Y. Rodriguez, J. P. Beltran Almeida, and C. A. Valenzuela-Toledo, *The different varieties of the Suyama-Yamaguchi consistency relation and its violation as a signal of statistical inhomogeneity*, *JCAP* **1304** (2013) 039, [arXiv:1301.5843].

[324] D. Seery and J. E. Lidsey, *Primordial non-Gaussianities from multiple-field inflation*, *JCAP* **0509** (2005) 011, [astro-ph/0506056].

[325] X. Gao, *Primordial Non-Gaussianities of General Multiple Field Inflation*, *JCAP* **0806** (2008) 029, [arXiv:0804.1055].

[326] M. Shibata and M. Sasaki, *Black hole formation in the Friedmann universe: Formulation and computation in numerical relativity*, *Phys. Rev.* **D60** (1999) 084002, [gr-qc/9905064].

[327] N. Deruelle and D. Langlois, *Long wavelength iteration of Einstein's equations near a space-time singularity*, *Phys. Rev.* **D52** (1995) 2007–2019, [gr-qc/9411040].

[328] D. Seery, J. E. Lidsey, and M. S. Sloth, *The inflationary trispectrum*, *JCAP* **0701** (2007) 027, [astro-ph/0610210].

[329] C. T. Byrnes, K. Koyama, M. Sasaki, and D. Wands, *Diagrammatic approach to non-Gaussianity from inflation*, *JCAP* **0711** (2007) 027, [arXiv:0705.4096].

[330] Z. Kenton and D. J. Mulryne, *The squeezed limit of the bispectrum in multi-field inflation*, *JCAP* **1510** (2015), no. 10 018, [arXiv:1507.0862].

[331] K. M. Smith, M. Loverde, and M. Zaldarriaga, *Universal Bound on N-Point Correlations from Inflation*, *Physical Review Letters* **107** (Nov., 2011) 191301, [arXiv:1108.1805].

[332] T. Suyama and S. Yokoyama, *Extension of local-type inequality for the higher order correlation functions*, *JCAP* **1107** (2011) 033, [arXiv:1105.5851].

[333] J. M. Maldacena and G. L. Pimentel, *On graviton non-Gaussianities during inflation*, *JHEP* **09** (2011) 045, [arXiv:1104.2846].

[334] E. Dimastrogiovanni, M. Fasiello, and M. Kamionkowski, *Imprints of Massive Primordial Fields on Large-Scale Structure*, arXiv:1504.0599.

[335] J. Fergusson and E. P. Shellard, *Primordial non-Gaussianity and the CMB bispectrum*, *Phys.Rev.* **D76** (2007) 083523, [astro-ph/0612713].